UNIVERSITÉ D'OTTAWA
UNIVERSITY OF OTTAWA

Abstract

Several surface processes have been examined over the years at metal single-crystal electrodes. At platinum, the most studied process is certainly the oxidation of small organic molecules that involve adsorbed carbon monoxide. Despite the very many papers that have appeared on the cathodic hydrogen evolution reaction (HER) since the time of Tafel's work (1905), surprisingly little is known about the actual details of the adsorption of the H-atom intermediate in this reaction and the states in which H is generated on polycrystalline or single-crystal surfaces of H_2 evolving cathodes. This problem arises due to difficulties of actually determining coverages, θ_H, by adsorbed H in the course of the HER at steady-state currents. However, substantially more is known from recent work about the states of underpotential deposited H (UPD) at well-defined, single-crystal surfaces.

Interest in the state of H, electrochemically generated at metal surfaces by discharge of H_3O^+ ions or from H_2O arises from two directions: a) the observation of the so-called underpotential deposition (UPD) of atomic H from aqueous solutions at Pt, Rh, Ir and Ru, which takes place distinguishably from the processes of proton discharge leading to molecular H_2 formation; b) the 2-e^- process of cathodic formation of molecular H_2, also involving an initial step of proton discharge but at an overvoltage.

The relation between the state of electrodeposited H in the "underpotential" voltage range and that of H involved in "overpotential deposition" in the course of the cathodic H_2 evolution reaction is a matter of substantial significance for electrocatalysis in the HER and for the surface electrochemistry of Pt. However, its possible involvement in the HER is not clearly understood since the H that is the intermediate in the HER is (overpotentially) deposited on a surface already containing a full monolayer of the underpotentially deposited H. While the cyclic voltammetry current profiles for UPD at several noble metals by H are relatively well characterized, no direct kinetic studies of such UPD processes are available. These studies are made difficult by the high rate-constants of the processes involved and by the small concentration of generated

surface species (of the order of 1 x 10^{15} atoms cm^{-2}, *i.e.* 1.66 x 10^{-9} mol cm^{-2}).

One of the most sensitive techniques available that can allow kinetic studies of the UPD of H to be made is ac impedance spectroscopy conducted at controlled electrode potentials. The principal aims of this part of the thesis work were to examine the dependence of the kinetics of the charge-transfer leading to H chemisorption in various states on various crystal-plane geometries of single-crystals of Pt through evaluation of the charge-transfer resistance, R_{ct}, and how this process depends substantially on the orientation and two-dimensional structure of the surface.

Analysis of the ac results by means of equivalent-circuit fitting allows determination of the double-layer capacitance, C_{dl}, and the H adsorption pseudocapacitance, C_p, which is determined by H (and anion) coverages, as well as the kinetics of the charge-transfer itself as a function of the potential.

Very good correlation between the results for total capacitance (C_{dl} + C_p's) determined by cyclic voltammetry and by impedance measurements was obtained for Pt(100), (111), (110) and (311) surfaces in 0.5 mol dm^{-3} H_2SO_4 solution, with allowance being made, where appropriate, for HSO_4^- ion co-adsorption. The variation of parameters with lowering of the temperature was also investigated for Pt(100), (111), (110) and (311) in 0.5 mol dm^{-3} H_2SO_4. This allowed determination of the apparent activation energy for the H adsorption-desorption process at Pt(100) and (311). The important influence of the geometry of the crystal face on the kinetics of the UPD process and on the thermodynamics of the interfacial process (C_{dl} and C_p's) was also evaluated.

In another main part of the work, the effects of chemisorbed acetonitrile on the UPD of H (and anion adsorption-desorption) in acidic solutions were evaluated. From studies of this process at polycrystalline Pt, acetonitrile was found to be reductively chemisorbed at Pt at the beginning of the "double-layer" potential region in the cyclic voltammogram for this electrode material, taken between 0.06 V and *ca.* 0.80 V *vs.* RHE. In this adsorbed state, it then undergoes an almost reversible stage of reoxidation or re-reduction, and slower further reduction over the potential range for UPD of H. In this respect, Pt, bearing a sub-monolayer of chemisorbed acetonitrile, was one of the first

"chemically modified electrodes" to be studied. These processes were investigated by means of cyclic voltammetry at the (111), (110) and (100) planes, together with the (311) stepped plane, of well characterized single-crystal Pt surfaces which exhibit, in the absence of adsorbed acetonitrile, the characteristically distinguished cyclic voltammograms demonstrated by Clavilier and other research groups for clean, well ordered surfaces. Complementary information on the reductive chemisorption of acetonitrile and competitive occupation of H sites was provided by recording of adsorption current transients at Pt surfaces when acetonitrile is added, at controlled potential, to an initially acetonitrile-free solution. In the range of potential for UPD of H, the resulting transient currents contain a component due to the "anodic H desorption effect".

The chemisorption and surface reactivity behaviour of acetonitrile at the above crystal planes is found to be very specific to the geometry of the surfaces and provides one of the clearest examples of such surface specificity in electrochemical surface science for an adsorbed organic molecule at Pt. Similarities to and contrasts with the surface-specific behaviour of the four crystal planes with respect to H UPD behaviour and HSO_4^- or ClO_4^- anion adsorption are observed and their significance is discussed.

Additionally, *in situ* infrared spectroscopy allowed further investigation of the mechanism of reactive chemisorption of acetonitrile by means of vibrational structural analysis of the potential-dependent adsorbates present on well-ordered Pt(111) and (100) surfaces. In accordance with the mechanism proposed from the electrochemical studies, the infrared spectra show, at potentials below 0.35 V *vs.* RHE on Pt(111), the presence of a reduced form of chemisorbed acetonitrile. This is supported by the observation of a >C=N- stretching frequency at 1630 cm^{-1} which is downshifted to 1614 cm^{-1} upon deuteration. A similar, albeit weaker, spectral feature was obtained upon reduction of adsorbed acetonitrile on Pt(100) which also develops with time, indicating slow reduction as can also be proposed on electrochemical grounds. Overall, the results illustrate the still seldom-exploited virtues of combined infrared-electrochemical measurements as an aid to the elucidation of adsorbate reaction pathways.

Publications and Oral Presentations

Some of the work described in this thesis has already been published or submitted for publication, and other parts are in preparation, as follows:

1. S. Morin and B.E. Conway, "Surface structure dependence of reactive chemisorption of acetonitrile on single-crystal Pt Surfaces", *J. Electroanal. Chem.*, **376** (1994) 135-150.

2. S. Morin, "Kinetics of underpotential deposition of hydrogen on Pt single-crystal electrodes using ac impedance spectroscopy", summary report to The Electrochemical Society for the 1995 Joseph W. Richards Research Fellowship, *Interface*, Summer 1996 issue.

3. S. Morin, H. Dumont and B.E. Conway, "Evaluation of the two-dimensional geometry of Pt single-crystal faces on the kinetics of UPD of H using impedance spectroscopy", *accepted for publication in J. Electroanal. Chem.*, in press.

4. S. Morin, B.E. Conway, G.J. Edens and M.J. Weaver, "The reactive chemisorption of acetonitrile on Pt(111) and Pt(100) electrodes as examined by in situ infrared spectroscopy", *accepted for publication in J. Electroanal. Chem.*, in press.

5. S. Morin and B.E. Conway, "Kinetics of UPD of H at the (110) and (311) surface of Pt single-crystal electrodes over a range of temperatures using impedance spectroscopy", *in preparation.*

During the course of this research, the work described in this thesis was presented at various conferences and symposia as follows:

1. S. Morin and B.E. Conway, "Electrochemical study of surface processes at platinum single-crystal electrodes: kinetic studies of the fast UPD of hydrogen and of the reactive chemisorption of acetonitrile", *invited speaker at the Steacie Institute for Molecular Sciences, National Research Council, Ottawa, Ontario, Canada*, July 1996.

2. S. Morin and B.E. Conway, "Surface structure dependence of the reactive chemisorption of acetonitrile on single-crystal Pt surfaces", *Student award lecture, The Electrochemical Society Inc. Canadian Section Symposium on Electrode Processes and Their Applications at the Canadian Society for Chemistry Conference, Guelph, Canada*, May 1995.

3. S. Morin, H. Dumont and B.E. Conway, "Studies of the kinetics of the underpotential deposition of H on different Pt monocrystal faces using ac impedance spectroscopy", *The Electrochemical Society Inc. Canadian Section Symposium on Electrode Processes and Their Applications at the Canadian Society for Chemistry Conference, Guelph, Canada*, May 1995.

4. S. Morin and B.E. Conway, "Reactivity of acetonitrile in the chemisorbed state on platinum single-crystal surfaces in aqueous acidic media", *Invited speaker at Exxon, Research and Engineering Company, Annandale, USA*, December 1994.

5. S. Morin and B.E. Conway, "Reactivity of acetonitrile in the chemisorbed state on Pt single-crystal surfaces in aqueous acidic media", *The Electrochemical Society Inc., Fall Meeting, Miami Beach, Florida, USA*, October 1994.

Acknowledgments

I have spent the past five years working in Prof. Conway's research group, this experience has undoubtfully provided me with invaluable knowledge of electrochemistry and other areas of surface science through numerous discussions, group seminars and Prof. Conway's graduate courses. Hence, I wish to express my sincere gratitude to Prof. Brian E. Conway whose generous help and guidance enabled me to pursue sucessfully my Ph.D. studies.

During the course of this research, I have also had the privilege to work with Dr. Jean Clavilier (CNRS, Meudon, France) and Prof. Mike Weaver (Dept. of Chemistry, Purdue University) and I would like to thank both of them for their scientific hospitality, allowing myself to work in their research facilities.

Conducting this research would have been impossible without electrochemical cells and other glass equipment built by Mr. Egon Kristof and Mr. John Hopkins, whom I thank very much for their help and professional advice. I would also like to extend my thanks to the personel of the Machine and Electric Shops, especially to Mr. Leonard Pement and Mr. Bob Hart for their help in machining pieces of equipment without which this research would not have been possible.

I wish to thank the Support Staff members and my colleagues at the department especially Ms. Eva Szabo for the Figures in Chapter 7, as well as my colleagues in Prof. Conway's research group for their friendship and especially Dr. Hubert Dumont for its collaboration on the UPD of H kinetics study.

At last, I would like to acknowledge the School of Graduate Studies, the FCAR founds from government of Quebec, the Ministry of Education an Training of the province of Ontario for two Ontario Graduate Scholarships, the Electrochemical Society Canadian section Inc. and the Electrochemical Society Inc. for their financial support throughout the course of my studies.

Table of contents

List of tables

List of figures

List of symbols

A	a) Area of the electrode b) $1/R_{ct}$ c) Frequency factor
a.u.	Absorbance units
b	Tafel slope
C	Capacitance, dq/dE
C_A	Adsorbate concentration in solution
C_{dl}	Double-layer capacitance
C_f	Faradaic capacitance
C_{H+}	Concentration de H^+
C_O, C_R	Redox species concentrations
C_p	Pseudocapacitance
C_{tot}	Total capacitance ($C_{dl} + C_p$)
C_W	Warburg pseudocapacitance
D_O, D_R	Diffusion constants of the redox species
E	Potential applied at the electrode
E_{ads}	Adsorption potential
E_C	Potential difference across a capacitance
E_{eq}	Equilibrium potential
E_f	Final potential
E_i	Initial potential
E_{peak}	Peak potential on the cyclic voltammogram recorded at a given *s* value
E_R	Potential difference across a resistance
$E(\omega)$	Sinusoidal potential
$E^{o'}$	Formal potential of the process studies
$E-E^{o'}$	Metal/solution potential difference
E_θ	Potential value in the UPD of H at coverage θ
$\tilde{E}_\theta$	Modulated potential around its equilibrium value
$E^o_{\theta=0.5}$	Standard state potential
f	Constant equal to nF/RT at a given temperature, T
F	Faraday constant
i_{dl}	Current corresponding to the double-layer charging
$i(\omega)$	Sinusoidal current
I_p	Absorbance intensity for p polarized light
I_s	Absorbance intensity for s polarized light
j	Current-density
j	Imaginary number
j_f	Faradaic current-density
$\tilde{j}_f$	Modulated current around its equilibrium value
j_o	Exchange current-density
$j_{o,E}$	Exchange current-density for the UPD of H

j_{peak}	Peak current-density on the cyclic voltammogram recorded at a given *s* value, Volts per second
k_s	Rate constant determined using the variation of sweep rate method
$k_{o,\theta}$	Exchange rate constant for the UPD of H
k_1	Forward specific rate constant
k_{-1}	Reverse specific rate constant
K_1	Equilibrium constant, k_1/k_{-1}
n	a) Width of the terrace in atoms b) Number of electron transferred
pzc	Potential of zero charge
pzfc	Potential of zero free charge
pztc	Potential of zero total charge
q	Charge
q_H	Charge associated with H UPD process
q_t or q_t'	Charge for adsorption on the terraces
q_T	Transient charge
$q_T(E_{ads})$	Maximum anodic transient charge recorded for H displacement
$q_T(E_{0.08V})$	Charge of the CO adsorption transient recorded at any potential E_{ads}
q(t)	Resulting charge q when a potential E(t) is applied to a capacitance
q_1	Charge corresponding to a monolayer of adsorbed species
q_{111}	Charge for a well-ordered (111) surface
$q_{100\ step}$	Charge for adsorption of H on the (100) step sites
$q_{110\ step}$	Charge for adsorption of H on the (110) step sites
R	a) Gas constant b) Resistance
R_f	Faradaic resistance
R_{ct}	Charge transfer resistance
RHE	Reversible hydrogen electrode
r_o	Rate of electron transfer
R_{sol}	Solution resistance
R_W	Warburg resistance
s	Sweep rate, dE/dt
s_o	Sweep rate value analogous to j_o
SCE	Saturated calomel electrode
SHE	Standard hydrogen electrode
t	Time
T	Temperature in K
TLK	Terrace, ledge and kink model
v	rate
v_o	exchange rate
$v_{o,\theta}$	exchange rate for the UPD of H
X_c	Capacitive reactance
Z	Impedance
Z'	Real component of the impedance Z

Z''	Imaginary component of the impedance Z
Z_{cp}	Impedance of the pseudocapacitance
Z_{Rct}	Impedance of the charge transfer resistance
Z_W	Warburg impedance
β	Transfer coefficient or barrier symmetry factor
ΔE_{peak}	Variation of E_{peak} with s
Δpzc	Variation of the potential of zero charge
Δq_T	Integration of the current response between two potential limits
ΔR	Change of reflectivity
ϕ	Phase angle between the imaginary and real components of impedance
Φ	Electron work function of the metal
θ	Coverage
$\tilde{\theta}$	Modulated coverage around its equilibrium value
θ_H	Hydrogen coverage
$\theta_{H,E}$	Hydrogen coverage in UPD of H region
ν	Frequency (cm^{-1})
ω	Frequency of the alternating signal
φ	Constant phase element exponent

Chapter 1
Introduction

1.1 Generalities

Information about two-dimensional and quasi-two-dimensional processes at electrodes is needed to understand and control reactions involved in many fields of fundamental and applied science, such as electrocatalysis, corrosion inhibition and plating, to name a few. However, it has been stated [1] that "there remains a gulf between those who developed electrode materials and those who seek to understand the physical chemistry of electrocatalysis". This, one can interpret as the relationship between structure and reactivity by studying electrochemical processes at well defined surfaces. In the present thesis work, the electrodes used were highly defined single-crystal faces. The use of such surfaces allows control over the surface crystallography which is the key to the understanding of phenomena occurring at the surface. Hence, by employing surfaces of different structure to study interfacial processes one can assess the effect of the surface crystallography, *i.e.* two-dimensional geometry and corresponding electronic properties, *e.g.* orbital emergence and electronic work function on phenomena involving adsorbed intermediates.

1.2 Scope and origin of the research described in this thesis

Some of the most original and significant research in Physical Electrochemistry is being conducted in the field of "surface electrochemistry", *i.e.* aspects of electrochemistry related to modern surface science. In a general overall sense, all electrochemical processes occur at the *interfaces* of metals and semiconductors. However, modern directions of work have emerged to address the specificities that arise in electrode-kinetic and electrosorption processes by using well defined single-crystal surfaces of metals, especially Pt and Au, to characterize and understand such processes. These surfaces offer highly specific surface geometries at which particular coordinations of adsorbates arise or at which particular kinetic pathways or activation energies arise in electrocatalysis.

An initial aim of the research project was to examine an interesting and unique surface electrochemical reaction, the reactive chemisorption of acetonitrile, that had been discovered in earlier work in this laboratory. It offered an excellent opportunity for examination of specificities of a surface reaction at single-crystal Pt electrodes cut to give different orientations of the electrode surface plane, and thus different coordination opportunities for chemisorption of acetonitrile and products of its electrochemical reduction. Such surfaces also provided simultaneous opportunities for quantitative examination of the role of underpotentially-deposited (UPD) hydrogen (H) (and also adsorbed anions) in the adsorptive and reactive pathways involved.

This led to a substantial record and complementary part of the work in which the effects of chemisorbed acetonitrile on the UPD H (and anions) in acidic solutions were evaluated and, more particularly, to a new direction of work on determination of the *surface specificity* of the kinetics of H deposition from H_3O^+ and anions in acid solution onto various single-crystal Pt surfaces in the potential region for UPD of H and anions. These experiments were conducted by means of cyclic voltammetry and ac impedance spectroscopy over the UPD H (and anion adsorption) region. Again, major specificities of the electrosorption kinetics to the surface geometries of Pt were found, and the energies of activation were also determined.

Finally, complementary to the electrochemical studies of acetonitrile electrosorption at Pt, and co-adsorption of H, *in situ* infrared absorption measurements were made on the states of chemisorbed acetonitrile at several well-ordered single-crystal Pt surfaces, as a function of electrode potential. The results obtained helped to provide a molecular-level basis for better understanding of the results derived by means of the cyclic voltammetry and adsorption charge transient measurements made by purely electrochemical means.

Overall, the experiments and results obtained provided a comprehensive understanding of a new surface electrochemical process, the reactive chemisorption of acetonitrile at Pt, as well as providing a kinetic picture of the H and anion adsorption-desorption processes at Pt single-crystals in acidic solution.

The results presented in this thesis are organized in two distinct Parts, the first

one, preceded by the Chapters on electrochemical characterization of Pt surfaces and methodologies, will deal with the results and discussion for the kinetics of the UPD H (and anions) at various Pt single-crystal surfaces and the second Part will deal with the reactive chemisorption of acetonitrile at Pt single-crystal surfaces. Each results and discussion Chapters include an introduction section, a relevant theoretical section, as well as a section containing more experimental details when appropriate; they will also include detailed discussion and conclusions sections. Finally, Chapter 8 will be concerned with general conclusions, followed by a list of achievements showing the relevance of this work.

1.3 Origins of specificity of surface geometries for surface reactions and chemisorption

A single-crystal is an array of atoms in a metal crystal, well ordered on a long-range scale. For metals such as gold, silver, copper and platinum the atoms crystallise in the face-centred cubic lattice arrangement. Each arrangement is generated by a repetition of a unit cell pattern. Various surface arrangements can be revealed by cross-sectioning a single-crystal with a dividing plane having a known orientation as illustrated in Fig. 1.1.

The specificity or anisotropy of surface reactions and chemisorption to various surface geometries was recognized very early as shown by ref. 2. The origin of this specificity lies in the following factors a) the differences in the potential of zero charge and hence work function (Φ) of the various surfaces geometries; b) the differences in double-layer structure at various surface geometries such as their respective specificity towards anion adsorption; and c) the different geometries of coordination of adsorbed species to the various surfaces. Each of these points will be elaborated below in their respective subsections.

1.3.1 Differences in the potential of zero charge for various surfaces

The environment of an electrode in contact with an electrolyte solution is complex; its treatment combines the established difficulties of conventional surface

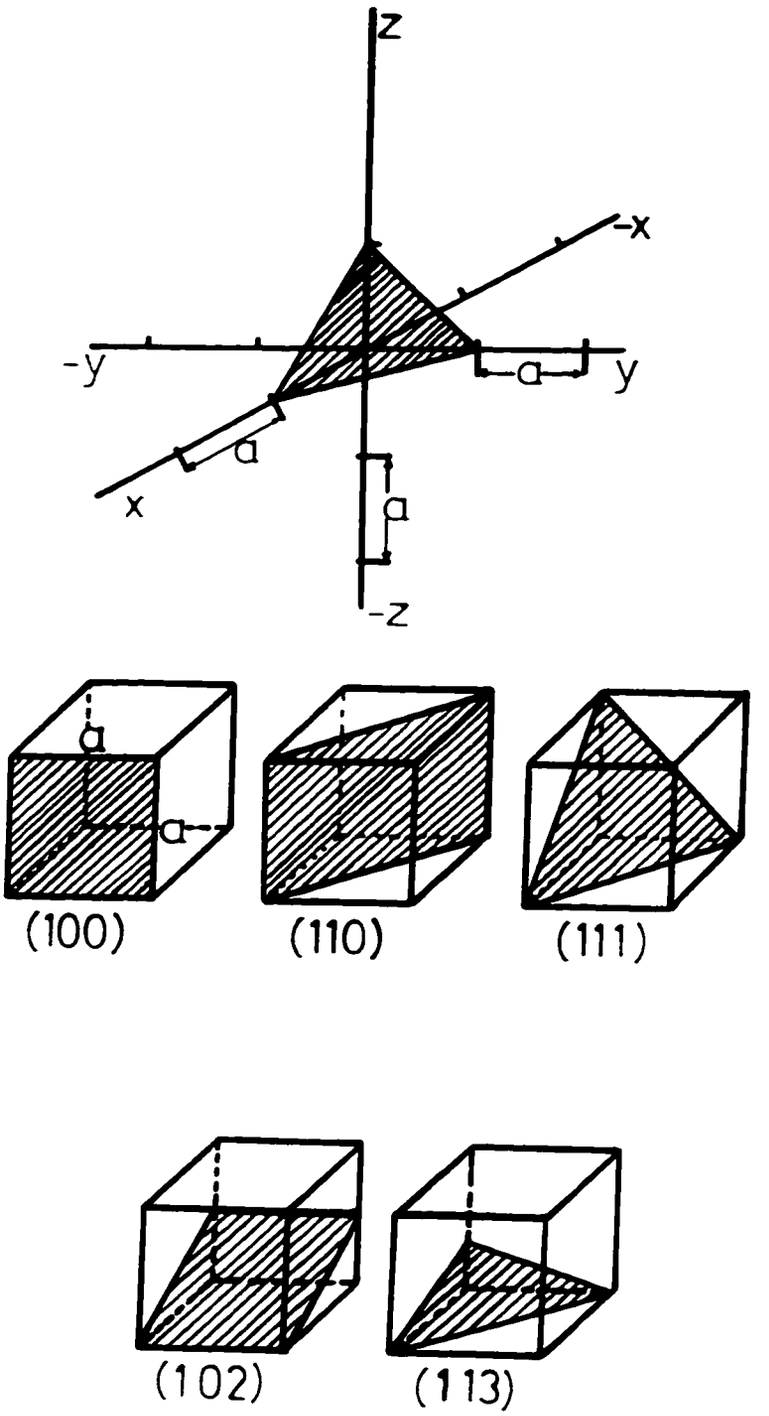

Fig. 1.1 The rectangular axes and the (111) plane for the cubic system. Some important planes and their Miller indices for the cubic system are shown [2].

studies with the complications associated with the disordered and mobile charge character of the liquid phase electrolyte. In the simplest case, when the electrode is in contact with water solvent containing a non-adsorbing electrolyte, a potential-dependent structure will be established at the metal solution interface. The formation of this structured layer (or layers) is driven by various factors, namely, the potential applied at the electrode (relative to some reference value) which will create an excess of positive or negative charges at the metal surface, the chemical nature and concentration of the electrolyte and the nature of the metal electrode itself.

The first modelling of the structured layer, referred to in some literature as the *interphase*, at the metal/solution interface is attributable to the early work of Helmholtz, Gouy and Chapman and Stern (see ref. 3 for further details) and a now well accepted representation of the structured interface is shown in Fig. 1.2 as proposed by Grahame [4]. In this representation the negatively charged electrode is in contact with a first layer composed of solvent molecules, *e.g.* water. For this sign of charge, the water molecule dipole moment tends to be oriented perpendicular to the plane of the surface, with its positive end towards it but this orientation is subject to thermal fluctuations. This is strictly an electrostatic response to the electric field created at the metal surface by the excess surface charge. The defining limit of this first layer when chemisorbed ions populate it (Fig. 1.5a) is called the *inner Helmholtz plane* [4]. In the absence of specific adsorption, *i.e.* chemisorption of the ions contained in the supporting electrolyte, a second plane (*outer Helmholtz plane*) is created by the locus of centres of solvated cations that accumulate near the surface also in response to the electrostatic field created by the applied potential. The different distances of closest approach of ions of the electrolyte to the electrode metal surface distinguish these two interphasial regions. The formation of these two layers, historically termed the *double-layer*, is the result of an interplay between the tendency of the charge on the metallic phase to attract or repel the charged species according to polarity and the tendency of thermal fluctuations to randomize them. This model therefore also involves a *diffuse layer* of charge towards the bulk of the solution phase, as first identified in the works of Gouy [5] and of

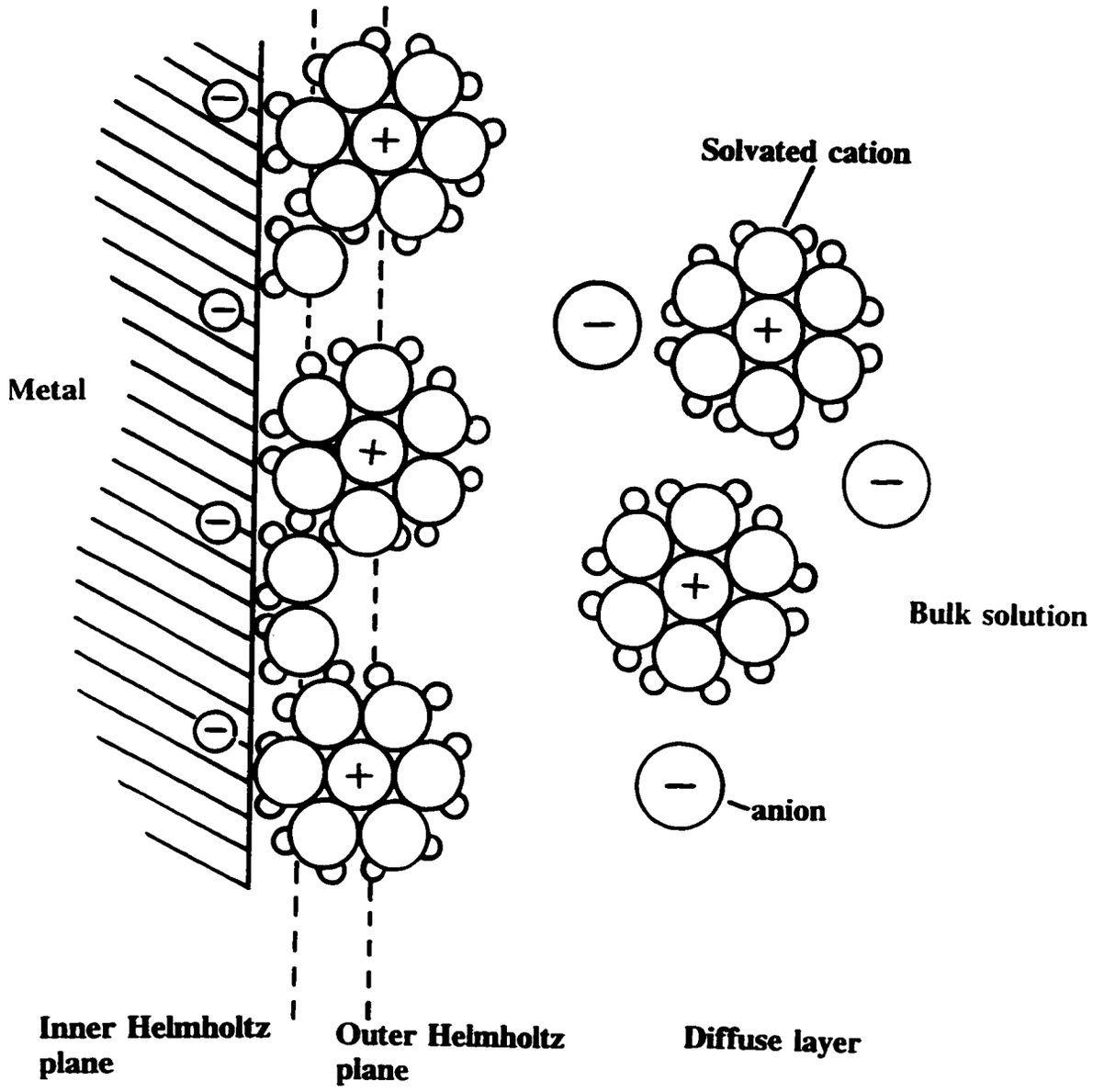

Fig. 1.2 Grahame's model of the interfacial region in the immediate vicinity of the electrode; + and - represent cations and anions respectively, and the remaining spheres on the diagrams are water molecules which may be free or involved in primary solvation. IHP and OHP are the inner and outer Helmholtz planes, respectively. This double-layer diagram is shown for the ideal case when there is no anion adsorption at the IHP.

Chapman [6]. Hence, the interphasial regions can be viewed in electrostatic terms as capacitors in series having their charge-bearing "plates" parallel to the electrode surface.

Various ways have been employed to characterise the metal/solution interface (for a summary, see ref. 7), but the most common procedure used for the study of the double-layer at solid electrodes is the determination of differential capacitance [8]. This method yields the relation between the capacitance at the plates of the model capacitor components and the applied potential. Hence, information on the structure of the interface can be obtained, *e.g.* by following the thermodynamic analysis given in detail by Grahame [4].

Figure 1.3, shows examples of differential capacitance curves for (100) single-crystal silver and mercury electrodes in NaF solutions. At low electrolyte concentrations a central minimum is clearly seen on the curves. This minimum corresponds to the potential of zero charge (*pzc*), *i.e.* to the potential at which the electrode charge is neither positive nor negative. This region represents the contribution of the diffuse part of the double-layer to the capacitance. Also, at this potential, the water molecules are almost randomly oriented at the interface, and the ions previously accumulated near the surface at the outer Helmholtz plane (OHP) and in the *diffuse layer* are now randomly distributed as if they were in the bulk. As the electrolyte concentration rises, there is a compression of the diffuse layer and a consequent rise in capacitance [4,6]. In the absence of specific adsorption, each side of the capacitance curve displays a broad region associated with the reorientation of the water molecules located in the inner Helmholtz plane (IHP). The capacitance associated with this reorientation process should have its maximum at the *pzc*, but since the *compact* and *diffuse-layer capacitances* are in series the total capacitance is governed by the smaller of the two components. In Fig. 1.3, as the concentration of NaF is increased, the contribution of the diffuse part of the *double-layer* becomes progressively less important and the depth of the minimum is reduced [9].

From differential capacitance measurements at various single-crystal planes of silver, the following relation was observed between the work function (as expressed by the authors [10] in terms of relative surface energies) as measured in UHV and the *pzc*

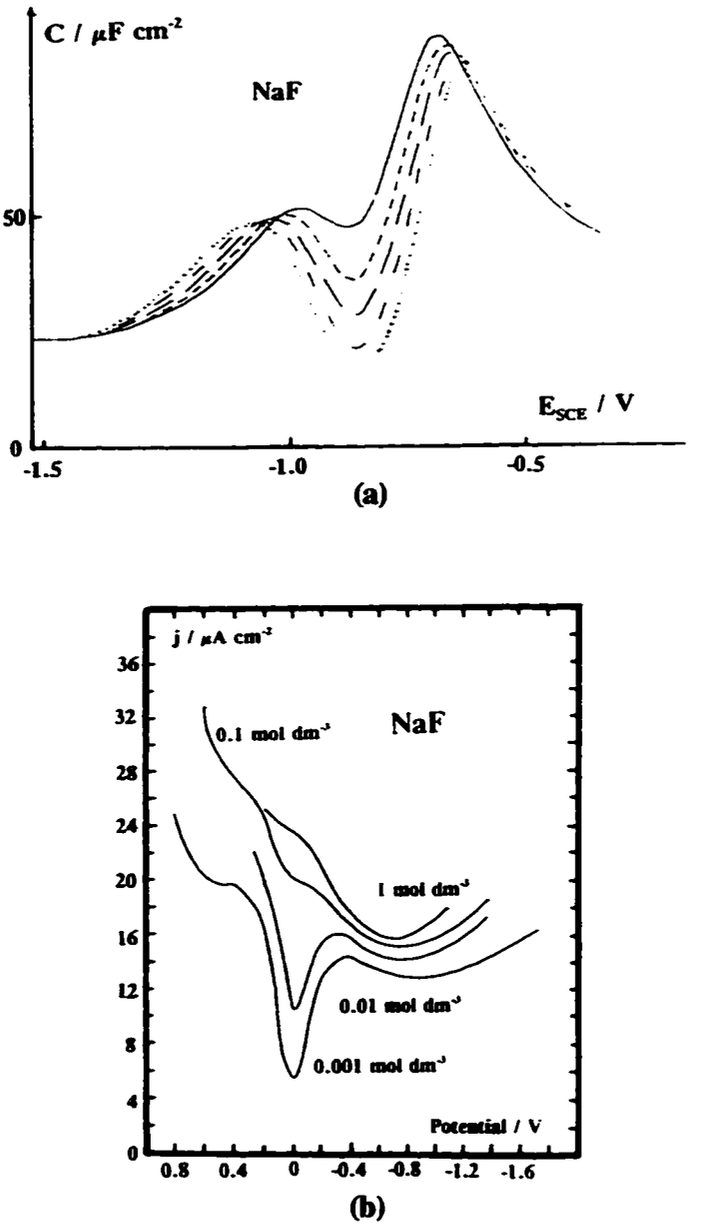

Fig. 1.3 Differential capacitance versus potential curves obtained by Valette (ref. 9) a) for the Ag(100) in aqueous NaF solutions of different concentrations: (solid line) 0.100, (- - -) 0.040, (-·-·-) 0.020, (-·····-·····) 0.010, and (· · ·) 0.005 mol dm^{-3}. Sweep rate = 5 mV s^{-1}; frequency = 20 Hz [9]; b) for the mercury electrode in aqueous NaF solutions of various concentrations as indicated on the figure [4]. Note in (b) that the potential scale is relative to the potential of the electrocapillary maximum [4], *i.e.* the potential of zero charge.

[10] (Fig. 1.4). In that figure the various single-crystal planes are denoted by their Miller indices. These indices correspond to the reciprocals of the intercepts of the atomic plane determined by the unit cell coordinates as was shown in Fig. 1.1. The resulting fractions are then reduced to the smallest integers having the same ratios. The resulting dependence of *pzc* values on crystal surface orientation is paralleled by relations to the work function (Φ) at the same metal surfaces (Fig. 1.4). Hence, the most densely packed metal faces are expected to have the most positive *pzc* since they have the highest work function values, while the "roughest" face on the atomic scale (*e.g.* (210)) should have the most negative *pzc* since it has the lowest electron work function. However, the linear relation between *pzc* and Φ does not necessarily hold for the case where adsorption is significant since that process modifies the surface dipole potential component of Φ [11].

Hitherto, results obtained mainly for gold and silver single-crystal electrodes have been discussed and interpreted. This arises from the fact that Pt-like metals display, in the potential region over which they are polarized, substantial pseudo-capacitive currents due either to hydrogen and/or oxygen adsorption being passed. This render the determination of the differential capacitance of the "real" double-layer very difficult. Thus such Pt-like metals are not "ideally" polarizable like Hg (or Au over some appreciable range of potentials).

Nevertheless, Frumkin *et al.* [12] used the notions of potential of zero total charge (*pztc*) as a means to evaluate the *pzc* at Pt-like metals. In the presence of excess of surface-inactive ions (no UPD H adsorption), the *pztc* can be regarded as the potential of zero free charge (*pzfc*) where the *pzfc* is an analogue of the *pzc* of metals not adsorbing hydrogen or oxygen. A summary of these results at various Pt-like metals is given in Table 1.1 below.

The implication of anisotropy of the *pzc* in the study of electrochemical adsorption processes is undeniable and it will be discussed in more detail later on in this work.

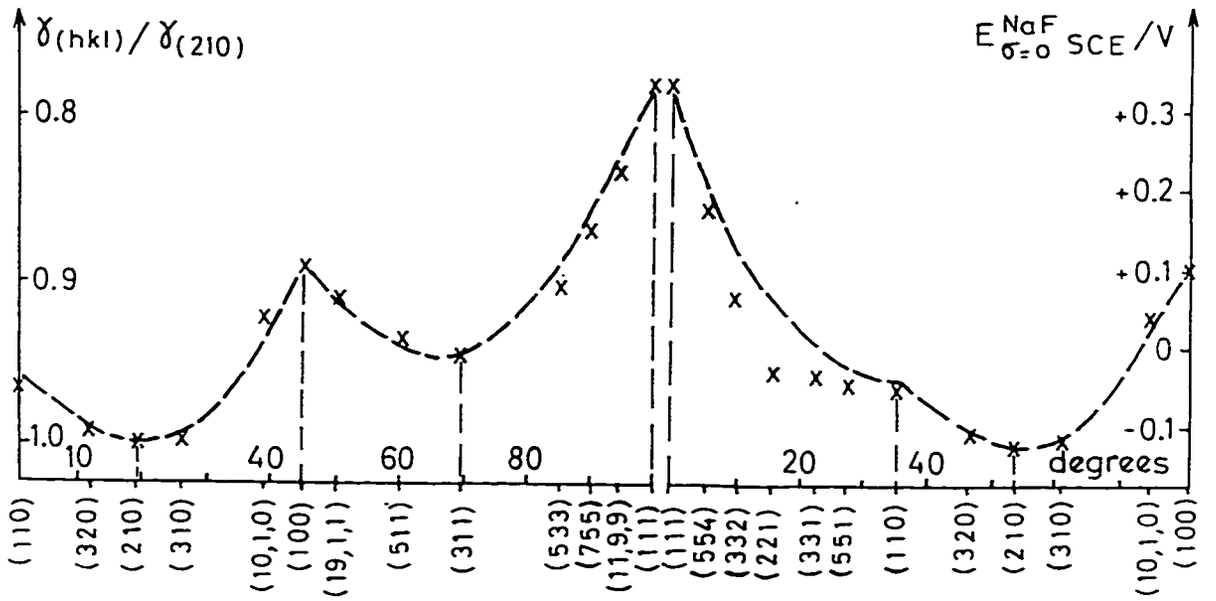

Fig. 1.4 Variation of the relative surface energy (- - -) and *pzc* of gold faces in 0.010 mol dm^{-3} NaF at room temperature with crystallographic orientation. Here (hkl) is a family of planes [10].

Table 1.1 Potential of zero charge for free and total charge* [12]

Metal	Solution	*pzfc* / V (vs. NHE)	*pztc* / V (vs. NHE)
Pt	0.3 mol dm^{-3} HF + 0.12 mol dm^{-3} KF (pH 2.4)	0.185	0.235
Pt	0.5 mol dm^{-3} Na_2SO_4 + 0.005 mol dm^{-3} H_2SO_4	0.16	0.2
Pt	0.5 mol dm^{-3} Na_2SO_4 + 0.001 mol dm^{-3} NaOH	---	-0.25
Pb	0.05 mol dm^{-3} Na_2SO_4 + 0.001 mol dm^{-3} H_2SO_4 (pH 3)	0.10	0.26
Rh	0.3 mol dm^{-3} HF + 0.12 mol dm^{-3} KF (pH 2.4)	-0.005	0.085
Rh	0.5 mol dm^{-3} Na_2SO_4 + 0.005 mol dm^{-3} H_2SO_4	-0.04	0.03
Ir	0.3 mol dm^{-3} HF + 0.12 mol dm^{-3} KF (pH 2.4)	-0.01	---
Ir	0.5 mol dm^{-3} Na_2SO_4 + 0.005 mol dm^{-3} H_2SO_4	-0.06	0.10

* The *pzc* of metals adsorbing hydrogen depends on solution pH. Here, only the values for pH = 2-3 and pH = 12 are given.

1.3.2 Differences in double-layer structure due to anion adsorption

In the previous subsection the concept of the double-layer structure was briefly introduced. For reasons of clarity, an important process influencing the double-layer was omitted: the specific adsorption of anions. This latter process is almost always present at the metal solution interface when anions such as F^-, ClO_4^-, SO_4^{-2}, Cl^-, Br^- and I^- are present in the supporting electrolytes. As illustrated in Fig. 1.5a, most anions are believed to be adsorbed with total or partial charge transfer to the electrode and this involves most probably coupled changes in the solvation shell around these ions. The strength of adsorption of these anions varies in the following order $F^- < ClO_4^- < SO_4^{-2} < Cl^- < Br^- < I^-$, where the extent of their adsorption varies greatly with the nature of the metal used as the electrode material, the ion/solvent and metal/solvent interactions, as well as the influence of these interactions on each other and especially the electron-pair donicity of the anions. This is illustrated in Fig. 1.5b by the anion adsorption effects on *pzc* at Hg electrodes in water [13]. The differential capacitance response also

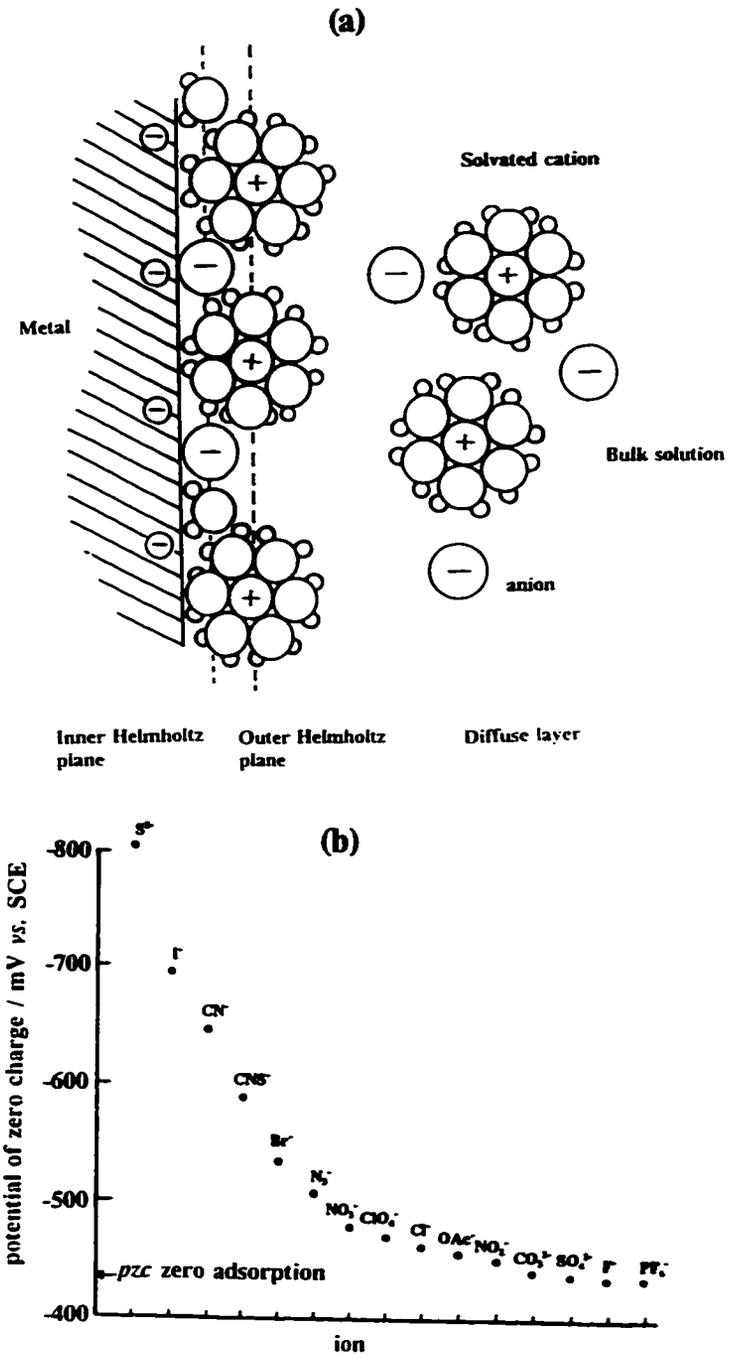

Fig. 1.5 a) As in Fig. 1.2 with the exception of anion specific adsorption; b) hierarchy of shift of *pzc* of Hg by various anions at 1 mol dm^{-3} concentration in water at 298 K, with decreasing values of Δpzc along the x-axis [13].

confirms the existence of such a process for gold as shown in Fig. 1.5c. Moreover, by the variation of the concentration of anions in solution, it was found that at Au strongest anion adsorption arise at those surfaces having the greatest packing density of atoms [14-16].

However, alkali and alkaline-earth cations have less tendency to be adsorbed on metal surfaces than anions, but it is well known that larger cations are adsorbed, where the extreme case of this behaviour is the underpotential deposition of a metal cation such as in the case of Pb^{2+} on gold single-crystal electrodes [17].

1.3.3 Differences between coordination of adsorbates at various surfaces

The interaction of molecules with electrode surfaces is one of the most critical aspects of electrochemical science and technology. It is also one of the more difficult processes to describe quantitatively, especially at the atomic level [18]. The coordination of an adsorbate molecule to a metallic surface depends strongly on the nature of the surface chemical bonds and, in electrocatalysis, it also depends on the applied potential. This last point obviously includes the other factors that were discussed earlier, namely, the position on the potential scale of the pzc value and any co-adsorption processes that could arise from anion and solvent adsorption.

In the past, investigations of adsorbed molecules or reaction intermediates at surfaces were limited by the electrochemical probes available, which restricted the information content to macroscopic properties of the electrode-electrolyte interface. Moreover, these investigations were focused mainly on the thermodynamic and kinetic aspects of the adsorption processes.

Based on earlier work on organic molecule adsorption at polycrystalline electrodes, three classes of adsorption processes where recognized [19,20]. One comprises molecules that can become coordinated to metal surfaces with or without bond rupture. This, for example, is the case of adsorption of pyridine at gold and silver surfaces [21]. The second class of compounds comprises molecules that decompose upon adsorption (dissociative chemisorption), resulting in the formation of surface-bonded intermediates. One good example of this type of surface reactivity is the decomposition

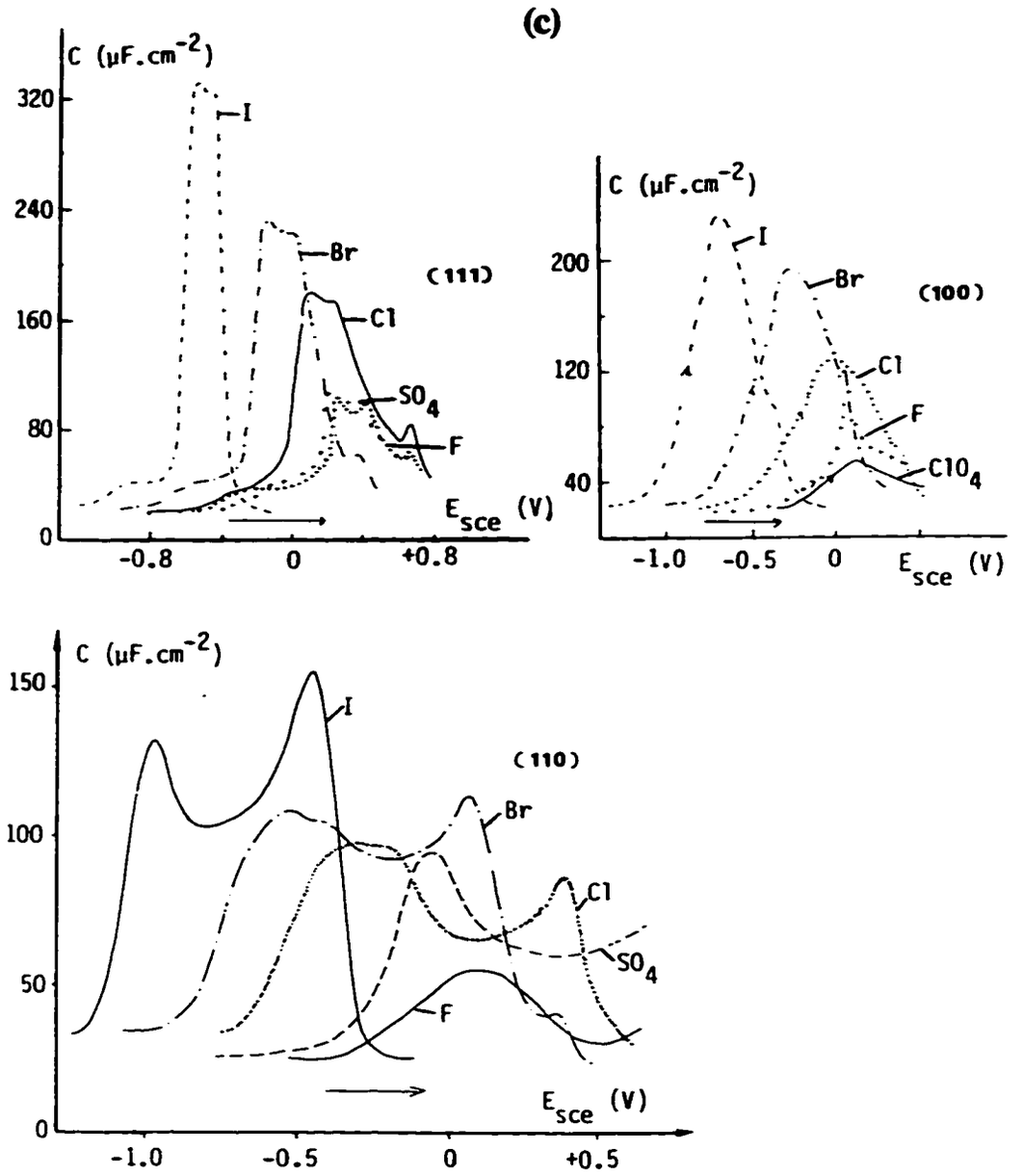

Fig. 1.5 c) Differential capacitance *vs.* potential curves for various anions in solution for the (111) [14], (100) [15], and (110) [16] faces of gold. For KI, KBr and KCl, concentration of the electrolyte is 0.100 mol dm^{-3}, frequency of the alternating signal is 80 Hz, and sweep-rate is 5 mV s^{-1}. For K_2SO_4, the same parameters are 0.200 mol dm^{-3}, 130 Hz and 100 mV s^{-1}, respectively; for NaF, 0.500 mol dm^{-3}, 20 Hz, and 5 mV s^{-1}; and $HClO_4$ 1mol dm^{-3}, 20 Hz, and 10 mV s^{-1}.

of methanol and formic acid to adsorbed carbon monoxide at Pt-like metals [22]. The third class is for molecules that interact only weakly with electrode surfaces, such as saturated carboxylic acids at Pt [23].

However, this classification is only phenomenological and it does not predict or explain the level of reactivity of molecules on a given metal electrode or the difference in reactivity at the various surface orientations of a given metal.

A more relevant approach is to explain chemisorption in terms of coordination of the adsorbate at various metal-atom sites (or metal surface orientations), *i.e.* through the "surface cluster" analogy [18]. This approach recognizes that chemisorption (surface coordination) must be considered in terms of the chemical properties of both the adsorbate (regarded here as a ligand) and the electrode or groups of metal atoms in its surface, (as the metal center). In this way a direct analogy can be drawn between interfacial structure and discrete molecules [24]. This allows surface intermediates to be modeled after well-characterized molecular [25] or cluster [26] complexes. This analogy is currently used to explain results at gas-metal surfaces and at solution-metal interfaces, as at electrodes.

However, one thing that must be considered, in drawing analogies between clusters and adsorbate bond-to-surface models, is that in the solid or on a surface, there is a very large number of electronic levels or states. In a discrete molecule it is usually possible to single out one orbital, or a small subgroup of orbitals (LUMO, HOMO), as being the frontier, or valence orbitals of the molecules, responsible for its geometry and reactivity. However, there is no way that a *single level* among the large number of orbitals of the crystal or of its surface will have the power to direct the geometry or reactivity of a given molecule in becoming adsorbed on its surface [24].

There is, however, a way to retrieve frontier orbital language for the solid state, using the concept of *density of states* (DOS) [24]:

$$DOS(E)dE = \text{number of levels between } E + dE \qquad (1.1)$$

where the shapes of DOS curves are predictable from the total number of occupied molecular orbitals (MO's). This number of MO's, multiplied by two, is the total number of electrons, and hence the DOS-curve plots the distribution of electrons in energy. The position of the Fermi level with respect to the DOS-curve plots is also an important factor in determining binding (chemisorption) and reactivity (catalysis) on metal surfaces [24].

1.4 Background to electrochemical adsorption measurements

One of the key recent developments in electrocatalysis and interfacial electrochemistry was the recognition of the need to use better defined electrode surfaces. Over the years, but especially in the last decade, this has given rise to many studies performed on single-crystal electrodes of mainly nickel, gold, silver and platinum [27].

As early as 1904, however, results by Pavlov were published which surprizingly claimed that potential differences could be observed between different copper single-crystal planes [28]. Following this pioneer work, many studies on single-crystal electrodes were undertaken. A review by Hamelin and de Becdelièvre [2], describes all the literature of papers published before 1968. The motivation behind these works was to verify how various specific electrochemical properties are affected by the surface geometry of the electrode material.

However, it took almost another ten years before sufficiently high standards in purity of water, chemicals and electrode surfaces were achieved to yield reliable results, reproducible from one laboratory to the next.

Most of the major modern development in this field originated from the C.N.R.S. in Meudon (France) from the laboratories of J. Clavilier and A. Hamelin. Meanwhile, in other research groups, high standards of purity of chemicals and water were also becoming an important issue in kinetic studies. Conway and his co-worker Angerstein-Kozlowska in this university contributed largely to the resolution of this issue by developing an efficient and effective water purification system based on pyrodistillation in oxygen [29] coupled with provision of general experimental guidelines for experimentation under very high-purity conditions [29]. Although some of these matters

were already addressed in the 'thirties by Frumkin [30] and other Russian researchers, and by Bockris and Conway [31] in the 'fifties and by Schudiner [32] in the 'sixties, the more recent experiments on highly clean and well-defined single-crystal surfaces have introduced increasing demands for purity of solutions and initial cleanliness of cells (*cf.* ref. 29) in order to obtain acceptable results. It can be said now that a consensus has been reached regarding experimental procedures required for performing highly sensitive surface electrochemistry, as well as for the actual preparation and characterisation of various metal single-crystal electrodes. As will be shown in Chapter 3, another approach involving the preparation of the electrode surface in an UHV chamber followed by transfer to the electrochemical cell has also proven valuable [33].

In the late 1980's important technological developments took place in the instrumentation for surface science which allowed characterisation via *in situ* methods for the electrode metal/solution interface and via *ex situ* methods for the interface, with the gas-phase, of a previously immersed electrode. These types of studies at single-crystal surfaces, especially of noble metals, constitute, nowadays, a major sector of the growing field of electrochemical surface science. Methods such as *in situ* FTIR, EXAFS, second-harmonic and sum-frequency generation, as well as STM, can yield types of information related to that provided by LEED, Auger and other UHV-based measurements.

The number of techniques available for both *in situ* and *ex situ* investigations are numerous and reference to some of these techniques will be made throughout the thesis. However it is not in the scope of this thesis to review these techniques in detail; the reader can consult references 7 and 34 for more detailed information.

Without any doubt, the classical electrochemical technique which is utilized the most in the characterisation of Pt single-crystal electrodes is cyclic voltammetry which provides a) high sensitivity of measurement; b) capability for excellent resolution of various processes occurring at different potentials and c) good facility for quantitative analysis of results, often by means of digital procedures.

1.4.1 Cyclic voltammetry

Cyclic voltammetry (CV) is the characterization technique most widely used in single-crystal studies since the current response for processes such as surface oxide formation in the case of gold or UPD of H in the case of platinum can be used to provide specific "fingerprints" corresponding to the different crystallographic orientations (see section 3.2.2). The procedure involves sweeping the potential, E, of the working electrode linearly between two limits, under the control of a potentiostat and a linear voltage-sweep generator, at constant sweep-rate, s ($V\ s^{-1}$), according to the equation

$$E = E_i + st \tag{1.2}$$

or

$$\frac{dE}{dt} = s \tag{1.3}$$

where E_i is the initial potential. In single-crystal work the choice of E_i is important; for example, in the case of Pt, it has to be located below the potential region for oxide formation and at a potential allowing rapid drying of the wall of the electrode when working with a hanging meniscus configuration. The dynamic current-density *vs.* potential profile resulting from this potential sweep gives a detailed picture of the process(es) taking place at the electrode surface as exemplified in Fig. 1.6.

The current response, j, to the applied potential, E, can be represented as the first derivative of charge, q. with respect to time:

$$j = \frac{dq}{dt} = \frac{dq}{dE} \cdot \frac{dE}{dt} \tag{1.4}$$

Since dq/dE = capacitance, C, and dE/dt = s, the current response can be represented equivalently by the well known relation

$$j = C\,s \tag{1.5}$$

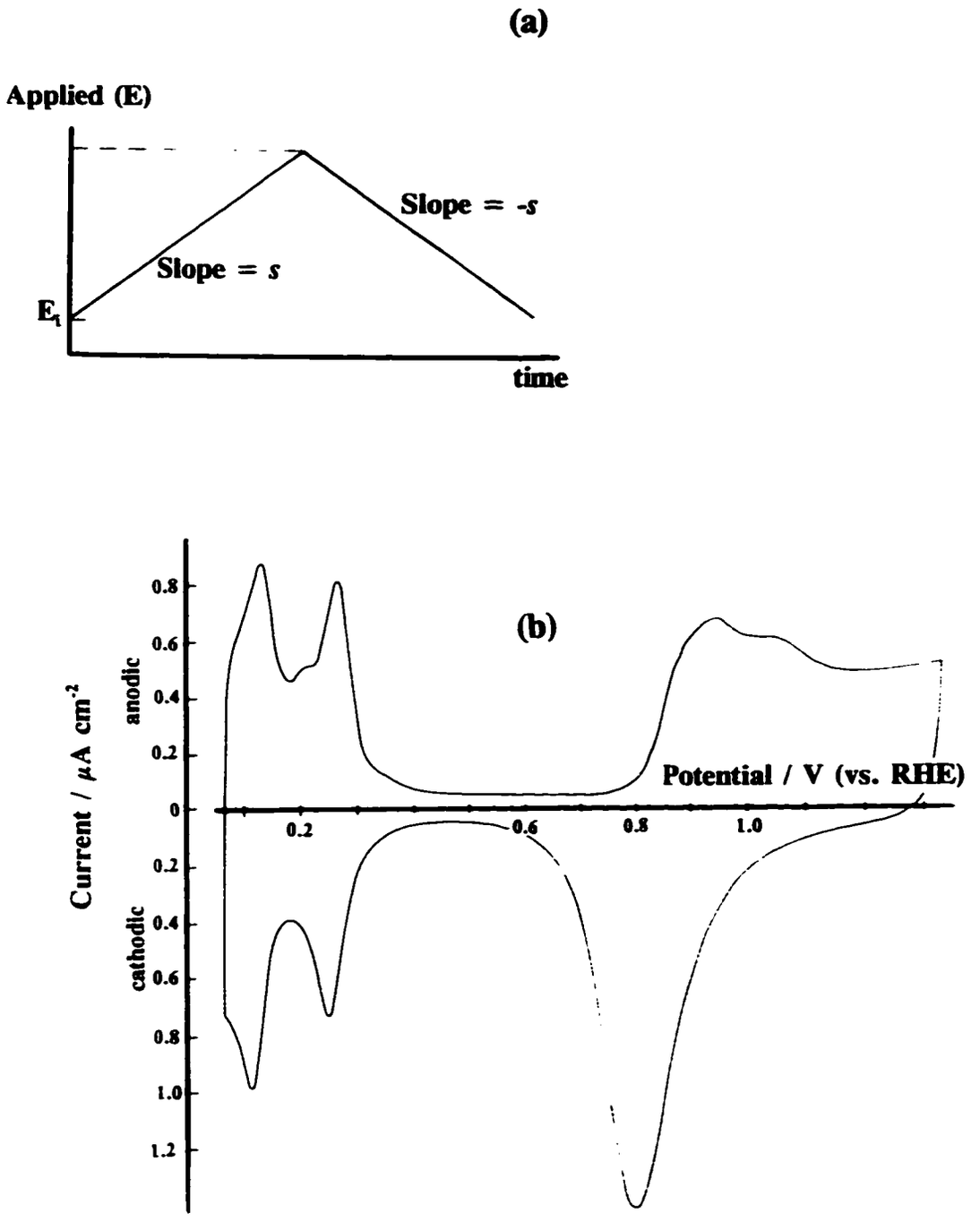

Fig. 1.6 a) Schematic diagram of the cyclic potential sweep applied at a polycrystalline Pt electrode; b) resulting current response giving cyclic voltammogram for a Pt polycrystalline electrode in contact with 0.5 mol dm^{-3} aqueous H_2SO_4 solution, sweep rate: 50 mV s^{-1} [29].

From the current-density *vs.* potential profiles, the total charge passed between two potential limits E_1 and E_2, can be evaluated from the following equation:

$$dq = j\,dt \tag{1.6}$$

Integration between these two potential limits allows determination of the charge, q:

$$q = \int_{E_1}^{E_2} j\,dt = \int_{E_1}^{E_2} C\,dE \tag{1.7}$$

where C can be a function of potential.

For surface processes, such as the underpotential deposition of H discussed at length later in this work, coverages, θ, can be determined using the equation

$$dq = q_1\,d\theta \tag{1.8}$$

where q_1 is the charge required to form a monolayer of the studied adsorbed species.

In the investigation of surface and interfacial processes at single-crystal electrodes, the cyclic voltammetry technique usually provides high resolution and sensitivity. It is able to determine surface coverage down to 5% of a monolayer ($\theta = 0.05$); to resolve states which differ in energy (electrochemical potential) by only 10 mV, i.e. with differences in Gibbs energy of about 965 J; and to characterize time effects in surface reconstruction processes down to the 10 μs time scale.

1.4.2 Cyclic voltammetry for adsorption processes

Application of this potential-sweep method to the study of adsorption of electrochemically active intermediates (i.e. species which can be formed on the surface or removed from it by steps involving charge transfer) was first made by Will and Knorr [35] and Srinivasan and Gileadi [36], who investigated the adsorption of hydrogen (as H) and oxygen (as OH and O) on noble metal electrodes experimentally and theoretically, respectively. Substantially earlier, work using a constant-current (so-called galvanostatic technique), was employed in Frumkin's School in Moscow in the 1930's, but gave less detailed information [37]. This broad topic has also been one of the main research

interests of Conway's research group for some years (see for example [38]). The work of Laviron [39] concerning kinetic modelling of cyclic voltammetry, chronopotentiometry and polarography responses of processes involving, for example, the oxidation and reduction of adsorbed intermediates has also contributed usefully to the understanding of electrochemical surface processes (see for example refs. 39a to d).

1.4.2.1 Reversible reaction case

The best way to describe the formation of a reversibly adsorbed species or intermediate is to consider the following reaction, eq. 1.9, at quasi-equilibrium. It is assumed that no diffusion limitations arise in process 1.9. This Faradaic surface process occurs by electron transfer between a metal site *M* and a solution species *A* (at a concentration, C_A) leading to the formation of a chemisorbed species *MB* but importantly only up to a fractional coverage, θ, = 1.

$$M + A + ne \underset{k_{-1}}{\overset{k_1}{\rightleftharpoons}} MB_{ads} \qquad (1.9)$$

The faradaic current j is expressed in the form of a Butler-Volmer equation [36,38]

$$j = nF(k_1 C_A (1 - \theta)\, e^{-\beta n(E - E^{o'})F/RT} - k_{-1}\, \theta\, e^{(1-\beta)n(E - E^{o'})F/RT}) \qquad (1.10)$$

where k_1 and k_{-1} are the respective forward and reverse standard rate constants, (E - E°') is the metal/solution potential difference where E°' represent the formal potential of the process studied, β is the transfer coefficient and θ is the fractional surface coverage by B_{ads} while 1-θ is the corresponding fraction of free sites of *M* available at which the process 1.9 can occur [36].

Under equilibrium conditions, the two sides of eq. 1.10 are equal and E = E_{eq}. An exchange current, j_o, can be determined as follows

$$j_o = nFk^o C_A\, e^{-\beta nF(E_{eq} - E^{o'})/RT} \qquad (1.11)$$

where the exchange rate constant $k^o = k_1 = k_{-1}$. The j_o value is an indication of how kinetically facile a given process is and it is also used widely as a characteristic parameter to compare activities of electrocatalytic materials.

From eq. 1.10, at equilibrium, it is seen that a change in potential will induce a change in coverage of B_{ads}, according to the following relation.

$$\frac{\theta}{(1 - \theta)C_A} = K_1 e^{-n(E - E^{o'})F/RT} \tag{1.12}$$

where $K_1 = k_1/k_{-1}$. In this treatment a simple Langmuir isotherm is used to describe the adsorption process (eq. 1.9); however, more complex isotherms have been used [38].

Following the treatment of ref. 36, the net (cathodic) Faradaic current may also be expressed as

$$j = -q_1 \frac{d\theta}{dt} \tag{1.13}$$

from which, by using eq. 1.12,

$$\frac{d\theta}{dt} = \frac{nF}{RT} \frac{K_1}{(e^{-(E - E^{o'})nF/RT} + K_1)^2} e^{-(E - E^{o'})nF/RT} \cdot s \tag{1.14}$$

for a sweep-rate, s (see eq. 1.5). The net current is then

$$j = \frac{q_1 nF}{RT} \frac{K_1 e^{-(E - E^{o'})nF/RT}}{(e^{-(E - E^{o'})nF/RT} + K_1)^2} s \tag{1.15}$$

where the term multiplying s is the expression for the adsorption pseudocapacitance, C_p [40]. The peak potential and current are then given by

$$E_{peak} = -\frac{RT}{nF} \ln K_1 \tag{1.16}$$

$$j_{peak} = \left(\frac{q_1 nF}{4RT}\right) s \tag{1.17}$$

For this case of a reversible adsorption process, the peak current is directly proportional to the sweep-rate whereas the peak potential is independent of s. The quantity ($q_1F/4RT$) is the maximum adsorption pseudocapacitance under the assumed conditions (see [36]), where, for all values of coverage, $C_p = (q_1nF/RT)\,\theta\,(1 - \theta)$.

1.4.2.2 Irreversible reaction case

In this particular case the reaction proceeds at a net rate almost equal to its forward rate; then eq. 1.10 reduces to

$$j = n F k_1' (1 - \theta) e^{-\beta n(E - E^{\circ'})F/RT} \tag{1.18}$$

or, in the differential form [36],

$$\frac{dj}{dt} = n F k_1' e^{-\beta n(E - E^{\circ'})F/RT} \left[\frac{d\theta}{dt} - (1 - \theta) \frac{\beta s nF}{RT}\right] \tag{1.19}$$

where in eqs. 1.18 and 1.19 the concentration of A is now included in k_1'. The current density, j, will be at its maximum when

$$\frac{d\theta}{dt} = (1 - \theta) \frac{\beta s nF}{RT} \tag{1.20}$$

By combining eqs. 1.13 and 1.20, the expression for the peak current is obtained:

$$j_{peak} = -(1 - \theta) \frac{\beta q_1 nF}{RT} s \tag{1.21}$$

Hence the peak current is again found to be proportional to the sweep-rate.

The potential at the maximum of the peak, E_{peak}, is obtained by combining eqs. 1.18 and 1.21 as

$$E_{peak} = -\frac{RT}{\beta nF} ln \frac{q_1 \beta}{k_1' RT} + \frac{RT}{\beta nF} ln (-s) \tag{1.22}$$

From eq. 1.22 a graph of E_{peak} as a function of the natural logarithm of the sweep-rate should yield a linear relation for the process described by eq. 1.18 [36].

By taking into account the considerations mentioned above, Conway *et al.* [38] proposed an original procedure to evaluate quantitatively the rate constant and reversibility parameters for surface reactions by the potential-sweep method. A characteristic quantity, s_o, analogous to the exchange current density, j_o (eq. 1.11), and related to the rate constant, was derived, giving s_o as follows:

$$s_o = \frac{RTk_s C_A^{(1-\beta)}}{q_1 \beta} \qquad (1.23)$$

where $k_s = k_1^{(1-\beta)} C_A^{(1-\beta)} K_{-1}^{\beta}$ and has units of mol cm^{-2} s^{-1}. The s_o for a given process is evaluated from the variation of the potential at the current maximum, ΔE_{peak}, as a function of log s. This graph is analogous to a Tafel line with a slope equal to 2.3 $RT/\beta nF$ and extrapolation to $\Delta E_{peak} = 0$ yields s_o.

In refs. 36 and 38, it is assumed that the back reaction rate is negligible; however, this might not be the case as pointed out by Lasia [41]. Nevertheless, at large enough values of s a linear relation should still be observed and the equations given above should still hold, as indicated by the results of simulation calculations presented in Fig. 1.7.

1.5 General objectives of the research

The first objective of this thesis work was to achieve the previous standards of experimentation reported in the literature concerning preparation of Pt single-crystal electrodes and their characterisation, as well as the high levels of solution purification required [29].

Once this objective had been achieved, the well defined Pt surfaces that had been prepared were used to study two distinct processes, although not entirely unrelated: i) the underpotential deposition of hydrogen (and anions) at Pt, usually termed UPD of H (Part I) and ii) the reactive chemisorption of acetonitrile at Pt (Part II).

In these two parts of the research reported in this thesis, the objectives were to

determine if the energetics and mechanisms of these processes are affected by the surface crystallography, both in terms of their respective kinetics and their thermodynamical behaviour. This former point should lead ultimately to a better understanding of the role of surface geometries in electrocatalytic reactions and related processes, such as chemisorption.

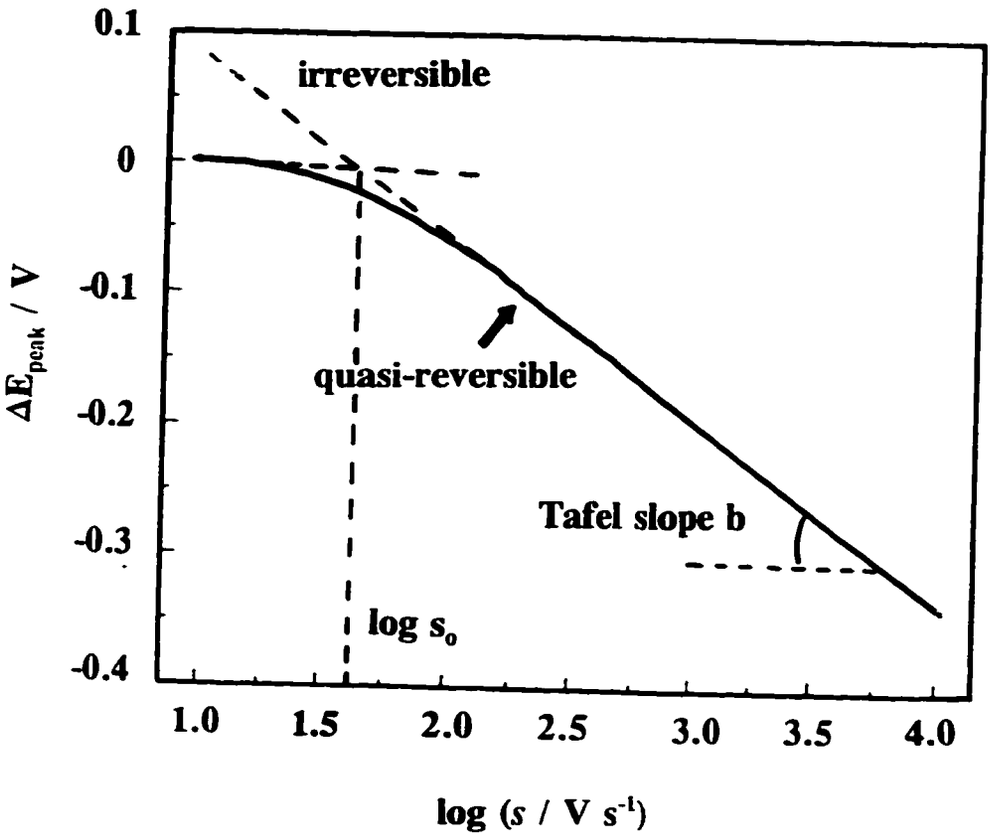

Fig. 1.7 Dependence of the hydrogen UPD peak potential on the sweep rate, k_s = 1.8 x 10^{-6} mol cm^{-2} s^{-1} for the quasi-reversible and irreversible models (adapted from ref. 41).

References

1. D. Pletcher, J. Appl. Electrochem.,14 (1984) 403.
2. A. Hamelin and J. de Becdelièvre, Traitement de surface, 85 (1969) 15.
3. P. Delahay, "Double Layer and Electrode Kinetics", Interscience Publishers, New York, 1965, 321 pages.
4. D.C. Grahame, Chem. Rev., 41 (1947) 441.
5. a) G. Gouy, J. Phys. Radium, 9 (1910) 457; b) G. Gouy, *ibid*, Compt. Rend., 149 (1910) 654.
6. D.L. Chapman, Phil. Mag., 25 (1913) 475.
7. J.O'M. Bockris and S.U.M. Khan, "Surface Electrochemistry: a molecular approach", Plenum Press, New York, 1993, 1014 pages.
8. A. Hamelin, in "Modern Aspects of Electrochemistry", B.E. Conway, J.O'M. Bockris and R.E. White (Eds.), Plenum, New York, 1985, Vol. 16, p.1.
9. G. Valette, J. Electroanal. Chem., 138 (1982) 37.
10. A. Hamelin, T. Vitanov, E. Sevastyanov and A. Popov, J. Electroanal. Chem., 145 (1983) 225.
11. R. Parsons, in "Modern Aspects of Electrochemistry", J.O'M. Bockris and B.E. Conway (Eds.), Butterworths, London, 1954, Vol. 1, Chapter 3.
12. A.N. Frumkin and O.A. Petrii, Electrochim. Acta, 20 (1975) 347, and references therein.
13. B.E. Conway, Electrochim. Acta, 40 (1995) 1510.
14. A. Hamelin, J. Electroanal. Chem., 144 (1983) 365.
15. A. Hamelin, J. Electroanal. Chem., 142 (1982) 299.
16. A. Hamelin, T. Vitanov, E. Sevatianov and A. Popov, J. Electroanal. Chem., 145 (1983) 225.
17. A. Hamelin, J. Electroanal. Chem., 165 (1984) 167.
18. a) A.A. Balandin, Zeit. Phys. Chem., B2 (1929) 289; b) A.A. Balandin, *ibid*, B3 (1929) 167 ; c) E. Muetterties, Science, 196 (1977) 839; d) M.P. Soriaga, in "Structure of Electrified Interfaces", J. Lipkowski and P.N. Ross (Eds.), VCH Publishers Inc., 1993, Chap.4, p. 103.

19. G. Horanyi, J. Electroanal. Chem., 51 (1988) 163.

20. a) A. Wieckowski, Electrochim. Acta, 26 (1981) 1121; b) A. Wieckowski, in "Modern Aspects of Electrochemistry", Vol. 21, R.E. White, J.O'M. Bockris and B.E. Conway (Eds.), Plenum, New York, 1990.

21. J. Lipkowski, L. Stolberg, D.-F. Yang, B. Pettinger, S. Mirwald, F. Henglein and D.M. Kolb, Electrochim. Acta, 39 (1994) 1045.

22. R. Parsons and T. Vandernoot, J. Electroanal. Chem., 257 (1988) 9.

23. M.P. Soriaga, in "Structure of electrified interfaces", J. Lipkowski and P.N. Ross (Eds.), VCH Publishers Inc., 1993, Chapter 4.

24. R. Hoffman, "Solids and Surfaces: A Chemist's view of Bonding in Extended Structures", VCH Publishers, New York, 1988.

25. a) M.P. Soriaga, Chem. Rev., 90 (1990) 771; b) B.G. Bravo, S.L. Michelhaugh, M.P. Soriaga, Langmuir, 5 (1989) 1092; and c) M.P. Soriaga, G.M. Berry, M.E. Bothwell, B.G. Bravo, G.J. Cali, J.E. Harris, T. Mebrahtu, S.L. Michelhaugh, J.F. Rodriguez, in "Electrochemical Surface Science: Molecular Phenomena at Electrode Surfaces", M.P. Soriaga (Ed.), ACS Books, Washington, DC, 1988.

26. G.J. Lewis, J.D. Roth, R.A. Montag, L.K. Safford, X. Gao, S.C. Chang, L.F. Dahl and M.J. Weaver, J. Am. Chem. Soc., 112 (1990) 2831.

27. R. Parsons, in "Electrified Interfaces in Physics, Chemistry and Biology", NATO ASI Series, R. Guidelli (Ed.), Vol. 355, Series C: Mathematical and Physical Sciences, 1992, p. 293.

28. P.N. Pavlov, Zap. Novoross. Obs. Lestvoisp., 25 (1904) 108 and 165.

29. See for example: H. Angerstein-Kozlowska, "Comprehensive Treatise of Electrochemistry", Vol. 9, E. Yeager, J.O'M. Bockris, B.E. Conway and S. Sarangapani (Eds.), Plenum Publishing Corporation, New York, 1984, 15.

30. M. Proskurina and A.N. Frumkin, Trans. Faraday Soc., 31 (1935) 110.

31. A.M. Azzam, J.O'M. Bockris, B.E. Conway and H.Rosenberg, Trans. Faraday Soc., 46 (1950) 918.

32. S. Schuldiner, B. Piersma and T.B. Warner, J. Electrochem. Soc., 113 (1966)

573.

33. a) F.T. Wagner and P.N. Ross, J. Electroanal. Chem., 150 (1983) 141; b) A.S. Homa, E. Yeager and B.D. Cahan, J. Electroanal. Chem., 150 (1983) 181; c) F.T. Wagner and P.N. Ross, Surf. Sci., 160 (1985) 305; d) M. Markovic, M. Hanson, G. McDougall and E. Yeager, J. Electroanal. Chem., 214 (1986) 555; e) D. Aberdam, R. Durand, R. Faure and F. El Omar, Surf. Sci., 171 (1986) 303; f) F. Wagner and P.N. Ross, J. Electroanal. Chem., 250 (1988) 301.

34. A. Zangwill, "Physics at Surfaces", Cambridge University Press, New York, 1990, 454 pages.

35. F.G. Will and C.A. Knorr, Z. Elektrochem., 64 (1960) 258 and 270.

36. S. Srinivasan and E. Gileadi, Electrochim. Acta, 11 (1966) 321.

37. a) A.N. Frumkin and A.I. Slygin, Acta Physicochim. U.R.S.S., 3 (1935) 791; b) A.N. Frumkin and A.I. Slygin, *ibid*, 4 (1936) 991.

38. a) H. Angerstein-Kozlowska, J. Klinger and B.E. Conway, J. Electroanal. Chem., 75 (1977) 45 and 61; b) H. Angerstein-Kozlowska and B.E. Conway, J. Electroanal. Chem., 95 (1979) 1; c) D.A. Harrington and B.E. Conway, Electrochim. Acta, 32 (1987) 1703.

39. a) E. Laviron, J. Electroanal. Chem., 39 (1972) 1; b) E. Laviron, *ibid*, 52 (1974) 355 and 395; c) E. Laviron, *ibid*, 63 (1975) 245; d) E. Laviron, *ibid*, 101 (1979) 19.

40. J. O'M. Bockris and H. Kita, J. Electrochem. Soc., 108 (1961) 676.

41. A. Lasia, Proceedings of the Symposium on "Electrochemistry and Materials Science of Cathodic Hydrogen Absorption and Adsorption", B.E. Conway and G. Jerkiewicz (Eds.), The Electrochemical Soc. Inc., New Jersey, Vol. 94-21, 1994, p. 261.

Chapter 2
Experimental

This chapter contains all the information pertaining to the preparation of the platinum single-crystal electrodes, the design of the electrochemical cells and the specifications about the water and chemicals employed in this work, as well as the instrumentation used to acquire the results.

2.1 Preparation of the platinum single-crystal electrodes

2.1.1 Crystallography

Platinum crystallizes in the face-centred cubic system and the orientation of the plane of interest in a single-crystal surface is identified by x-ray diffraction patterns. Because of the high level of symmetry of pure metals, the stereographic projection of a cubic crystal shows that all types of planes can be represented around one unit stereographic triangle. Figure 2.1 shows a) the stereographic projection [1a] and b) the unit projection stereographic triangle [1b] for cubic crystals. The distance between crystallographic planes in a unit stereographic triangle can be expressed in terms of angles between these planes with the help of tables of crystallographic data [2].

In the research reported in this thesis, studies on the (100), (111), (110) and (311) planes of platinum are reported. This choice was made because the (110), (100) and (111) surfaces are low-index planes located at the extremities of the stereographic triangle for the fcc unit cell (see Fig. 2.2) and they are the smoothest on the atomic scale. Hence, these faces are the most suitable for exhibiting the largest differences in their adsorption or catalytic behaviour in comparison with that at a polycrystalline electrode. On the other hand, the (311) surface represents the turning point of the [011] zone on the stereographic triangle (Fig. 2.2), i.e. it is the limiting case for stepped faces with terraces having the (111) orientation, denoted Pt(S) (n(111)-(100)) by the TLK (terrace, ledge and kink) model [3] where n is the number of atomic rows determining the width of the terrace; in the case of the (311) plane, n = 2. Accepting that the atoms are hard

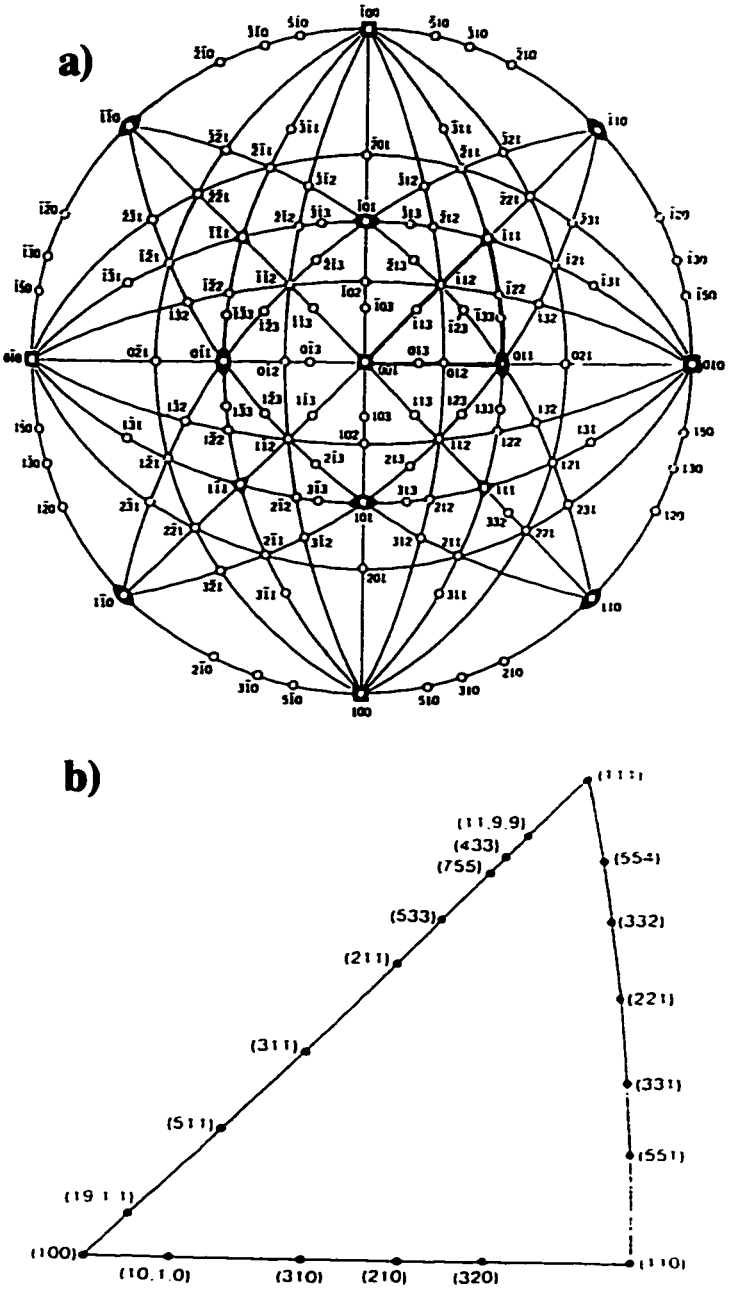

Fig. 2.1 a) The standard (001) stereographic projection [1a] and b) the unit projected stereographic triangle for a cubic crystals [1b].

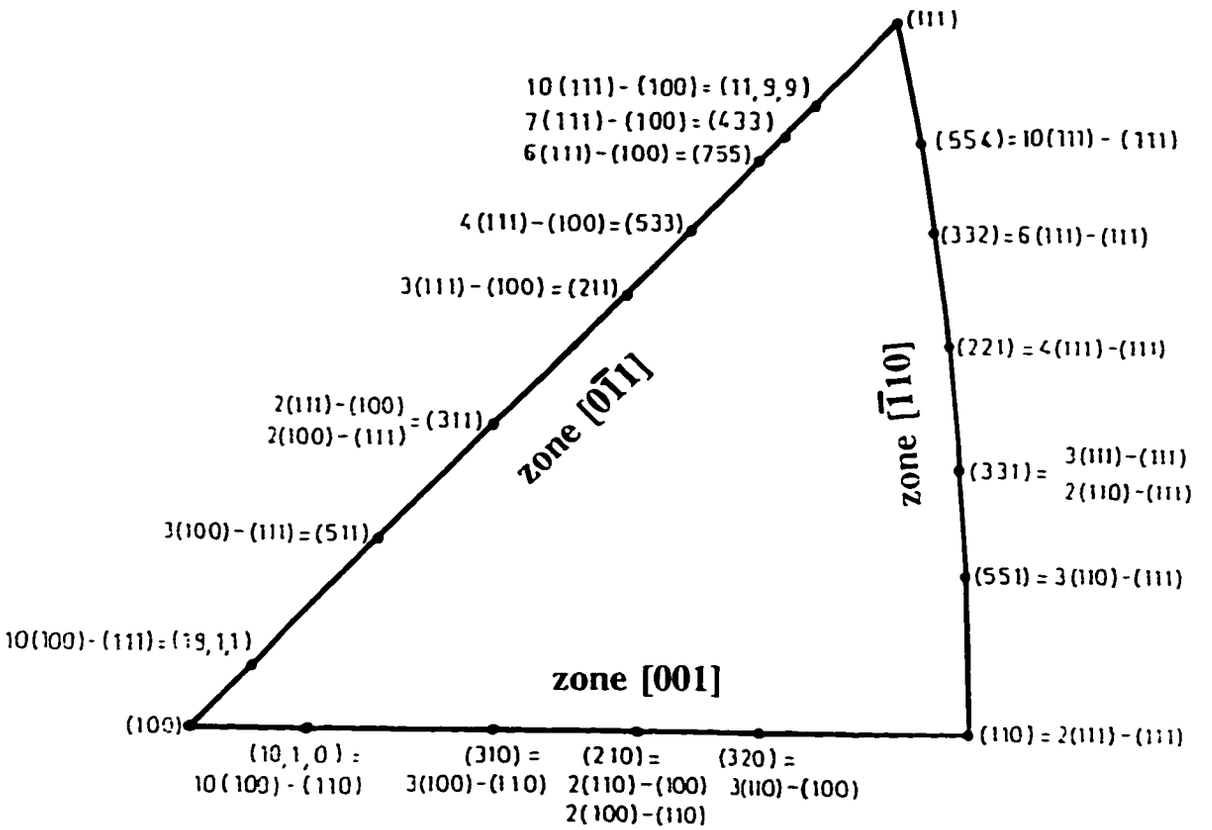

Fig. 2.2 Unit projected sterographic triangle for the fcc structure with the (100) face at the centre of the projection. Faces are also designated according to the notation n (h_t k_t l_t) - (h_s k_s l_s), where (h_t k_t l_t) and (h_s k_s l_s) represents the Miller index of the crystallographic orientation of the terraces and the steps, respectively, and n measures the width of the terrace in number of atoms [1b].

spheres, the surfaces can be described by the following "ball models" [1] (see Fig. 2.3), where each face is shown with its unit cell delineated by a dotted line and where the first, second and third layers of atoms are denoted respectively by 0, 1 and 2. From the "ball models" it becomes clear that each surface displays different types of sites; the (111) has a threefold symmetry with two types of unequivalent hollow sites (see Fig. 2.3); the (100) has fourfold symmetry and the (110) and (311) surfaces have a significant increase in the number of types of sites available in comparison to the (111) and (100) surfaces. This increase of types of sites on the (110) and (311) surfaces is a consequence of the more open nature of the structure of these two surfaces.

2.1.2 Preparation of platinum single-crystal electrodes

Spherical platinum single-crystals of the desired orientations were obtained by melting the extremity of a high-purity Pt wire [4], using a gas-oxygen flame, blowing in the vertical direction, in order to maximize the size of the prepared monocrystals [5]. Once a drop of melted platinum of an appreciable size was obtained, the flame was slowly lowered to ensure proper recrystallisation, allowing time for diffusion of possible metal impurities to the surface, and opportunity for catalytic oxidation of any carbonaceous and/or sulphurous impurities by oxygen in the air [6]. The resulting metal bead has the shape of a drop and displays small flat areas equally spaced (90° apart) corresponding to the face of the fcc cube. These facets are of the (111) orientation and they are usually larger than the (100) orientation facets whereas the (110) facets are very difficult to observe because of their extremely small size [7]. Lehmpfuhl and Uchida have used reflection electron microscopy to show that the centre part of the (111) facets display flat and smooth areas with only a few monatomic steps [7].

The Pt (Johnson Matthey) used to make the crystals was of 99.9995% purity, supplied as a wire 1 mm in diameter; the surface of the wire was first etched in *aqua regia* before melting to eliminate any surface impurities. The monocrystalline beads of platinum obtained after melting were about 3 mm in diameter and were aligned using the back-von-Laüe X-ray diffraction method, and then cut and polished along the chosen crystallographic orientation according to the procedure described in reference 8. This

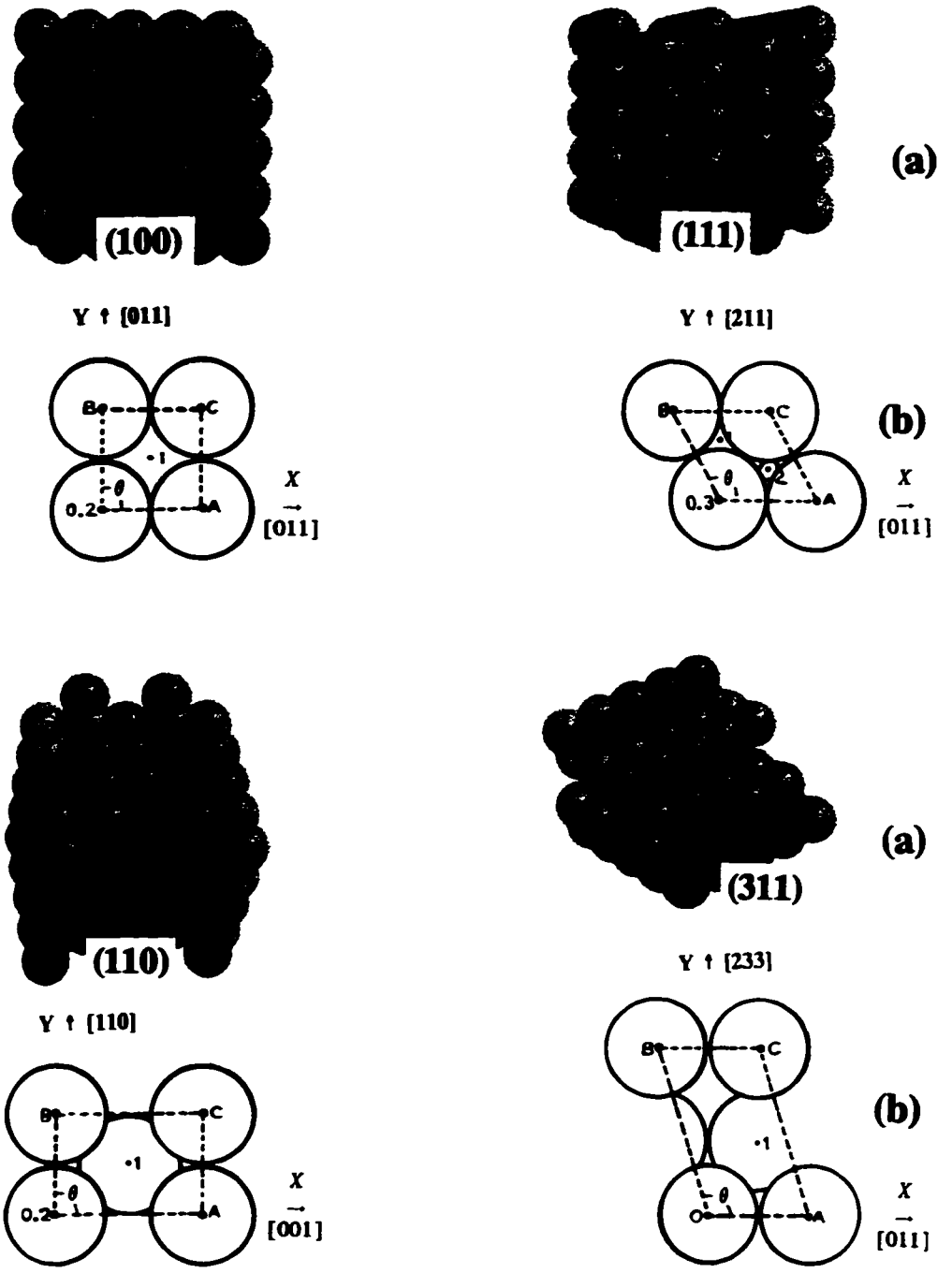

Fig. 2.3 Ball models for five faces of the fcc system. a) Photographs; b) drawing looking normally at the models [1b]. The unit cell boundary is delimited by a dotted line and the first, second, and third layers of atoms are denoted by 0, 1, and 2 (0.2 implies that one atom lies directly behind the other).

method is quite different from the one used by Clavilier and co-workers [9]. In the present work the appropriate crystallographic orientation was determined by X-ray diffraction in the way described by Hamelin for gold and silver single-crystals in ref. 10. First the crystal is placed in a Kel-F holder, **H** (Fig. 2.4a), and secured using some epoxy resin (Epofix, Struers) **E** (Fig. 2.4b). Then the crystallographic orientation of its main axis is determined by a first X-ray diagram. According to the observed angle between the desired face and the main axis of the crystal, the stem is bent if necessary close to the sphere so as to have the desired face perpendicular to the main axis $\pm$ about 8° (Fig. 2.4a). The Kel-F holder fits exactly into the orientable "head" represented in Fig. 2.4c. The first version of this "head" was designed and constructed in LEI-CNRS, Bellevue (France).

A second X-ray diagram is taken to determine the precise angle to which the holder of Fig. 2.4a has to be tilted in order to orientate the desired face precisely perpendicular to the axis of the "head" of Fig. 2.4c; this is done by means of two of the four screws, **S**, of the "head". The "head" is designed so that one turn of a screw corresponds to 2°; a precise dial is fixed on the allen key used to turn the screws so that precise orientation could be set.

Each step of this alignment procedure was checked by an X-ray diagram. This alignment procedure is explained in detail in ref. 10. It consists in reading angular relations on the back reflection films using a Gerninger chart [11] and a table of the angles between the different faces (both are reproduced in ref. 10 for a crystal at 3 cm distance from the X-ray film). In our case the Gerninger chart was for a crystal positioned at 6 cm from the X-ray film, hence increasing the precision of the measured angles.

Once the orientation is completed, the cutting of the crystal is simply performed by placing the "head" in cylinder **C** (Fig. 2.4c) in order to keep the crystal in the proper position. Then, the crystal and resin were ground on fine-grade silicon carbide paper of three different grades until nearly half of the sphere was removed, followed by polishing the surface using 0.25 micron diamond compound (Metadi II, Tech-Met), 0.1 and 0.05 micron diamond suspensions (Metadi Supreme, Tech-Met). X-ray diagrams are made

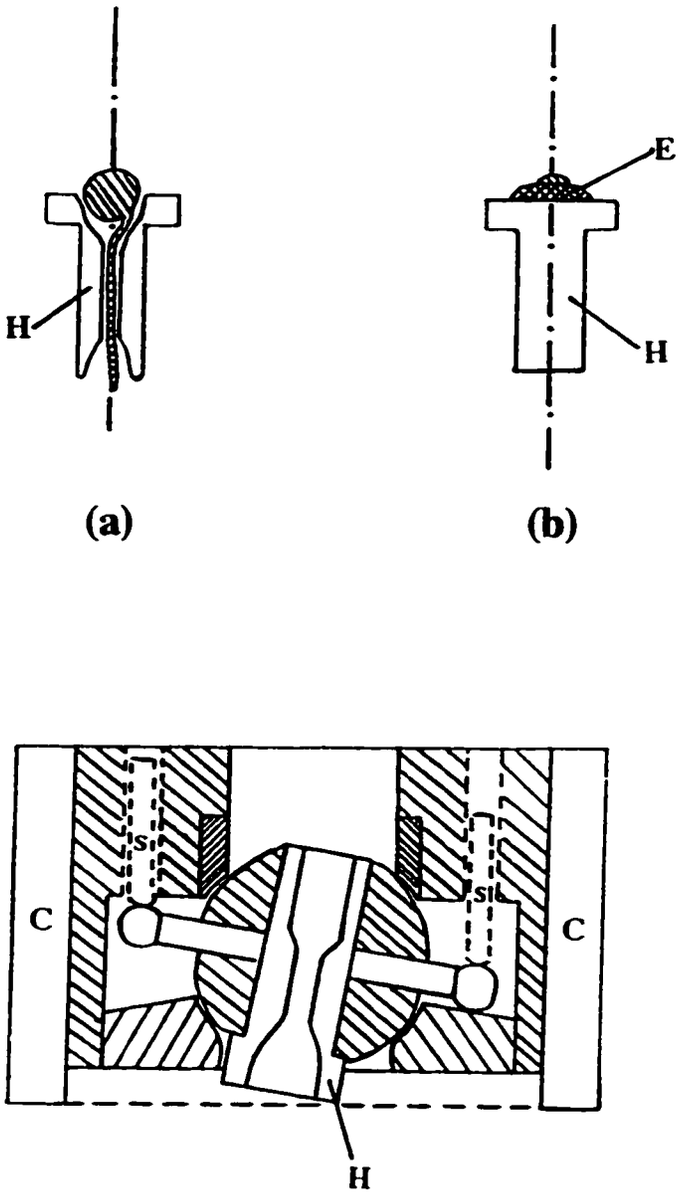

Fig. 2.4 a) Crystal holder (H); b) crystal secured by epoxy resin (E) in holder (H); c) goniometer "head" designed for the orientation of the crystal in the cylinder (C), used to keep the crystal in the proper position. S: screws used for positioning. (Reproduced from ref. 8).

to follow the elimination of the disturbed layer created at the surface by the cutting. This method of orientation and cutting was successful for a number of metals, namely for gold, silver and platinum single-crystals.

The Pt single-crystals are then removed from the Kel-F holder by dissolving the resin in chloroform. The monocrystals were then annealed following the procedure descirbed in Chapter 3 (section 3.2).

A polyoriented platinum electrode used for comparative experiments (see chapter 6) was a spherical single-crystal bead attached to a wire. The advantage of using this type of electrode is that its surface is comprised of many types of sites, including (111) facets, and is also quite smooth. The polycrystalline electrode that was used in comparative experiments was made of a Pt wire (Johnson Matthey) also of 99.9995% purity. In Chapter 7, the Pt(111) and (100) crystals (*ca.* 9 mm diameter, 4 mm thick) were obtained from the Materials Preparation Facility of Cornell University and were oriented within 1°, as verified by X-ray diffraction. In that part of the work, the preparation of the ordered (111) surface followed the procedure described in ref. 14 and referred to as the I_2 adsorption-CO exchange method (see Chapter 7), whereas the ordered (100) surface was annealed and cooled in an H_2 + Ar atmosphere [13].

Before each experiment was commenced, the respective electrode was heated in a gas-oxygen flame in order to decontaminate the surface and it was then either cooled down in air to about 300 °C and a drop of Milli-Pore water was attached to the surface [12], or cooled down in a mixture of H_2 and Ar [13], and then a drop of deoxygenated pure water was attached to the surface. The type of cooling procedure used will be indicated for each of the cyclic voltammograms presented in the figures which follow in section 3.2.2.

2.2 Reference electrodes

The reversible hydrogen electrode, H^+, H_2 (Pt), (RHE) was used throughout this work; it is normally made of platinized Pt (99.99 % purity, 100 mesh, Johnson Matthey Inc.) gauze. H_2 gas was continuously bubbled into the reference compartment of the cell. All the potentials, if not stated otherwise, are given on the RHE scale.

2.3 Counter electrodes

Two counter electrodes were used in this work, one was made of a coiled Pt wire (99.9998% purity, 0.5 mm diameter, Johnson Matthey Inc.) the other one was a Pt gauze with the same characteristics as the one used to make the reference electrode. Both had a large surface area to minimize the Faradaic current-density of the oxygen evolution process which arises at the counter electrode during polarization experiments.

2.4 Water and chemicals

Supporting electrolyte solutions were prepared from a Milli-Q UV-plus ultra-pure water purification system (Millipore); the resulting water had a resistivity of 18.2 MΩ cm. The electrolytes used were 0.02, 0.5 and 2.0 mol dm^{-3} aqueous sulphuric acid (Seastar Chemicals) solution and 0.1 mol dm^{-3} aqueous perchloric acid (Seastar Chemicals) solution. These two acids were of the highest purity commercially available and were chosen as supporting electrolytes in order to be able to generate reproducibly the substantially different background voltammograms that are known for various single-crystal planes from Clavilier's work [15].

As described in Chapter 3, carbon monoxide adsorption transients which gave information on displacement of previously chemisorbed H and/or HSO_4^- ions, were measured for three single-crystal surfaces. The CO (Ultra High Purity Grade, Air Products) was introduced in the gas atmosphere of the cell as a mixture of CO and Ar, and the CO was allowed to diffuse to the metal/solution interface (see next Chapter for more details).

In Part II of this work, the acetonitrile solution were prepared during the experiments by injecting pure acetonitrile (CH_3CN) (BDH, HPLC grade) or CD_3CN (Aldrich) or a 0.1 vol% solution of acetonitrile into the electrolyte already in the electrochemical cell, using a 10 or a 100 μl microsyringe (Hamilton). In Chapter 7 (Part II) the doubly-distilled, high purity sulphuric and perchloric acids, used as supporting electrolytes, were from G.F. Smith Co., and were diluted with either 99.8% deuterium oxide (Cambridge Isotopes) or Milli-Q water (Millipore).

High purity H_2 gas (Air Products), passed through a gas purification line, was

used for the RHE reference electrode. The H_2 gas purification treatment in the gas line consisted in passing the gas first through $Mg(ClO_4)_2$ as a drying agent, then, molecular sieve (BDH type 4A), then through an oven containing Cu turnings and palladized asbestos at 623 K to remove traces of oxygen, and finally through activated charcoal traps in liquid nitrogen.

Oxygen was removed from the solutions before each experiment by purging them with high purity Ar (Research Grade, Air Products). The solution was blanketed throughout the experiments with Ar and all runs were carried out at room temperature (294 K) unless otherwise specified.

In Chapters 4 and 5, the effect of the variation of the temperature was investigated for the kinetics of deposition and desorption of hydrogen; in that part of the work, the temperature of the electrochemical cell was regulated by means of a thermostated bath (HAAKE F3 and C, Germany).

2.5 Electrochemical cells

The cells (three of them) used during the course of this work were all made out of pyrex glass and their design varied depending on the experimental needs. Figs. 2.5a and b show two types of cell used in this thesis work. Each cell comprised three electrodes: the single-crystal working electrode, the RHE reference in a separate compartment and a Pt counter electrode. In the cell shown in Fig. 2.5a the Pt counter electrode could be flame-annealed for cleaningliness. In the cell shown in Fig. 2.5b the counter electrode is a Pt gauze attached to a wire and sealed in soft glass; this electrode could not be flame-annealed but was cleaned in hot sulphuric acid prior to use in experiments. Two cells were necessary in some parts of this work in order to check the state of the electrode surface during experiments when one of the cells already contained an organic additive (see Part II). The cell used in the work described in the first part of the thesis was of a three-compartment design (not shown) where the working electrode compartment is designed for a rotating electrode. A glass cup attached at the top of the cell could be filled with water so that a Teflon cap attached to the rotating electrode could be immersed in the water, creating a gas seal and hence preventing the main

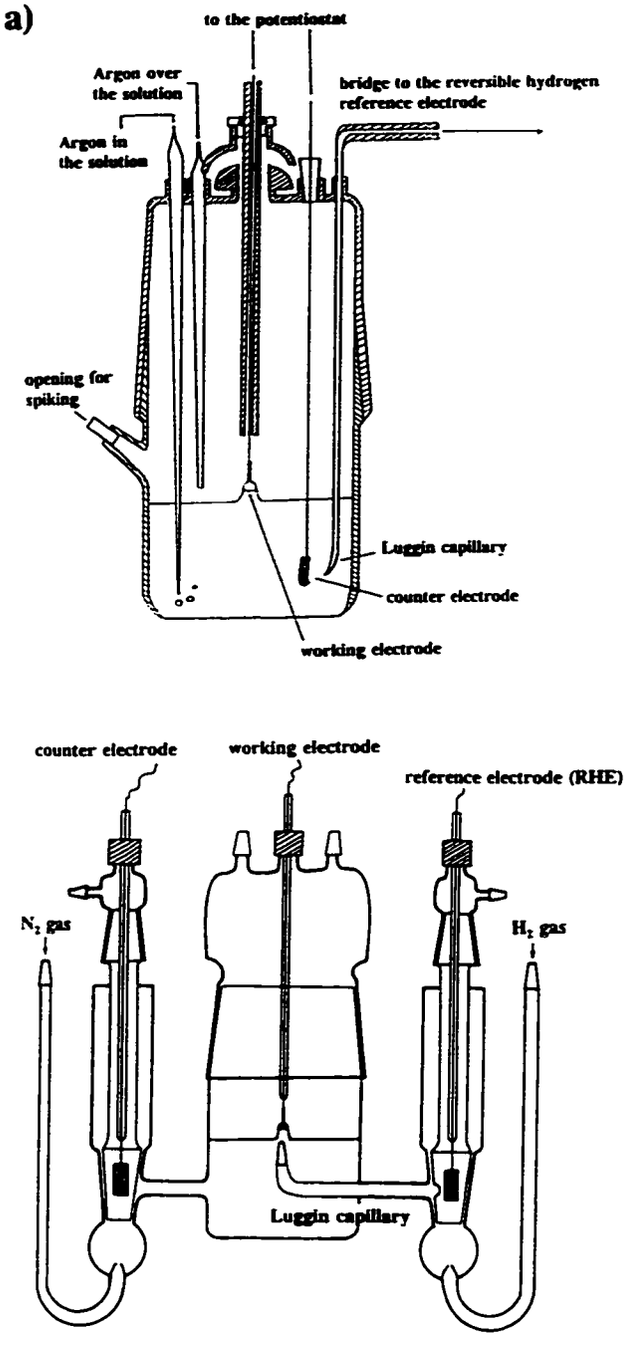

Fig. 2.5 Two versions (a and b) of the electrochemical cell used in this work (see text).

compartment of the cell from becoming contaminated by atmospheric oxygen. Special care was taken to minimize the iR drop by having the Luggin capillary located at the centre of the cell; this was essential for fast response measurements, as in ac impedance spectroscopy.

Prior to each experiment, the electrochemical cell was taken apart and soaked in hot sulphuric acid for about 15 minutes. After having been left to cool (not completely) the cell was rinsed thoroughly with MilliPore water. An identical cleaning procedure was applied to all the glassware used for preparing solutions.

2.6 Instrumental set-up

Since the experimental aspects of the work described in this thesis are formatted in two distinct parts (I and II), the further details concerning the use and evaluation of the current transients, impedance spectroscopy and *in situ* FTIR spectroscopy techniques will be given prior to the presentation of the respective results in the appropriate later chapters. This should avoid the reader having to go from chapter to chapter when looking for details concerning the methodology employed.

2.6.1 Cyclic voltammetry (CV)

Standard instruments for CV measurements were used. They consisted of a function generator (Model HB-104, HD Ltd., Japan) which provides a linearly-varying, time-dependent input potential to a potentiostat (Model HA-501, HD Ltd., Japan) which controls potentials and monitors current responses; an X-Y recorder (Model 7045 B, Hewlett Packard, USA) was used to record the current responses as a function of the varying potential applied.

Cyclic voltammetry experiments were conducted at sweep-rate of 20 mV s^{-1} for Pt(311) in order to optimize recording of the sharpness of the observed peak and at 50 mV s^{-1} for the other electrodes surfaces investigated, except in experiments where the effect of variation of sweep-rate was to be investigated.

2.6.2 Current transients

Current (charge) transients arise in the UPD H potential range when substitutional adsorption of H by a chemisorbed organic substance takes place, an effect first discovered in this laboratory [16]. Such current transients arise upon addition of acetonitrile (or carbon monoxide) to an initially uncontaminated electrode (see Chapters 3 and 6) held at constant potential (using the same potentiostat as above) and were recorded using the X-Y recorder specified above or a two-channel digital oscilloscope (Model 310, Nicolet).

2.6.3 Impedance spectroscopy

The system used for impedance measurements consisted of a Solartron 1255 Frequency Response Analyzer in conjunction with a SI 1287 Solartron Potentiostat, controlled by Zplot Software (Scribner Associates Inc.). The generator provided an output signal of known amplitude (smaller or equal to 5 mV r.m.s. in the present case) and the frequency range was typically 1.0×10^5 to 0.01 Hz. The impedance spectra were fitted by means of a complex, non-linear, least-squares immitance fitting program, LEVM [17]. As will be shown in Chapters 4 and 5, this technique allowed sensitive kinetic measurements to be made on distinguishable adsorption states of H and anions at submonolayer coverages at various Pt single-crystal electrodes.

2.6.4 *In situ* FTIR spectroscopy

The infrared spectrometer was an IBM (Bruker) IR-98-4A vacuum Fourier-transform instrument with a Globar light source and an MCT narrow-band detector (Infrared Associates). The radiation incident upon the sample was p-polarized by means of a wire grid KRS-5 thallium bromiodide polarizer (Harrick). The polarizer was positioned on the optical bench such that the infrared radiation was polarized prior to reflection into the spectroelectrochemical cell. The combined electrochemical-infrared measurements were performed after pushing the disk electrode up to a bevelled CaF_2 prism to form a thin (*ca.* 5 μm) solution layer. A diagram of the thin-layer cell is shown in Fig. 2.6; it consists of a Pt wire counter-electrode, a silver/silver chloride reference

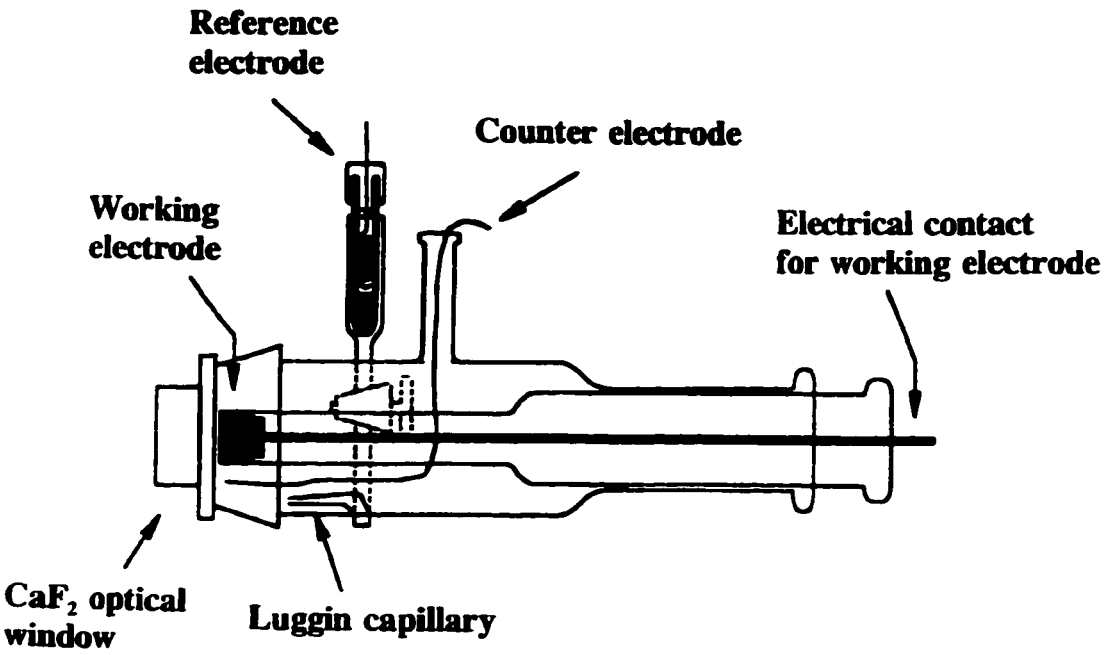

Fig. 2.6 Diagram of the thin-layer cell (cell design from Prof. M.J. Weaver's laboratory, Purdue University).

electrode as well as the Pt single-crystal working electrode under investigation. This instrument is located, and was used, in the research laboratory of Prof. M.J. Weaver at Purdue University. The experiments were conducted there by the author of this thesis as no suitable spectrometer was available in this department at the time such experiments were required. Digital processing of the spectral results was conducted in the usual way.

References

1. a) E.A. Wood, Crystal Orientation Manuel, Culombia Uinv. Press, New York, 1963; b) J.F. Nicholas, "An Atlas of Models of Crystal Surfaces", Gordon and Breach (Eds.) New York, 1965.
2. C.S. Barret and T.B. Massalski, "Structure of Metals: Crystallographic Methods, Principles and Data", McGraw-Hill, London, 1966.
3. B. Lang, R.W. Joyner and G.A. Sormorjai, Surf. Sci., 30 (1973) 454.
4. R. Kaischew and B. Mutaftschiew, Zeit. Phys. Chem., 204 (1955) 334.
5. J. Clavilier and R. Pineaux, C.R. Acad. Sci., Paris, 260 (1965) 891.
6. J. Clavilier and J.P. Chauvineau, J. Electroanal. Chem., 100 (1978) 461.
7. G. Lehmpfuhl and Y. Uchida, Surf. Sci., 235 (1990) 295.
8. A. Hamelin, S.Morin, J. Richer and J. Lipkowski, J. Electroanal. Chem., 285 (1990) 249-262.
9. J. Clavilier and J.P. Chauvineau, J. Electroanal. Chem., 100 (1979) 461.
10. A. Hamelin, in "Modern Aspects of Electrochemistry", B.E. Conway, J. O'M. Bockris and R.E. White (Eds.), Plenum, New York, 1985, Vol. 16, Chap. 1.
11. a) A.B. Greninger, Trans. AIME, 117 (1935) 61; b) *ibid*, Z. Krist., 91 (1935) 424.
12. J. Clavilier, R. Faure, G. Guinet and R. Durand, J. Electroanal. Chem., 107 (1980) 205.
13. S. Motoo and N. Furuya, J. Electroanal. Chem., 172 (1984) 339.
14. D. Zurawski, L. Rice, M. Hourani and A. Wieckowski, J. Electroanal. Chem., 230 (1987) 221.
15. J. Clavilier, A. Rodes, K. El Achi and M.A. Zamakhchari, J. Chim. Phys., 88 (1991) 1291.
16. B.R. MacDougall, B.E. Conway and H.A. Kozlowska, J. Electroanal. Chem., 32 App. (1971) 15.
17. J.R. Macdonald, Electrochim. Acta, 35 (1990) 1483.

Chapter 3

Characterisation of Pt single-crystal electrodes

This chapter is concerned with the most important experimental aspect of the investigation of electrochemical processes at Pt single-crystal electrodes: their surface electrochemical characterisation. This step is essential and needs to be performed prior to any electrosorption or electrocatalysis measurements that are made at these surfaces; *e.g.* in the present work, where studies on UPD of H and reactive chemisorption of acetonitrile were made.

3.1 Developments in surface electrochemistry at Pt single-crystal electrodes

The adsorption of intermediates that arise in many electrode processes plays a key role in electrocatalysis, such as in the case of the hydrogen evolution reaction (HER) from the reduction of water molecules or protons. However, little is known about the coordination and physical situations of the(se) adsorbed specie(s) and how, in particular, the different states available at platinum surfaces, exhibiting various coordinating geometries, affect these adsorption processes. Most of the studies that have been conducted on the HER were performed at polycrystalline Pt electrodes. The heterogeneity of the sites and hence of the surface states at such electrodes does not then allow any quantitative evaluation of the effect of surface crystallography and site specificity on the adsorption of H in the HER regime or in related UPD processes below the HER reversible potential.

However, the adsorption of H on Pt single-crystals has been studied widely since the beginning of the '80's. Pt (like Ir and Rh) exhibits a characteristic behaviour at potentials *positive* to the H_2 reversible potential; in this potential region, H atoms are adsorbed reversibly on the Pt surface. This sub-Nernstian adsorption is termed Underpotential Deposition (UPD) of H and it can be represented by the following equation:

$$H_3O^+ + Pt + e \rightleftharpoons Pt\text{-}H_{ads} + H_2O \quad \text{(acidic medium)}$$

where "Pt" represents some particular site geometry on the platinum electrode surface. In this region of potential the adsorbed H can be studied electrochemically in a quantitative way by evaluation of the charge required to adsorb or desorb H and by knowing the type of sites involved. Using cyclic voltammetry, an "electrochemical spectrum" of H adsorption and desorption at various extents of coverage of the surface can be sensitively obtained with remarkable resolution (see Chapter 1, section 1.3.1).

The above UPD process arises when the bond of H to the substrate metal (Pt) has a lower Gibbs energy (*i.e.* a larger negative value) than half of that for formation of a molecule of H_2 from two H atoms.

The study of the influence of the crystallographic orientation of the selected electrode surface on its adsorptive and electrocatalytic properties is very important in both the fundamental and technological aspects of surface electrochemistry. Hydrogen being the smallest adsorbed species, and because of its involvement in the HER and other electro-reduction processes, the UPD H on Pt single-crystals is a process of great interest and importance.

Already since the discovery of UPD of H at polycrystalline Pt, it was proposed that such surfaces comprise different adsorption sites. In order to characterise the nature of those sites, Will [1] investigated Pt single-crystals having the (100), (111) and (110) orientations and concluded that two or three adsorption states can be present simultaneously on each face but in different surface fraction ratios. In 1974, these experiments were extended by Conway and co-workers [2]; in their work, characterisation of the surfaces was performed in a UHV chamber prior to electrochemical experiments using Low Energy Electron Diffraction (LEED). In ref. 2 the surfaces were investigated by electrochemical and *ex situ* UHV techniques in two separate experiments. Although the UHV study confirmed that the surfaces were well ordered, direct transfer to the electrochemical cell was not possible at that time so that direct correlation between the results (electrochemical *vs.* UHV) had to be made with some reservations.

Hence, one of the next steps in the development of surface electrochemistry at Pt was to adapt UHV chambers to allow *direct transfer* of the electrode crystal to an

electrochemical cell under an highly controlled environment without exposure to the ambient atmosphere [3-6]. In these pioneer works [3-6] on low index [(111), (100) and (110)] single-crystal planes, contamination from adsorption of oxygen during the transfer experiments or by "impurities" was still a problem that was often solved by cycling the electrode into the oxide potential region over a long period of time. This procedure is now known to modify the surface order of atoms at the Pt single-crystal surfaces.

It was at the beginning of the '80's, that the CV for flame-treated Pt(111), (110) and (100) surfaces was reported for the first time by Clavilier *et al.* [7-9]. Figures 3.1a to 3.1c reproduce the CV's for these three planes in contact with 0.5 mol dm^{-3} aqueous H_2SO_4 solution at 298 K. Additionally, in Fig. 3.1b, the CV's are shown comparatively for Pt(111) in contact with 0.5 mol dm^{-3} H_2SO_4 and 0.1 mol dm^{-3} $HClO_4$ solutions. In this figure, the now well recognized characteristic but unusual adsorption states, which are sensitive to the nature of the anions present, are clearly visible (see arrows, Fig. 3.1d) [8,9]. Initially the unusual states reported in refs. 7-9 were associated with intrinsic properties of the (111) [as well as of the (100)] surface and were assigned to the adsorption of hydrogen (as H) on a highly ordered surface [9]; they correspond to 1/3 of an H monolayer charge. Both the simplicity of the flame treatment and the interesting behaviour of Pt(111) and (100) surfaces prompted many other research groups to investigate the quality of the Pt single-crystal surfaces produced by this treatment as well as the resulting characteristic current responses generated in cyclic voltammetry experiments.

Hence, Pt surfaces were reexamined by electrochemical means as well as by methods such as the UHV-electrochemical technique or by using new approaches combining electrochemistry with other surface-sensitive techniques such as radiochemistry, *in situ* scanning tunnelling microscopy, *in situ* IR spectroscopy, second harmonic generation and UV-visible spectroscopy. This multiplicity of approaches has served to provide evidence for the complexity of solving this problem at the microscopic level in order to explain the characteristic adsorption behaviour of H related to the geometries and corresponding specific electronic properties of these surfaces.

Since the number of references dealing with this interesting behaviour is now very

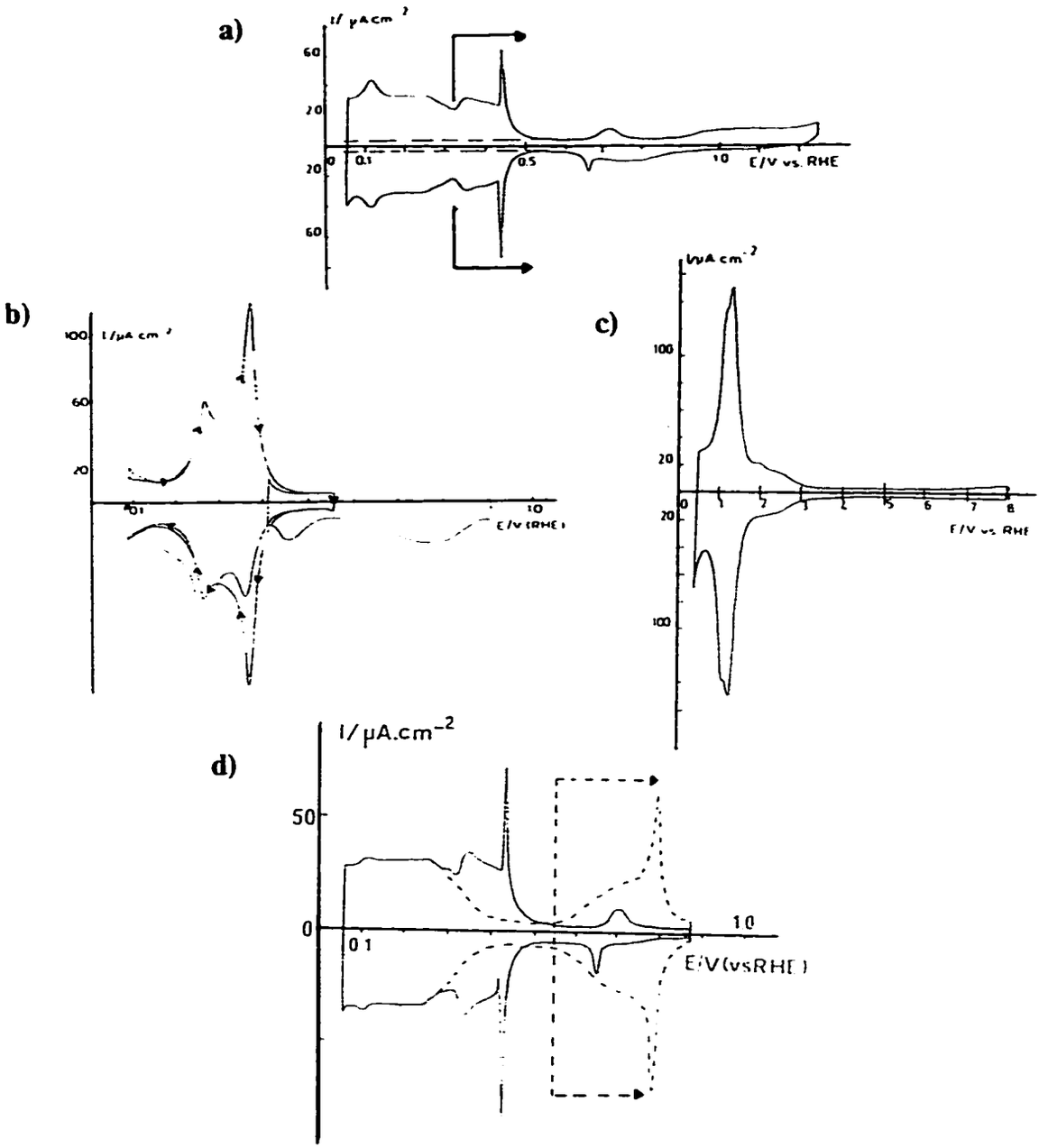

Fig. 3.1 Cyclic voltammograms for flame treated Pt surfaces: a) Pt(111) [9]; b) Pt(100) [8] (curve indicated by arrows); c) Pt(110) [7] in contact with 0.5 mol dm^{-3} H_2SO_4 solution; and d) cyclic voltammograms of Pt (111). Solid line in 0.5 mol dm^{-3} H_2SO_4 and dashed line 0.1 mol dm^{-3} $HClO_4$ [10].

large, the reader will be referred to the thorough review by Clavilier [10] for all of the publications by various authors prior to 1991.

3.1.1 Interpretation of adsorption states at Pt (111)

As reviewed in 1991 by Clavilier *et al.* [10], the origin of the unusual electrochemical adsorption properties of Pt(111) was interpreted in various ways from one research group to another. A first interpretation in terms of surface defects and a second one in terms of surface impurities were proposed by various authors. For example, in some studies it was believed that surface defects develop in the form of Pt adatoms or clusters of adatoms during the thermal treatment of Pt(111) and create states for adsorption of H with high energy bonding. These defects could be eliminated after a few cycles in the oxygen adsorption-desorption potential range and resulted in the gradual disappearance of the unusual states. This latter conclusion was contradicted by preliminary LEED studies by Aberdam *et al.* [11] of thermally treated Pt(111) before and after cycling of the surface in the oxygen adsorption-desorption potential range. The latter work demonstrated that cycling in the oxygen adsorption-desorption region causes micro-roughening, involving faceting of the surface.

In a series of publications, Scortichini and co-workers [12] characterized the Pt low-index planes using both UPD of H as well as UPD of Cu. From this work, they concluded that the pretreated flame-annealed and quenched surface contained a high density of defects such as vacant Pt atom sites and clusters of Pt atom sites. According to these authors, only a few cycles in the oxygen adsorption region in either H_2SO_4 or $HClO_4$ are necessary to yield an hydrogen adsorption-desorption profile that compares closely with those published by authors [3-6] who established the structures using the LEED technique, but without the flame treatment.

It is to be noted that initial cyclic voltammograms after the pretreatment are identical with those initially reported in refs. 7-9. Scortichini *et al.* [12] also noted an increase in the width of the copper adatom stripping peak after cycling of the electrode to the oxide region; this point somewhat contradicts their first observation.

The invalidity of the surface defect or impurity interpretation was partly refuted

by the work Wagner and Ross [13] and Homa *et al.* [14]. In the former work, Pt(100) and (111) surfaces were prepared, and produced well-ordered surfaces as verified by the observed LEED patterns. In 0.3 mol dm^{-3} HF solution, the CV current response for the (111) surface was found to be similar to that recorded in 0.1 mol dm^{-3} $HClO_4$ [10] (see Fig. 3.1b for the CV in $HClO_4$). Cycling of the (100) surface well into the oxygen electrosorption region (to 1.58 V *vs.* RHE) produced LEED patterns characteristic of the formation of random monoatomic-height steps on the surface, and a mean terrace width of 4-6 atoms was estimated [13]. These authors [13] interpreted the unusual adsorption state as being either due to reversible OH adsorption or surface impurity effects.

Using the UHV-electrochemistry transfer technique to investigate Pt(111), (100) and (110) surfaces, as in [13], Homa *et al.* [14] observed similar behaviour for (100) but no unusual adsorption states were observed and only 35% of an H monolayer was detected [14]. However, these studies [11,13,14] did not succeed in reproducing exactly the respective current features observed in Clavilier *et al.* [7-9] for the (100), (110) and (111) surfaces.

Using cyclic voltammetry, Motoo and Furuya [15], studied the effect of the temperature on the thermal re-ordering of a Pt(111) surface electrochemically perturbed by one cycle of oxygen (as OH/O) adsorption-desorption. They suggested that thermal treatment in non-oxidizing atmospheres (H_2 + Ar mixture) favours the migration of surface atoms toward their equilibrium positions, i.e. restoring the long-range ordering on the surface exhibiting the presence of the unusual adsorption states, which are then attributed to H adsorption. These results are in agreement with those obtained in the work of refs. 7-9.

Two more studies corroborated the invalidity of the involvement of the defects as the reason for appearance of the unusual adsorption states. From carefully controlled emersion and transfer to the UHV system with minimum contamination, Aberdam *et al.* [16] succeeded in reproducing the electrochemical results yielded by the Pt(111) plane prepared by the thermal treatment, including the unusual adsorption state corresponding to 1/3 of a monolayer (assuming 1e being transferred per Pt atom). Cycling of this

surface in H_2SO_4 or $HClO_4$ to the oxygen adsorption-desorption potential region causes the disappearance of these unusual adsorption states and was paralleled in the UHV study by the development of monoatomic steps.

Then Itaya *et al.* [17] performed an *in situ* STM observation of a spherical Pt single-crystal: wide, atomically flat (111) domains were observed and, as then expected, the surface became highly disordered after cycling into the oxygen region.

A year later, Feddrix *et al.* [18], using transfer experiments to and from the UHV and the electrochemical cell, succeeded in reproducing the now accepted cyclic voltammograms for the three low-index planes, *i.e.* as found by Clavilier.

3.1.2 The nature of the adsorbed species in the unusual adsorption state region

One of the most important points requiring clarification before advancing this discussion further is the nature of the species present on the Pt(111) (as well as on the other surfaces) at the onset of the UPD profile. In ref. 10 the authors initially believed that the unusual adsorption state at Pt(111) could be interpreted as "strongly adsorbed hydrogen". However, several groups have disputed this interpretation, suggesting that in sulphuric and hydrochloric acids this state is more likely to be due to anion adsorption [19-21] and, in perchloric acid or hydrofluoric acid, it was due to adsorbed -OH [13,19,21].

The idea that (bi)sulphate anion adsorption could explain the pseudocapacitive currents of the unusual adsorption states in H_2SO_4 (see Fig. 3.1a and b) was introduced by Scherson and Kolb [19a]. These authors compared convincingly the cyclic voltammetry behaviour of Au(111) and Ag(111) in the presence of specifically adsorbed anions with that observed for Pt(111) in aqueous H_2SO_4 electrolyte and demonstrated similarities between the current responses for the surfaces investigated [19a]. In addition, from integration of the current under the voltammogram peaks for Au(111) in contact with solution containing Cl^-, Br^-, I^- and SO_4^{2-} the authors obtained charge values corresponding to about 1/3 of a monolayer for a fully discharged univalent species. In a later publication, Kolb and co-workers [19b] also show the effect of bisulphate anion concentration on the voltammetric current reponse for Pt(111); again the evidence pointed

to the involvement of anions instead of H in this particular process [19b].

In recent publications by Wagner and Ross [20a], and Ross [20b], the local work function concept is used to explain the unique sensitivity of the "anomalous" features to the atomic flatness [20]. From the work function measurements at various stepped surfaces it was shown that the local work function at defects in the stepped surface is lower in energy than that of the surrounding flat (111) domains. Thus, the local pzc at the defect is less positive than the pzc of the flat area. This difference in pzc controls the coupling of the processes of hydrogen adsorption and anion desorption. Hence, on all the faces except the (111) co-adsorption of hydrogen and anions is expected around the pzc, whereas for (111) these processes are decoupled due to its very positive pzc (high work function).

In another study involving electrochemical experiments at large Pt single-crystals prepared by H_2 + O_2 or H_2 + air flame annealing, followed by cooling in H_2 gas, Markovic *et al.* [21] observed similar adsorption/desorption behaviour to that of crystals prepared in the UHV and outside the UHV chamber. These authors also confirmed that the current response in the UPD region is very specific to the crystallographic orientation of the Pt single-crystals and that very small concentrations of anions can induce profound changes in the H electrosorption isotherm.

Contradictory conclusions to those of refs. 19-21, were reached from the interpretation of second harmonic generation (SHG) results at Pt(111), (100) and polycrystalline Pt [22]. Using the SHG technique, Campbell and Corn [22a] investigated the potential dependence of optical SHG from polycrystalline Pt electrodes in the presence of aqueous sulphuric and perchloric acid solution. Both the processes of specific adsorption of anions and H atom chemisorption increase the SHG signal from the Pt surface, where the chemisorption of bisulphate ions in the double-layer potential region varies with potential, reaching a minimum near the pzc.

Similarly, Lynch and co-workers [22b,22c] investigated the SHG signal from a flamed-annealed Pt(111) surface transferred to solution with a protective iodine overlayer [23] and cleaned through an iodine-CO exchange reaction followed by electrochemical CO oxidation. This surface preparation method was developed by Wieckowski and co-

workers [24] and was shown to produce highly ordered (111) surfaces (for examples see ref. 22b). The utilization of this surface preparation technique is unavoidable in complex *in situ* experiments where a simple transfer of a water covered surface to the electrochemical cell is not sufficient to avoid surface contamination.

The potential dependence of the SHG signal from the well-ordered Pt(111) surface in $HClO_4$ is associated with an ordered overlayer of hydrogen species; this conclusion was reached from the differences between the SHG signals observed from Pt(100) [22c], polycrystalline Pt [22a] and from Pt(111). However, the identity of the chemisorbed species cannot be determined unambiguously from such SHG measurements [22c].

This analysis of the significance of SHG signals was supported by an electrochemical investigation of Pt(111) UPD in $HClO_4$ using N_2O as a probe [25]. In this work [25], the reactivity of N_2O with adsorbed H is used to probe the presence of the latter adsorbate. The reduction of N_2O on Pt(111) occurs below 0.75 V in $HClO_4$ and below 0.5 V in H_2SO_4, respectively, suggesting that adsorbed H *is* involved in the unusual adsorption states [25].

On the other hand, the involvement of bisulphate anions in the UPD region of Pt(111) and (100) in contact with sulphuric acid has been clearly demonstrated by using radiotracer labelling and voltammetry [26]. In that work, marked differences were observed in the behaviour of bisulphate ion adsorption, for which the coverage is much smaller on Pt(100) than on Pt(111). According to these authors, a possible explanation is that there is a perfect symmetry match between bisulphate oxygen (triangular) ligands and the hexagonal (111) site geometry of Pt atoms, as emphasized for sulphate on Au(111) [27].

However, more divergent conclusions were obtained from electroreflectance measurements at well-defined Pt surfaces [28]. In that work, the authors concluded that the major species present in the UPD H region are also present in the unusual state on (111) surface.

In a series of publications, Kunimatsu *et al.* [29] reported *in situ* FTIR reflection absorption spectroscopy (IRAS) behaviour for polycrystalline Pt in contact with sulphuric acid [29a,29b,29d], NaOH containing $NaSO_4$ (pH = 11.5) as well as H_2SO_4 containing

$NaSO_4$ (pH = 3.4) [29c]. They found a strong dependence of the anion adsorption (HSO_4^- and SO_4^{-2}) with pH of the solution, as well as with the electrode potential. Similar conclusions were reached by Nart and Iwasita [30] for a polycrystalline Pt surface also probed by IR spectroscopy for pH's values varying between 0.2 and 3 using fluoride supporting electrolyte and K_2SO_4 as the anion source.

In another study using *in situ* IR spectroscopy, Faguy and co-workers [31] showed convincingly that the anomalous voltammetry on Pt (111) in sulphuric acid is due to the specific adsorption of bisulphate anions. However, in some other studies, different conclusions were reached concerning the nature of the adsorbed anion; for instance, from an *in situ* FTIR spectroscopy study, the unusual states were attributed to the presence of adsorbed sulphate anions at each of the (111), (100), and (110) surfaces [32]. This difference in the nature of the anion adsorbed at Pt(111) and (100) might be attributed to the absence of a large amount of HSO_4^- in the thin layer due to careful control of the pH (*i.e.* determining changes in the SO_4^{-2}/HSO_4^- ratio in the solution phase) [32].

Using a different approach, Adzic and co-workers [33] probed the adsorption of copper and lead adatoms, and of carbon monoxide at Pt(111) in H_2SO_4 and $HClO_4$ solutions in order to gain information on the species involved in the unusual adsorption states. In H_2SO_4 solution, these three adsorbates caused extensive blocking of H adsorption and a decrease of the "anomalous peak" ascribed previously to HSO_4^- adsorption [31], while, in $HClO_4$ solution, the unusual state was only slightly perturbed by Cu and Pb adatoms suggesting to these authors that Pt/OH is the species involved in the unusual state [33].

The involvement of bisulphate anions in the unusual state was also inferred by the work of Ogasawara *et al.* [34], who reported *in situ* FTIR spectra at Pt(111) in contact with 0.5 mol dm^{-3} H_2SO_4 solution as well as the *ex situ* FTIR spectra after transfer of the Pt(111) to an UHV chamber to record the LEED patterns of the adsorbed layer. From, this study, the nature of the species adsorbed in the unusual-state potential region was believed to be bisulphate anions. Moreover, in that work, it was also clearly shown that these adsorbates exhibit a ($\sqrt{3}$ x $\sqrt{3}$)-R30° array structure. The same structure was

reported by Michaelis *et al.* [35] for bisulphate anion adsorbed on top of an UPD Cu layer.

Recently, Faguy *et al.* [36] have investigated the pH effect on anion adsorption at Pt(111) electrodes from acidic sulphate solutions. Unlike the other studies mentioned so far, these authors observed more IR spectroscopic features related to the anomalous peak region of the cyclic voltammetry of Pt(111) electrodes: two due to the adsorbate species itself and one due to the loss of the adsorbing anion in the thin-layer cell. One of the bands due to adsorption of anions was not observed in earlier work [31-34] and it is assigned, here, to the S-O stretch of an adsorbed ion-pair having the following structure: $Pt\cdots O_3SO^{2-}\cdot H_3O^+$ rather than $Pt\cdots O_3SOH^-$ [36].

Shingaya and Ito [37] also reported the electrode potential-dependent IRAS of ClO_4^- on Pt(111) as part of a study of anion adsorption on clean and copper-modified Pt(111) and Rh(111) electrode surfaces. There results show that ClO_4^- anions begin to become adsorbed on Pt(111) at potentials more positive (*ca.* 500 mV *vs.* SHE) than that for the bisulphate anion adsorption (*ca.* 100 mV more positive).

Other recent publications seem to confirm the suggestion that anions are the main species present at the surface [38-40] in the unusual adsorption state region and that, in the case of H_2SO_4 electrolyte, bisulphate rather than sulphate anions are the species adsorbed [41].

Another electrochemical procedure for examination of adsorbed species is an adaptation of a method developed by Conway *et al.* [42] for polycrystalline Pt electrodes. It allowed electrochemical characterisation of the species present at the surface by measuring the current transient that arises upon addition of carbon monoxide to an initially clean surface in contact with the electrolyte solution and maintained at a constant potential; the strongly adsorbed CO replaces any previously adsorbed species, *e.g.* H and/or HSO_4^- on the surface. This method was first tested on an iodine-precovered surface [43] and demonstrated that CO could be used as a neutral probe in the replacement process when it adsorbs on Pt under electrochemical conditions.

This method was then employed to study the UPD region of the low-index planes

in various electrolytic media such as $HClO_4$ [38], H_2SO_4 [39] and, $H_2C_2O_4$ (oxalic acid), HCl, CH_3COONa and KBr added to an $HClO_4$ supporting electrolyte solution [40].

As shown in Fig. 3.2a-d for Pt(111) in H_2SO_4, the adsorption current transients recorded at potentials positive to *ca.* 0.3 V are cathodic (Fig. 3.2a) and those recorded at potentials less positive than this limit are anodic (Fig. 3.2c). This indicates clearly that the nature of the species being desorbed by CO is different, *i.e.* anionic *versus* proton (from adsorbed H), respectively.

Integration of the charges under the voltammograms compares very well with the charges recorded from the transient charge differences, as shown in Fig. 3.2e.

The transient charge differences, q_T, are expressed as follows:

$$q_T = q_T(E_{0.08V}) - q_T(E_{ads}) \qquad (3.1)$$

where q_T ($E_{0.08V}$) corresponds to the maximum anodic transient charge recorded for H displacement and q_T (E_{ads}) to the charge of the CO adsorption transient recorded at any potential E_{ads}. In Fig. 3.2e, the curve labelled 2 is for a disordered Pt(111) surface. It was observed by these authors that the adsorption transients recorded for the disordered surface were displaying cathodic charge changes at potentials less positive than those respectively for the ordered Pt(111). The potential corresponding to zero desorption charge was observed on this face at a value much less positive for the disordered surface in comparison with that for the well-ordered one. This is indicated in Fig. 3.2e by the arrows: this potential is referred to as the *pztc* (see Chapter 1, section 1.2.1), the "potential of zero total charge".

From the integration of the charge under the current transient, the maximum H coverage near the threshold of the HER is estimated to be near 2/3 of a monolayer for the ordered Pt(111) and close to a monolayer for Pt(100) (cooled in H_2-Ar) and Pt(110) (the charge being calculated for a (1 x 1) structure). In the case of the (100) and (110) surfaces, the maximum charges recorded under the cathodic adsorption transients were much less than in the case of the (111) surface, i.e. around -60 μC cm^{-2} where the onset of anion adsorption occurs around the maximum of the desorption peak (the most positive hydrogen desorption peak in the case of (100)).

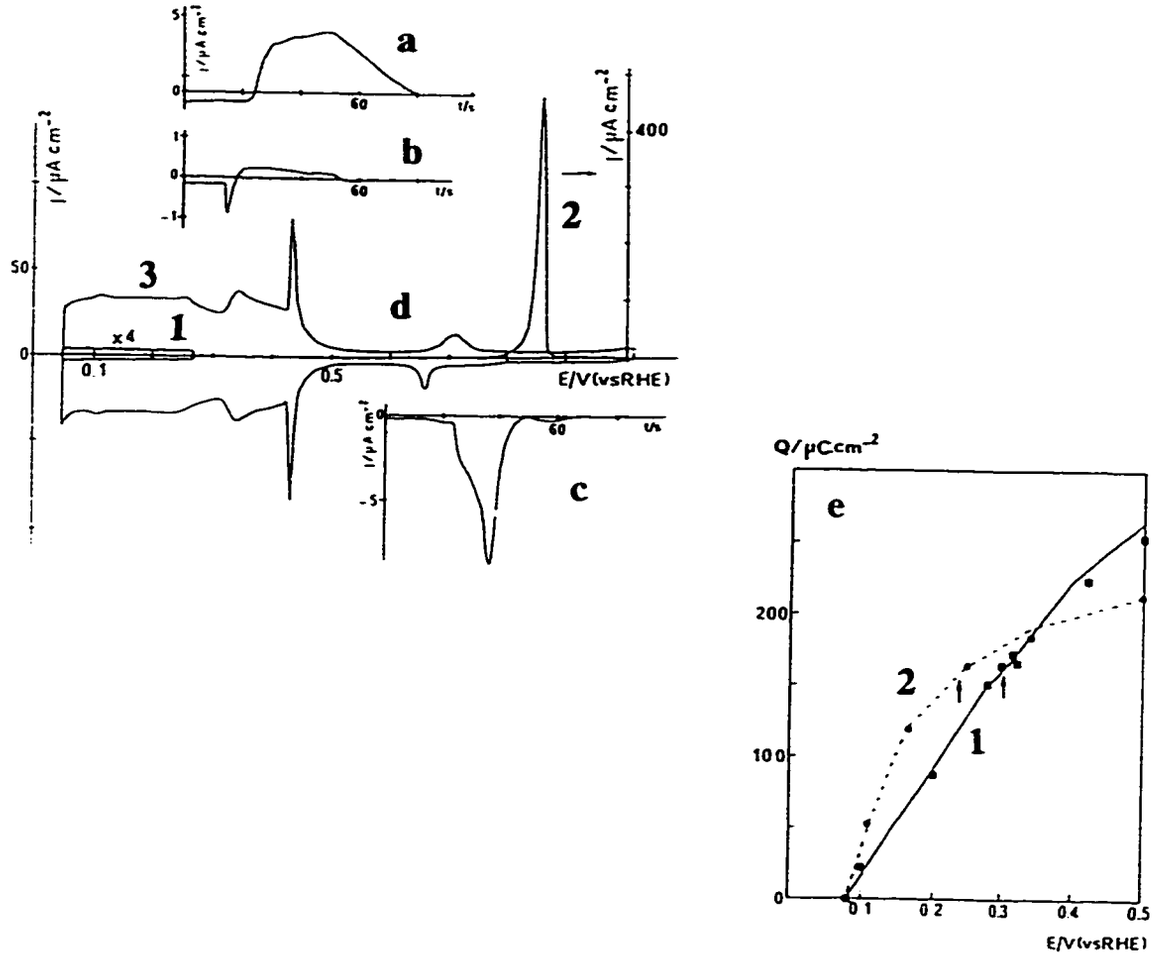

Fig. 3.2 a), b), c) Current density-time transients corresponding to CO adsorption experiments on a well ordered Pt(111) electrode in 0.5 mol dm^{-3} H_2SO_4 (E_{ads} = 0.08, 0.30 and 0.50 V *vs.* RHE, respectively); d) Voltammograms for the same electrode in the CO-free electrolyte, after CO adsorption: (1) control of the surface blocking by adsorbed CO (50 mV s^{-1}, enlarged by a factor of 4); (2) stripping of adsorbed CO (20 mV s^{-1}); (3) recovery of the initial voltammetric profile (50 mV s^{-1}) [39a]. e) Plots of the charge densities obtained from voltammogram integration (starting at the less possitive limit: 0.08 V) (solid and dashed lines) and those obtained from transient charge differences, q_T data points *versus* electrode potential for (1) for a well ordered Pt(111) and (2) perturbed Pt(111). The arrows indicate the potential region where net total transient charge becomes zero (*pztc*) [39b].

In the presence of $HClO_4$ the adsorption transient at Pt(110) indicated a much smaller effect of ClO_4^- anion adsorption (-38 μC cm^{-2} at 340 mV). In the case of Pt(111), cathodic transients were recorded at potentials between those for the H UPD and the unusual state regions; however, the charges were small *ca.* -20 μC cm^{-2}, and might be associated with changes in the double-layer structure induced by the CO adsorption. The unusual state region could not be investigated because it coincides with the CO oxidation-potential region.

Using chronocoulometry and Gibbs thermodynamics of interfaces, Savich and co-workers [41] investigated bisulphate adsorption at the Pt(111) surface by varying the concentration of H_2SO_4 in a 0.1 mol dm^{-3} $HClO_4$ supporting electrolyte.

From these authors' analysis, the surface concentration of sulphate/bisulphate adsorbed at Pt(111) attains a maximum value of 5 x 10^{14} ions cm^{-2}, corresponding to 1/3 of a monolayer (ML) coverage where one ML corresponds to a Pt atom density of 1.5 x 10^{15} atoms cm^{-2}. The 1/3 ML coverage correlates well with the ($\sqrt{3}$ x $\sqrt{3}$)R30° pattern discussed earlier. A second quasi-plateau in the surface concentration *versus* potential graph corresponds to 0.4 ML and could be represented by an ordered ($\sqrt{3}$ x $\sqrt{7}$) anion overlayer.

3.1.3 Effect of long-range surface ordering on the unusual adsorption states

Another approach to increase the level of understanding regarding the characteristic CV profiles of Pt(111) (and (100)) surfaces, and the effect of long-range order on these two atomically flat surface domains, is the use of stepped surfaces [6,10,44-53] for comparative purposes.

As described in Chapter 2, section 2.1.1, stepped surfaces are "located" in the stereographic triangle (Fig. 2.1) between the low-index plane apices and they possess, according to their angle with respect to these planes, characteristic orientations of their terraces and steps (see Fig. 2.2).

Many studies using this approach started to emerge in the mid-'eighties [44-48]. On the basis of the results for four stepped surfaces, Ross [6] arrived at the conclusion that the multiple peaks for H UPD were due primarily to the intrinsic heterogeneity

arising from different types of sites on the single-crystal surface. Love *et al.* [44,47] have invoked the "induced heterogeneity" concept [54] to explain the multiple peaks. Adzic and co-workers [46], on the other hand, have demonstrated the sensitivity of hydrogen adsorption to the step-density and step-orientation, and have noticed the stability of some stepped surfaces towards oxidation. A similar conclusion had been reached by Clavilier *et al.* [45].

Of the first studies reported on stepped surfaces that by Motoo *et al.* [48] was the most complete. These authors reported a detailed study of stepped surfaces in the three zones spanning a wide range of n values (n = terrace width in atoms) up to 40. Their results show that the voltammetric profiles are highly dependent on the step-density and terrace-width, allowing direct correlation with the incidence of step and terrace sites, respectively (see Fig. 3.3). These authors utilized their modified "Clavilier method" of annealing and quenching by cooling the stepped surface in a flow of H_2 and Ar mixture instead of air [15,48]. This modification of the procedure was prompted by the UHV studies of Blakely and Sormorjai [55], who had shown that instability (formation of multiple steps and faceting) of clean stepped surfaces arises under UHV conditions when such surfaces are annealed and exposed to oxygen.

At the beginning of the 'nineties more quantitative analyses of H adsorption states at various stepped surfaces arising over the three zones (see Table 3.1, Fig. 3.3b) were performed [10,49-53].

For instance, Marković *et al.* [49,51] investigated stepped Pt surfaces from the [110] zone, *i.e.* surfaces with steps and terraces of the (111) and (100) orientations, and from the [1$\bar{1}$0] zone, *i.e.* surfaces with steps and terraces of the (111) and (110) orientations, in contact with H_2SO_4 solution and for some of these faces, also in $HClO_4$ solution [49,51]. These authors also applied the H_2-cooling method to avoid possible disordering of the stepped surfaces (due to O_2 adsorption) during the cooling procedure. The quality of the data is quite remarkable and it is discussed in terms of H and HSO_4^- / SO_4^{2-} adsorption, and in terms of ClO_4^- adsorption, although the latter is much less adsorbed than the former. Similar to results reported in ref. 45, linear relations are

a)

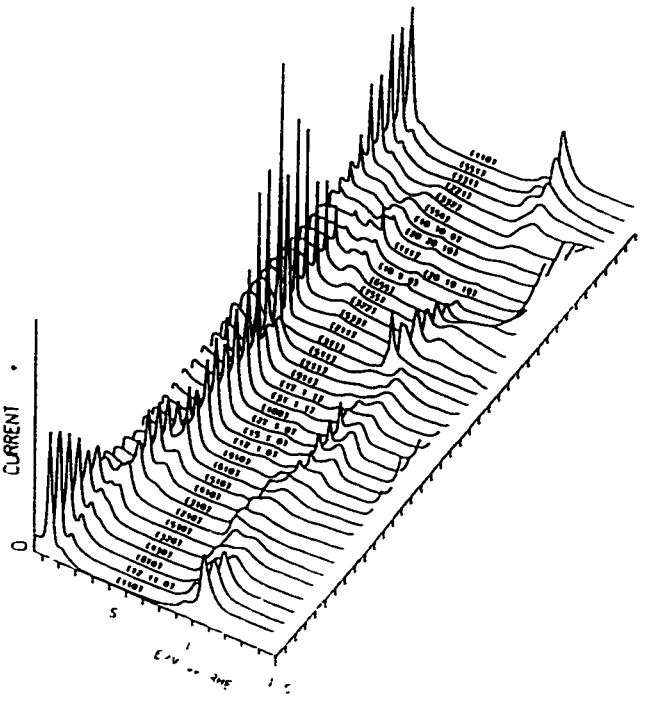

b) Table 3.1 The various zones of the stereographic triangle containing stepped surfaces with their t l k notations†

Various zones of higher Miller indices	tlk notations†	examples
from (110)‡ to (20 20 19)	n(111)-(111) or (n-1)(111)-(110)	(332) = 6(111)-(111) = 5(111)-(110)
from (111) to (311)**	n(111)-(100)	(533) = 4(111)-(100)
from (311)** to (100)	n(100)-(111)	(511) = 3(100)-(111)
from (100) to (210)*	n(100)-(110)	(12 1 0) = 12(100)-(110)
from (210)* to (110)	n(110)-(100)	(430) = 4(110)-(100)

† see chapter 2, section 2.1.1
‡ (110) = 2 (111)-(111)
** turning point in the zone between the (110) and (111) planes. (311) = 2(111)-(100) = 2(100)-(111).
* turning point in the zone between the (100) and (110) planes. (210) = 2(110)-(100) = 2(100)-(110).

Fig. 3.3 a) Voltammograms for surfaces of higher Miller indices consisting of steps and terraces in contact with 0.5 mol dm^{-3} H_2SO_4 solution [48]; b) table of the various zones containing stepped surfaces and their TLK notations.

found between the charge associated with the H adsorption process and that for the unusual states, as well as for the step-density for the n (111) - (100) surfaces [49] and n(111)-(111) surfaces [51]. However, as pointed out by Clavilier [10], this quantitative approach was limited to three surfaces with narrow terraces and might not reflect the situation at surfaces exhibiting wider terraces ($n \geq 6$).

In ref. 49, the unusual states are associated with anion adsorption/desorption on the (111) terraces and the sharp feature at *ca.* 250 mV to H UPD on the (100) sites but coupled with anion desorption/adsorption on the (111)-(100) sites [49]. A similar interpretation was given for the stepped surfaces with terraces of the (100) orientation and (111) monoatomic steps, as well as for some n(100)-(110) surfaces [49].

In the case of stepped surfaces having n(111)-(111) and n(110)-(111) notations, a sharp feature was observed at *ca.* 100 mV and it was associated with coupling of desorption of bisulphate with adsorption of H on those sites [51]. From a comparison of these results [49,51], it is believed that anions are more strongly adsorbed at the steps than at the (111) oriented terraces. The latter process occurs at potentials more positive than that at the steps and hence it is affected by anions already adsorbed at such step sites [51].

A 1991 review by Parsons and Ritzoulis [50] compares the results obtained between various laboratories for the current responses for various adsorption processes on stepped surfaces of platinum and gold single-crystals. This review clearly revealed good agreement in the observed features of the voltammograms obtained by various workers for a number of stepped surfaces. However, the authors of this review seem to favour the scenario ascribing the unusual states to the adsorption/desorption of hydrogen rather than to anions. This is attributable to the convincing quantitative analysis provided by Clavilier and co-workers [10] for the behaviours at stepped surfaces containing terraces of (111) orientation. In order to perform quantitative analysis, a large number of stepped surfaces are required in a given zone. In order to prepare high quality stepped surfaces, only a few degrees apart, Clavilier developed a new method of surface preparation that has angular accuracy down to 3 minutes of arc [10].

From their study the critical size of the two-dimensional domains for which

unusual states are observed was determined, knowing that on a highly ordered (111) surface those states account for 1/3 of the total charge. Two types of stepped surfaces having (111) oriented terraces were examined: one having monoatomic steps consisting of (100) and the other steps of (110) sites.

The cyclic voltammograms for the desorption of H for a series of stepped surfaces with (110) and (100) monoatomic steps are shown in Figs. 3.4a and 3.4b, respectively. On both of these figures, the sharp peak increases with decrease in terrace length (or increase in step-density). The sharp peaks are observed at the same respective potentials as reported earlier [45,48,49,51], where the peaks corresponding to the (110) steps are observed at *ca.* 100 mV and those for the (100) steps at *ca.* 250 mV, where the areas under these peaks correspond to the adsorption charge of H on the step sites. The rest of the charge under the voltammogram is that for the terrace plus the charge of the double-layer.

Using a hard-sphere model (see Figs. 3.5a and 3.5b) and allowing one electron to be transferred per Pt atom, a relation between the adsorption charge-density for the steps and terraces, and n, can be compared to the experimental values for each type of surface. From such comparisons, it is clear that the unusual adsorption states no longer correspond to 1/3 of the terrace sites on narrow terraces ($n < 7$) for the (110) steps. Moreover, by comparing the charge from the cyclic voltammograms and that estimated from the ball model for the step sites, the authors [10] realised that the (100) and (110) step sites occupy different areas of the total surface. Hence, the (110) step sites according to the model, occupy an area 1/3 greater than that of the terrace sites [10] while the (100) step sites an area 1/3 less [10], as may be seen by inspection of models (*cf.* Figs. 3.5a and b). This difference arises from the position of the rows of atoms in the steps *versus* the rows of atoms in the terraces. This can be expressed for the two types of step sites by the following two relations:

$$q_t = q_{111} - \frac{4}{3} q_{110\ step} \qquad (3.2)$$

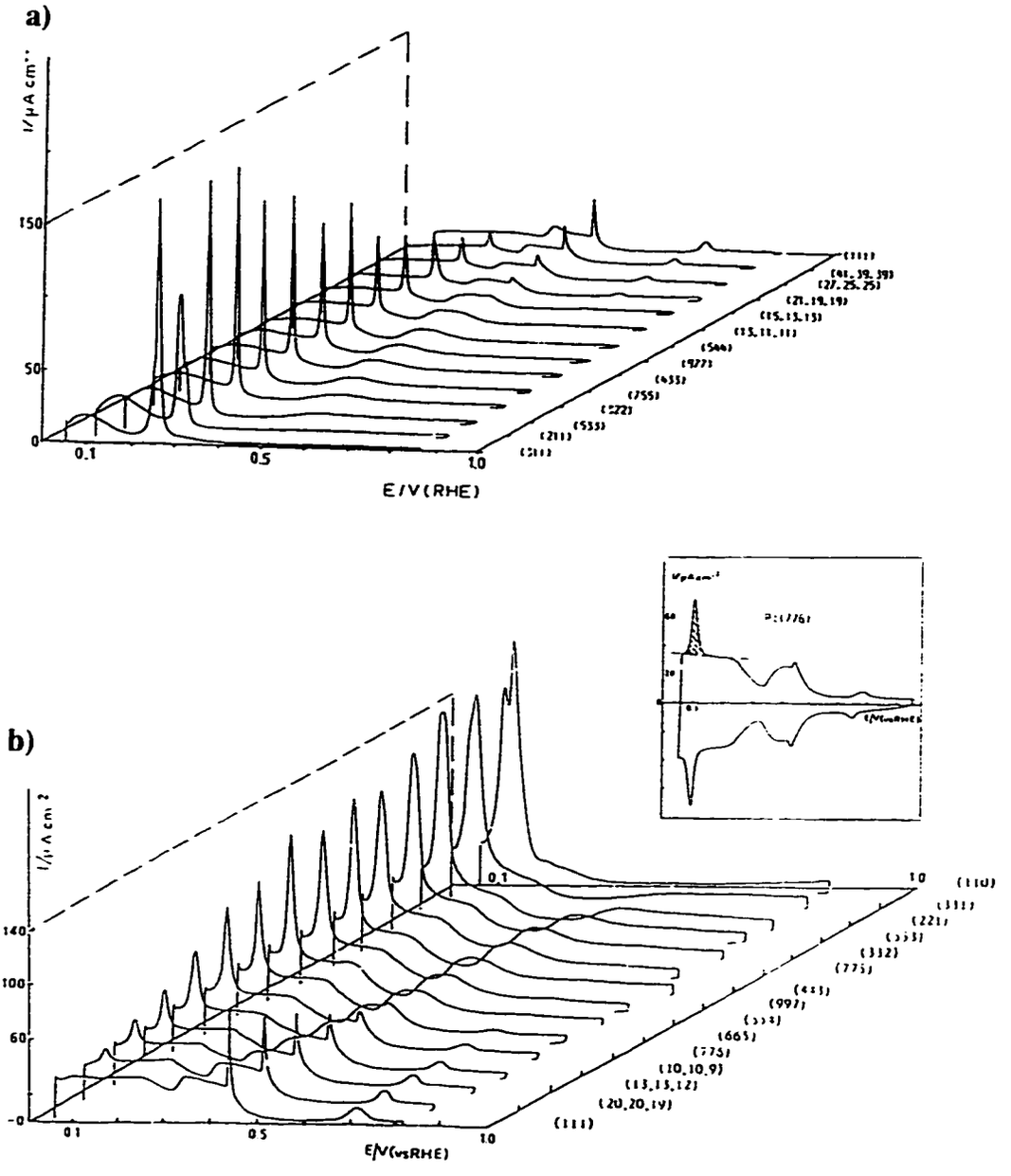

Fig. 3.4 a) Positive-going sweep of the voltammograms of Pt(111) and Pt n(111)-(100) surfaces investigated with n = 2-9, 12, 14, 20, 26 and 40 in 0.5 mol dm^{-3} H_2SO_4 (sweep rate: 20 mV s^{-1}) [56]; b) Positive-going sweep of the voltammograms of the surfaces investigated in this work in 0.5 mol dm^{-3} H_2SO_4. The inset shows the separation between the step (shaded area) and terrace electric charge contribution for H desorption from one of the stepped surfaces [57].

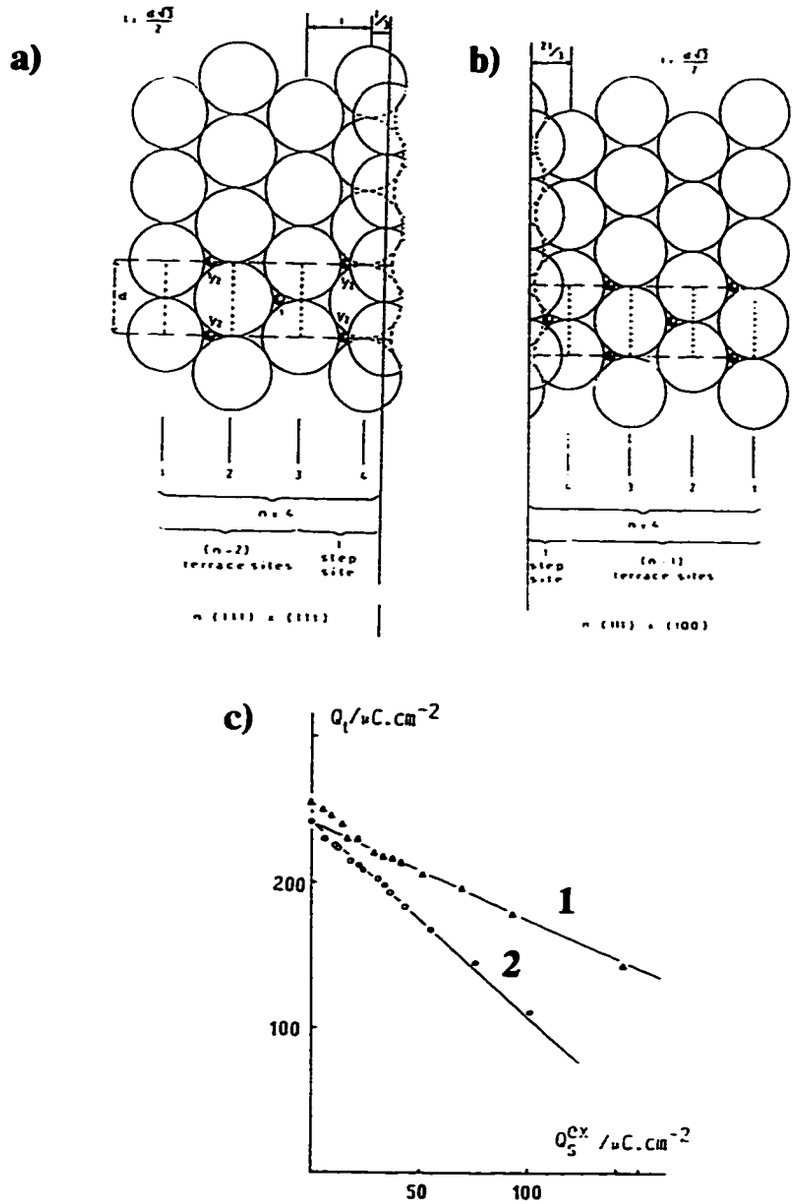

Fig. 3.5 a) Projection on the terrace plane of the hard-sphere model of a stepped surface of the n(111)-(111) or n-1(111)-(110) type showing the surface unit cell [56,57]; b) top view of the hard sphere model of a n(111)-(100) stepped surface showing the surface unit cell, enclose by the dashed line [10]; c) experimental terrace charge density after double-layer correction for 1) Pt n (111)-(111) and 2) Pt n(111)-(100) as a function of the corresponding experimental step charge densities. The full lines correspond to theoretical relations with slopes -4/3 (see eq. 3.2) and -2/3 (see eq. 3.3), respectively. 0.5 mol dm^{-3} H_2SO_4 [10].

$$q_t' = q_{111} - \frac{2}{3} q_{100\ step} \qquad (3.3)$$

where q_t and q_{step} are the charges for the terrace and the step, respectively, and q_{111} is the charge for a well-ordered (111) surface. Figure 3.5c, shows a graph for q_t and q_t' *vs.* $q_{110\ step}$ and $q_{100\ step}$, respectively.

Clavilier and Rodes [52,53] also quantified the effect of oxygen adsorption and high-temperature quenching on the ordering of step surfaces. One of these works [53] was performed on a series of stepped surfaces with (111) terraces and (100) step sites, and showed the appearance of the (110) sites after adsorption of oxygen and correspondingly a reduction of the number of (100) step sites. This behaviour was explained quantitatively using a hard-sphere model assuming a step reconstruction that creates indentations made of (110) sites [53].

In the case of a surface of the (n-1)(111)-(110) type, with $n < 8$, thermal shock developed the unusual states. This is associated with the formation of wider terraces made of atoms from the monoatomic steps [52]. Hence there is formation of multiatomic steps in order to conserve the average structure of the surface. These two studies yielded results that were in good quantitative agreement with the two proposed models for the reconstruction of stepped surfaces due to thermal treatment.

In refs. 10, 52 and 53, discussion concerning the adsorption on the step and terraces was not given in terms of adsorption of HSO_4^- in the unusual state region. However, in ref. 10, for both the n(111)-(100) and (n-1)(111)-(110) surfaces, the charge assigned and measured for the unusual state is 1/3 of q_t for terraces with $n > 7$, making the model proposed still valid if q_t is interpreted as corresponding to 2/3 of H and 1/3 HSO_4^-. At the time refs. 10, 52 and 53 were published, the respective authors assigned the sharp features in the unusual states to the effect of a surface phase transition of adsorbed sulphuric anions on the adsorption isotherm of hydrogen. This was supported by the decoupling of the unusual hydrogen adsorption state and the surface phase transition observed by varying the terrace width, where each effect (the broader feature and the sharp peak) appeared at a different characteristic terrace width [10].

It is fair to say that consensus has now emerged on the relation between the surface long-range order and the unusual adsorption states. Figure 3.6a shows typical voltammograms for flame-treated Pt(111), (100) and (110) surfaces cooled in an H_2 + Ar atmosphere in contact with 0.5 mol dm^{-3} H_2SO_4 solution. The H_2 + Ar treatment introduced by Motoo and Furuya [15] produces surfaces that exhibit different CV characteristics from those for surfaces cooled in air except for Pt (111) which remains unchanged [10].

Further discussion of the characteristics of the current responses of Pt single-crystals will be given in the next section (especially for Pt(100) and (110)) where the qualitative and quantitative evaluation of the quality of the Pt surfaces produced for the electrocatalysis studies on the reactive chemisorption of acetonitrile will be treated.

3.2 Single-crystal surfaces used in the present work: electrochemical characterisation techniques and results

Analysis of the surfaces produced by the present author in our laboratory will now be discussed with reference to the information referred to in the previous section. Mainly, three characterisation techniques were used in the present work: a) electrochemical monitoring of the thermal reordering of the Pt(111); b) cyclic voltammetry; and c) the adsorption replacement technique, using CO as the competitive adsorbate.

3.2.1 Initial electrochemical monitoring of the thermal reordering of the Pt(111) surface

This characterization procedure was performed immediately after the polishing of the electrode (see section 2.1.2 of Chapter 2, for details on the polishing procedure). This allows any atomic reorganization of the perturbed surface to be followed electrochemically by first performing a thermal decontamination [58]. The latter treatment consists in raising the temperature of the crystal just above 100°C for a few seconds. The voltammogram of the resulting decontaminated surface, in contact with a 0.5 mol dm^{-3} H_2SO_4 solution, is shown in Fig. 3.7; it looks very similar to that for a

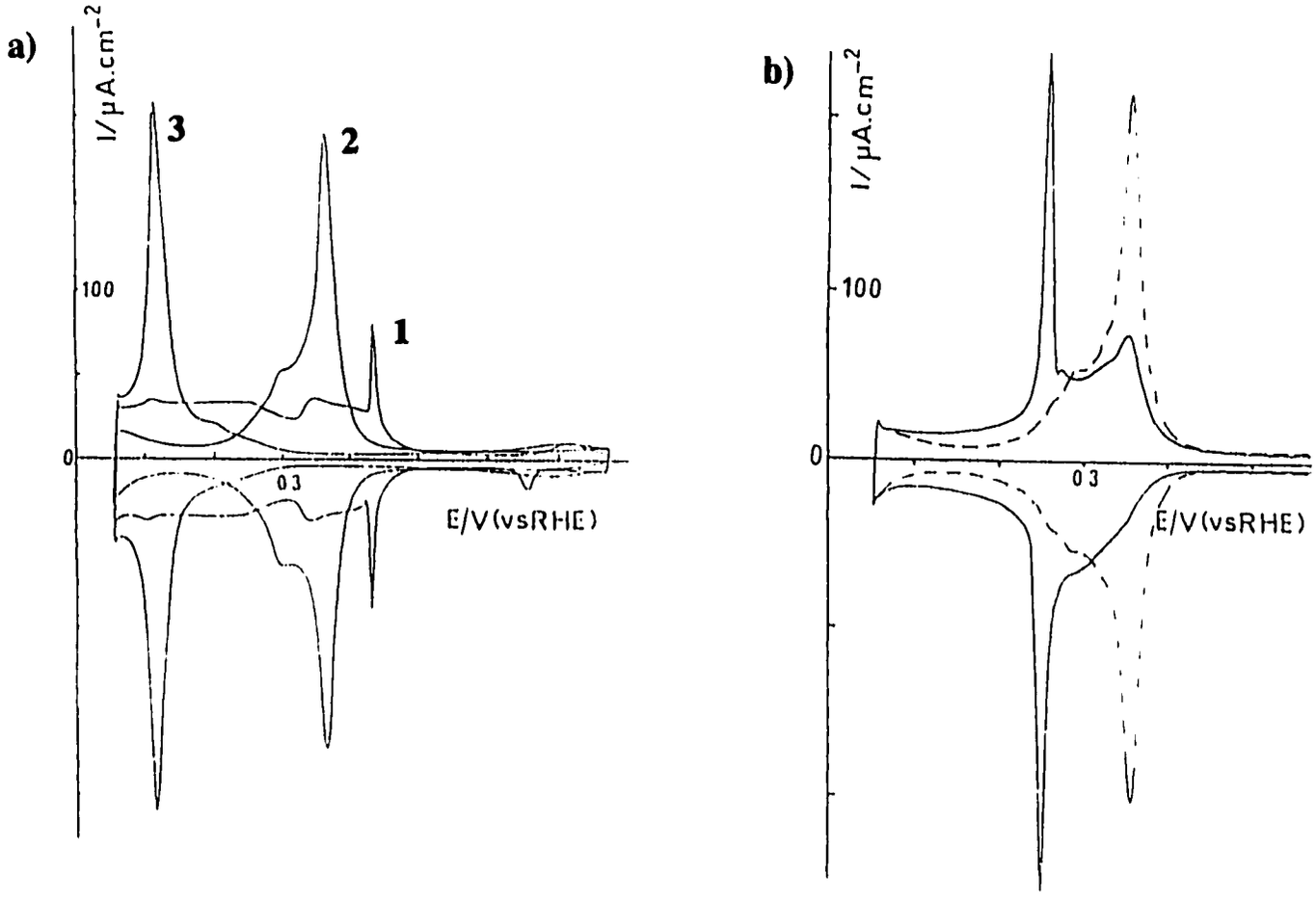

Fig. 3.6 Cyclic voltammograms of a) Pt(111): 1, Pt(100): 2 and Pt(110): 3 in 0.5 mol dm^{-3} H_2SO_4; b) Pt(100) for a surface cooled in air (solid line) and for a surface cooled in an H_2 - Ar mixture (dashed line) [10].

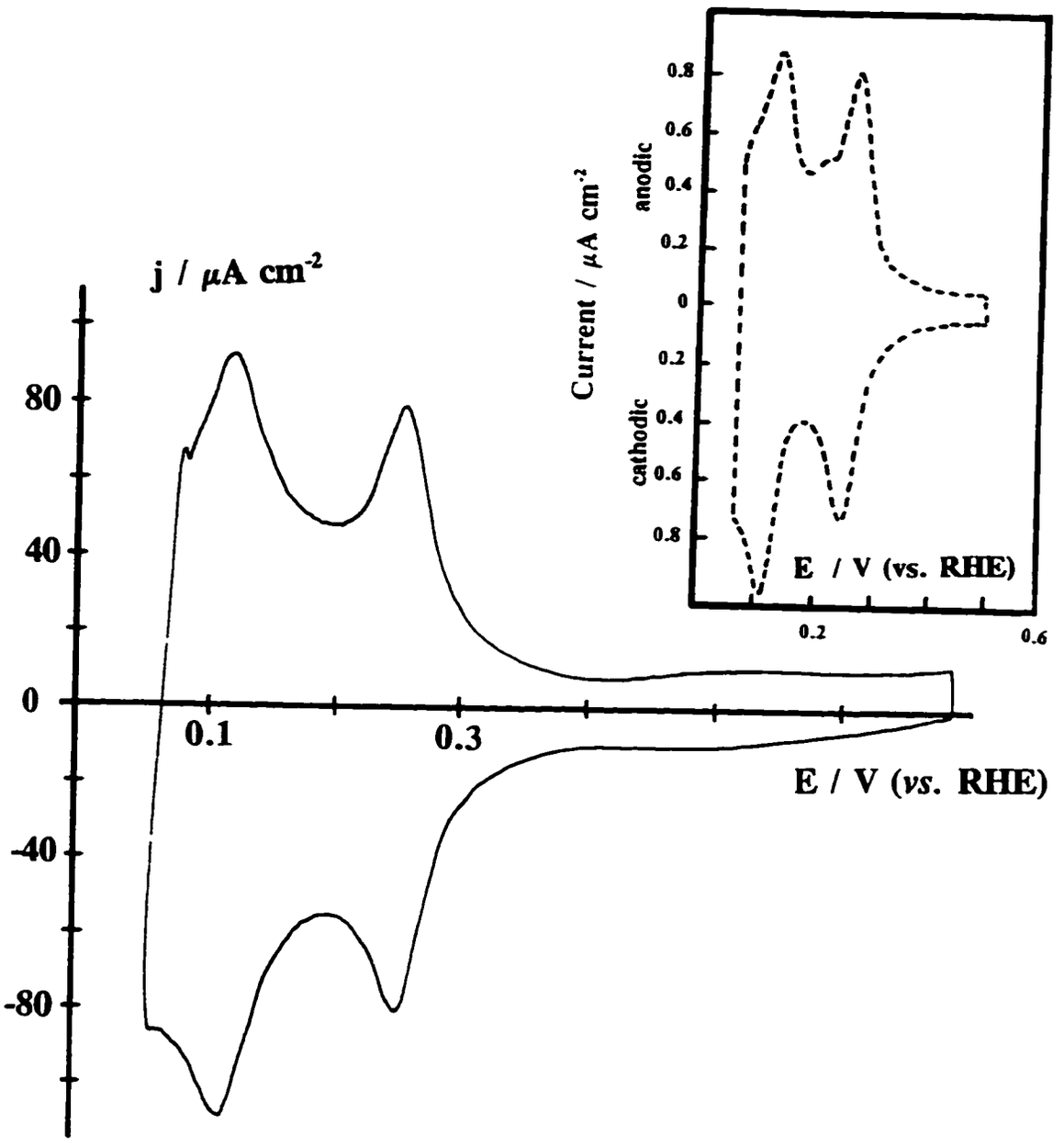

Fig. 3.7 Cyclic voltammogram of a freshly prepared Pt(111) surface in 0.5 mol dm^{-3} H_2SO_4 solution after applying a decontamination treatment, see text. Inset: cyclic voltammogram of a Pt polycrystalline electrode in contact with the same solution.

polycrystalline surface (inset, Fig. 3.7) indicating that sites with the three basal (low-index) symmetries are present at the surface and no net preferential site distribution is observed. The CV shows that the surface does not contain large (111) ordered surface domains, as indicated by the absence of a marked unusual hydrogen adsorption state (see section 3.1.1) in the potential region between 0.3 and 0.5 V. From the results reported on the voltammetric features of stepped surfaces containing (111) sites [ref. 10 and the discussion above in section 3.1.3], it is possible that the slight increase of currents around 0.5 V is due to very narrow (111) terraces (*ca.* 3 atomic rows [10]). The main peaks seen on the CV of Fig. 3.7 correspond to randomly distributed (110) and (100) steps of various heights. The mean total electric charge passed between 0.055 V and 0.685 V is equivalent to 215 μC cm^{-2}, including that for double-layer charging.

Following decontamination, the surface is then annealed by gradually increasing the temperature of the crystal and the time of annealing. Figure 3.8 shows the voltammograms of the successive states of reordering of a newly polished Pt (111) oriented surface obtained by applying thermal treatment. The two variables in this treatment are temperature and annealing time; both were increased slowly in order for the effect shown in Fig. 3.8 to be seen.

As was reported earlier by Clavilier *et al.* [58], the information contained in Fig. 3.8 is very valuable and shows clearly the ordering effect of thermal annealing on the structure of the (111) surface. First, the peaks at 0.11 V and 0.26 V ascribed earlier to (110) and (100) defects created by the cutting and polishing procedures are decreased significantly, while the adsorption states between 0.3 and 0.5 V increase in response-current intensity, including the current spike at 0.43 V. This spike is characteristic of this surface in contact with 0.5 mol dm^{-3} H_2SO_4. It is only observed in very clean solutions and when large ordered (111) domains have been created [58]. The appearance of this spike is also sensitive to the amount of sulphate/bisulphate anions present, as discussed previously. The mean total electric charge for curve between 0.055 V and 0.6 V is substantially less than that following decontamination (not shown in Fig. 3.8) and is another indication of the ordering.

It was also shown by Clavilier [58] that the change of the CV profile in the UPD

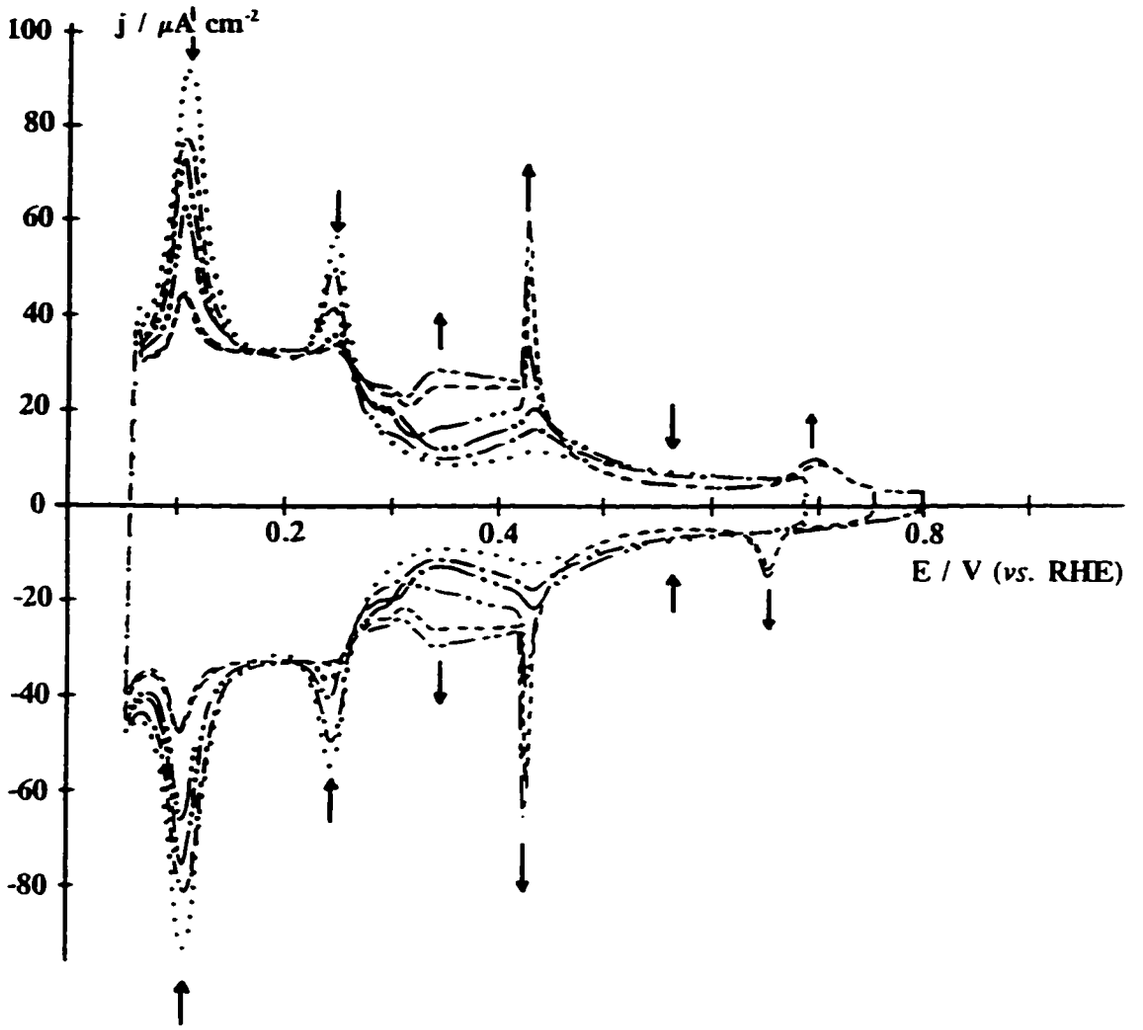

Fig. 3.8 Modification of the voltammetric profile in the UPD region for Pt(111) in contact with 0.5 mol dm^{-3} H_2SO_4 solution. Each curve corresponds to a different stage of annealing of the electrode shown in Fig. 3.7. Curves (••••) and (- • -) show the voltammograms of the electrode surface after annealing at about 500°C for a few seconds in each case. Curve (- •• -) is after annealing at *ca.* 800°C for 1-2 sec, curve (- ••• -) after annealing at *ca.* 900°C for 30 sec, curve (- - -) after annealing at *ca.* 900°C for 2 min and finally curve (- -- -) for annealing at *ca.* 900°C for 15 min.

region was paralleled by changes in the oxygen adsorption region. These authors have recorded the CV over the OH/O adsorption region for each stage of annealing and shown that the initial oxygen adsorption region was very similar to that for a polycrystalline surface subjected to cleaning by electrochemical cycling (see Fig. 3.9a). This current profile was decreased in intensity drastically to yield finally the current response profile shown in Fig. 3.9b. In the absence of defects in a (111) surface both current responses are almost identical regardless of the mode of cooling, i.e. in air or in H_2-Ar mixture. This last point demonstrates the unique stability of the (111) ordered domains, which arises, presumably, because this has, amongst the low-index planes, the largest (6) two-dimensional Pt atom coordination number.

The current response for one of our electrodes is also shown in Fig. 3.10a; it was obtained after further annealing of the electrode at 1300°C for *ca.* 15 min. In this figure the current corresponding to adsorption of oxygen species is almost non-existent and only small additional currents pass due to hydrogen adsorption on the residual (110) and (100) defect sites at 0.11 V and 0.26 V, respectively. The mean charge between 0.06 V and 0.75 V is 302 μC cm^{-2}, or 237 μC cm^{-2} after subtracting the double-layer contribution.

In the case where there is an error in the procedure for cutting of the Pt (111) surface as shown in Fig. 3.10b, the thermal reordering procedure will not yield the right final UPD H profile. This is illustrated for a Pt single-crystal mis-oriented by about 3° to the (111) plane (Fig. 3.10b). In this case, subsequent flame annealing did not yield an increase in the charge for the unusual state nor a decrease in the magnitude of the current peaks at 0.11 V and 0.26 V which correspond to sites of the (110) and (100) geometries, respectively. Hence, the observation of these types of sites was not caused by surface roughness produced in the polishing procedure.

This technique of electrochemical monitoring of the thermal reordering is applicable to all crystallographic orientations of Pt single-crystals and is a useful tool for *in situ* sensitive characterization of the surfaces. It also gives information on both the amount and nature of species initially present on the surface (thermally adsorbed oxygen [58] as well as on the nature, amount and distribution of surface defects). Modification of the distribution of the platinum adsorption sites can be correctly monitored by

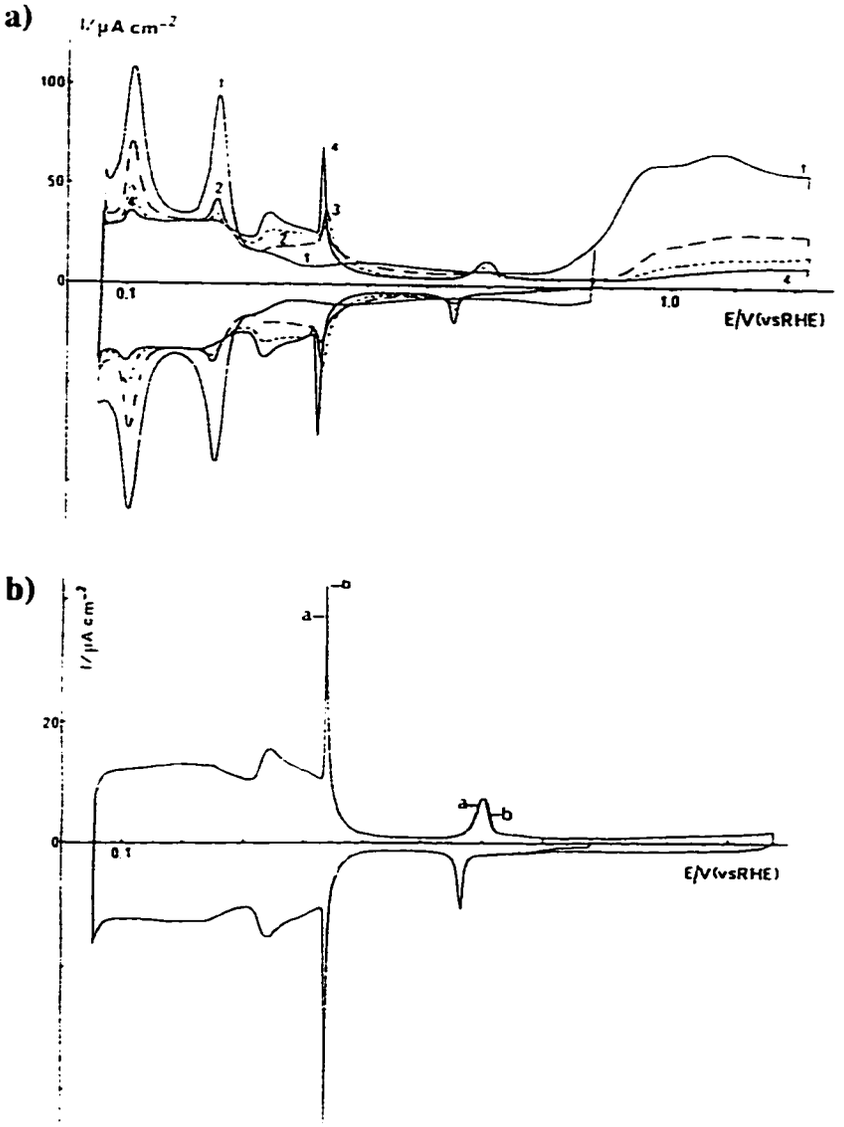

Fig. 3.9 a) Modification of the hydrogen and oxygen adsorption-desorption voltammetric profiles for various stages of annealing of a newly polished Pt(111) sample. Curve 1: Voltammogram of the electrode surface after decomtamination. Curves 2 and 3: After two successive annealings between 500 and 600°C for a few seconds. Curve 4: After annealing between 1300 and 1400°C for 10 s [58]; b) voltammograms of a fully ordered Pt(111) electrode surface after annealing for 15 min between 1300 and 1400°C. Curve a: After flame cleaning and cooling in a stream of a mixture of hydrogen and argon before isolation of the surface by a droplet of ultrapure water. Curve b: Sample cooled in air before water isolation. Sweep rate: 20 mV s^{-1} [58].

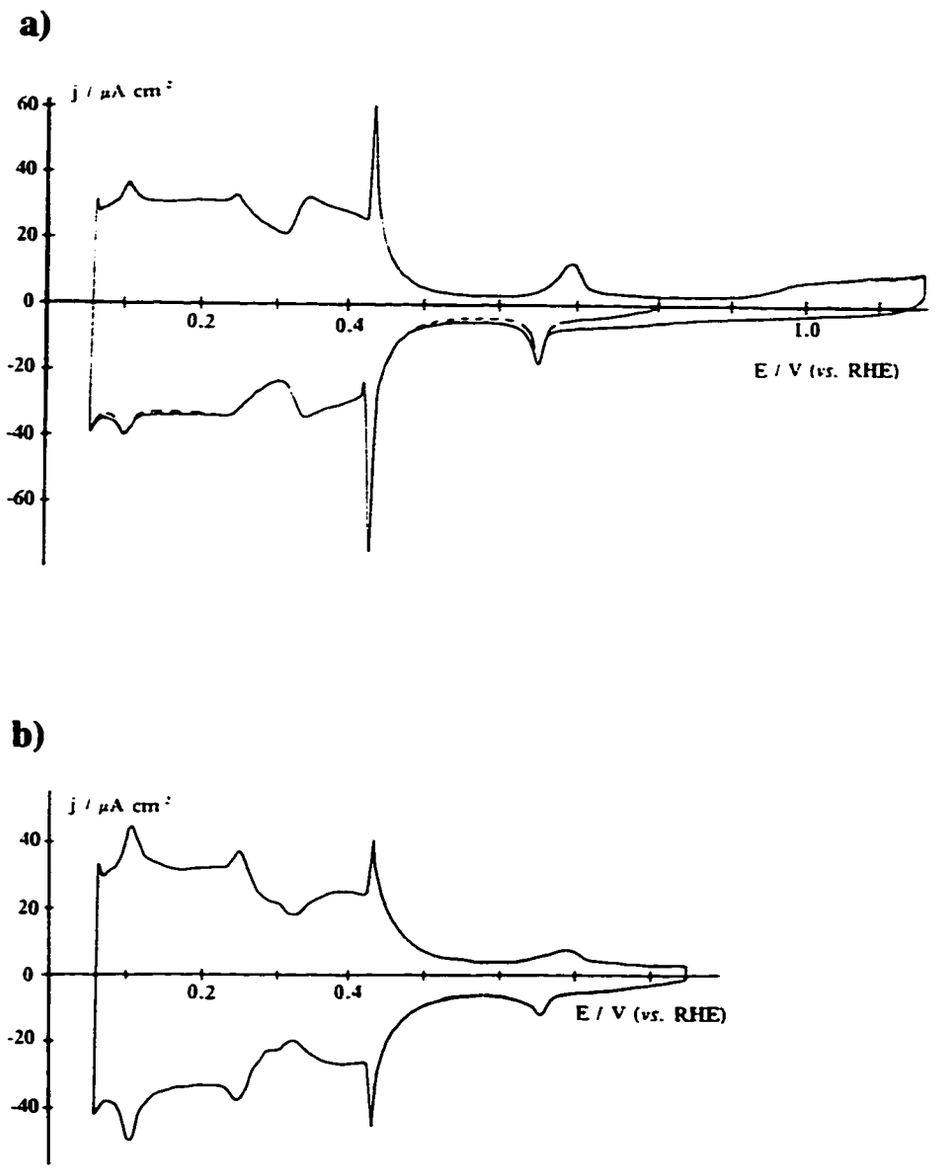

Fig. 3.10 a) Cyclic voltammogram for Pt(111) of Figs. 3.7 and 3.8 in contact with 0.5 mol dm^{-3} H_2SO_4 after further annealing at 1300°C for *ca.* 15 min; b) cyclic voltammogram for Pt(111) mis-oriented by about 3° of the (111) plane in contact with 0.5 mol dm^{-3} H_2SO_4 after monitoring of the thermal reordering (sweep rate 50 mV s^{-1}).

voltammetry particularly when such a modification leads to an increase of surface order [58].

3.2.2 "Finger printing" of the single-crystal electrode current response prior to electrocatalysis studies

In this thesis work, interest was directed to the investigation of electrocatalytic processes at single-crystal electrodes. Hence, the first step in such work is to ensure that the surface that will be investigated is well prepared. The usual method to characterize a Pt single-crystal electrode (outside a UHV system) after the initial annealing is to record the current response for that electrode in contact with an acidic solution and compare the current response and amount of charge passed during the deposition and stripping of UPD H with the literature values for the same experimental conditions. This gives a very good evaluation of the quality of the surface in terms of density of defects at the surface and the cleanliness of the solutions, as indicated in section 3.1.

The main goal at this point in such experiments is to obtain for the clean Pt planes in contact with the various electrolytes, the same CV shapes and total charges as those respectively reported in the literature by various authors for the same planes.

Table 3.2 gives the H UPD charge values determined for each of the faces investigated in this work, together with the literature sources of the reference data with which these results were compared, and the expected charges calculated from hard-sphere models. The latter allow the calculation of the density of sites, which is then converted into the corresponding charge for a monolayer of H adsorbed on those sites. These data provide the reference information required for discussion of results given in the next four chapters.

This Table shows that the CVs reported in this thesis, as obtained in the experimental work, are closely similar to those in the referenced publications (see Table 3.2) regarding form and details of the current-potential profile characteristic for each face; the corresponding UPD H charges will be discussed below.

3.2.2.1 Charge analysis for the cyclic voltammograms for Pt(111)

For Pt (111), the UPD charges (see Table 3.2) obtained from the curves in Fig.

3.10 and 3.11 are in good agreement with previously published results and also with calculated values [10,49,59]. As discussed in the previous section, two thirds of the UPD H charge corresponds to the H-adsorption region on the (111) hexagonal sites while the remaining charge that corresponds to one third of the calculated UPD charge, is most likely due to adsorbed bisulphate anions in Fig. 3.10 and adsorbed perchlorate or hydroxyl anions in Fig. 3.11 (see section 3.1.2).

Table 3.2 Measured and calculated UPD charges for the various Pt single-crystal surfaces studied

Pt surface (Miller index)	Supporting electrolyte	UPD H charge / μC cm^{-2} Experimental (± 3%)	Literature	Calculated
(111)	0.5 mol dm^{-3} H_2SO_4	237 (Fig. 3.10a)	240 [10]	243 [7]
	0.1 mol dm^{-3} $HClO_4$	239 (Fig. 3.11)	249 [59] 243 [49]	
(100)	0.5 mol dm^{-3} H_2SO_4	215* (Fig. 3.12 inset) 217** (Fig. 3.12)	214*,** [60] 205-215 [8,10,12c,49] 217** [60]	209 (1x1) [10]
	0.1 mol dm^{-3} $HClO_4$	253** (Fig. 3.13)	258** [10] 255** [60]	258 (5x20) [10]
(110)	0.5 mol dm^{-3} H_2SO_4	206* (Fig. 3.14 inset) 217** (Fig. 3.14)	220* [7] 199 [12b] 218*,** [61]	148 (1x1) [61]
	0.1 mol dm^{-3} $HClO_4$	201** (Fig. 3.15)	180-190 [12b,18] 166** [62]	222 (1x2) [61]
(311)	0.5 mol dm^{-3} H_2SO_4	252** (Fig. 3.16a)	251.6 [10,56] 245 [49]	251.9 [49]
	0.1 mol dm^{-3} $HClO_4$	248** (Fig. 3.16b)	212 [49]	

* flame-treated surface cooled down in air
** flame-treated surface cooled down in Ar-H_2 mixture

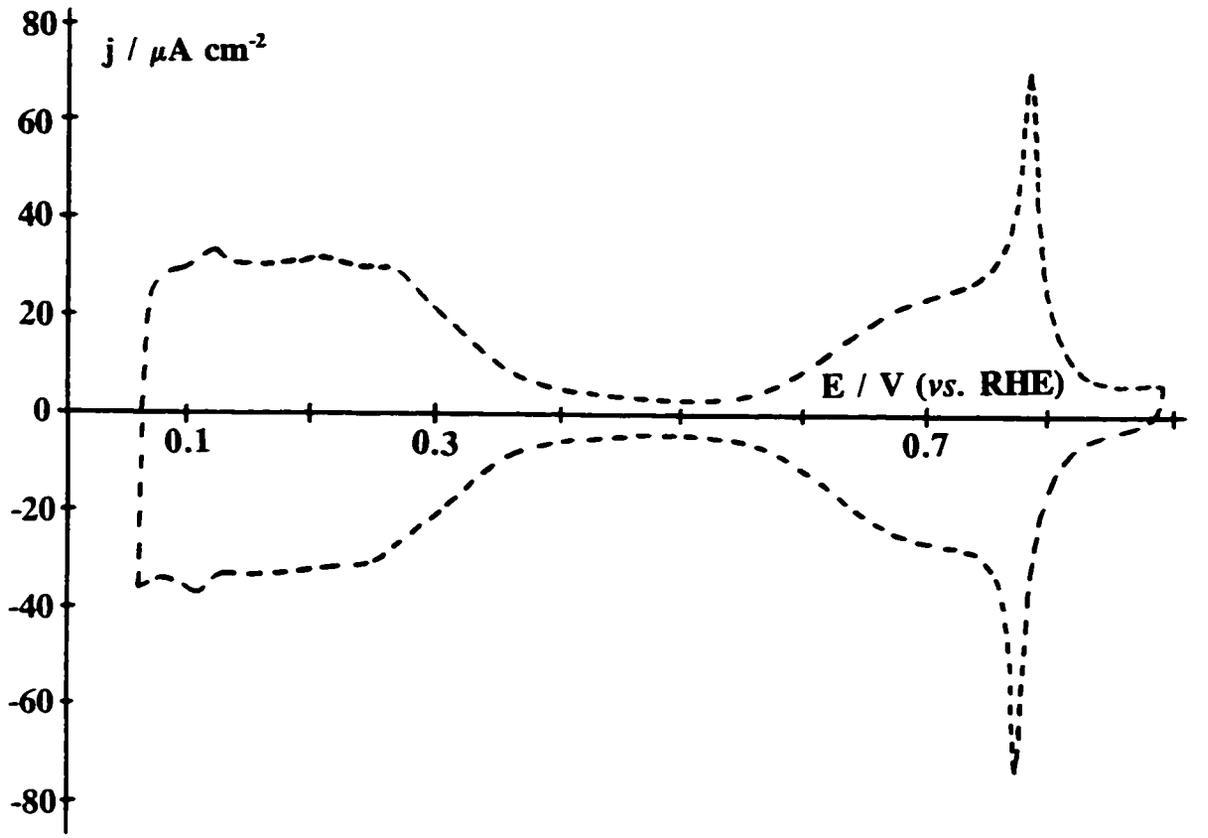

Fig. 3.11 Cyclic voltammogram obtained for flame-treated Pt(111) after cooling in air in contact with a 0.1 mol dm^{-3} aqueous $HClO_4$ solution.

3.2.2.2 Charge analysis for the cyclic voltammograms for Pt(100)

Similarly to the properties of Pt(111), the (100) surface also displays long-range ordering [10]. However, contrarily to Pt(111), the (100) surface is very sensitive to conditions of surface preparation [8b] (see Fig. 3.6b). Moreover, it was shown that a Pt(100), perturbed by a few cycles of oxygen adsorption-desorption, can be restored (in 0.5 mol dm^{-3} H_2SO_4) to its initial state using a fast cycling electrochemical procedure [10]. Other authors [12c,13a,18,63] have also reported unusual adsorption states in 0.1 mol dm^{-3} $HClO_4$ for a H_2-O_2 flame cleaned Pt (100) surface.

It was reported that the various voltammetric profiles in H_2SO_4 [10,13b] gave nearly the same capacitive charge; hence possible surface geometry assignment from the voltammetry alone is rendered difficult, since both are nearly equal to the charge evaluated for a (1x1) structure [10,60]. However, since the current response profile of the Pt(100) cooled in H_2-Ar mixture or to which a fast cycling procedure was applied, displayed the most developed unusual states and hence long-range ordering, these surfaces are believed to be the more ordered compared with those resulting from the cooling-in-air procedure.

However, this is not that simple; for example in the UHV-electrochemical transfer experiment of Aberdam *et al.* [64], a UHV-prepared (100) surface gave a (5x20) reconstructed structure while the post-electrochemical LEED pattern revealed structural changes to a (1x1) arrangement with good long-range ordering. According to Clavilier and co-workers [10] the electrochemical behaviour could have some similarities to what was observed for Pt(100) in the gas phase, where a clean (5x20) structure was observed to become converted to the (1x1) upon immersion of the hexagonal surface structure in water or electrolyte solutions as determined by *ex situ* electron diffraction [13b] as well as *in situ* x-ray diffraction studies [64].

This behaviour is not consistent, however, with the fact that the adsorption charge for the current-response profile is substantially increased by the presence in solution of anions being strongly adsorbed. From these observations Clavilier *et al.* [10] proposed that the Pt(100) surface could be stabilized by the anion adsorption and maintain an hexagonal or (5x20) surface structure. However, as pointed out by these authors, some

other explanation is then necessary to explain the unusually large charge measured for Pt(100) in $HClO_4$ [10].

In the case of our Pt(100) in 0.5 mol dm^{-3} H_2SO_4, the UPD H charge obtained for the flame-annealed surface cooled in air after two fast cycling procedures (see Fig. 3.12 inset, dashed trace) agrees with other published results [8,10,12c] and with the calculated UPD H charge for Pt(100) in a (1x1) structure. However, since the charges for the two curves recorded in the inset of Fig. 3.12 are almost identical, this assignment has to be made with some reservation.

In 0.1 mol dm^{-3} $HClO_4$, Pt(100) (see Fig.3.13) yields a UPD H charge which is greater by 22% than that obtained for Pt(100) in a (1x1) surface structure, which is consistent with previous published results [60]. As mentioned above, this behaviour is still not totally explained, since such an excess is not found when this electrode is in contact with H_2SO_4 solution. However, a similar charge was found using solutions containing chloride anions [59] and oxalate bi-anions [66] for Pt(100) cooled in air. The first cycle into the oxide region (up to 1.1 V) is also shown in Fig. 3.13 and it is in good agreement with previously published voltammograms [65].

Figure 3.12 shows an example for the same surface flame-annealed and cooled in H_2-Ar mixture; this procedure can yield charges as high as 235 $\mu C\ cm^{-2}$ and shows an increase of the ordering at the surface, *i.e.* the UPD region is displaced towards more positive potentials (see the CV for the same surface in Chapter 4, Fig. 4.5). This charge is larger than that calculated for a (1x1) surface *i.e.* 209 $\mu C\ cm^{-2}$ but smaller than that expected for a (5x20) reconstructed surface *i.e.* 258 $\mu C\ cm^{-2}$ [10].

A recent *in situ* STM study of a flame-treated Pt(100) cooled down in iodine vapour, followed by an exchange with CO, was performed in the presence of CO, CN^-, S^{2-} and I^- in the supporting electrolyte [67]. While no atomic resolution images of the CO and CN^- covered surfaces could be obtained reproducibly, S^{2-} and I^- yielded ordered overlayers on top of a Pt(100) (1x1) lattice [67]. However, no imaging of the Pt(100) surface is available under the conditions for which the CV's are reported in this thesis work.

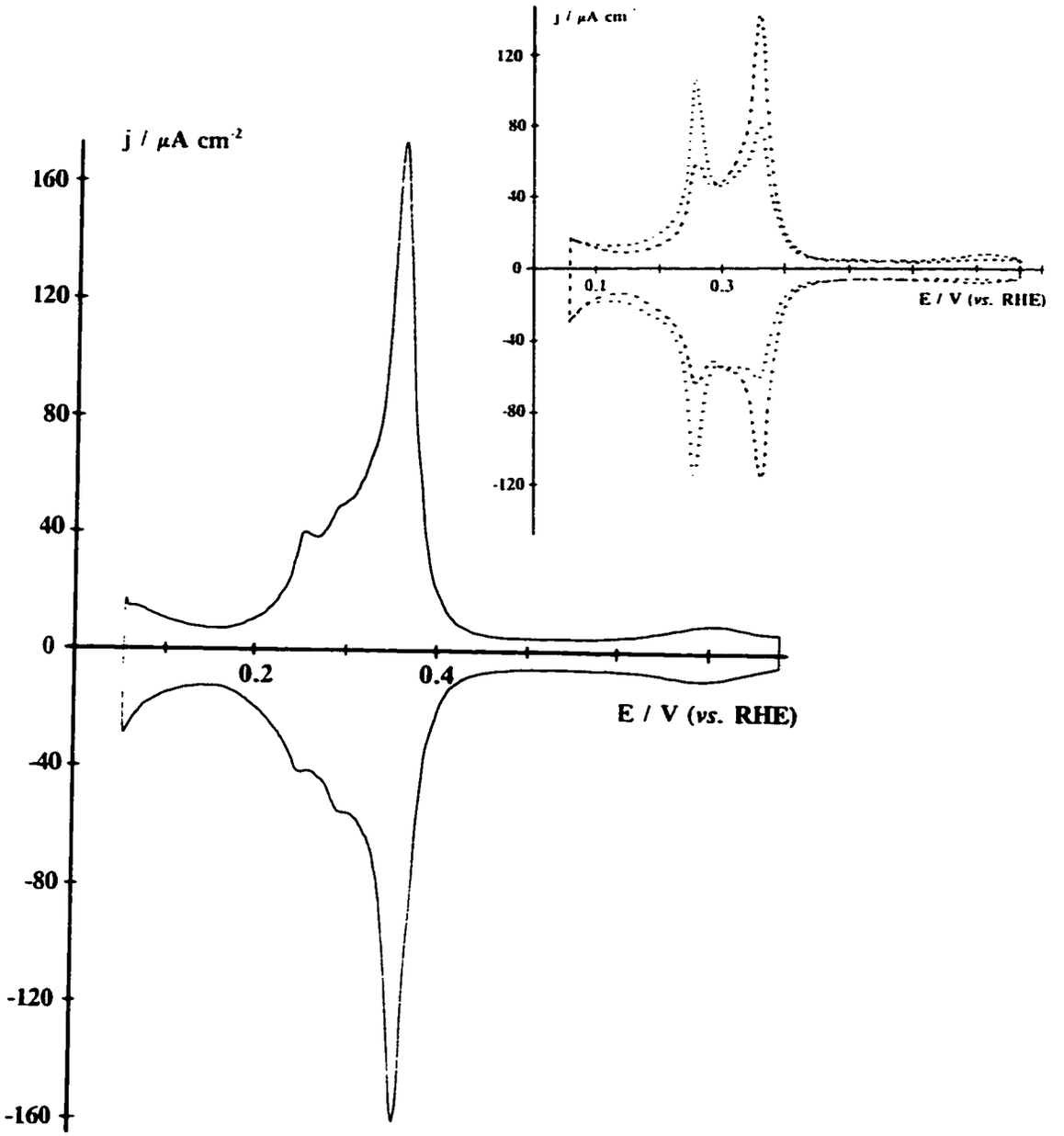

Fig. 3.12 Cyclic voltammogram obtained for a flame-treated Pt(100) after cooling in H_2 + Ar in 0.5 mol dm^{-3} H_2SO_4 solution. Inset: Cyclic voltammogram obtained in the same conditions but for a flame-treated Pt(100) after cooling in air (dotted trace) and the same surface after two fast cycling (100 V s^{-1}) up to *ca.* 1 V for 30 s (dashed trace).

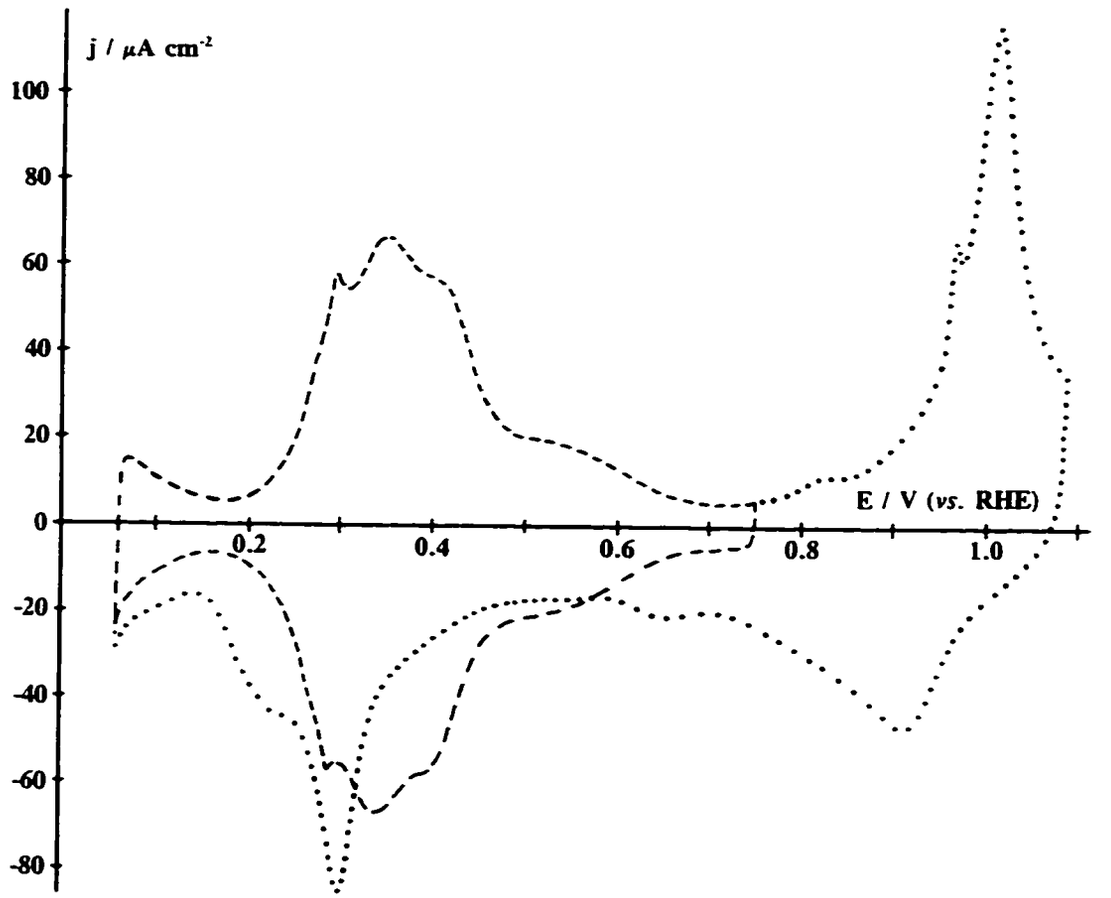

Fig. 3.13 Cyclic voltammogram obtained for flame-treated Pt(100) after cooling in H_2 + Ar in a 0.1 mol dm^{-3} $HClO_4$ solution, first cycle (between 0.75 and 0.06 V) (dashed trace), second cycle up to 1.1 V (dotted trace) and back to 0.06 V.

3.2.2.3 Charge analysis for the cyclic voltammograms for Pt(110)

Similarly to Pt(100), Pt(110) surfaces are also sensitive to the surface preparation; for instance Fig. 3.14 and its inset show the cyclic voltammetry current responses for a surface flame-treated and cooled in the H_2-Ar mixture and in air, respectively, in contact with 0.5 mol dm^{-3} H_2SO_4 solution. These results, reported here, are for an electrode cycled between 0.06 V and 0.80 V for *ca.* 5-10 cycles; in both cases the charges due to adsorbed species are 206 μC cm^{-2} and 217 μC cm^{-2}, respectively; both are in good agreement with those reported earlier [5,7,58,62,61,68,69]. It is to be noted here that unlike Pt(100) there is no known electrochemical treatment showing a clear transformation from one structure to another for Pt(110) [10].

These latter charges are found to be approximatively 1.5 times that corresponding to the atomic density of the topmost layer of the unreconstructed surface (0.92×10^{15} atom cm^{-2}) [61]. This electrochemical result suggested to the authors of ref. 61 that Pt(110) surfaces prepared following either of these procedures were reconstructed in acidic solution, where a (2x1) surface reconstruction was proposed. This missing row model accounted for the charge value considering octahedral sites for H adsorption. The differences then observed in voltammetric current profiles (Fig. 3.14 and inset) could be associated with differences in the distribution of reconstructed domains [61].

Unlike the other two surfaces discussed so far, Pt(110) often displays a third UPD desorption peak [61,68]. This is similar to what is often observed for polycrystalline Pt in the same solution at *ca.* 200 mV [70]. However, in the case of Pt(110) this peak tends to disappear after a few cycles in the UPD region (note that this peak is visible only in the inset of Fig. 3.14). From careful control of the surface preparation and monitoring of the charge for H adsorption and oxide formation (first cycle), it was proposed [61] that the appearance of the third adsorbed H oxidation peak occurs only when (110) surface domains are of a minimum size. Conversely, using stepped surfaces having (110) sites for the steps and by varying the length of the terrace made of (111) or (100) sites, it was found [61] that the third adsorbed H oxidation peak was observed only when the (110) domains were not far apart from each other.

Two recent *in situ* STM studies investigated the structure of Pt(110) in contact

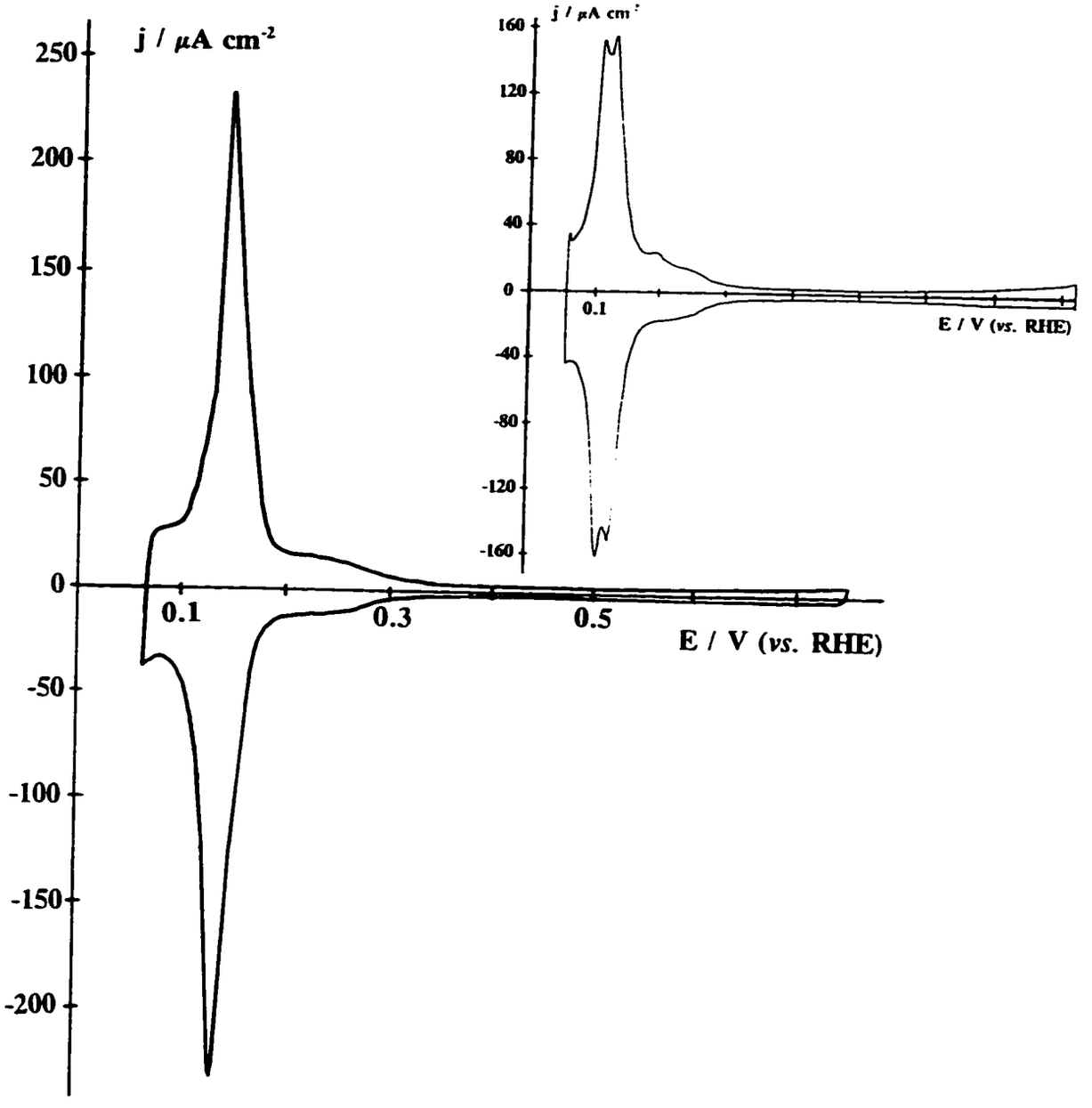

Fig. 3.14 Cyclic voltammogram obtained for a flame-treated Pt(110) after cooling in H_2 + Ar in a 0.5 mol dm^{-3} H_2SO_4 solution. Inset: Under the same conditions, cyclic voltammogram for a Pt(110) cooled in air.

with H_2SO_4 solution, amongst other systems [71,72]. The authors of the first study [71] reported the structure of a flame-annealed Pt(110) cooled in iodine vapour, following the removal of the adsorbed I layer: an unreconstructed (1x1) surface was observed [71].

The other STM study [72] showed that the (1x2) missing-row reconstructed surface topography was formed during flame annealing but was lifted during cooling down or during immersion of the sample into the electrolyte H_2SO_4, in this case, at the open-circuit potential. The (1x2) missing-row reconstructed surface has also been observed for a clean Pt(110) in a vacuum environment [73]. However, these observations do not explain the fact that two different current responses result from the cooling procedure (see Fig. 3.14).

In this section, the current response for Pt(110) in contact with 0.1 mol dm^{-3} $HClO_4$ is also included, and yielded an UPD charge of 201 $\mu C\ cm^{-2}$ (Fig. 3.15). This CV is again in good agreement with other published results; for example, in ref. 61 the authors reported a similar curve. Nervertheless, our CV displays some differences from that previously reported: on the cathodic scan there is a splitting of the UPD peak at *ca.* 110 mV (see Fig. 3.15) and the first cycle in the oxide region shown in Fig. 3.15 is also somewhat different: a shoulder is visible on the main anodic peak while the ratio of the current maxima of the two smaller peaks at 800 mV and 900 mV, are opposite to what is reported in ref. 61.

3.2.2.4 Charge analysis for the cyclic voltammograms for Pt(311)

Finally, the UPD H charges measured between 0.06 and 0.60 V for Pt (311) in contact with 0.5 mol dm^{-3} H_2SO_4 (Fig. 3.16a for CV) and with 0.1 mol dm^{-3} $HClO_4$ (Fig. 3.16b for CV) were found to be in very good agreement with the value previously reported [48,53] and obtained after the same thermal and cooling (Ar + H_2) procedure, *viz.* 252 $\mu C\ cm^{-2}$ and 248 $\mu C\ cm^{-2}$, respectively. An interesting feature of this surface is that the charge associated with adsorption on the steps and the terrace are the same *i.e.* 126 $\mu C\ cm^{-2}$. However, anion co-adsorption could occur in the UPD H potential region around 375 mV. This point will be discussed further in the next section.

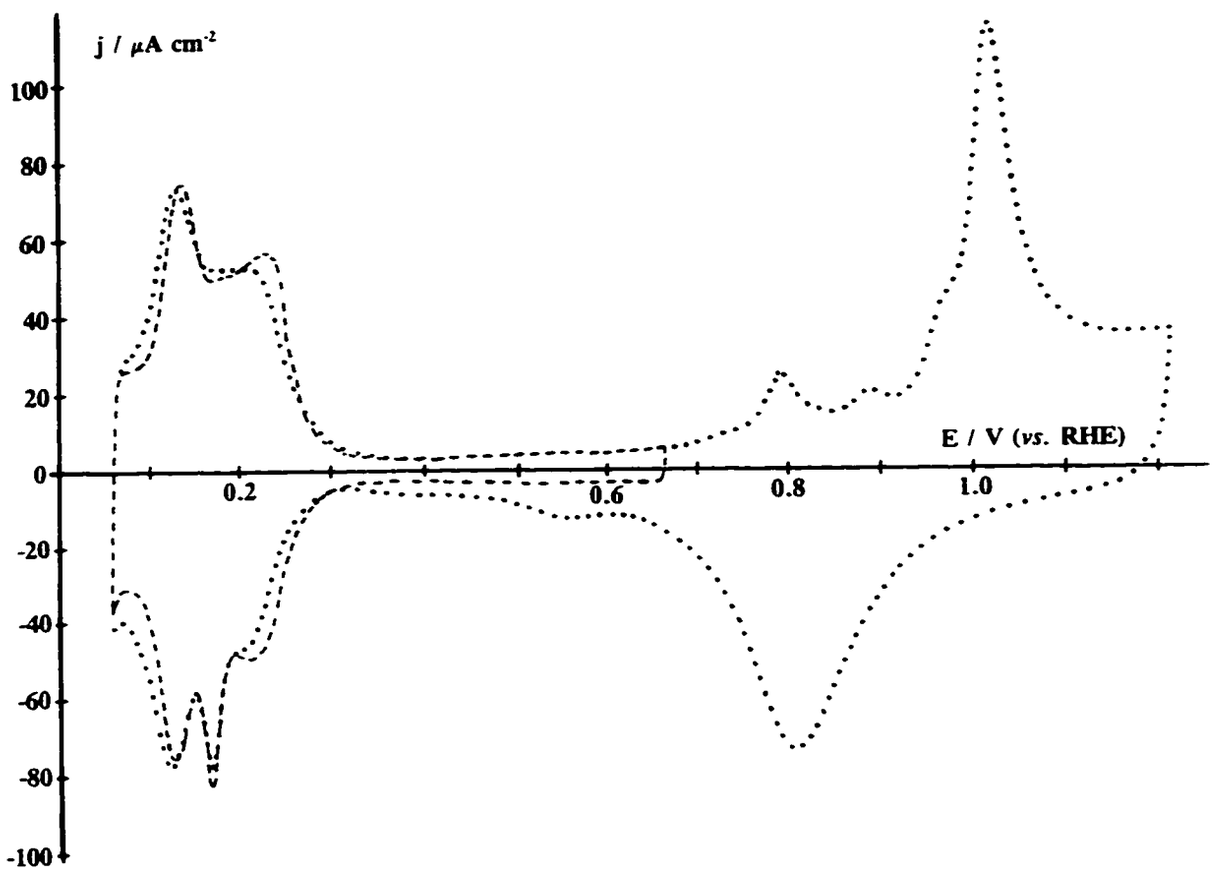

Fig. 3.15 Cyclic voltammogram obtained for flame-treated Pt(110) after cooling in H_2 + Ar in 0.1 mol dm^{-3} $HClO_4$ solution, first cycle between 0.67 and 0.06 V (dashed trace); second cycle recorded up to 1.2 V shows the effect of the adsorption-desorption of oxygen on the UPD region (dotted trace).

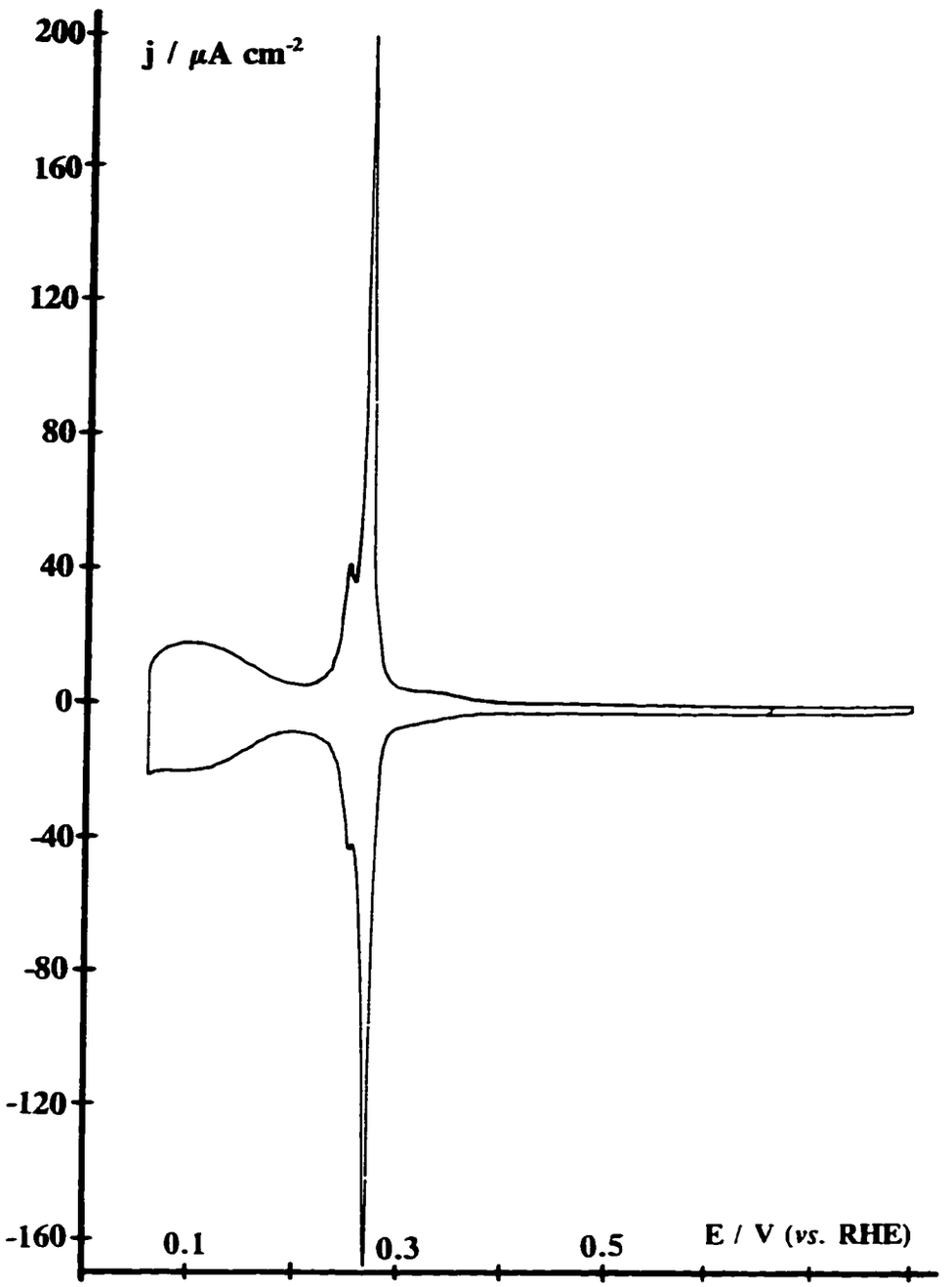

Fig. 3.16 a) Cyclic voltammogram obtained for flame-treated Pt(311) after cooling in Ar + H_2 in a 0.5 mol dm^{-3} H_2SO_4 solution.

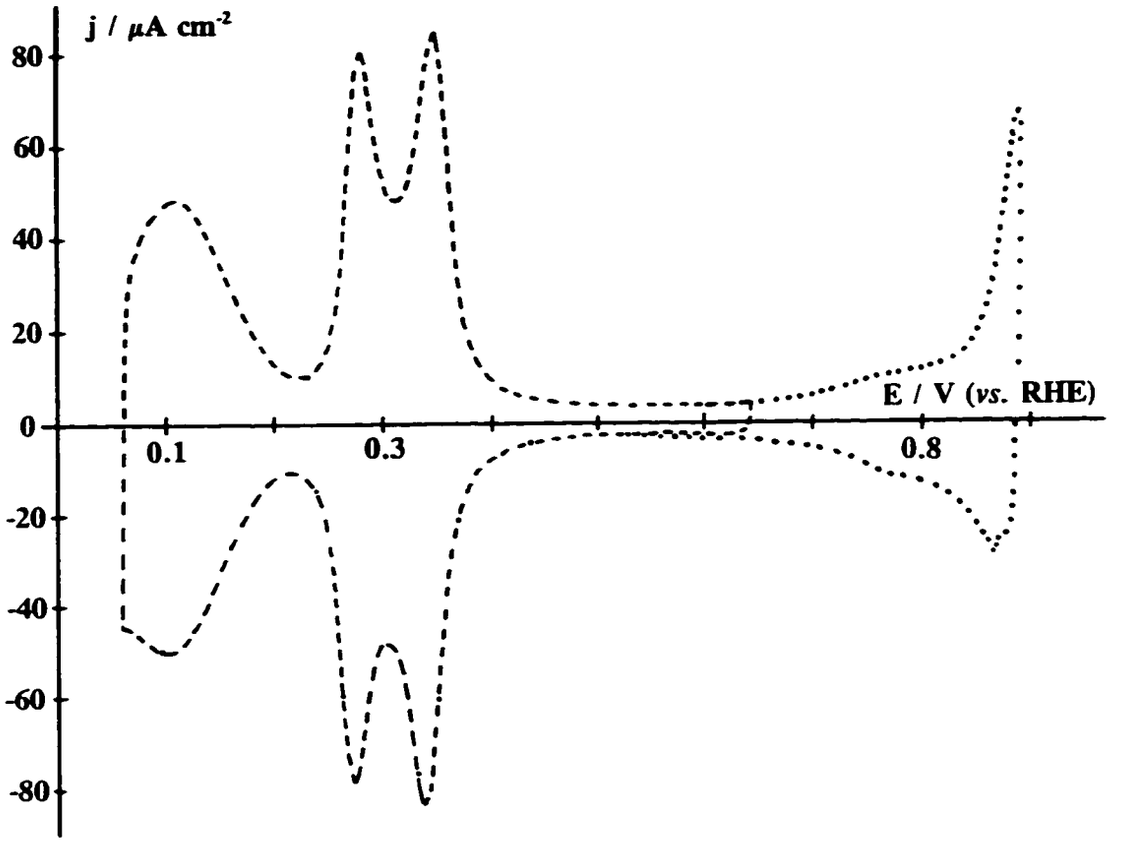

Fig. 3.16 b) Cyclic voltammogram for flame-treated Pt(311) after cooling in Ar + H_2 mixture in a 0.1 mol dm^{-3} $HClO_4$ solution (dashed trace); the dotted trace corresponds to the current response for cycling the surface up to 0.9 V and its little effect on the current response in the UPD region.

3.2.3 Adsorption replacement technique

As mentioned in section 3.1.2, this technique using CO as a surface probe was recently reported [38-40,43], and allowed determination of the nature of the species present in the interfacial region as a function of potential.

The experimental strategy, discussed in section 3.2.1, was employed to evaluate the amounts of H and anions present at a Pt(311) surface in contact with 0.5 mol dm^{-3} H_2SO_4. This information was needed in order to evaluate and help assign the identity of the electron transfer processes, the rates of which were measured using impedance spectroscopy, to either H or anion adsorption (see Chapters 4 and 5).

As discussed earlier, the current transient resulting from displacement of the initially adsorbed H or the anion by adsorbed CO can yield information on the nature of these species: that is, the displacement of hydrogen by CO will induce an *anodic* transient while that of anions will induce a *cathodic* current independently, however, of their location at the surface. In this process, adsorbed CO will decrease considerably the value of the double-layer capacitance as well as displace less strogly adsorbed species. Moreoever, it was shown in ref. 43 that CO acted as a neutral probe under these experimental conditions.

The voltammetric profile of the flame-treated Pt(311) cooled in H_2 - Ar mixture was discussed in the previous section 3.2.2.4 and it is shown again in Fig. 3.17. Additionally, this figure also gives the voltammogram recorded for the surface blocked with adsorbed CO and that recorded after CO oxidation. Contrary, to its behaviour at the three low index planes, CO adsorption and/or CO oxidation has an irreversible effect on the voltammogram. Hence, the flame-treatment and cooling procedure needed to be performed between each transient.

Using eq. 3.1, direct comparison between the charge density obtained from the voltammogram (Fig. 3.18, solid line) and that from the current transient resulting from CO adsorption (q_T) can be made (see Fig. 3.18). For the sake of comparison with the result of ref. 39, the integration origin for the voltammogram is taken at $E_{0.075V}$. From Fig. 3.18 good agreement is found between the two ways of determining the total charge passed at the interface between $E_{0.075V}$ and any value E_{ads}. This indicates that the

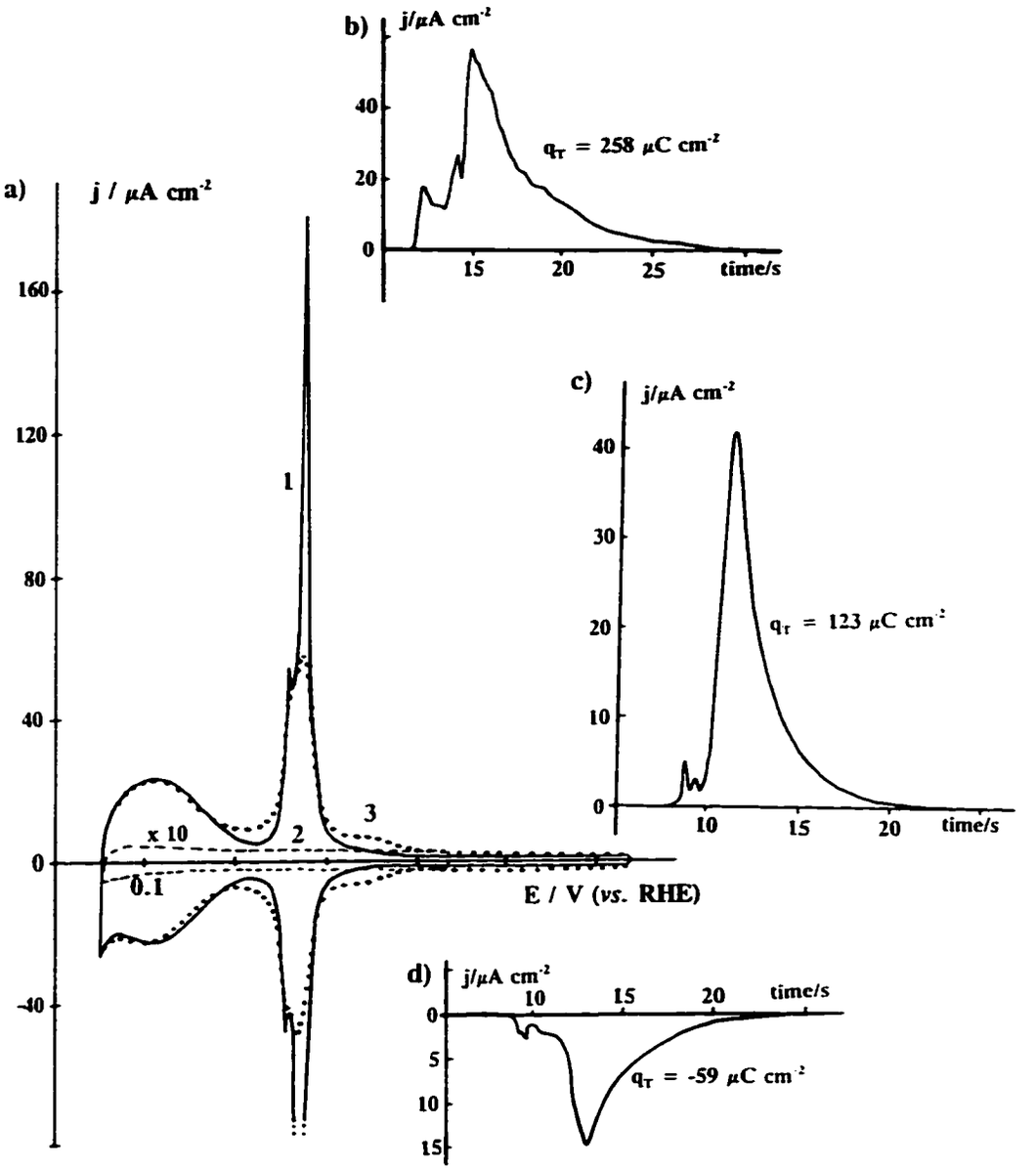

Fig. 3.17 a) Curve 1: Voltammogram for a flame-treated Pt(311) cooled down in H_2-Ar atmosphere in contact with 0.5 mol dm^{-3} H_2SO_4 (20 mV s^{-1}); curve 2: control of the surface blocking by adsorbed CO (20 mV s^{-1}, sensitivity increased x10); curve 3: cyclic voltammogram after stripping of adsorbed CO (20 mV s^{-1}). b), c) and d): Current transients for E_{ads} = 0.075, 0.25 and 0.4 V, respectively.

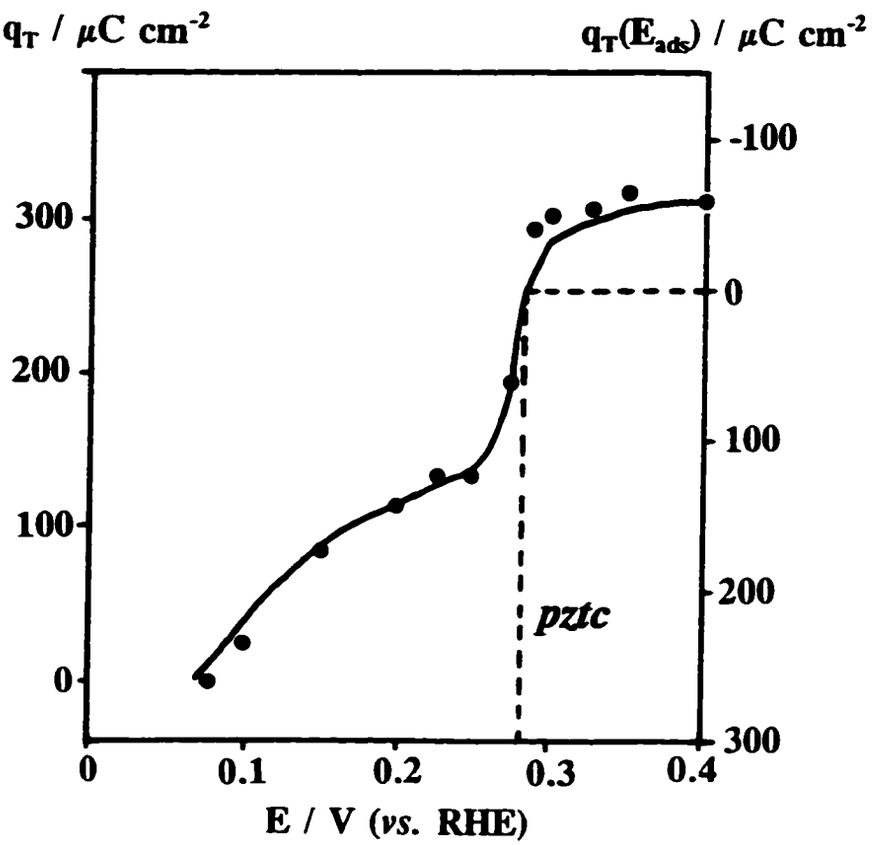

Fig. 3.18 Plot of the charge densities obtained from the integration of the voltammogram (solid line) and those obtained from transient charge differences (q_T, see eq. 3.1) versus the electrode potential for Pt(311) cooled in H_2-Ar atmosphere (see also Fig. 3.17).

modification in the voltammogram following CO oxidation has little effect on the recorded charge and that it must arise during CO oxidation rather than CO adsorption.

The curve for q_T *versus* potential also allows the estimation of the *pztc* [74]; this value is indicated in Fig. 3.18 by the intercept of the curve with $q_T(E_{ads}) = 0$ on the horizontal axis.

CO adsorption transients were also recorded at the surface discussed in the previous section in contact with 0.5 mol dm^{-3} H_2SO_4 solution. Essentially identical results were obtained for the transient charge to those reported by Clavilier and co-workers [39]. For example, at a Pt(111) surface a total cathodic transient of -92 $\mu C\ cm^{-2}$ corresponding to anion adsorption was recorded at $E_{ads} = 0.5$ V (an identical value is reported in ref.39), while at $E_{ads} = 0.08$ V an anodic H displacement transient of 164 $\mu C\ cm^{-2}$ was recorded (*versus* 161 $\mu C\ cm^{-2}$ in ref. 39). This is consistent with the situation where, at potentials less positive then 0.3 V, the surface is covered by H with a maximum coverage corresponding to 2/3 of an H monolayer and, at potentials positive to this value, anions (HSO_4^- in this case) are being adsorbed corresponding to 1/3 of the UPD total charge.

In the present work, agreement with previous results was found for Pt(100) where a maximum cathodic CO adsorption transient of -59 $\mu C\ cm^{-2}$ was recorded at $E_{ads} = 0.45$ V (*vs.* -57 $\mu C\ cm^{-2}$ [39]). As concluded by Clavilier *et al.* [39], adsorption of anions is most important in terms of the amount of charge transferred on Pt(111) (*ca.* -92 $\mu C\ cm^{-2}$) while, for the other faces flame-treated and cooled in H_2 - Ar mixture, the integrated cathodic charge transients give very similar values (around -60 $\mu C\ cm^{-2}$). An interesting point to be mentioned about Pt(110) is that anodic transients (for H desorption) of *ca.* 140 $\mu C\ cm^{-2}$ at 0.1 V were recorded for both types of surface treatment (cooled in air or in Ar - H_2); this tends to indicate that both surface treatments yield an unreconstructed surface assuming a (1x1) surface structure with one hydrogen atom per supposed heptacoordinated surface atom [39]. The usefulness of these results will be emphasised in Chapters 4 and 5.

3.3 Summary of conclusions from the above review that are more relevant to the present work

Although several years have passed since the first CV's were reported for well-ordered Pt single-crystal surfaces [7-9], there remains a number of questions unanswered concerning the possible reconstruction of Pt(110) and (100) surfaces as well as the coordination of H and anions on these surfaces. This is mainly due to the more complex behaviour of these surfaces in comparison with that of Pt(111), which shows remarkable stability towards thermally adsorbed oxygen and electrochemically formed oxide layers that are formed at potentials positive to 1.2 V *vs.* RHE.

For the purposes of interpretation of new results that have arisen in the course of the present thesis project, the following experimental observations, reported in the literature discussed in detail above, will be accepted:

a) In the UPD of H region, the Pt(111) surface in contact with 0.5 mol dm^{-3} H_2SO_4 is covered at potentials less positive than 325 mV by 2/3 of a monolayer of adsorbed H, while at potentials more positive than this limit it is covered by 1/3 of a monolayer of adsorbed HSO_4^-. In $HClO_4$, the "unusual adsorption states" are displaced to more positive potentials and could be arising from adsorption of ClO_4^-, or even OH^-.

b) In the case of Pt(100), only data for the surface preparations involving the flame-treatment followed by the cooling in the H_2-Ar mixture will be utilized, since this procedure yields a more ordered surface exhibiting long-range ordering. Anion adsorption also occurs on this surface in both H_2SO_4 and $HClO_4$ solutions, but it arises to a lesser extent in comparison with the other two low-index planes. No reference will be given in this work with regard to the actual structure of this surface, since no means of imaging of the Pt(100) surfaces was available under the conditions for which the CV's are reported in this Chapter and the subsequent ones.

c) Similarly to Pt(100), the Pt(110) and (311) surfaces were prepared in the present work using the cooling procedure (H_2-Ar) which prevents the formation of adsorbed oxygen species; again it is believed this procedure gives rise to "unreconstructed" surfaces. However, as discussed above in the case of Pt(110), there is the possibility that both cooling procedures, in fact, yield the same surface geometry.

References

1. F.G. Will, J. Electrochem. Soc., 112 (1965) 451.
2. H. Angerstein-Kozlowska, W.B.A. Sharp and B.E. Conway in M.W. Breiter (ed.) Proc. of the Symposium on Catalysis, The Electrochemical Society Inc., Princeton, N.J., 1974, p. 94.
3. a) R.M. Ishikawa and A.T. Hubbard, J. Electroanal. Chem., 69 (1976) 317; b) A.T. Hubbard, R.M. Ishikawa and J. Katekaru, J. Electroanal. Chem., 86 (1978) 271.
4. a) W.E. O'Grady, M.Y. C. Woo, P.L. Hagans and E. Yeager, J. Vac. Sci. Technol., 14 (1977) 365; b) E. Yeager, W.E. O'Grady, M.Y.C. Woo and P.L. Hagans, J. Electrochem. Soc., 125 (1978) 348; c) E. Yeager, W.E. O'Grady, B.D. Cahan and D. Scherson, J. Vac. Sic. Technol., 20 (1982) 628.
5. K. Yamamoto, D.M. Kolb, R. Kötz and G. Lehmpfuhl, J. Electroanal. Chem., 96 (1979) 233.
6. a) P.N. Ross, J. Electroanal. Chem., 126 (1979) 67; b) *ibid*, Surf. Sci., 102 (1981) 463.
7. J. Clavilier, R. Faure, G. Guinet and R. Durand, J. Electroanal. Chem., 107 (1980) 205.
8. a) J. Clavilier, R. Durand, G. Guinet and R. Faure, J. Electroanal. Chem., 127 (1981) 281; b) J. Clavilier, D. Armand and B.L. Wu, J. Electroanal. Chem., 135 (1982) 159.
9. J. Clavilier, J. Electroanal. Chem., 107 (1980) 211.
10. J. Clavilier, A. Rodes, K. El Achi and M.A. Zamakhchari,J. Chim. Phys., 88 (1991) 1291.
11. D. Aberdam, C. Corotte, D. Dufayard, R. Durand, R. Faure and G. Guinet, Le vide, les couches minces (Suppl. Proc. 4th Int. Conf. Solid Surfaces, Cannes) 1980, p. 622.
12. a) C.L. Scortichini and C.N. Reilley, J. Electroanal. Chem., 139 (1982) 233; b) C.L. Scortichini and C.N. Reilley, *ibid*, 139 (1982) 247; c) C.L. Scortichini, F.E. Woodward and C.N. Reilley, *ibid*, 139 (1982) 265.

13. a) F.T. Wagner and P.N. Ross, J. Electroanal. Chem., 150 (1983) 141; b) F.T. Wagner and P.N. Ross, *ibid*, Surf. Sci., 160 (1985) 305.
14. A.S. Homa, E. Yeager and B.D. Cahan, J. Electroanal. Chem., 150 (1983) 181.
15. S. Motoo and N. Furuya, J. Electroanal. Chem., 172 (1984) 339.
16. D. Aberdam, R. Durand, R. Faure and F. El Omar, Surf. Sci., 171 (1986) 303.
17. K. Itaya, S Sugawara, K. Sashikata and N. Furuya, J. Vac. Sci. Technol. A, 8 (1990) 515.
18. F.H. Feddrix, E.B. Yeager and B.D. Cahan, J. Electroanal. Chem., 330 (1992) 419.
19. a) D.A. Scherson and D.M. Kolb, J. Electroanal. Chem., 176 (1984) 353; b) K. Al-Jaaf-Golze, D.M. Kolb and D. Scherson, J. Electroanal. Chem., 200 (1986) 353.
20. a) F. Wagner and P.N. Ross, J. Electroanal. Chem., 250 (1988) 301; b) P.N. Ross, J. Chim. Phys., 88 (1991) 1353.
21. M. Markovic, M. Hanson, G. McDougall and E. Yeager, J. Electroanal. Chem., 214 (1986) 555.
22. a) D.J. Campbell and R.M. Corn, J. Phys. Chem., 92 (1988) 5796; b) M.L. Lynch and R.M. Corn, J. Phys. Chem., 94 (1990) 4382; c) M.L. Lynch, B.J. Barner and R.M. Corn, J. Electroanal. Chem., 300 (1991) 447.
23. R.F. Lane and A.T. Hubbard, J. Phys. Chem., 79 (1975) 808.
24. D. Zurawski, L. Rice, M. Hourani and A. Wieckowski, J. Electroanal. Chem., 230 (1987) 221.
25. H. Ebert, R. Parsons, G. Ritzoulis and T. Vandernoot, J. Electroanal. Chem., 264 (1986) 181.
26. a) A. Wieckowski, P. Zelenay and K. Varga, J. Chim. Phys., 88 (1991) 1247; b) M.E. Gamboa-Aldeco, E. Herrero, P.S. Zelanay and A. Wieckowski, J. Electroanal. Chem., 348 (1993) 451.
27. a) H. Angerstein-Kozlowska, B.E. Conway, A. Hamelin and L. Stoicoviciu, Electrochim. Acta, 31 (1986) 1051; b) *ibid*, J. Electroanal. Chem., 228 (1987) 429.

28. F.V. Molina and R. Parsons, J. Chim. Phys., 88 (1991) 1339.

29. a) K. Kunimatsu, M.G. Samant, H. Seki and M.R. Philpott, J.Electroanal. Chem., 243 (1988) 203; b) K. Kunimatsu, M.G. Samant and H. Seki, *ibid*, 258 (1989) 163; c) K. Kunimatsu, M.G. Samant and H. Seki, *ibid*, 272 (1988) 185; d) M.G. Samant, K. Kunimatsu, H. Seki and M.R. Philpott, *ibid*, 280 (1990) 391.

30. F.C. Nart and T. Iwasita, J. Electroanal. Chem., 322 (1992) 289.

31. P. Faguy, N. Markovic, R. Adzic, C. Fieiro and E. Yeager, J. Electroanal. Chem., 289 (1990) 245.

32. a) F.C. Nart, T. Iwasita and M. Weber, Electrochim. Acta, 39 (1994) 961 and 2093; b) T. Iwasita, F.C. Nart, A. Rodes, E. Pastor and M. Weber, Electrochim. Acta, 40 (1994) 53.

33. R.R. Adzic, F. Feddrix, B.Z. Nikolic and E. Yeager, J. Electroanal. chem., 341 (1992) 287.

34. H. Ogasawara, Y. Sawatari, J. Inukai and M. Ito, J. Electroanal. Chem., 358 (1993) 337.

35. R. Michaelis, M.S. Zhai and D.M. Kolb, J. Electroanal. Chem., 339 (1992) 299.

36. P.W. Faguy, N.S. Marinkovic and R.R. Adzic, Langmuir, 12 (1996) 243.

37. Y. Shingaya and M. Ito, J. Electroanal. Chem., 372 (1994) 283.

38. J. Clavilier, R. Albalat, R. Gomez, J.M. Orts, J.M. Feliu and A. Aldaz, J. Electroanal. Chem., 330 (1992) 489.

39. a) J.M. Feliu, J.M. Orts, R. Gomez, A. Aldaz and J. Clavilier, J. Electroanal. Chem., 372 (1994) 265; b) J. Clavilier J.M. Orts, R. Gomez, J.M. Feliu and A. Aldaz, Proceedings of the symposium on "Electrochemistry and Materials Science of Cathodic Hydrogen Absorption and Adsorption", (eds. B.E. Conway and G. Jerkiewicz) The Electrochem. Soc. Inc., New Jersey, Vol. 94-21, 1994, p.167.

40. J.M. Orts, R. Gomez, J.M. Feliu, A. Aldaz and J. Clavilier, Electrochim. Acta, 39 (1994) 1519.

41. W. Savich, S.-G. Sun, J. Lipkowski and A. Wieckowski, J. Electroanal. Chem., 388 (1995) 237.

42. a) B.E. Conway, B. MacDougall and H. Angerstein-Kozlowska, J. Chem. Soc., Faraday Trans. I, 68 (1972) 1566; b) *ibid*, J. Electroanal. Chem., 32 (1971) 477.
43. J. Clavilier, R. Albalat, R. Gomez, J.M. Orts and J.M. Feliu, J. Electroanal. Chem., 360 (1993) 325.
44. B. Love, K. Seto and J. Lipkowski, J. Electroanal. Chem., 199 (1986) 219.
45. J. Clavilier, D. Armand, S.-G. Sun, and M. Petit, J. Electroanal. Chem., 205 (1986) 267.
46. a) R.R. Adzic, A.V. Tripkovic and V.B. Vesovic, J. Electroanal. Chem., 204 (1986) 329; b) A.V. Tripkovic and R.R. Adzic, *ibid*, 205 (1986) 335.
47. B. Love, K. Seto and J. Lipkowski, Rev. Chem. Intermediates, 8 (1987) 87.
48. S. Motoo and N. Furuya, Ber. Bunsenges. Phys. Chem., 91 (1987) 457.
49. N.M. Markovic, N.S. Marinkovic and R. Adzic, J. Electroanal. Chem., 241 (1988) 309.
50. R. Parsons and G. Ritzoulis, J. Electroanal. Chem., 318 (1991) 1.
51. N.M. Markovic, N.S. Marinkovic and R.R. Adzic, J. Electroanal. Chem., 314 (1991) 289.
52. J. Clavilier and A. Rodes, J. Electroanal. Chem., 348 (1993) 247.
53. A. Rodes and J. Clavilier, J. Electroanal. Chem., 344 (1993) 269.
54. M. Boudart, J. Am. Chem. Soc., 72 (1952) 3566.
55. D.W. Blakely and G.A. Somorjai, Surf. Sic., 30 (1972) 440.
56. A. Rodes, K. El Achi, M.A. Zamakhchari and J. Clavilier, J. Electroanal. Chem., 284 (1990) 245.
57. J. Clavilier, K. El Achi and A. Rodes, Chem. Phys., 141 (1990) 1.
58. J. Clavilier, K. El Achi, M. Petit, A. Rodes and M.A. Zamakhchari, J. Electroanal. Chem., 295 (1990) 333.
59. D. Armand and J. Clavilier, J. Electroanal. Chem., 270 (1989) 331.
60. A. Rodes, M.A. Zamakhchari, K. El Achi, J. Clavilier and A. Rodes, J. Electroanal. Chem., 305 (1991) 115.
61. R. Gomez and J. Clavilier, J. Electroanal. Chem., 354 (1993) 189.
62. D. Armand and J. Clavilier, J. Electroanal. Chem., 263 (1989) 109.

63. F. El Omar and R. Durand, J. Electroanal. Chem., 178 (1984) 343.
64. D. Aberdam, S. Traore, R. Durand and R. Faure, Surf. Sci., 180 (1987) 317.
65. I.M. Tidswell, N.M. Markovic and P.N. Ross, Phys. Rev. Lett., 71 (1993) 1601.
66. J.M. Orts, J.M. Feliu, A. Aldaz, J. Clavilier and A. Rodes, J. Electroanal. Chem., 281 (1990) 199.
67. I. Villegas and M.J. Weaver, J. Electroanal. Chem., 373 (1994) 245.
68. a) F.E. Woodard, C.L. Scortichini and C.N. Reilley, J. Electroanal. Chem., 151 (1983) 109; b) C.L. Scortichini and C.N. Reilley, *ibid*, 152 (1983) 255.
69. N. Furuya, S. Motoo and K. Kunimatsu, J. Electroanal. Chem., 239 (1988) 347.
70. third oxidation peak on Pt polycrystalline
71. A.M. Bittner, J. Wintterlin and G. Ertl, J. Electroanal. Chem., 388 (1995) 225.
72. G. Beitel, O.M. Magnussen and R.J. Behm, Surf. Sci., 336 (1995) 19.
73. H.P. Bonzel and R. Ku, Surf. Sci., 33 (1972) 91.
74. A.N. Frumkin and O.A. Petrii, Electrochim. Acta, 20 (1975) 347.

Part I

Chapter 4

Evaluation of the effect of two-dimensional geometry of Pt single-crystal faces on the kinetics of UPD of H using impedance spectroscopy

4.1 Introduction

The study of the states of adsorbed hydrogen, as H, electrochemically generated by discharge of H_3O^+ ions or from H_2O, has formed a major area of electrochemical surface science for many years, as reviewed in Chapter 3. Interest in this topic arises from two directions: a) the observation of so-called underpotential deposition (UPD) of atomic H from aqueous solutions at Pt, Pd, Rh, Ir, and Ru, which takes place distinguishably from the processes of proton discharge leading to molecular H_2 formation at potentials negative to the reversible H_2 electrode (RHE). b) The 2-e process of cathodic formation of molecular H_2 also involving an initial step of proton discharge and H chemisorption but at an overvoltage, *i.e.* at potentials negative to that of the RHE.

The relation between the state of electrodeposited H in the "underpotential" voltage range (0.0 to *ca.* 0.35 V, RHE on polycrystalline Pt) and that of H "overpotential-deposited" (OPD) [1] in the course of the cathodic H_2 evolution reaction (HER) is a matter of substantial significance for electrocatalysis in the HER and for the surface electrochemistry of Pt. On the noble metals, such as Pt, Rh, Ir, Ru and Pd, H that is the intermediate in the HER is (overpotentially) deposited on a surface *containing already* a full monolayer of underpotentially-deposited H. While the two kinds of H thus involved are, of course, atomically identical, their bound state(s) at e.g. a Pt surface must be different, or a new communal state of adsorbed H for "fractional" coverages (θ_H) formally greater than one (in the OPD case) is generated. Rather little attention to this point has been given in previous literature on mechanisms of the HER, although some authors have suggested it [2-7] but confusion has existed. In fact, it may well be that the high j_o value for Pt, at the top of the "volcano curve" [8] for HER rates, is not due to

an optimal intermediate value of the standard Gibbs energy of chemisorption directly to the metal (cf. ref. 9) but to the special situation that the OPD H intermediate has to be deposited on to, or amongst, an *already complete* monolayer of UPD H. Thus, the so-called Volmer step of H deposition (see eqs. 4.28 a and b) from H_3O^+ ion or H_2O in the mechanism of the HER at noble metals (except Au) is probably different, in surface-chemistry terms, from that for deposition of H on such metals as Au, Ag, Cu, Sn, etc which do not exhibit significant coverage by UPD of H [10], nor by OPD of H even at appreciable overpotentials.

While the study of the kinetics of the overall reaction of H_2 formation has been one the major topics of the field of electrode processes since Tafel's classical work in 1905, much less work has been carried out on the kinetics of UPD of H. Because the latter process cannot take place in a continuous way (since coverage by H is limited at $\theta_H \rightarrow 1$), like H_2 evolution, special non-steady-state techniques are required, principally ac impedance spectroscopy [11-18] as well as the charge-step method [19,20], fast-sweep cyclic voltammetry [21,22] and ac voltammetry [23] where non-steady current responses to potential, linearly or periodically changing with time, can be recorded and provide the required kinetic information.

In the work described in the present chapter, the method of a.c. modulation was used to examine the kinetics of H electrosorption and desorption under near-equilibrium conditions at Pt single-crystal surfaces over the UPD potential range [24].

4.1.1 Literature overview

Although the HER has been examined in great detail [25] on polycrystalline or porous materials and on Hg, only few attempts been made to examine the specificity of such a process to the individual geometries and electronic properties of respective Pt single-crystal surfaces [3-5,26-28]. Such studies have been attempted [26,27], but the electrodes were activated and cleaned anodically (at 1.2 V) for 20 s [26] up to a period of days [27]; this procedure is now known to introduce serious and irreversible perturbation of the surface structure [29]. In ref. 28, the overall HER was studied in aqueous $HClO_4$ solution at Pt (100), (111) and (511) surfaces but the same kinetic

parameters for the reaction, which thus involved OPD processes, were obtained for all three surfaces, whereas the UPD of H is very sensitive to the surface structure [30]. At activated Pt surfaces, it has been argued [11b] that the kinetics of the HER are influenced by H_2 supersaturation and diffusion of H_2 away from the electrode but contrary conclusions were reached by Kita *et al.* [3] and in Bai and Conway's work [1] using a rotated-disc active-Pt electrode. This point is important since mass-transfer control would be insensitive to the surface structure and exhibit a quasi-thermodynamic Tafel slope of 30 mV, i.e. one not determined in the usual way [31] by H recombination-controlled kinetics.

Studies of the HER on Pt single-crystals have hitherto been conducted mainly by potential-step techniques [28], steady-state polarization [3] and slow potential-sweep experiments [4,5] but no quantitative kinetic data were determined, *e.g.* for rate constants of the individual reactions or surface coverages by adsorbed, OPD H except on polycrystalline Pt [1].

On the other hand, through use of Pt single-crystal surfaces, the isotherms for UPD of H are now better understood [30] but direct kinetic studies of the H UPD processes are made difficult by their high rate constants. We believe that the OPD of H can be better understood if the differences of the kinetics in the UPD region at the different crystallographic planes are determined.

During the last 50 years, various investigations of the dynamics of H adsorption-desorption processes at polycrystalline Pt in H_2SO_4 have been reported [11-23]. Dolin and Ershler [17] were the first to study the kinetics of the "ionization of adsorbed hydrogen" by impedance measurements on a Pt electrode in a variety of electrolytes, followed by a various other studies, e.g. by Breiter *et al.* [11] using cyclic voltammetry and impedance methods, by Petrii *et al.* [13] on the kinetics as a function of potential and anion concentration at Ir, Rh and Pt (exchange current-densities increased in the order $F^- < SO_4^{-2} < Cl^- < Br^-$ and Ir < Rh < Pt), and by Flinn *et al.* [19,20] who found the current-density for H^+/H exchange at Pt to exhibit a reaction order in $[H^+]$ of 0.5 but to be independent of potential within the UPD range. Using another approach,

Angerstein-Kozlowska and Conway [21] investigated the kinetics of UPD of the several H states resolvable at polycrystalline Pt by determining the value of s_o [21] (which is the analogue of j_o, see eqs. 1.23 and 1.11, respectively) using a fast sweep method. Ohsaka *et al.* [16] found the best fit to their experimental results for H UPD kinetics when the data were treated in terms of an equivalent circuit comprised of a pseudocapacitance and a Faradaic resistance in series, the value of which was 0.58 Ω cm^2 (at E = 150 mV vs RHE) at Pt in 1 mol dm^{-3} H_2SO_4, the largest value reported for this process. Durand [14], evaluated kinetic parameters for UPD of H at Pt monocrystal sphere electrodes, which exhibited facets of various orientations, especially (111); the impedance method was employed up to 1 MHz using Pt microelectrodes. The kinetics both of H UPD and the HER were investigated at non-activated and anodically pretreated Pt electrodes. In another publication [15], Durand determined the electrosorption valency for H adsorption from 1 mol dm^{-3} $NaSO_4$ + 0.01 mol dm^{-3} H_2SO_4 also using the impedance method. Recently, Harrington [23] investigated the UPD of H on Pt as a model reaction to validate his extension of impedance theory to the technique of ac voltammetry and Lasia [22] discussed various modulation techniques for the study of H UPD at polycrystalline Pt electrodes.

Although most studies at polycrystalline Pt involve surfaces having both macroscopic and microscopic structural differences (*e.g.* roughness factor, mixture of more active versus less active sites), the results obtained have been largely in mutual agreement. A charge-transfer resistance (R_{ct}) of about 0.05 Ω cm^2 was observed at 50 mV (vs RHE) in refs. 12-14, 17 and 20 for 1 mol dm^{-3} H_2SO_4 solutions and corresponds to an apparent rate constant of approximately 5 x 10^{-6} mol^{½} cm$^{-½}$ s^{-1} (calculated using eqn. 4.35, section 4.1.3). Using a relation given in ref. 20, the R_{ct} at 50 mV, for 0.5 mol dm^{-3} H_2SO_4 solution [20], is 0.06 Ω cm^2 (*i.e.* corresponding to a rate of charge transfer of 4 x 10^{-6} mol s^{-1} cm^{-2}).

Using potential-step relaxation, Woodard and co-workers [32b] concluded that the mechanism for the UPD of H involved "instantaneous" surface equilibration between several co-existing but different adsorption states. This mechanism was supported by the dependence of the adsorption kinetics on electrode crystal face, electrode potential and

solution pH. (These latter results will be discussed further in section 4.3.5.) However, it seems that a better model is one in which, at each coverage, with increasing potential, new *communal* arrangements of adsorbed H atoms arise [33] corresponding to communal changes of the electronic properties of the metal surface with increasing θ_H as recognized in refs. 34 and 35.

In the case of single-crystal Pt electrodes, Oelgeklaus *et al.* [36] determined the rates of H and iodine adsorption on polycrystalline and Pt (111) electrodes. In iodide-free 1 mol dm^{-3} KOH solution, the specific rate of H adsorption in 1 mol dm^{-3} KOH was found to be higher on Pt(111) (R_α = 4 Ω cm^2 at 100 mV) than on a polycrystalline electrode (39 Ω cm^2) by one order of magnitude. These authors surprisingly found no influence of iodine adsorption on the kinetics of UPD of H on the polycrystalline electrode, whereas the rates were markedly lower on Pt (111), even for quite low coverages of iodine. Nishihara and Nozoye [37] examined the kinetics of the processes (possibly involving HSO_4^-/SO_4^{2-} anion adsorption [38]) which arise at Pt (111) in 0.5 mol dm^{-3} H_2SO_4 solution over the more positive potential region, 600 to 800 mV.

No studies are, however, available comparatively on the kinetics of UPD of H on two or more Pt *single-crystal* electrodes that have *well-ordered* (cf. ref. 39 and Chapter 3) surface structures; hence the present study is the first that reports the kinetics, and surface specificity thereof, of this process, including measurements at several temperatures, on such types of surfaces. Such information is of obvious relevance to the resolution of multiple-state adsorption [30] of H on single-crystal Pt surfaces and as well as to the influence of co-adsorbed anions, and additionally to the behavior of OPD H in the HER.

4.1.2 Impedance spectroscopy method

When a potential varying sinusoidally in time, $E(\omega) = E \sin \omega t$, is applied to an electrical system, the alternating response current that results is influenced by the electrical components of that system. The impedance (Z) of this system is then defined according to Ohm's law by the ratio $E(\omega)/I(\omega)$. The electrical components of the system being either in series or in parallel, the laws of Kirchoff can be applied.

For example, if this sinusoidal potential is applied to a pure resistance, R, the resulting current is the following, according to Ohm's law:

$$i(\omega) = \frac{E(\omega)}{R} = \frac{E}{R} \sin\omega t = I \sin\omega t \qquad (4.1)$$

It will be noticed that in this case the two signals, i(ω) and E(ω), are *in phase* as is shown in Fig. 4.1a [40]. The impedance of this circuit element is then equal to the nominal value of the resistance.

In the case of a pure capacitance (C), its charge (q) varies with potential according to the following equation:

$$q(\omega) = CE(\omega) \qquad (4.2)$$

By writing the derivative of eq. 4.2 with respect to time, the charging current of the capacitance is:

$$i(\omega) = C\omega E \cos\omega t = \frac{E}{X_c} \sin(\omega t + \frac{\pi}{2}) \qquad (4.3)$$

where $X_c = 1/(\omega C)$ and is the so-called capacitive reactance [40]. In the case of the capacitance, the resulting current and the applied potential are out of phase by $\pi/2$ (90°) as shown in Fig. 4.1b [40]. This angle is generally termed the phase angle, ϕ. This 90° phase angle can be represented in complex notation using j, $j = \sqrt{(-1)}$, for a planar system. Hence, eq. 4.3 becomes:

$$E(\omega) = -jX_c\, i(\omega) \qquad (4.4)$$

In electrochemistry, an ideally polarizable electrode can be represented by a circuit containing a resistance corresponding to the solution resistance in series with a capacitance corresponding to the double-layer capacitance. The potential difference applied to this electrochemical cell should be equal to the sum of the potential differences across each component of this equivalent circuit, *i.e.*:

$$E(\omega) = E_R + E_C = i(\omega)\,(R + jX_C) \qquad (4.5)$$

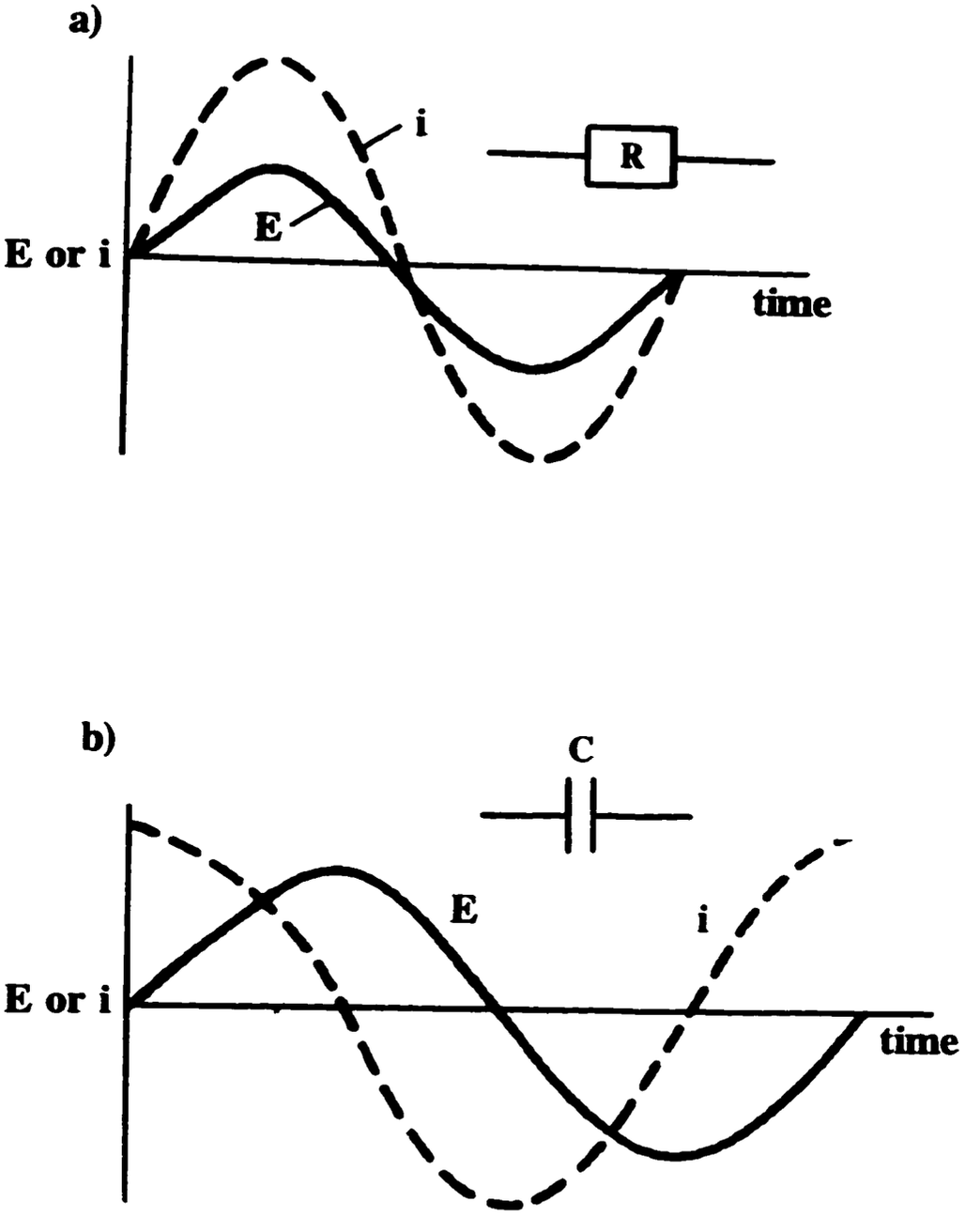

Fig. 4.1 Relationship between the applied potential in a sinusoidal regime and the resulting current response when applied to a) a pure resistance and b) a pure capacitance [40].

and the impedance Z is then equal to the sum of the impedance of the resistance in series with a capacitance, $R + jX_C$ according to Kirchoff's second law. If the impedance of this circuit can be decomposed into its real $Z' = R$, and imaginary $Z'' = jX_C = -j/\omega C$, components, the Nyquist representation of this equivalent circuit is obtained (Fig. 4.2a) [40]. This development corresponds to ideal conditions and it has been observed in the work presented here (section 4.3) as well as on mercury electrodes [41] which display smooth and homogeneous surfaces.

On the other hand, in the case of inhomogeneous surfaces, displaying surface defects, porosity, pits and dentrites, *etc.*, the ideal behaviour shown in Fig. 4.2a is no longer observed; instead the impedance response is inclined as illustrated in Fig. 4.2b; this behaviour is related to the inhomogeneous distribution of current caused by such structural inhomogeneities [40]. The angle of inclination observed in the impedance spectrum (complex-plane plot) (Fig. 4.2b) is independent of frequency, ω, and is modelled by substituing the capacitance by a new quantity T, which displays a phase angle φ independent of ω [42a]. This term originates from analogous behaviour that arises in the impedance of diffusion-controlled processes where the Warburg impedance element has real and imaginary components each dependent on $\omega^{-1/2}$, thus giving a constant phase angle of $\pi/4$, independent of ω. This angle, φ, is generally termed the "constant phase element" (CPE) [42a]. The impedance of the CPE element is:

$$Z_{CPE} = \frac{1}{T\,(j\omega)^{\varphi}} \qquad (4.6)$$

From the new circuit element T the surface average double-layer capacitance can be determined using eq. 4.7:

$$T = C_{dl}^{\varphi}\,(R_{sol}^{-1} + A)^{1-\varphi} \qquad (4.7)$$

where $A = 1/R_{\alpha}$ (see below for the definition of R_{α}).

When the polarization of the electrochemical metal/solution interface causes an electron transfer, the rate of the electron transfer accross the interface becomes an important factor in the resulting current measured for the system. In this case, the complexity of the current response will be related to the various steps involved in the

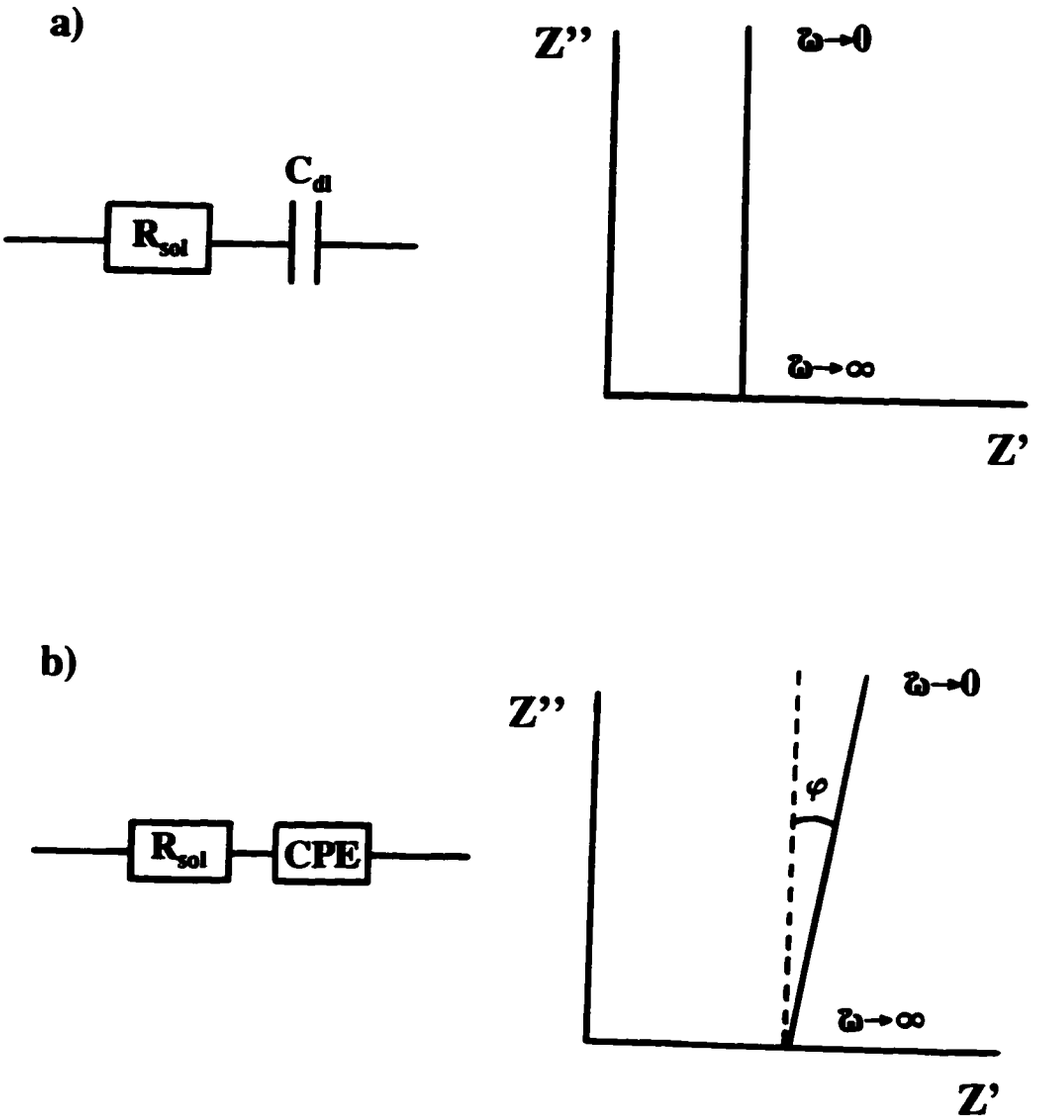

Fig. 4.2 a) Equivalent circuit for an ideally polarized electrode and the correponding Nyquist representation for this circuit; b) equivalent circuit for an inhomogeneous ideally polarized electrode and the corresponding Nyquist representation for this circuit (adapted from ref. 42a).

overall mechanism, such as adsorption-desorption and diffusion limitation. As well as the homogeneity of the electrode surface, i.e. roughness, porosity, electrode material dissolution.

It was also shown recently by Pajkossy that for macroscopically smooth electrodes this kind of CPE behaviour could not be attributed to surface geometric defects but rather to an interfacial origin such as an adsorption effect [42b].

For reasons of simplicity the case of the simple outer-sphere electron transfer process (given in eq. 4.8) will be discussed in this introduction:

$$O + ne \rightleftharpoons R \tag{4.8}$$

where both species O and R of the redox pair are soluble.

First let it be assumed that the impedance associated with the Faradaic process can be represented by a combination of a resistance, R_f, and a capacitance, C_f, in series. Similarly to the previous examples, the potential is dictated by Kirchoff's law and

$$E = iR_f + C_f^{-1} \int i\,dt \tag{4.9}$$

The perturbation dE/dt for a sinusoidal current is

$$\frac{dE}{dt} = R_f i\omega \cos \omega t + C_f^{-1} i \sin \omega t \tag{4.10}$$

Since the current is also a function of the concentrations of the redox species, $E f(i, C_O, C_R)$, the following relation is obtained:

$$\frac{dE}{dt} = \frac{\delta E}{\delta i}\frac{\delta i}{\delta t} + \frac{\delta E}{\delta C_O}\frac{\delta C_O}{\delta t} + \frac{\delta E}{\delta C_R}\frac{\delta C_R}{\delta t} \tag{4.11}$$

This equation can be simplified to

$$\frac{dE}{dt} = R_\alpha \frac{\delta i}{\delta t} + \beta_O \frac{\delta C_O}{\delta t} + \beta_R \frac{\delta C_R}{\delta t} \tag{4.12}$$

Obtaining an expression for dE/dt depends on the evaluation of the six factors on the right-hand side of eq. 4.12. The three parameters R_{ct}, β_O and β_R are specifically related to the kinetic properties of the electron transfer reaction.

While, the three remaining factors can evaluated from the current flow according to eq. 4.5, where

$$\frac{di}{dt} = I\omega \cos \omega t , \tag{4.13}$$

the other two parameters are evaluated by considering mass transfer, using Fick's law of diffusion [40] and are equal to:

$$\frac{dC_O}{dt} = \frac{i}{nFA} \left(\frac{\omega}{2D_O}\right)^{1/2} (\sin \omega t + \cos \omega t) \tag{4.14}$$

and

$$\frac{dC_R}{dt} = \frac{i}{nFA} \left(\frac{\omega}{2D_R}\right)^{1/2} (\sin \omega t + \cos \omega t) \tag{4.15}$$

By substituing eq. 4.14 and 4.15 in eq. 4.12, and knowing that eq. 4.10 and eq. 4.12 are equivalent, the following expression is obtained:

$$\begin{aligned} &R_f(i\omega \cos \omega t) + C_f^{-1}(i \sin \omega t) = \\ &\left(R_{ct} + \frac{\sigma}{\omega^{1/2}}\right) (i\omega \cos \omega t) + \sigma\omega^{1/2} (i \sin \omega t) \end{aligned} \tag{4.16}$$

From eq. 4.16, the following expressions are obtained for the faradaic resistance and capacitance:

$$R_f = R_{ct} + \frac{\sigma}{\omega^{1/2}} \tag{4.17}$$

and

$$C_f = \frac{1}{\sigma\omega^{1/2}} \tag{4.18}$$

where R_{ct} is determined by the kinetics of charge transfer and σ takes into account the diffusional mass transfer and is equal to $(\beta_O/D_O^{1/2} - \beta_R/D_R^{1/2})$ $(nFA\sqrt{2})^{-1}$.

The Faradaic impedance Z_f can be expressed as

$$Z_f = R_{ct} + Z_W = R_{ct} + R_W - j\frac{1}{\omega C_W} \tag{4.19}$$

where Z_W is the so-called Warburg impedance, composed of a resistance, $R_W = \sigma/\omega^{1/2}$ in series with a diffusional pseudocapacitance, C_W.

The complete equivalent circuit for the electrochemical process given in eq. 4.8 is shown in Fig. 4.3a [40]. The total impedance can be expressed in a form where the real (Z') and imaginary (Z'') components are separated, *viz.*:

$$Z' = R_{sol} + \frac{R_{ct} + \sigma\omega^{-1/2}}{(C_{dl}\sigma\omega^{1/2} + 1)^2 + \omega^2 C_{dl}^2 (R_{ct} + \sigma\omega^{-1/2})^2} \tag{4.20}$$

and

$$Z'' = \frac{\omega C_{dl} (R_{ct} + \sigma\omega^{-1/2})^2 + \sigma\omega^{-1/2} (\omega^{1/2} C_{dl}\sigma + 1)}{\omega^{1/2} C_{dl}\sigma + 1)^2 + \omega^2 C_{dl}^2 (R_{ct} + \sigma\omega^{-1/2})^2} \tag{4.21}$$

Two limiting cases can be envisaged: one for the high frequency limit and the second for the low frequency end of the spectrum. At high frequencies, the resistance and capacitance terms associated with the Warburg impedance tend toward 0, and Z_W is negligible. Hence, Z' becomes:

$$Z' = R_{sol} + \frac{R_{ct}}{1 + \omega^2 C_{dl} R_{ct}^2} \tag{4.22}$$

and correspondingly

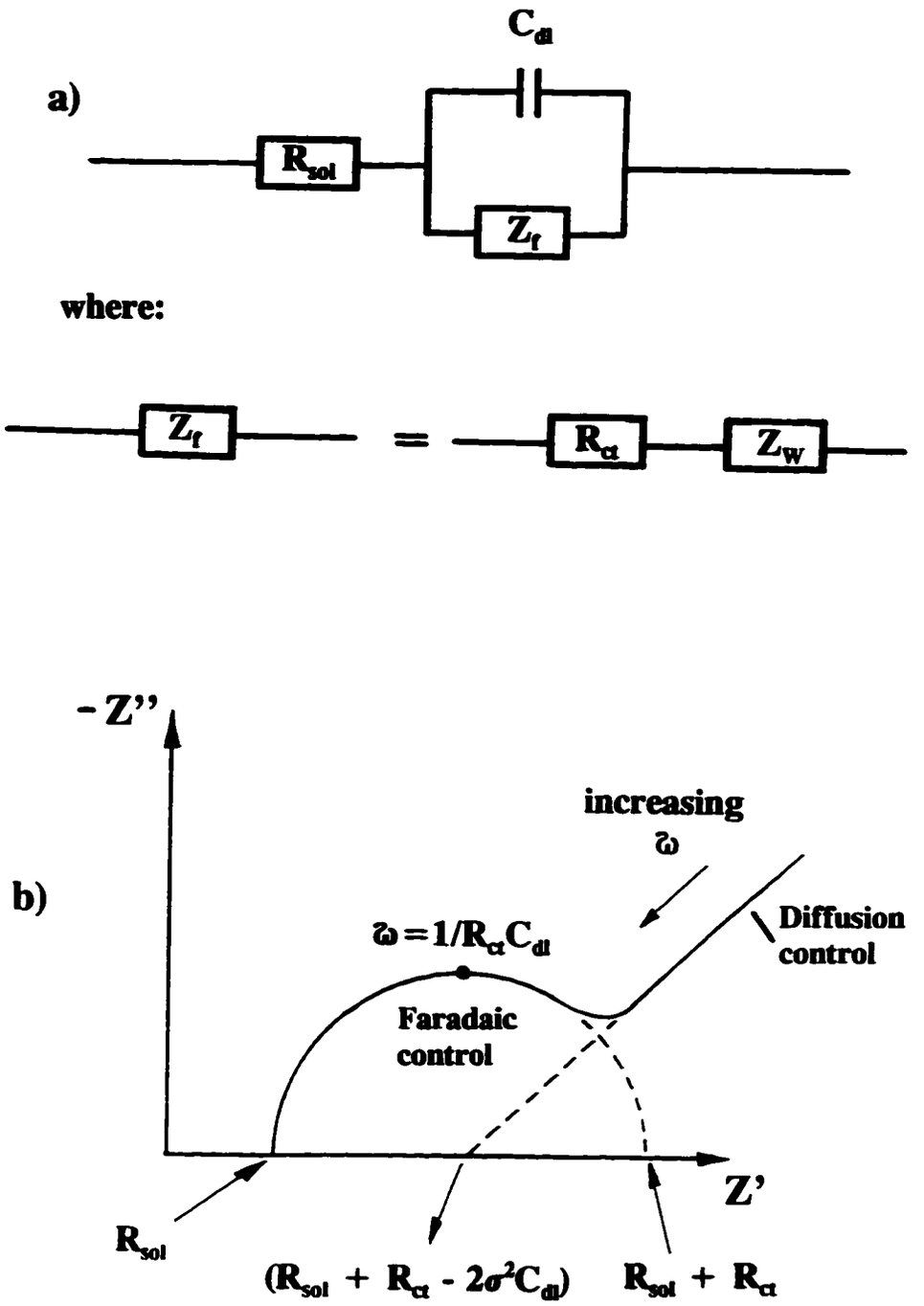

Fig. 4.3 a) Equivalent circuit for the process described in eq. 4.1 [40]; b) Nyquist representation of the impedance of the circuit shown in a) [43].

$$Z'' = \frac{\omega C_{dl} R_{ct}^2}{1 + \omega^2 C_{dl}^2 R_{ct}^2} \quad (4.23)$$

By isolating ω in eq. 4.22 and substituing it in Z'' the following relation is obtained:

$$(Z' - R_{sol} - \frac{R_{ct}}{2})^2 + (Z'')^2 = (\frac{R_{ct}}{2})^2 \quad (4.24)$$

Eq. 4.24 represents the equation of a circle centred on $Z' = R_{sol} + R_{ct}/2$ with a radius of $R_{ct}/2$. To this value of Z', is also associated a frequency value, ω, which is equal to $1/R_{ct} + C_{dl}$.

At the low frequency limit, eqs. 4.20 and 4.21 become:

$$Z' = R_{sol} + R_{ct} + \sigma \omega^{-1/2} \quad (4.25)$$

and

$$Z'' = \sigma \omega^{-1/2} + 2\sigma^2 C_{dl} \quad (4.26)$$

By eliminating ω between these two equations,

$$Z'' = Z' - R_{sol} - R_{ct} + 2\sigma^2 C_{dl} \quad (4.27)$$

This latter case shows a linear relation between Z'' and Z' with a unit slope, the plot for which intersects the Z' axis at $R_{sol} + R_{ct} - 2\sigma^2 C_{dl}$ (see Fig. 4.3b described previously).

A plot of the whole frequency range for the expression of Z'' (eq. 4.21) *versus* Z' (eq. 4.20) has the form shown in Fig. 4.3b [43]. In this plot both the kinetically-controlled and diffusion-controlled regions are resolved and displayed which provides a major advantage of employing this experimental methodology.

4.1.3 Kinetic aspects of the UPD of H

At the Platinum metals, Pt, Rh, Ir, Ru and Pd, UPD of H, and also of base metal atoms [44], is observed indicating strong energy of interaction between the H [45] or metal adatoms and the metal surface; this situation leads to well ordered, 2-dimensional

arrays before bulk-phase deposition commences above the reversible potential. The H UPD reaction formally corresponds to the analogous well known Volmer step of the HER (eqn. 4.28):

$$H_3O^+_{(aq)} + M(\theta_H<1) + e(M) \underset{k_{-1}}{\overset{k_1}{\rightleftharpoons}} M\,H_{ads}(\theta_H \leq 1) + H_2O \quad (acidic\ media) \quad \textbf{(4.28a)}$$

$$H_2O_{(aq)} + M(\theta_H<1) + e(M) \underset{k_{-2}}{\overset{k_2}{\rightleftharpoons}} MH_{ads}\,(\theta_H \leq 1) + OH^- \quad (alkalin\ media) \quad \textbf{(4.28b)}$$

However, it must be remarked that the kinetic behaviour of UPD processes, e.g. the dependence of R_{ct} on potential, is quite different from that under OPD conditions. Thus, at each potential, E_θ, in the UPD range, a separate *equilibrium state*, characteristic of the coverage, $\theta_{H,E}$, at that potential is involved and R_{ct} values measure the exchange current-density, $j_{o,E}$, at that potential and coverage. Only for sufficiently fast modulation, e.g. in fast linear-sweep voltammetry as employed in ref. 18, is a polarization (overvoltage) involved in the kinetics of the UPD process, as treated theoretically in refs. 46a and 46b. On the contrary, at potentials a little, or substantially, displaced negatively from the H_2 reversible potential, the adsorbed H that is then involved is a species *overpotentially deposited* in the HER under non-equilibrium conditions. Then, only for cases where the rate-constant for either of the desorption steps in the HER is substantially smaller than that for H^+ discharge to adsorbed H (eq. 4.28a), is the latter step almost at equilibrium but then at some potential *negatively displaced* from the overall equilibrium potential, and thus also to the UPD region.

R_{ct} is determined by a small modulation (δE_θ) around *each* equilibrium potential, corresponding to a series of UPD H coverages ($\theta_{H,E}$) which are themselves related thermodynamically to potential (E_θ) according (for a simple 1-state adsorption) to eqn. 4.29, where K is the equilibrium constant for the reaction given in eq. 4.28a and f has its usual meaning (f=F/RT):

$$\theta_{H,E} = \frac{K\, C_{H^+}\, exp\ -fE_\theta}{1 + C_{H^+}\, K\, exp\ -fE_\theta} \qquad (4.29)$$

Hence, R_α will not be related to potential through the usual Tafel exponent αEF/RT, but rather to some quasi-Nernstian function involving the changing reversible E_θ value related to $\theta_{H,E}$, as above. Equation 4.29 is an electrochemical Langmuir relation for electrosorption of H on M according to reaction 4.28a.

The kinetic equation for the UPD reaction 4.28 is as follows, derived for an electrochemical process involving adsorption of H at the surface of an electrode [21,46]. In the case of eqn. 1, the net rate of the process, subject to a small applied perturbation, δ, of potential (such as a.v. modulation [δE_θ] used in impedance measurements) is:

$$v = k_1\,(1-\theta_{H,E})\; C_{H^+}\; exp[-\beta\, f\,(E_\theta \pm \delta E_\theta)] - k_{-1}\,(\theta_{H,E})\; exp[(1-\beta)\, f\,(E_\theta \pm \delta E_\theta)] \qquad (4.30)$$

where δE_θ is a small ($F\delta E_\theta \ll RT$) perturbation of potential from its equilibrium value, E_θ, (see eqn. 4 below) for a given value of θ_H in the UPD H profile. Note that eq. 4.30 includes both forward and backward reaction rate terms corresponding to a Butler-Volmer relation written for a surface process including coverage [θ and (1-θ)] terms.

For the H UPD process, the potential at such a given coverage is given (cf. eqn. 4.29) by:

$$E_\theta = E^o_{\theta=0.5} + \frac{RT}{nF}\, ln\, \frac{(1 - \theta_{H,E})\; C_{H^+}}{\theta_{H,E}} \qquad (4.31)$$

with the $E^o_{\theta=0.5}$ in the Nernst equation (4.31) being defined for a standard state θ_H=0.5. Note that this standard reversible potential for the UPD process is thus the potential of the current peak in cyclic voltammetry (for a *given* adsorption state or for single-state adsorption) associated with the process, if a Langmuirian type of isotherm (e.g. eqn. 4.29) is assumed or indicated (in the absence of co-adsorbed anions).

In eqn. 4.30, the exponential factor describes how the Gibbs energy of activation in k_1 and k_{-1} is modified by the small potential perturbation, ($E_\theta \pm \delta E_\theta$), through an electrochemical Brønsted (barrier symmetry) factor β ($\simeq$ 0.5). Formally, eqn. 4.30

relates the dependence of i on E_θ and $\theta_{H,E}$. Note that in cyclic voltammetry of the UPD process for $s < s_o$, *both* terms of the Butler-Volmer eq. 4.30 remain significant at all E_θ values (eq. 4.31). As the potential E_θ is changed, i at first increases exponentially with E_θ when $\theta_{H,E}$ is small but must decrease as $\theta_{H,E} \rightarrow 1$ (cf. eqn. 4.30). A maximum is attained at some intermediate value of $\theta_{H,E}$, usually, 0.5 if 4.28a is a single-state reversible process, as is well known, e.g. ref. 46. However, since the process of UPD of H involves the formation of a monolayer of adsorbed H which is limited by the number of sites available, the current is non-continuous and can be observed only in a non-steady-state experiment as $0 < \theta_{H,E} < 1$. The main difference between H UPD and H OPD processes is that for the UPD of H, at each value of E_θ, the *net* rate v (eqn. 4.30) is virtually zero. Thus, the high reversibility of the UPD H process at every potential allows an exchange rate v_o (i.e. corresponding to an exchange current-density, j_o) to be defined which characterises the dynamics of the equilibrium of the UPD H at any given potential corresponding to a particular H coverage. As shown in eqn. 4.32, $v_{o,\theta}$ is given by:

$$v_{o,\theta} = \frac{d\theta_{H,E}}{dt} = k_1 (1 - \theta_{H,E}) C_{H^+} \exp [\beta f (E_\theta \pm \delta E_\theta)] - k_{-1} \theta_{H,E} \exp [(1 - \beta) f (E_\theta \pm \delta E_\theta)] \quad (4.32)$$

Then

$$k_{o,\theta} = k_1 \exp [-\beta f (E_\theta \pm \delta E_\theta)] = k_{-1} \exp [(1 - \beta) f (E_\theta \pm \delta E_\theta)] \quad (4.33)$$

When eqn. 4.30 is taken at the standard state (i.e. $\theta_{H,E} = 0.5$ and $C_{H+} = 1$ mol dm^{-3}), and introduced in eqn. 4.32, the standard rate constant, $k_{o,\theta}$, for the process of UPD of H at a given $\theta_{H,E}$ is obtained as:

$$k_{o,\theta} = k_1^{(1 - \beta)} k_{-1}^{\beta} \quad (4.34)$$

The exchange rate at any potential or corresponding coverage value can then be expressed in the form of $k_{o,\theta}$ from eqns. 4.33 and 4.34:

$$v_{o,\theta} = k_1 (1 - \theta) C_{H^+} \frac{(1 - \theta_H)^{-\beta} C_{H^+}^{-\beta}}{\theta_H^{-\beta}} \frac{k_1^{-\beta}}{k_{-1}^{-\beta}} = k_{o,\theta} C_{H^+}^{(1-\beta)} (1 - \theta_H)^{(1-\beta)} \theta_H^{\beta} \quad (4.35)$$

Since the H-adatoms are small compared to the first nearest-neighbour distances in the fcc lattices of M, a localized one-to-one adsorption is expected which, however, may be influenced by lateral interactions and the extent of anion co-adsorption, leading to non-commensurate adsorbed H lattices.

Harrington and Conway [47] developed a generalised approach for the treatment of ac impedance of electrochemical reactions involving one or two adsorbed intermediates by considering that the faradaic current passing, corresponding to the rate of electron transfer (r_o), is proportional to the sum of the rates of the individual electrochemical steps. In the case of UPD of H, the only electron-transfer reaction involved is that in eqn. 4.28 and the ac current obtained will then be simply the ac response of the reversible exchange rate according to eqn. 4.35, *viz.*:

$$j_f = F r_o = F v_{o,\theta} = q \frac{d\theta}{dt} \quad (4.36)$$

where q_1 is the charge for monolayer formation or desorption. Then for small potential perturbation of the rate, $\delta v_{o,\theta}$ can be derived using a Taylor series, giving (where $\delta\theta = \tilde{\theta} \exp(j\omega t)$):

$$\delta v_{o,\theta} = q/F \frac{d\delta\theta}{dt} = q/F \tilde{\theta}\, j\omega\, e^{j\omega t} = \left(\frac{\partial v}{\partial E_\theta} \delta E_\theta\right) + \left(\frac{\partial v}{\partial \theta} \delta\theta\right) \quad (4.37)$$

With $\delta E_\theta = \tilde{E}_\theta \exp(j\omega t)$, $\tilde{\theta}$ defined in the following way:

$$\tilde{\theta} = \frac{\frac{F}{q}\left(\frac{\partial v}{\partial E_\theta}\right) \tilde{E}_\theta}{j\omega - \frac{F}{q}\left(\frac{\partial v}{\partial \theta}\right)} \quad (4.38)$$

is obtained, where $\tilde{E}_\theta$ and $\tilde{\theta}$ are the modulated potential and coverage around there equilibrium values, respectively. Similarly the complex component of the ac current is obtained by re-introducing eqn. 4.37 into eqn. 4.36:

$$\delta j_f - \tilde{j}_f e^{j\omega t} - F\left[\left(\frac{\partial v}{\partial E_\theta}\,\delta E_\theta\right) + \left(\frac{\partial v}{\partial \theta}\,\delta\theta\right)\right] \tag{4.39}$$

By solving for the modulated current around its equilibrium value, $\tilde{j}_f$, we obtain:

$$\tilde{j}_f - F\left[\left(\frac{\partial v}{\partial E_\theta}\,\tilde{E}_\theta\right) + \left(\frac{\partial v}{\partial \theta}\,\tilde{\theta}\right)\right] \tag{4.40}$$

The Faradaic admittance is obtained by dividing the modulated $\tilde{j}_f$ by the modulated $\tilde{E}_\theta$ and introducing the resulting modulated $\tilde{\theta}$, giving:

$$Y_f - -F\left(\frac{\partial v}{\partial E_\theta}\right) - \frac{\left[F\left(\frac{\partial v}{\partial E_\theta}\right) F/q\left(\frac{\partial v}{\partial \theta}\right)\right]}{j\omega - F/q\left(\frac{\partial v}{\partial \theta}\right)} - A - \frac{AB}{j\omega + B} \tag{4.41}$$

where $A = -F\,(\partial v / \partial E_\theta)$ and hence is equal to $1 / R_{ct}$, and $B = -(F / q)\,\partial v / \partial E_\theta$.

The adsorption pseudocapacitance of H can be obtained [47] as:

$$C_p - q\,\frac{\partial \theta}{\partial E_\theta} - q\left(\frac{\partial \theta}{\partial \upsilon}\right)\left(\frac{\partial v}{\partial E_\theta}\right) - \frac{A}{B} \tag{4.42}$$

The faradaic impedance is thus:

$$Z_f - \frac{1}{Y_f} - \frac{1}{A} + \frac{1}{j\omega\,(A/B)} - R_{ct} + \frac{1}{j\omega C_p} \tag{4.43}$$

This relation directly demonstrates, of course, that the faradaic impedance can be represented by an equivalent circuit containing a resistance in series with a capacitance to which meaningful physical values can be attributed. The electrical circuit equivalent to the Pt electrode adsorbing H must, of course, also include a capacitance representing charging of the double-layer in parallel with the faradaic impedance, as shown in Fig. 4.4a, in the well known way. The impedance measurements on such an equivalent circuit will give rise to two limiting cases: first, at high frequencies, the more rapid electrochemical process is being stimulated and only the charging of the double-layer at the electrode/solution interface and the solution resistance will be measured. At sufficiently low frequencies, all processes will be stimulated regardless of their rates and

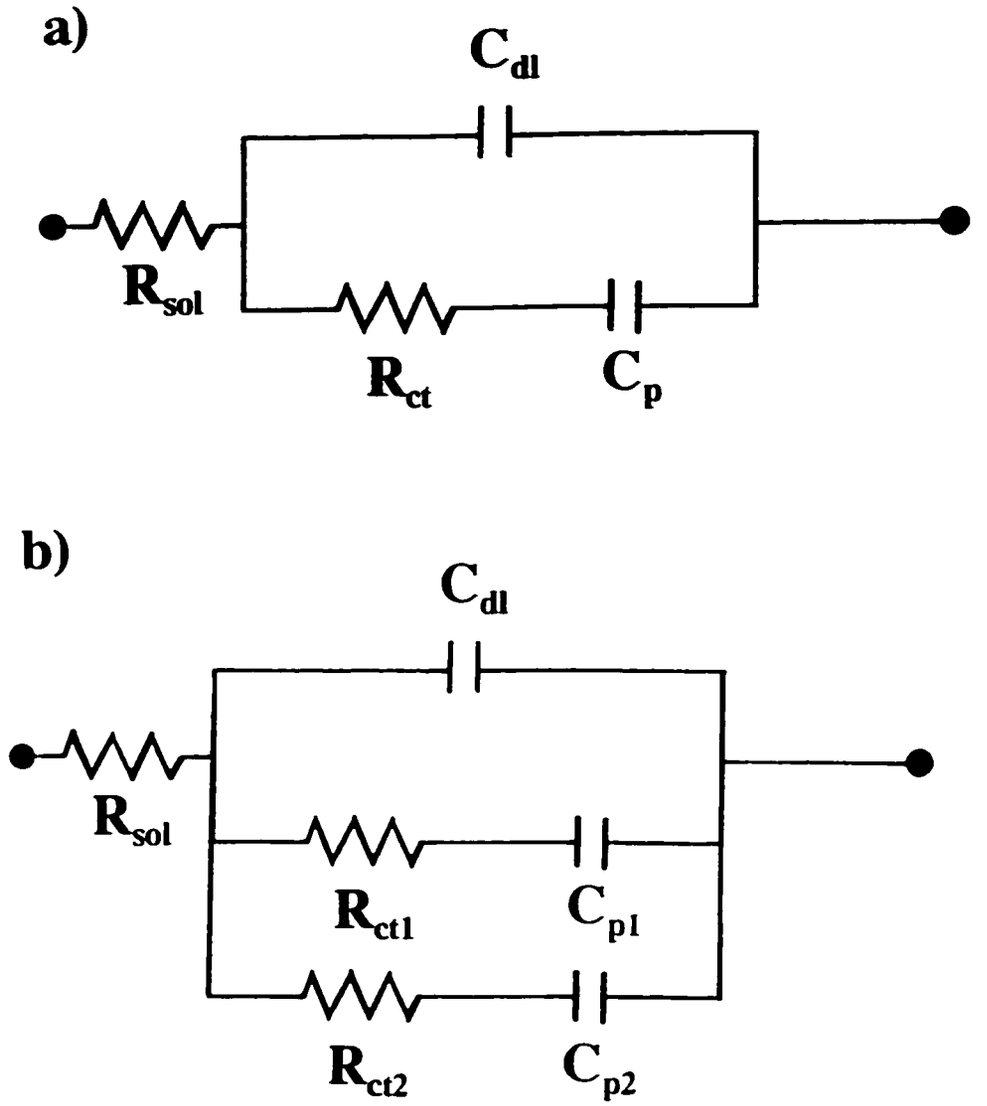

Fig. 4.4 Equivalent circuit for H UPD corresponding to the kinetic model: a) in the absence of anion co-adsorption and b) in the presence of anion co-adsorption.

a purely capacitive behaviour of the impedance will be observed with decreasing frequency. This impedance response is then limitingly associated with the sum of the two capacitances (C_{dl} and C_p) in parallel. Considering the equivalent circuit in Fig. 4.4a, C_{dl} and C_p only become additive when $Z_{Rct} << Z_{Cp}$, and are then not separately resolvable. Since, of these impedances, only Z_{Cp} is frequency dependent, being inversely determined by the product of frequency and C_p, the above condition is reached at some sufficiently low frequency, depending on C_p. In our case, for the (100) and (311) surfaces, this frequency limit is about 1000 Hz. For the (111) and (110) surfaces, however, the results indicate that the limit is much higher, so that only capacitive behaviour is observed over the accessible range of scanned frequency; then R_{ct} is not experimentally determinable in that frequency range.

4.2 Experimental

Cyclic voltammetric experiments were conducted at sweep rates of 50 mV s^{-1} with the Pt single-crystal electrodes in a hanging meniscus configuration (Fig. 4.5). Cyclic voltammograms were recorded after each surface preparation in order to verify a correct and clean state of the surface. This procedure was repeated also after each potentiostatic series of ac measurements to ensure that no poisoning or reconstruction of the surface had occurred during the time of the data acquisition. In practice, two ac measurements could be performed before a new surface preparation was required. The reversible hydrogen electrode (RHE) was used as the reference electrode and all potentials, if not stated otherwise, are given on the RHE scale.

As mentioned in section 2.6.3 of Chapter 2, the magnitude of the ac perturbation was chosen to be 5 mV r.m.s.; if the guidelines given in ref. 48 are followed, an amplitude of about a tenth of the voltage width of the linear-sweep current peak at half height should be adequate to yield results relatively free from distortion. In the present work, the width of the capacitive peak on Pt (100) is about 35 mV at half height while for (311) it is much smaller (10 mV). Hence, much care must be taken in the measurement of the impedance on the (311) face in the potential region where the peaks are appearing, since for that face the width is considerably smaller than that for the

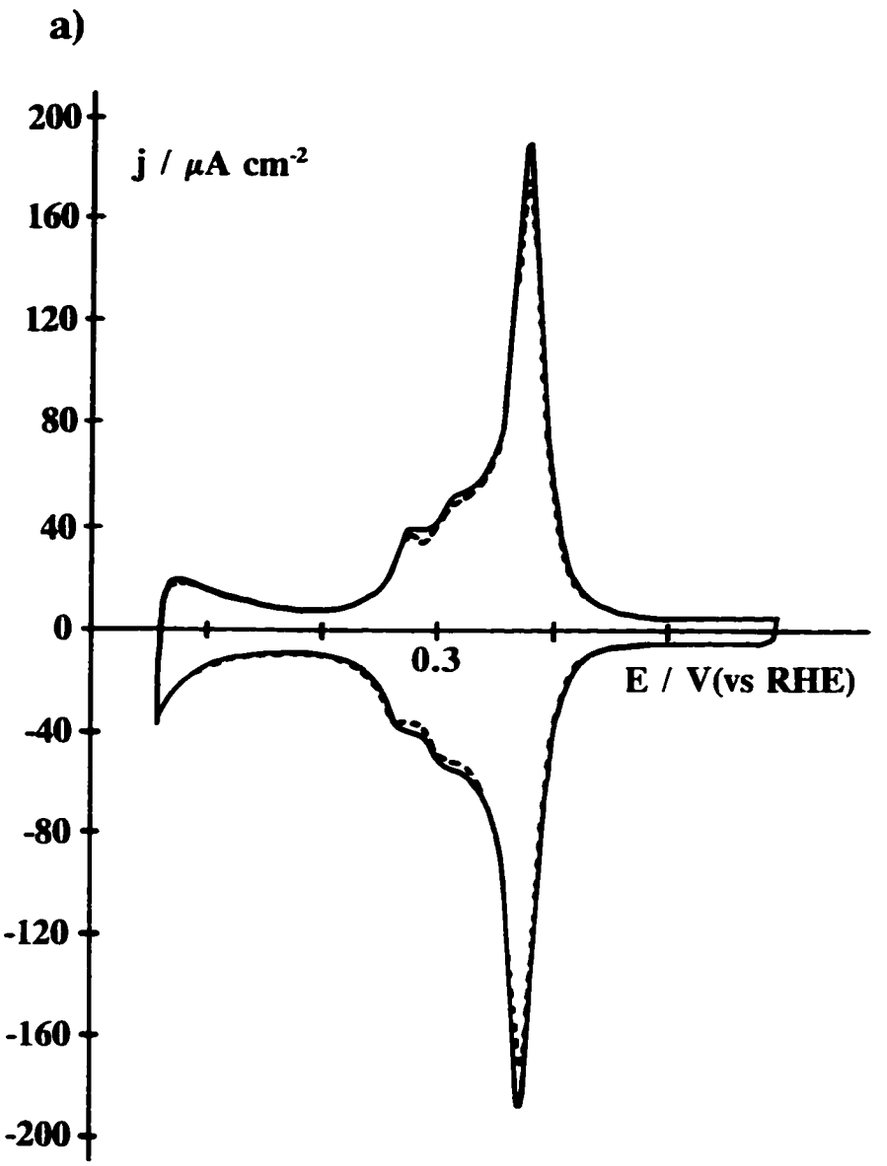

Fig. 4.5 Cyclic voltammograms a) for Pt (100) in 0.5 mol dm^{-3} aqueous H_2SO_4 solution for one surface preparation before (solid line) and after (dashed line) two consecutive series of impedance measurements (duration *ca.* 1.5 min). The sweep rate for Pt (100) was 50 mV s^{-1}. b) on following page.

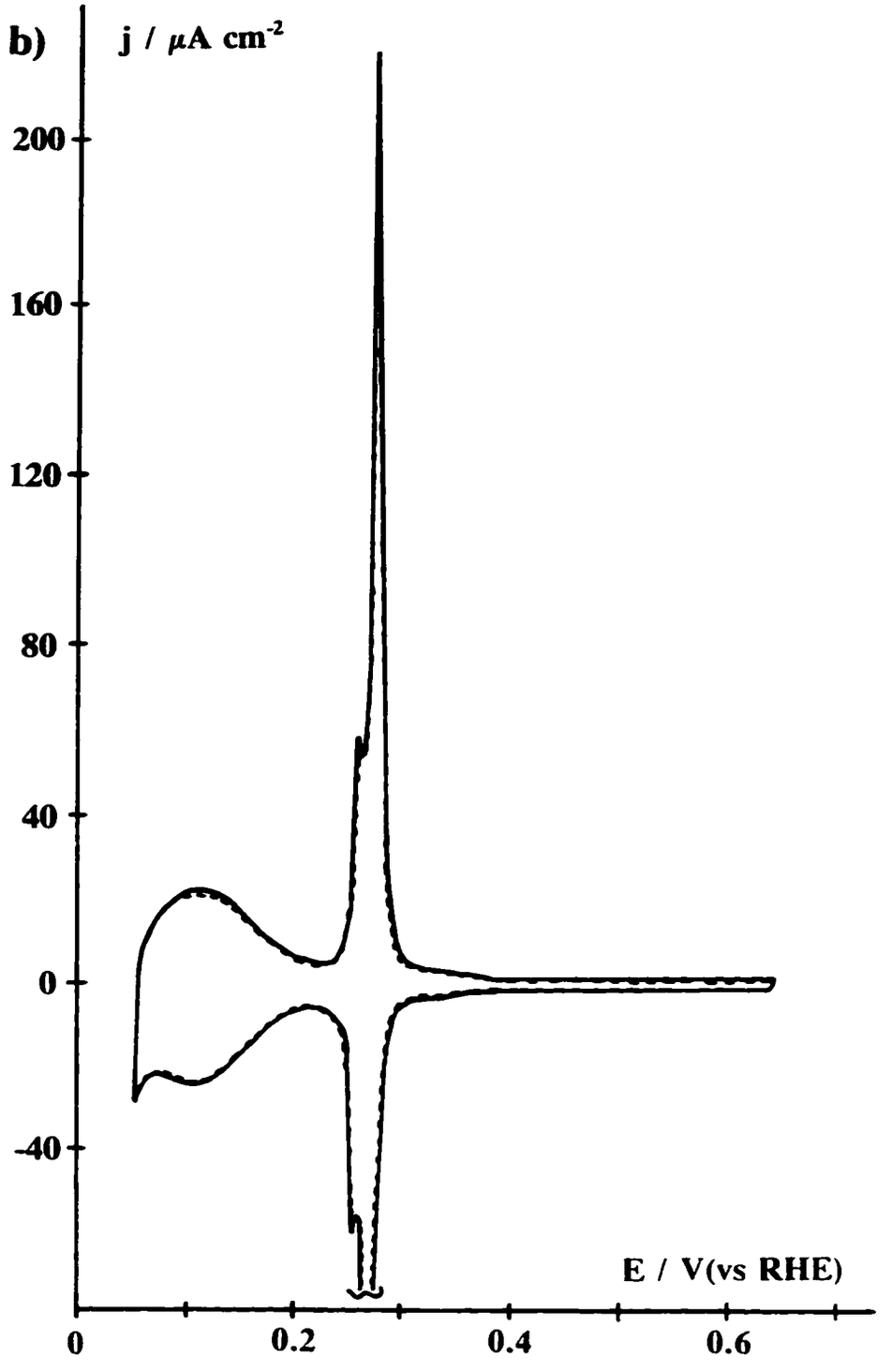

Fig. 4.5 b) same conditions as a) but this time for Pt(311). The sweep rate for (311) was 20 mV s^{-1}.

others. This problem was dealt with by measuring the impedance responses at the peak potential at lower amplitudes, going from 2.5 mV down to 0.5 mV r.m.s.. However, the noise level increased appreciably as the amplitude was lowered, as is to be expected. The impedance spectra were fitted by means of a complex, non-linear, least-squares immitance fitting program, LEVM [49] and the resulting impedance yielded the same kinetic parameters for all amplitudes.

4.3 Results and Discussion

For all the results reported in this work it was very important that the cleanliness and ordering of the single-crystal surfaces remained unaltered throughout the respective ac impedance measurements; hence cyclic voltammograms were recorded before and after each potentiostatic ac series of frequency-scan measurements. In most cases two sets of ac impedance measurements could be recorded before the H UPD charge became reduced significantly (more than 5 %). For all the data reported here, only experiments for which the total charge lost in this way was less than 5% were considered as being acceptable.

Figs. 4.5a and b, show the cyclic voltammograms for Pt (100) and (311) for one surface preparation before and after two consecutive series of ac impedance scan measurements. It is clear from these curves that the electrochemical interface remained almost unchanged during the course of the ac measurements. Once this level of cleanliness had been achieved, ac impedance measurements were recorded over the whole range of potentials within which the UPD behaviour is observed.

From recent results, as discussed in detail in Chapter 3, it is now strongly believed that the UPD H region on single-crystal Pt faces involves, in fact, a combination of H as well as anion adsorption at potentials positive to the *pzc* (chapter 1, section 1.2.1) [50-52]. Moreover, the surface concentrations of hydrogen atoms and anions present will vary with the crystallographic orientation, as shown by Clavilier et al. [50,51] for various crystallographic orientations studied in sulphuric and perchloric acid solutions. From what is already known about these two surfaces ((100) and (311)) in H_2SO_4 [50,51], at the potential values corresponding to the maximum of the current

peaks on the voltammogram for both surfaces as shown in Figs. 4.5a and b, the surfaces are partially covered by adsorbed bisulphate anions [50-52].

Since these two processes are parallel surface reactions in the UPD behaviour, the equivalent circuit has to include two branches representing both these adsorption processes, $R_{ct1} + C_{p1}$ and $R_{ct2} + C_{p2}$, acting in parallel. Following the above considerations, the measured current responses were thus fitted to the equivalent circuits shown in Fig. 4.4a or b, the latter if anion co-adsorption is expected. The presence of the second adsorption process will be manifested by the appearance of a second semi-circle in the complex-plane plots. The circuit shown in Fig. 4.4a is a simplification of that in Fig. 4.4b when the participation of one of the two adsorption processes is negligible, i.e. when its R_{ct2} becomes large. In the former case, another charge-transfer resistance and anion adsorption pseudocapacitance is required.

In Figs. 4.6a and b, the complex-plane impedance and the Bode phase-angle plots, are shown for two values of potential for Pt (100) where there is only H adsorption-desorption occurring at the surface at these two potential values over a range of frequency from 100 kHz to 100 Hz. The evidence for the assignment of the electron transfer process to H adsorption-desorption comes from the CO-adsorption transient experiments in 0.5 mol dm^{-3} [50] where the majority of the species desorbing from the surface upon adsorption of CO at these two potentials (see Fig. 4.6) were being oxidized, *i.e.* they became of cationic nature and therefore originated from adsorbed H. The data plotted in this figure were compensated, for purposes of clarity, for the small but significant solution resistance effect that arises in the hanging meniscus electrode/solution configuration. These figures 4.6a and b clearly show the two main features expected from the kinetic treatment of the impedance results for these two faces: a small semi-circle observed at high frequencies followed by a purely capacitive response at lower frequencies.

Table 4.1 records the values obtained from the LEVM fitting for Pt (100) in 0.5 M H_2SO_4 for each component of the circuit for a series of potential values and the corresponding standard deviations from the fits. It also includes the resulting R_{ct}, C_p and C_{dl} values for the ac results shown in Figs. 4.6a and b at 200 and 300 mV. The

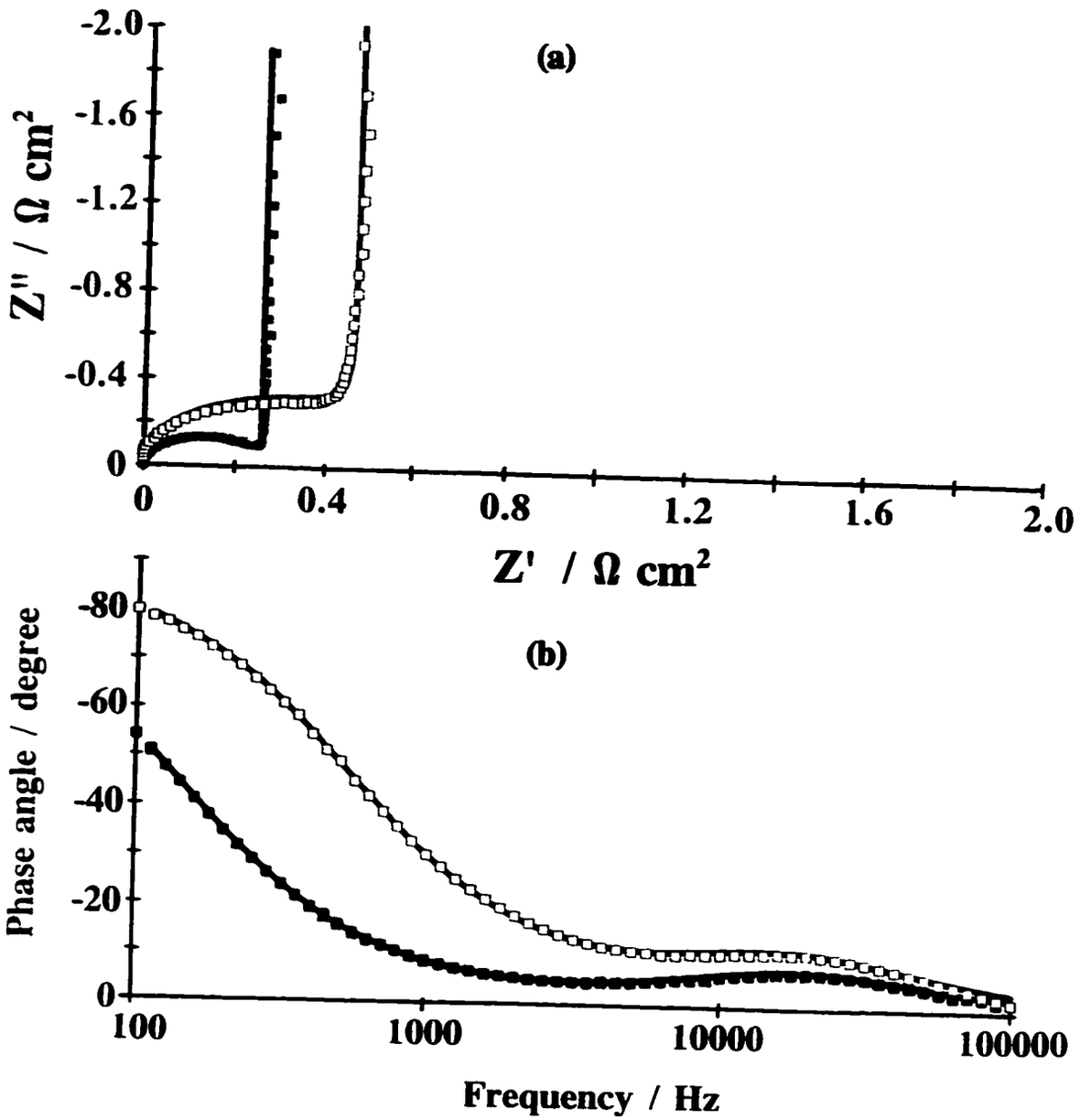

Fig. 4.6 a) Complex-plane impedance plots; and b) Bode phase-angle plots for Pt (100) in 0.5 mol dm^{-3} aqueous H_2SO_4 at 293 K for the two given potential values (■) 300 mV and (□) 200 mV. The solid lines correspond to fitting of the data using the equivalent circuit in Fig. 2a. Note that the solution resistance was compensated in these figures and the Z' and Z'' values are in Ω cm^2.

observed standard deviations from the fitting are much smaller than cumulative errors of surface area of the electrodes (about 3 %) together with change in the total capacitance on the CV due to contamination during the ac measurements (< 5 %).

Table 4.1 Parameters for UPD of H obtained by fitting to the proposed equivalent circuit (Fig. 4.4a) the ac impedance data for Pt (100) in contact with 0.5 mol dm^{-3} H_2SO_4 solution (at 293 K)*

E_θ (mv)	R_{ct1} Ω cm^2	C_{pl} 10^6 F cm^{-2}	C_{dl} 10^6 F cm^{-2}
125	0.361 ± 0.004	147.8 ± 0.06	23.0 ± 0.4
200	0.588 ± 0.005	146.8 ± 0.04	19.5 ± 0.3
250+	0.300 ± 0.003	377 ± 0.3	33.2 ± 0.5
275+	0.284 ± 0.002	630 ± 0.7	41.3 ± 0.7
290	0.349 ± 0.002	733 ± 0.2	33.9 ± 0.5
300+	0.259 ± 0.002	812 ± 0.2	34.5 ± 0.7
315	0.428 ± 0.002	970 ± 3	42.2 ± 0.9
325	0.228 ± 0.002	1020 ± 2	61 ± 1
350	0.401 ± 0.004	1180 ± 1	110 ± 2
355	0.431 ± 0.004	1480 ± 1	124 ± 2
365	0.350 ± 0.004	2070 ± 2	172 ± 4
375	0.392 ± 0.005	1750 ± 2	171 ± 5
385	0.518 ± 0.008	931 ± 0.9	167 ± 4
395	0.632 ± 0.010	610 ± 0.5	156 ± 3
400+	0.839 ± 0.001	410 ± 0.3	141 ± 3
450	2.5 ± 0.4	35 ± 0.2	99 ± 2

* The errors given correspond to the standard deviations from the fits.
+ At the given potentials, the parameters shown are the averages of the values obtained and their corresponding standard deviations.

The ac impedance data shown in the Table were fitted entirely using the circuit in Fig. 4.4a (see section 4.3.2).

It should be mentioned here that inclusion of constant phase elements (CPE's) in the equivalent circuits was unnecessary in the fitting of the data shown below mainly because, on the type of surface examined in this study, we believe there is little surface inhomogeneity on the well prepared single-crystal surfaces used. However, the effect of addition of a CPE *was* investigated and, from this, two things were observed: a) the optimum value of the CPE dimensionless φ parameter, which is used in the CPE representation [42], had to be very close to 1 and b) inclusion of the CPE had the effect of diminishing the precision of the fits. The conclusion then is that an inclusion of a CPE is unnecessary.

4.3.1 Results for the kinetics of H UPD on various single-crystal surfaces of Pt

In the course of this work, ac frequency scans were performed on the following single-crystal faces; Pt (100), (110), (111) and (311). At 293 K, it is important to mention that rates of H UPD were accessible, *i.e.* determinable (at frequencies < 300 kHz) only on the Pt (100) and (311) surfaces. The rates for UPD of H on the two other surfaces studied, (111) and (110), were clearly much greater than on the former two faces. In order to quantify the kinetic differences, low-temperature ac impedance studies are required (see Chapter 5). Hence, for now, the discussion of the results will be focused on the data for the two faces that did give an accessible impedance response, i.e. R_{ct} for the charge-transfer process studied.

Figs. 4.10 and 4.11, displayed later (pages 131 and 132), show the results derived from the fitted data for Pt (100) and (311) surfaces, respectively, for each component of the circuit, namely C_{dl}, C_p's and R_{ct}'s over the whole range of potentials (100 to 450 mV) investigated. According to Fig. 4.4b, each of the Faradaic branches of the equivalent circuit are labelled R_{ct1}, C_{p1} and R_{ct2} and C_{p2}, respectively. In the case of C_p for Pt (100) (Fig. 4.10a) and C_{p1} and C_{p2} for Pt (311) (Fig. 4.11a) it is clear that the derived values follow the features of the profiles of H UPD observed in cyclic voltammetry, which was to be expected from what is already known for such processes [11,17].

As a matter of fact, for all the faces studied (including Pt (111) and (110)), the total capacitance values obtained from the cyclic voltammogram profiles correspond almost exactly to the sum of the C_p's and C_{dl} obtained from the fitted impedance data. However, as mentioned earlier, we shall see that some care must be taken in the interpretation of the impedance results, since bisulphate anions are almost certainly co-adsorbed on these two faces at potentials positive to 375 mV in the case of Pt (100) [50,52] and positive to 275 mV for Pt (311) [51,52]. Hence, it is only for potential values less positive than those mentioned above that the measured kinetics solely apply to the process of UPD of H and correspond to the equivalent circuit given in Fig. 4.4a.

4.3.2 Consistency between the total capacitance and the corresponding UPD voltammogram

As an internal check on the results, the total capacitance (C_{dl} + C_p's = C_{tot}) was plotted as a function of potential in Figs. 4.7 and 4.9 for Pt (100) and (311), respectively. These figures compare C_{tot}'s obtained from the impedance results with those calculated from the respective cyclic voltammograms. It is clear from these results that in the absence of substantial surface contamination during the ac frequency scan the total capacitance values are in very good agreement with each other in the case of Pt (311) (Fig. 4.9). In the case of Pt (100), the C_{tot} values are also in good agreement with each other but only for potentials less positive than 375 mV which is the potential of the maximum of the largest UPD H peak for this face.

The disagreement observed above 375 mV can be explained in terms of the cyclic voltammograms shown in Fig. 4.8, where a change of cyclic voltammetry response current due to some "labile" surface modification arises on Pt (100) in 0.5 mol dm^{-3} H_2SO_4 upon performing an ac frequency-scan above 375 mV (see caption to Fig. 4.8). We have referred to this surface modification as "labile" since the surface goes back to its initial state as soon as the potential scan is reversed at the less positive end of the potential range investigated (i.e. 60 mV). This apparent loss in C_{tot} for this surface in reality corresponds to the calculated capacitance of the modified surface (Fig. 4.8, dotted

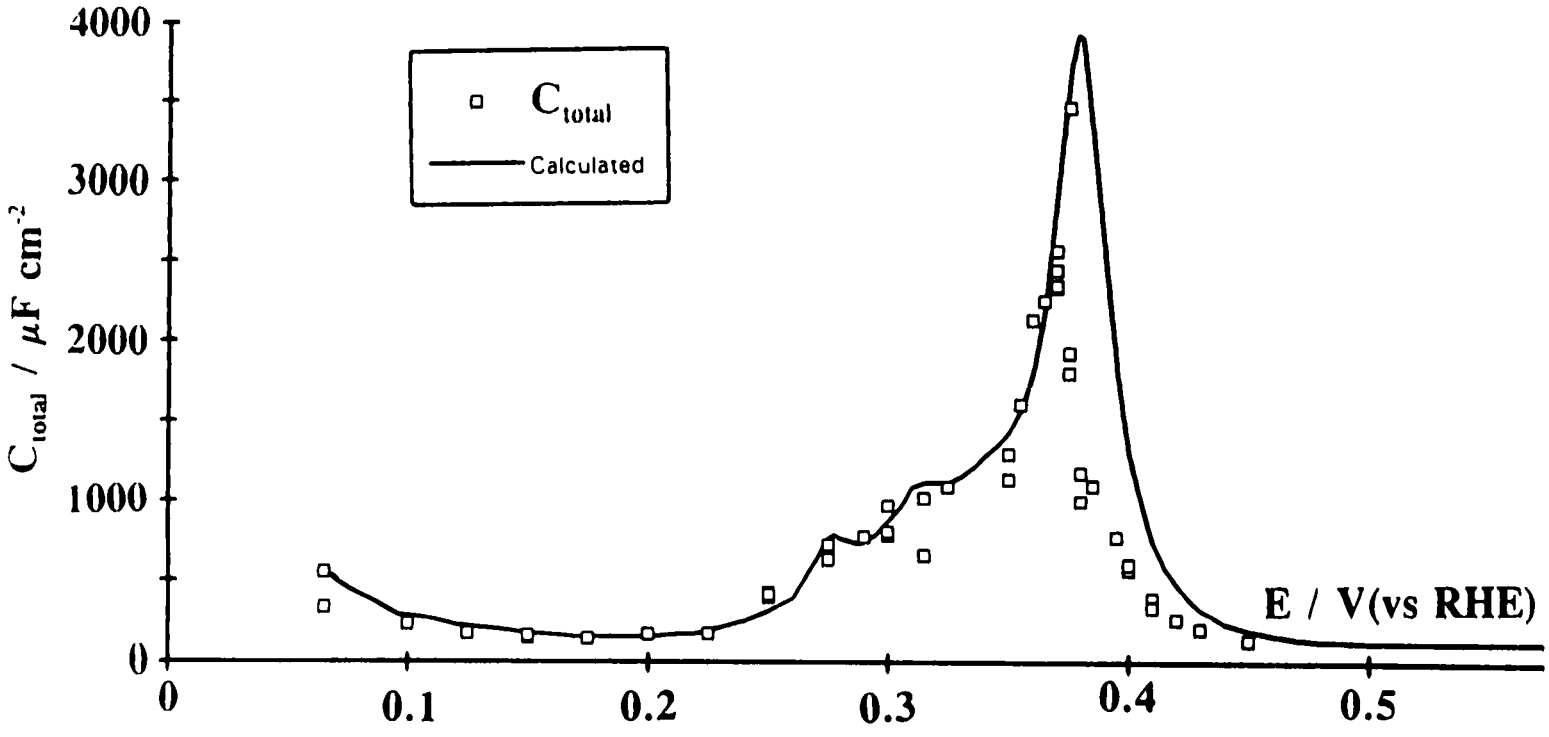

Fig. 4.7 Total capacitance (C_{tot}) as a function of the applied potential (vs RHE) for the adsorption-desorption of H on Pt (100) in contact with a 0.5 mol dm^{-3} aqueous H_2SO_4 solution at 293 K. The solid line corresponds to the C_{tot} calculated from the cyclic voltammogram (current-density / sweep rate = total capacitance); it is not drawn as a fit to the experimental □ points.

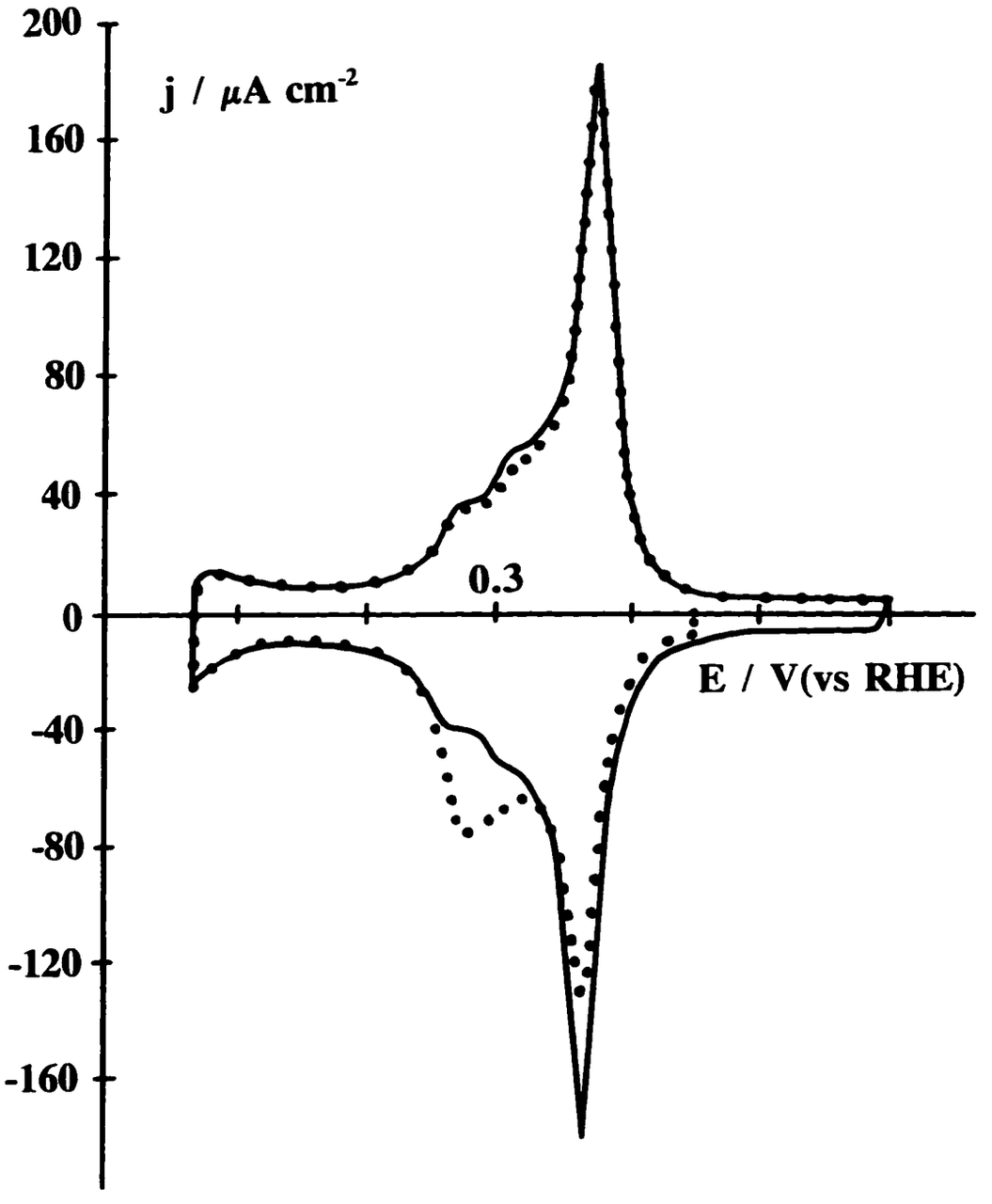

Fig. 4.8 Cyclic voltammogram for Pt (100) in 0.5 mol dm^{-3} aqueous H_2SO_4 solution before (solid line) and after holding at potentials greater than 275 mV (dashed line); see text for explanation.

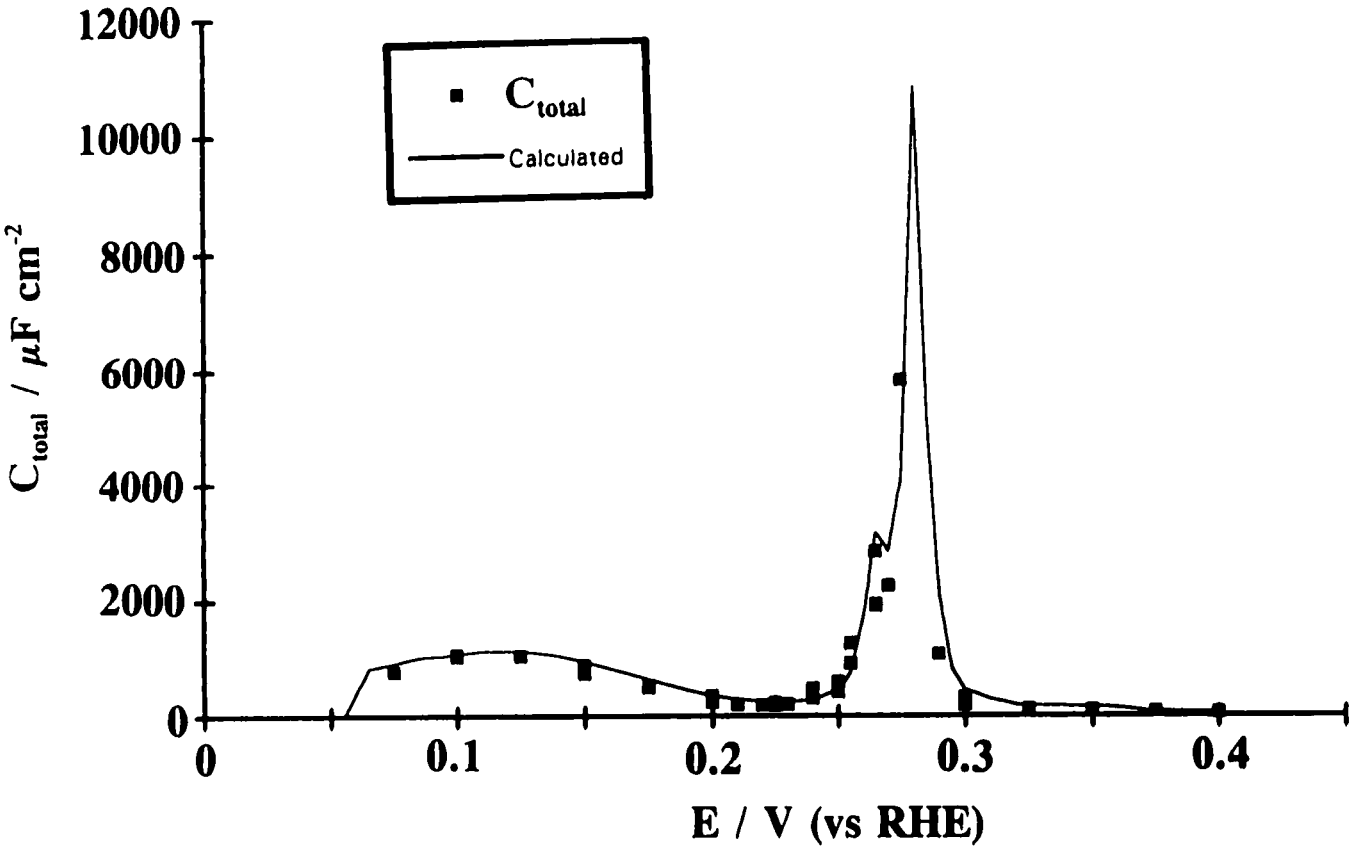

Fig. 4.9 Total capacitance (C_{tot}) as a function of the applied potential (vs RHE) for the adsorption-desorption of H on Pt (311) in contact with a 0.5 mol dm^{-3} aqueous H_2SO_4 solution at 293 K. The solid line corresponds to the C_{tot} calculated from the cyclic voltammogram (current-density / sweep rate = total capacitance); it is not drawn as a fit to the experimental ■ points.

trace). Hence, this surface modification effect is not only reversible but the modification(s) can also be formed rapidly, *i.e.* during the high frequency scan (in a few seconds). A similar "labile" state has been observed after oxidation of adsorbed carbon monoxide on Pt (100) in H_2SO_4 [50]. However, since the surface state is changing, caution is needed when discussing the ac results for this face at potentials greater than 375 mV.

The fitting of the results in this potential range using the circuit shown in Fig. 4.4b was not successful, possibly because of this surface reorganisation during the ac scan. However, the use of the equivalent circuit 4.4a yielded good fits for R_{ct}, C_{dl} and C_p associated with the fast electron-transfer process related to either H or HSO_4^- electrosorption in the potential range refered to above. The resulting C_p values then correspond to the total pseudocapacitance for both anion and hydrogen adsorption. This fitting procedure still yields good fits for the high and low frequency ends of the spectrum since the distortions observed (between 375 and 400 mV) in the ac results always occur outside these frequency regions and hence the corresponding data points add only a small statistical weight.

As was mentioned earlier, in the cases of Pt (111) and (110), for which no R_{ct} could be measured (i.e. it is too small) up to 100 KHz, a purely capacitive behaviour is then observed over the whole range of potentials. In this case, C_{tot} is observed and, as in the cases discussed above, follows the observed C_{tot} calculated from the CV's.

4.3.3 Impedance results at potentials less positive than 375 mV and 275 mV, for Pt (100) and (311), respectively

Over the above two ranges of potentials, C_p represents the H adsorption pseudocapacitance which varies with potential in the same way as the current-density in the cyclic voltammetry profiles (Figs. 4.10a and 4.11a). The corresponding C_{dl} values (Figs. 4.10b and 4.11b) for Pt (100) are almost constant and an average of the C_{dl} values is $30 \pm 6\ \mu F\ cm^{-2}$ for potentials ranging between 100 and 315 mV. On the other hand, in the case of Pt (311) (Fig. 4.11b) the C_{dl} values tend to decrease as the potential is swept from 150 to 225 mV, indicating that C_{dl} in this region of potential is larger for the

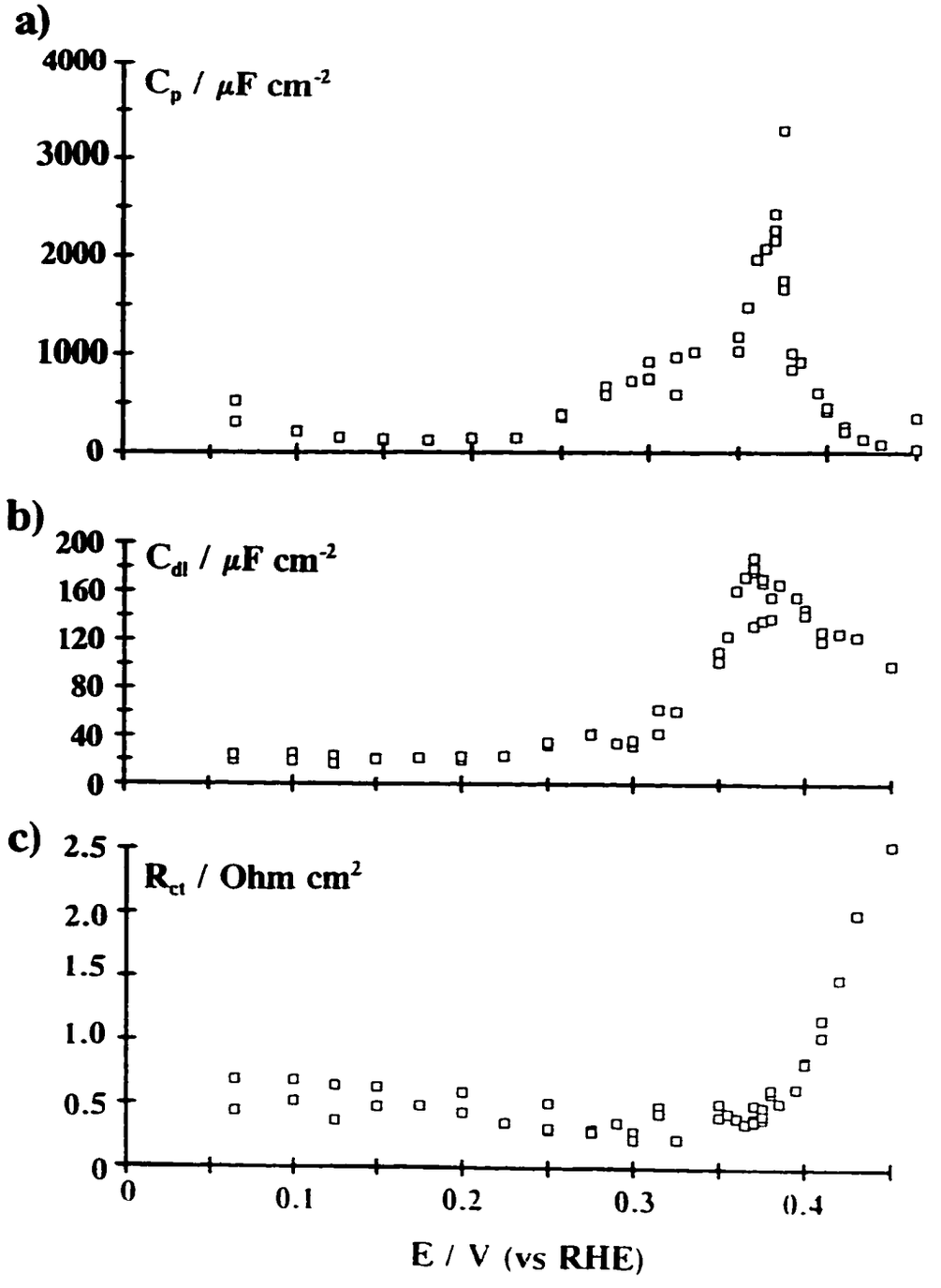

Fig. 4.10 a) Pseudocapacitance (C_p), b) double-layer capacitance (C_{dl}) and c) charge-transfer resistance (R_{ct}) as a function of the applied potential (vs RHE) for the adsorption-desorption of H on a Pt (100) surface in contact with a 0.5 mol dm^{-3} aqueous H_2SO_4 solution at 293 K.

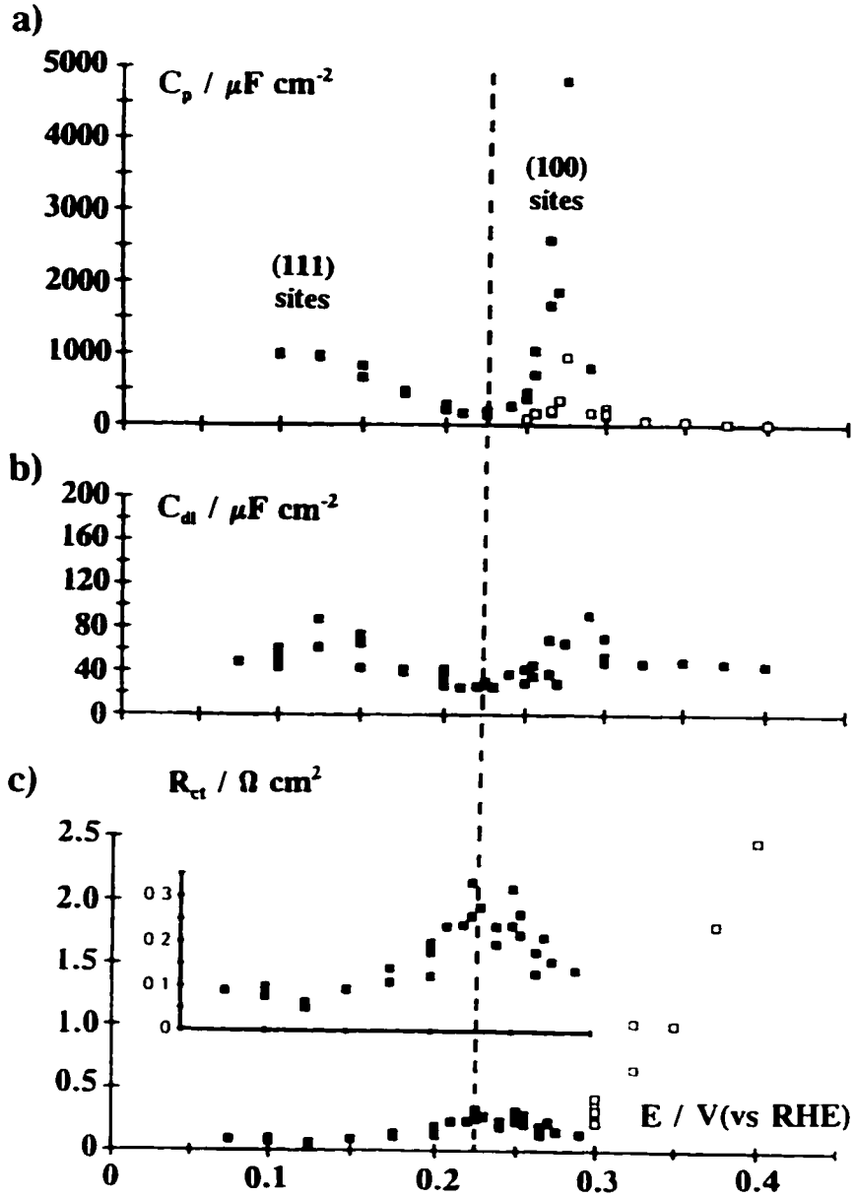

Fig. 4.11 a) Pseudocapacitance (C_{p1}, ■ and C_{p2}, □), b) double-layer capacitance (C_{dl}) and c) charge-transfer resistance (R_{ct1}, ■ and R_{ct2}, □) as a function of the applied potential (vs RHE) for the adsorption-desorption of H on a Pt (311) surface in contact with a 0.5 mol dm^{-3} aqueous H_2SO_4 solution at 293 K. A dashed line is drawn on the figure to separate the UPD of H (■) in two regions corresponding to adsorption at the (111) and (100) sites, as shown. Also, c) includes an inset of the R_{ct} data on a larger R_{ct} scale.

(111) site arrays than at those for (100). Moreover, between 200 and 250 mV, the C_{dl} values for Pt (311) (Fig. 4.11b) are evidently close to those obtained for Pt (100) (Fig. 4.10b).

The corresponding R_{α} values, which are proportional to the inverse of the exchange rate of the process of UPD of H, are shown in Figs. 4.10c and 4.11c, for Pt (100) and (311), respectively. In the region of potential referred to in this section, the exchange rate is virtually constant with changing potential for Pt (100), where the average R_{α} value is $0.37 \pm 0.08\ \Omega\ cm^2$. Using the known relation between R_{α} and $\nu_{o,\theta}$ ($\nu_{o,\theta} = RT / nF^2 R_{\alpha}$), the average rate of charge transfer, found equal to 7×10^{-7} mol s^{-1} cm^{-2}, was calculated. In the case of Pt (311) (Fig. 4.11c) R_{α} is smaller (on the average $0.09 \pm 0.02\ \Omega\ cm^2$) indicating that the rate is faster on the (111) sites (3×10^{-6} mol s^{-1} cm^{-2} on the average between 75 and 200 mV) than on the (100) sites of the (311) surface, reaching the value observed for the well-ordered (100) surface (7×10^{-7} mol s^{-1} cm^{-2}, see also Fig. 4.10c) around 250 mV. The fact that the H adsorption-desorption is faster (by four times) on the (111) sites is consistent with the observations on the (111) surface mentioned in the previous section. By examining the R_{α} values for Pt (311) (Fig. 4.11c) more closely, it is seen that these values increase to reach a maximum around 240 mV which coincides, on the CV profile (Fig. 4.5b), with the minimum in the CV current. Moreover, as the adsorption or desorption current starts to increase markedly ($E > 240$ mV) corresponding to the onset of adsorption of H on the (100) sites of the (311) plane, the resulting R_{α} values decrease slightly, corresponding to faster kinetics.

The fact that R_{α} remains *constant* for Pt (100) with potential over some 250 mV in Fig. 4.10c may seem surprising. However, R_{α} for the UPD manifold should not vary with potential in that range in the same way as a Tafel relation (like that for OPD) but rather refers to a range of adsorbed H states at various coverages, θ_H, each always near equilibrium at all respective E_{θ} potentials (eq. 4.31) in the UPD region, as was emphasised in section 4.1.3.

4.3.4 Impedance results for potential values around the capacitance peaks of Pt (100) and (311)

For potential values beyond 275 mV on Pt (311), the response is not solely associated with H adsorption-desorption but also with HSO_4^- adsorption-desorption [50] over a narrow potential region more positive to the current maximum in the CV. Using the circuit in Fig. 4.4b to fit the data, it was found that the exchange rate ($1/R_{ct1}$) (see Figs. 4.11c and 4.12) remains almost unchanged over this potential region while the exchange rate ($1/R_{ct2}$) for the other process (Fig. 4.12) increases markedly from 250 mV to 290 mV and a slow increase is observed in the C_{dl} values over that potential range. The corresponding C_p's (C_{p1} and C_{p2}) are shown in Fig. 4.11a where the C_{p2} values associated with the large R_{ct2} are the open squares in Fig. 4.12 and the C_{p1} are associated with the small R_{ct1} values (Fig. 4.12, filled squares). It is clear, by considering the magnitude of the C_p's, that the R_{ct2} values can be associated with species being adsorbed to a smaller extent at these potentials whereas the R_{ct1} corresponds to the majority species present at the surface. From what is already known about the adsorption of anions on Pt (311) and (100) [50-52], the anion adsorption is least on these two faces (about 60 μC cm^{-2} passes when anions are displaced using CO adsorption [50-52]). Moreover, for the concentration of electrolyte studied (0.5 mol dm^{-3}), the C_{dl} values would obviously not show any feature related to the diffuse part of the double-layer; instead a maximum in C_{dl} would, if anything, be observed around the *pzc* [53]. Similar behaviour of C_{dl} was observed by Flinn *et al.* [19] for two concentrations of H_2SO_4 (1 mol dm^{-3} and 9.5 x 10^{-3} mol dm^{-3}) at a Pt polycrystalline electrode whereas, for a concentration of 3.6 x 10^{-4} mol dm^{-3} H_2SO_4, these authors observed a minimum in C_{dl} around 240 mV (vs NHE) [19]. From these considerations, we believe that the onset in the increase of C_{dl} (Fig. 4.11b) corresponds to the onset of anion adsorption, and further increase in the anion coverage (increase in C_{p2}) corresponds to a decrease of the R_{ct2} values (Fig. 4.12). However, in refs. 50-52, it is seen that around the maximum of the capacitance peak the majority species adsorbed are negatively charged; hence, to which of H or HSO_4^- should be assigned C_{p1} or C_{p2}, becomes difficult.

The inset in Fig. 4.12 gives one example of a complex-plane plot that clearly

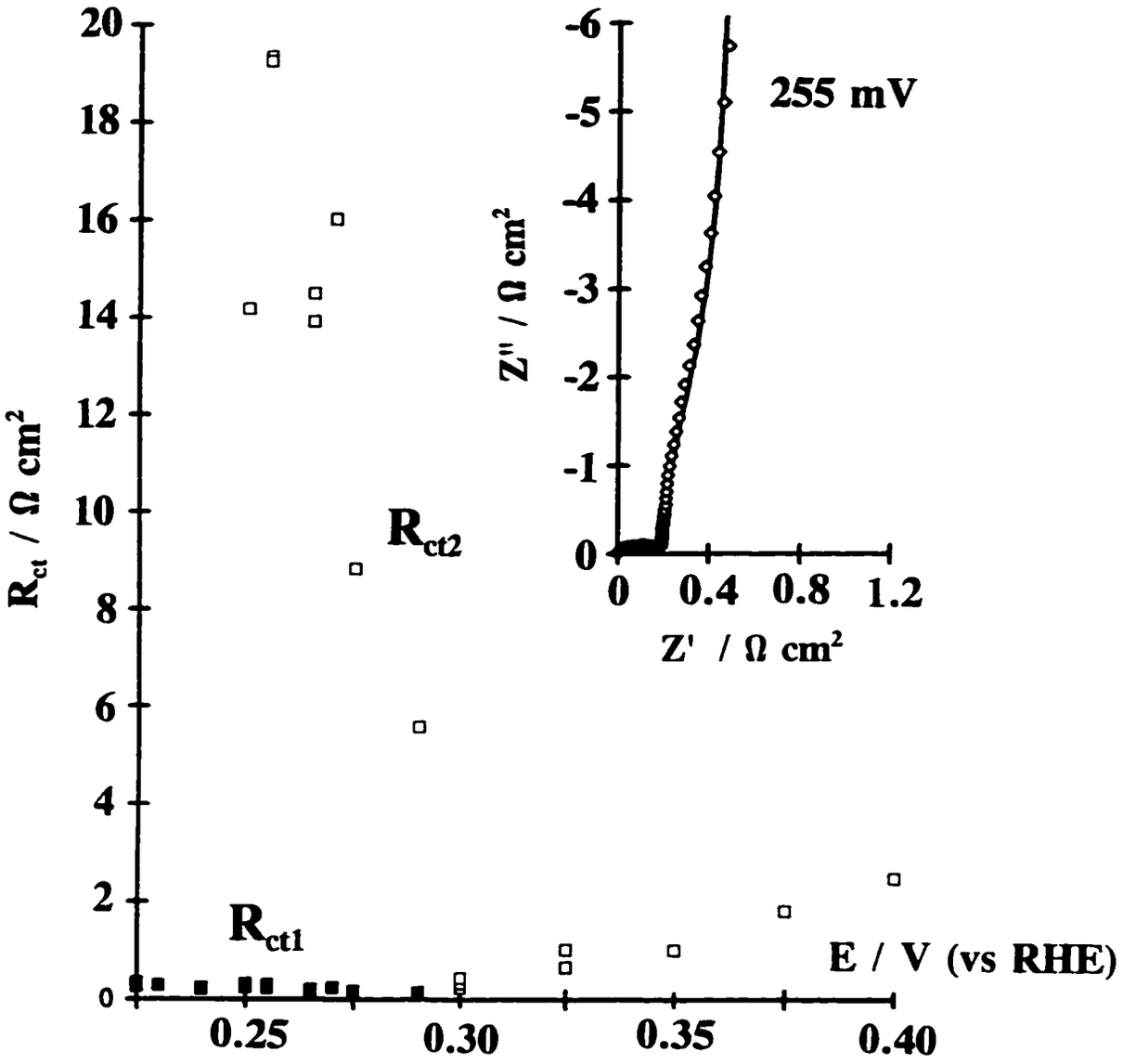

Fig. 4.12 Charge-transfer resistances (R_{ct1}, ■ and R_{ct2}, □) as a function of the applied potential (vs RHE) for the adsorption-desorption of H on Pt (311) in contact with a 0.5 mol dm^{-3} aqueous H_2SO_4 solution at 293 K, for the potential region (250 mV to 300 mV) where anion co-adsorption can be detected (see text). *Inset*: Complex-plane impedance plots for Pt (311) for an applied potential of 255 mV (◇). The solid line corresponds to the fitting of the data using the equivalent circuit in Fig. 2b. Note that the solution resistance was compensated in this figure and the Z' and Z" values are in Ω cm^2.

shows the presence of two charge-transfer processes occurring at 255 mV for Pt (311), the first semi-circle is located between 0 and 0.2 Ω cm^2 on the Z' axis while only part of the second one is resolved beyond this resistance value; nevertheless, the diameter of the second semi-circle is clearly much bigger corresponding to a larger R_{ct}. The treatment of these data as well as those for potentials between 250 and 290 mV (Fig. 4.12), using the equivalent circuit in Fig. 4.4b, produces fits with standard deviations for C_{dl}, R_{ct1}, C_{p1}, C_{p2} in general higher than those reported in Table 4.1, where the standard deviation on R_{ct2} can be as big as 20 % in comparison with 2% for R_{ct1}. In Fig. 4.12 (inset) the standard deviation on R_{ct2} was 10%, 5% for C_{dl} and C_{p2}, and 2% for C_{p1} and R_{ct1}. The kinetic parameters plotted in Figs. 4.11 and 4.12 for potential values between 250 and 290 mV have larger fitting errors, which are almost certainly due to the increase of the number of circuit elements to be fitted at a given potential as well as the number of points associated with each semi-circle (statistical weight).

4.3.5 Impedance results for potentials positive to 375 mV and 275 mV for Pt (100) and Pt (311), respectively

At potentials more positive than those of the capacitance peaks, at 300 mV in the case of Pt (311), only one C_p and R_{ct} was required in the equivalent circuit to achieve a good fit of the data and any attempt to use the circuit in Fig. 4.4b, yielded values of C_{p2} and R_{ct2} that had no physical significance. From the R_{ct}, C_p and C_{dl} values it seems that coverage by HSO_4^- almost reaches a limit with potential, leading to small C_p values and almost constant C_{dl} values for both Pt (100) and (311) (Figs. 4.10b and 4.11b). This clearly shows that the applied ac perturbation leads to only minor modulation of the HSO_4^- coverage. On the other hand, the exchange rate decreases ($\propto 1/R_{ct}$, Figs. 4.10c and 4.11c) considerably when the potential is made more positive; this could be ascribed tentatively to significant interaction between adsorbed bisulphate, partially hindering its own further adsorption.

Hence, the slower kinetics could indicate that, at these potential values, the adsorbed HSO_4^- layer becomes increasingly compact and tends toward monolayer coverage, taking account of the site requirements for chemisorption of HSO_4^- with

discharge. The anomalous apparent entropy of chemisorption of H in one of the states resolved at polycrystalline Pt was already attributed in ref. 54 in 1978 to such HSO_4^- adsorption. A study by Parsons and co-workers [55] dealt with anion adsorption on Ag (111); in the case of 1 x 10^{-2} mol dm^{-3} $NaOOCCH_3$ a minimum charge-transfer resistance of 100 Ω cm^2 was measured; the reason for the slow adsorption was tentatively assigned to bond formation as well as desolvation. For the adsorption of SO_4^{2-} (1 x 10^{-2} mol dm^{-3}) at the same electrode surface, a minimum charge-transfer resistance of 60 Ω cm^2 was observed.

From the experimental results on the kinetics of H adsorption-desorption on polycrystalline electrodes [12-14,17,20], it is possible to compare the rates observed in those studies and in that reported here. The general trend observed is that the (average) rate of UPD of H on polycrystalline Pt is greater than the rates on Pt (100) and (311) surfaces.

As was observed in some studies on polycrystalline Pt [18,20,11b], the rate of UPD of H on Pt (100) is observed to be almost independent of potential. However, on the (311) stepped face, the rate ($1/R_\alpha$) varies with potential according to the type of sites available in a given range of potential. As was observed by Durand [8] for a polyoriented Pt monocrystal sphere, the observed rates of UPD of H follow the capacitance peak of the UPD profile; this behaviour was not observed, however, on a contaminated surface where the rate was indeed almost constant with potential.

4.3.6 Variation of the charge-transfer resistance with potential

In the case of the kinetic, R_α, data for Pt (311), shown in Fig. 4.11c, the dependence of R_α on potential, E, follows, for this case, the variation of C_p with E in Fig. 4.11a. However, for Pt (100) (Fig. 4.10), the R_α values decline uniformly with potential from 0.06 V to 0.37 V without exhibiting a minimum (≡ maximum rate) at the potential, 0.365 V, of the maximum in C_p (Fig. 4.10a) or the maximum in the cyclic voltammetry current profile (Fig. 4.8). This result seems anomalous but it may be due to the effect of HSO_4^- adsorption which leads to an increase (inhibiting effect) of R_α on this (100) face as seen in the rising region of the R_α *vs* E plot in Fig. 4.10c at potentials

just above 0.37 V.

In the paper of Woodard *et al.* [32a], theoretically calculated correlations between C_p (written in their paper as C_ϕ) and log R_{ct} (written as log R_f) were shown in which log R_f exhibited a minimum at the C_p maximum, the potential of which ($E^{o'}$) they identified as a standard reversible potential. They supposed, and their calculations showed, that at potentials sufficiently displaced from $E^{o'}$, the log [kinetic parameter] would supposedly vary linearly with E in a Tafel-like function with slopes determined by the transfer coefficient for the kinetics. However, we believe this modelling of the kinetic behaviour is incorrect since displacements of potential from the maximum of the C_p profile do not result in a Tafel-type change of rate-constant but rather, simply, a change of rate or R_{ct} due to the potential-dependent change of *equilibrium coverage* according (Langmuir case) to eqn. 4.29. Thus, the transition to Tafel-type behaviour is not expected just because E diverges appreciably from $E^{o'}$ [32] but rather only when $s \gg s_o$ or equivalently at high ω. Hence a minimum in R_{ct} or log R_{ct} is not necessarily to be expected for kinetic reasons in modulation experiments *except* when high frequencies or large sweep-rates, $s \gg s_o$ [21], are applied. This point was already noted in a general way earlier in section 4.1.3.

In the region where both anions and H are present at the (311) surface (Figs. 4.11c and 4.12) the variation of R_{ct} with potential is more consistent with a variation of the rate with coverage. Similar variations of R_{ct} with potential were observed in ref. 55 for the adsorption of anions at an Ag (111) electrode. In our case, however, the adsorption cannot be treated by a simple Langmuir isotherm. This is seen in the CV's from the appearance of large narrow current peaks on Pt (100), (311) and (110) in the potential regions where there is both H and bisulphate adsorption [50-52].

The quasi absence of variation of R_{ct} with coverage, hence potential, at the Pt (100) surface in the case of the UPD process, as well as an almost constant energy of activation (see the following Chapter 5) for intermediate coverages, was not an expected behaviour and, at the moment, remains unexplained, except for the possibility suggested earlier in this section of interaction effects due to co-adsorbed HSO_4^-.

4.4 Conclusions

By comparing the various ac modulation responses obtained on (100) and (311) surfaces and the literature values for a polycrystalline electrode [12-14,17,20], the $H/H^+ + e$ exchange rates are shown to vary in the following order as a function of the surface geometry: [(111) and (110)] > polycrystalline > (100). The turn-over rate calculated from the surface concentration of H at the various surfaces yielded values as high as *ca.* 16000 monolayers of H per second for (111) and significantly slower for (100), *ca.* 350 monolayers s^{-1}. The evaluation of the turn-over rate on (111) was extrapolated from the results of ref. 36, where the exchange rate for UPD of H at polycrystalline Pt was found to be ten times smaller than that observed at a (111) surface in 1 mol dm^{-3} KOH solution.

At the (311) stepped surface the observed exchange rates were faster (*i.e.* 4 times) at the (111) than at the (100) sites, where the observed exchange rates for the latter show no variation from the values derived for the homogeneous (100) surface (*ca.* 7×10^{-7} mol s^{-1} cm^{-2}).

In summary, the kinetics of UPD of H on well ordered Pt (100) and (311) in contact with an H_2SO_4 solution have been determined for the first time, and are found to be characteristically different, and also substantially slower than on Pt (111) and (110) geometries. This information is essential to the understanding of the effect of surface geometry in electrocatalysis of H discharge and chemisorption below a monalayer, and also in the OPD of H involved in the HER. It is also clear from the present double-layer capacitance results on Pt (100) and (311) that each surface atomic arrangement, including surface structures with steps and terraces, has a distinct double-layer structure and corresponding capacitance, as is known also at Au [56].

References

1. L. Bai and B.E. Conway, J. Electroanal. Chem., 198 (1986) 149.
2. R.J. Nichols and A. Bewick, J. Electroanal. Chem., 243 (1988) 445.
3. H. Kita, S. Ye and Y. Gao, J. Electroanal. Chem., 334 (1992) 351.
4. J. Clavilier, J.M. Feliu, A. Fernandez-Vega and A. Aldaz, J. Electroanal. Chem., 294 (1990) 193.
5. R. Gomez, A. Fernandez-Vega, J.M. Feliu and A. Aldaz, J. Phys. Chem., 97 (1993) 4769.
6. H. Ogasawara and M. Ito, Chem. Phys. Lett., 221 (1994) 213.
7. A. Peremans and A. Tajeddine, J. Chem. Phys., 103 (1995) 7197.
8. a) S. Trasatti, Electrochim. Acta, 32 (1987) 369; b) R. Parsons, Trans. Faraday Soc., 34 (1958) 1093.
9. R. Parsons, Trans. Faraday Soc., 56 (1960) 1340.
10. B.E. Conway and L. Bai, Electrochim. Acta, 31 (1986) 1013.
11. a) M. Breiter, H. Kammermaier and C.A. Knorr, Zeit. Elektrochem., 60, 37 (1956); b) M. Breiter, Transactions of the Symposium on Electrode processes, (Ed. E. Yeager), Wiley, New York (1961) p. 307.
12. V.I. Luk'yanycheva, E.M. Strochkova, V.S. Bagotskii and L.L. Knots, Elektrokhimiya 7 (1971) 267.
13. a) O.A. Petrii, A.N. Frumkin, V.A. Safonov and I.G. Shchigorev, Elektrokhimiya 7 (1971) 1352; b) V.A. Safonov, V.D. Dishel and O.A. Petrii, Elektrokhimiya, 9 (1973) 264; c) N.A. Epshtein, B.I. Podlovchenko, O.A. Ptrii and V.A. Safonov, *ibid*, 10 (1974) 561; d) V.A. Safonov, B.I. Podlovchenko and O.A. Petrii, *ibid*, 12 (1976) 1601.
14. a) R. Durand, Electrochim. Acta, 24 (1979) 1095; b) R. Durand, C.r. hebd. Séanc. Acad. Sci., Paris 278C (1974) 821.
15. R. Durand, J. Electroanal. Chem., 97 (1979) 293.
16. T. Ohsaka, Y. Sawada, T. Yoshida and K. Nihei, J. Electrochem. Soc., 123 (1976) 1339.
17. P. Dolin and B. Ershler, Acta Physicochim. URSS, 13 (1940) 747.

18. J. Honz and L. Němec, Coll. Czech. Chem. Commun., 34 (1969) 2030.
19. D.R. Flinn, M. Rosen and S. Schuldiner, Coll Czech. Chem. Commun. 36 (1971) 454; and M. Rosen, D.R. Flinn and S. Schuldiner, J. Electrochem. Soc., 116 (1969) 1112.
20. D.R. Flinn and S. Schuldiner, Electrochim. Acta, 19 (1974) 421.
21. H. Angerstein-Kozlowska and B.E. Conway, J. Electroanal. Chem., 95 (1979) 1.
22. A. Lasia, Proceedings of the symposium on "Electrochemistry and Materials Science of the Cathodic Hydrogen Absorption and Adsorption", (eds. B.E. Conway and G. Jerkiewicz) The Electrochemical Soc. Inc., New Jersey, Vol. 94-21, 1994, p. 261.
23. D.A. Harrington, J. Electroanal. Chem., 355 (1993) 21.
24. S. Morin, H. Dumont and B.E. Conway, accepted for publication J. Electroanal. Chem., February 13, 1996.
25. B.E. Conway and B.V. Tilak, Advances in Catalysis, 38 (1992) 1, and references therein.
26. I.I. Physnogreva, A.M. Skundin, Yu. B. Vasiliev and V.S. Bagotsky, Elektrokhimiya, 6 (1970) 142.
27. S. Schuldiner, M. Rosen and D. Flinn, J. Electrochem. Soc., 117 (1970) 1251.
28. K. Seto, A. Iannelli, B. Love and J. Lipkowski, J. Electroanal. Chem., 226 (1987) 351.
29. J. Clavilier, K. El Achi, M. Petit, A. Rodes and M.A. Zamakhchari, J. Electroanal. Chem., 295 (1990) 333.
30. D. Armand and M.L. Rosinberg, J. Chim. Phys., 88 (1991) 1401.
31. J.O'M. Bockris, Modern Aspects of Electrochemistry, Butterworths, London, Vol. 1, 1954, Chapter 4.
32. a) F.E. Woodard, M.K. Hanafey and C.N. Reilley, J. Electroanal. Chem., 167 (1984) 43; b) F.E. Woodard and C.N. Reilley, J. Electroanal. Chem., 167 (1984) 65.
33. B.E. Conway and H. Angerstein-Kozlowska, Acc. Chem. Res., 14 (1981) 49.

34. D.M. Newns, Phys. Rev., 178 (1969) 1123.

35. K. Christmann, Surf. Sci. Reports, 9 (1988) 1, section 3 and 4, and references therein.

36. R. Oelgeklaus, J. Rose and H. Baltruchat, J. Electroanal. Chem., 376 (1994) 127.

37. C. Nishihara and H. Nozoye, J. Electroanal. Chem., 379 (1994) 527.

38. W. Savich, S. Sun, J. Lipkowski and W. Wieckowski, J. Electroanal. Chem., 388 (1995) 237.

39. J. Clavilier, A. Rodes, K. El Achi and M.A. Zamakhchari, J. Chim. Phys., 88 (1991) 1291.

40. A.J. Bard and L.R. Faulkner, "Electrochemical Methods: fundamentals and applications, John Wiley and Sons, Inc., New York, 1980, 718 pages.

41. D.C. Grahame, Chem. Rev., 41 (1947) 441.

42. a) G.J. Brug, A.L.G. van der Eeden, M. Sluyters-Rehbach and J.H. Sluyters, J. Electroanal. Chem., 176 (1984) 275; b) T. Pajkossy, J. Electroanal. Chem., 364 (1994) 111.

43. R. Greef, R. Peat, L.M. Peter, D. Pletcher and J. Robinson, "Instrumental Methods in Electrochemistry, Ellis Horwood seires in physical chemistry, New York, 1990, 443 pages.

44. D.M. Kolb, Adv. Electrochem. Electrochem. Eng., 11 (1978) 125.

45. M. Breiter, Electrochim. Acta, 7 (1962) 25.

46. a) S. Srinivasan and E. Gileadi, Electrochim. Acta, 11 (1966) 321; b) H.A. Angerstein-Kozlowska, J. Klinger and B.E. Conway, J. Electroanal. Chem., 75 (1977) 45.

47. D.A. Harrington and B.E. Conway, Electrochim. Acta, 32 (1987) 1703.

48. T. Wandlowski and R. de Levie, J. Electroanal. Chem., 388 (1995) 199.

49. J.R. Macdonald, Electrochim. Acta, 35 (1990) 1483.

50. a) J. Clavilier, J.M. Orts, R. Gómez, J.M. Feliu and A. Aldaz, Proceedings of the symposium on "Electrochemistry and Materials Science of Cathodic Hydrogen Absorption and Adsorption", (eds. B.E. Conway and G. Jerkiewicz) The

J.M. Orts, R.Gómez, A.Aldaz and J. Clavilier, J. Electroanal. Chem., 372 (1994) 265.

51. R. Gómez, Ph.D. Thesis, Universitat d'Alacant, Alacant, Spain, 1994.
52. These results were verified in this work using carbon monoxide adsorption to displace anions from the surface, as employed in refs. 41 and 42.
53. D.C. Grahame, Chem. Rev., 41 (1974) 441.
54. B.E. Conway, H.A. Angerstein-Kozlowska and W.B.A. Sharp, J. Chem. Soc., Faraday Transactions I, 78 (1978) 1373.
55. V.D. Jović, R. Parsons and B.M. Jović, J. Electroanal. Chem., 339 (1992) 327.
56. A. Hamelin, in "Modern Aspects of Electrochemistry", B.E. Conway, J.O'M. Bockris and R.E. White (Eds.), Plenum, New York, 1985, Vol. 16, Chapter 1.

Chapter 5

Effect of temperature on the kinetics of the UPD process and determination of the apparent activation energy ($E_a^{\ddagger}$)

5.1 Introduction

It is an experimental fact that most rate constants, k, of solution-phase reaction vary with temperature following the well known Arrhenius relations:

$$k = A\, e^{-\Delta E_a^{\ddagger}/RT} \qquad (5.1)$$

where $E_a^{\ddagger}$ is the activation energy and the coefficient A is generally known as the frequency factor. The latter originates from the interpretation based on the energy barrier and, according to the absolute rate theory, for an heterogeneous reaction A is equal to the product of κ, the transmission coefficient and Z given by $k_B T\delta/h$ where δ is a reaction length of the order of a molecular diameter. Z can also be interpreted as the upper limit to the heterogeneous rate constant set by the vibrations of the transition state, and it is commonly taken to have a value between 10^4 to 10^5 cm s^{-1} [1].

In the condensed phase, $\Delta E_a^{\ddagger} \sim \Delta H^{\ddagger}$ and the Arrhenius equation could be rewritten as

$$k = A\, e^{-\Delta H^{\ddagger}/RT} \qquad (5.2)$$

where A could be expressed as the product A' exp ($\Delta S^{\ddagger}/R$). From this, two equations equivalent to the Arrhenius one (eq. 5.1) can be written:

$$k = A'\, e^{-(\Delta H^{\ddagger} - T\Delta S^{\ddagger})/RT} \qquad (5.3)$$

$$k = A'\, e^{-\Delta G^{\ddagger}/RT} \qquad (5.4)$$

where the Gibbs activation energy, $\Delta G^{\ddagger}$, is also a function of the standard free energy of the reaction, the work required to bring the reactant or products to a giving distance and it is also a function of the so-called reorganisation energy, λ [1].

This reorganisation energy is the sum of the energies for the changes in the bond

lengths of the reactants in order to form the products and that corresponding to the changes in solvent orientation coordinates; this value is usually evaluated by treating the medium as a dielectric continuum [1].

Electrochemical processes differ from other heterogeneous process since their rate constants are affected by the potential difference at the electrode/solution interface. Hence, the Gibbs activation energy for an electron transfer process, $\Delta G^{\ddagger}$, depends by a fraction (β, the barrier symmetry coefficient) of the energetic changes of the electrons in the metal resulting from the polarisation of the interface:

$$\Delta G^{\ddagger} = \Delta G^{o\ddagger} \pm \beta nFE \qquad (5.5)$$

where $\Delta G^{o\ddagger}$ is the Gibbs standard activation energy when the potential difference at the interface (E) is equal to zero and n normally has a value of 1.

However, determinations of the heats of activation of electrochemical reactions is obscured by the fact that they are deduced from j_o values at constant electrode potential referred to a reversible reference electrode in the electrochemical cell [2]. When both the working and reference compartment of the cell are kept at the same temperature and the temperature of the whole cell is varied, the absolute metal/solution potential difference of the reference electrode will also vary in an experimentally undeterminable manner [2]. Hence, a true heat of activation at constant electrode potential cannot be determined, so that only an *apparent* activation energy can be measured [2]. However, extra-thermodynamic corrections can be applied in a moderately reliable manner to convert apparent $\Delta H^{\ddagger}$ values to real ones with an accuracy of about 10%.

In this chapter, the apparent activation energy ($E_a^{\ddagger}$) for the processes of UPD of H was evaluated for Pt(100) and (311), and the effect of temperature on the exchange rate as well as on the measured C_{dl} and C_p examined. Moreover, low temperature measurements, at *ca.* 273 K, allowed determination of the kinetics of UPD of H at a Pt(110) surface, *i.e.* the surface for which the process was too fast to be determined at 294 K.

5.2 Results and discussion

5.2.1 Evaluation of the kinetics of UPD of H for the Pt(110) and Pt(111) surfaces

As mentioned in Chapter 4, at room temperature, the charge transfer rates at Pt(111) and (110) in contact with 0.5 mol dm^{-3} H_2SO_4 were not accessible at modulation frequencies smaller than 300 kHz; hence, low-temperature ac impedance studies were required in order to diminish the respective rate-constants so that any surface-specific differences might then be detectable.

5.2.1.1 Results for the kinetics of H UPD at the Pt(110) surface at 273 K

The results discussed in this section were acquired according to the methodology described in Chapter 2 (section 2.6.3), where the amplitude of the ac modulation was taken as 3 mV *r.m.s.* (instead of 5 mV).

The kinetic studies were performed on a flame-treated Pt(110) surface cooled in a mixture of H_2-Ar. The resulting CV for such a surface preparation was shown in Fig. 3.14 for a 0.5 mol dm^{-3} H_2SO_4 solution at 293 K.

The capacitances (C_{dl} and C_p's) and R_α's values are shown as a function of potential in Fig. 5.1 and Fig. 5.2, respectively. Contrarily to what was observed in the case of Pt(311), the C_p values recorded for the adsorption-desorption of H and HSO_4^- show significant contributions from both of these adsorption processes over an appreciable potential range, *i.e.* 0.125 to 0.280 V, where the maximum in C_p's are observed at almost the same potential, *i.e.* around 0.15 V.

When these results are compared with those obtained using the CO adsorption displacement method [3] (this procedure was outlined in section 3.2.3), very good agreement is observed between the results obtained from the two methods. For instance, in ref. 3b the amount of cathodic transient charge corresponding to bisulphate anion adsorption is almost half of the anodic transient charge at maximum H coverage (close to $\theta=1$). This also seems to be the case in the present data when comparing the area under the C_p curves associated, respectively, with the H and HSO_4^- adsorption-desorption processes (see Fig. 5.1), where the potentials for onset of the charge dependence for the two adsorption processes differ by *ca.* 25 mV.

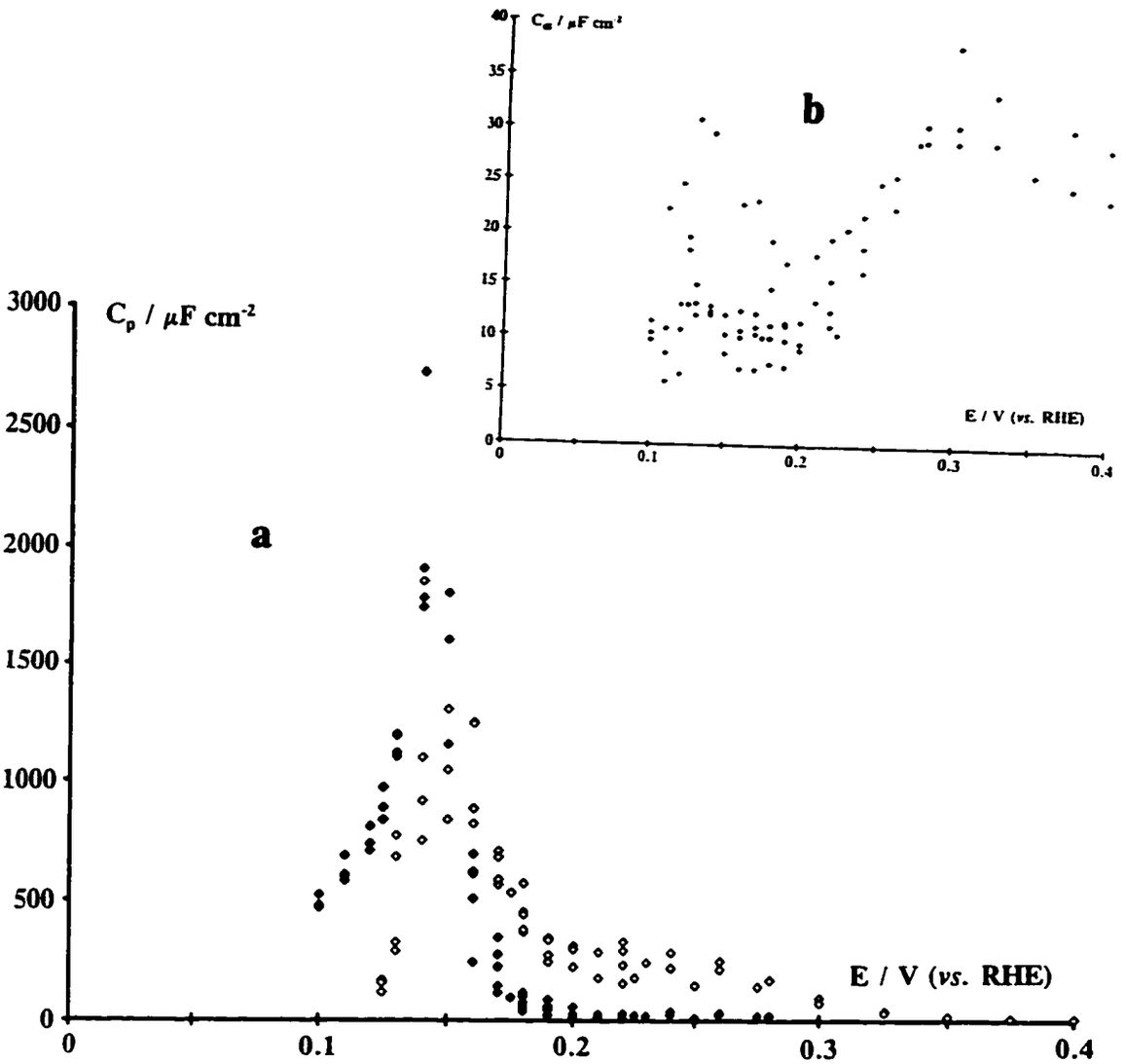

Fig. 5.1 a) Pseudocapacitances C_{p1} (◆) and C_{p2} (◇) and b) double-layer capacitance C_{dl} as a function of the applied potential (*vs.* RHE) for the adsorption-desorption of H on a Pt(110) surface in contact with a 0.5 mol dm^{-3} aqueous H_2SO_4 solution at 273 K.

These observations seem to justify the assignments of the open symbols in Figs. 5.1 and 5.2 to anion adsorption-desorption while the closed symbols are to be associated with data for the process of UPD of H.

The C_{dl} values are displayed as a function of potential in the inset of Fig. 5.1; this graph shows appreciable scattering in the data between 0.1 and 0.2 V, and a possible explanation for the origin of this behaviour will be given latter on in the discussion.

The resulting R_{ct1} and R_{ct2} values are shown in Fig. 5.2 and it should be noted here that the scatter observed in the C_{dl} values is not observed as far as the R_{ct} values are concerned. Moreover, similarly to what was observed for Pt(100) (although anion adsorption-desorption was not considered) the R_{ct}'s remain almost constant with potential when the coverage of the co-adsorbed species (either H or HSO_4^-) is small enough. It is only at potential values around the maximum of the current peak on the CV at *ca.* 0.15 V (see Fig. 3.14, p.83) that the R_{ct}'s values vary more. Similarly to what was recorded in Chapter 4, variations in R_{ct2} also occur over the potential region (> 0.25 V) where the charge for adsorption of HSO_4^- remains almost constant.

The average exchange rate for the process of UPD of H between 0.1 and 0.15 V is 1.3×10^{-6} mol s^{-1} cm^{-2} and corresponds to a turn-over rate of about 1000 monolayers s^{-1}.

Similarly to the procedure in section 4.3.2, as an internal check of the results, the total capacitance (C_{dl} + C_p's = C_{tot}) was plotted as a function of potential for Pt(110) in Fig. 5.3 where the solid line on this graph represents the capacitance calculated from the cyclic voltammograms. The agreement between the C_{tot} obtained from the ac impedance experiments and that from cyclic voltammetry is very good. However, some discrepancies are observed between 0.2 and 0.3 V, these differences are attributed to the dependence of this region of potential on the history of this electrode surface [4]. For instance, repeated cycling of Pt(110) over the UPD region will result in the diminution of the capacitive current in this region of potential, *i.e.* between 0.2 and 0.3 V, while holding of the potential would result in a marked increase in the capacitive voltammogram current over the same potential region.

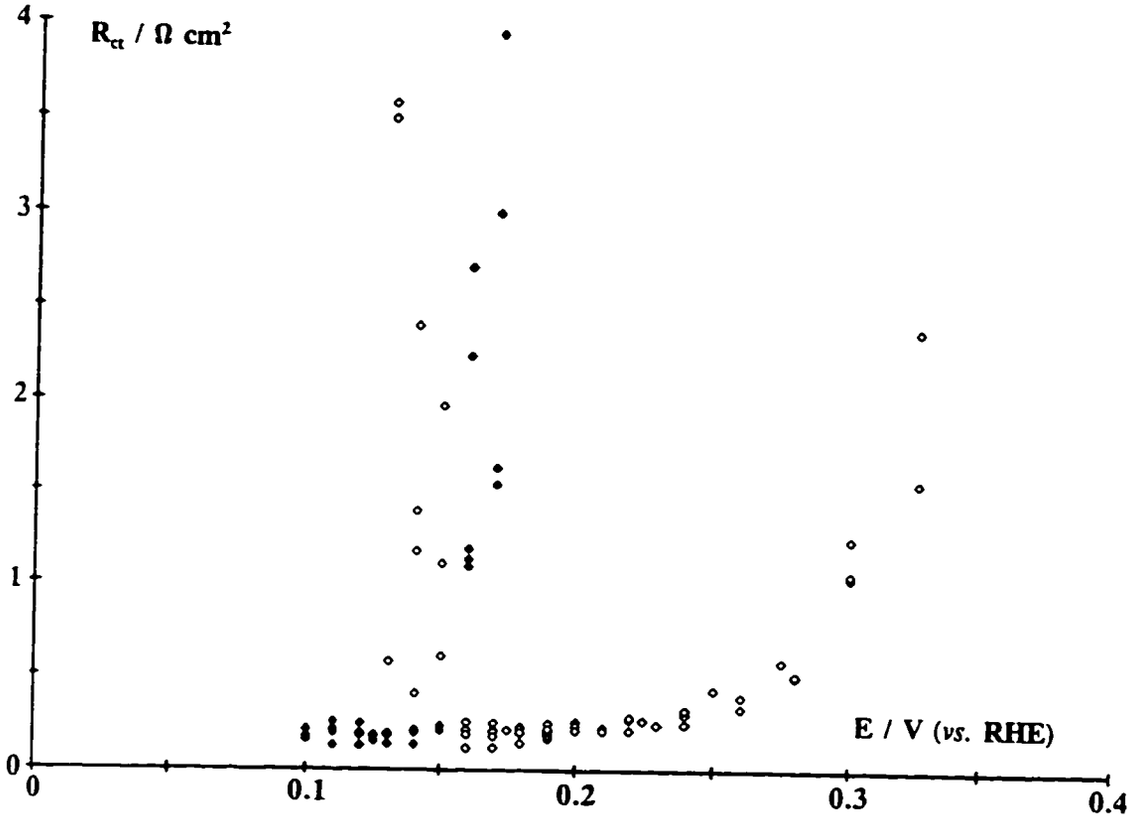

Fig. 5.2 Charge-transfer resistance R_{ct1} (◆) and R_{ct2} (◇) as a function of the applied potential (*vs.* RHE) for the adsorption-desorption of H on a Pt(110) surface in contact with a 0.5 mol dm^{-3} aqueous H_2SO_4 solution at 273 K.

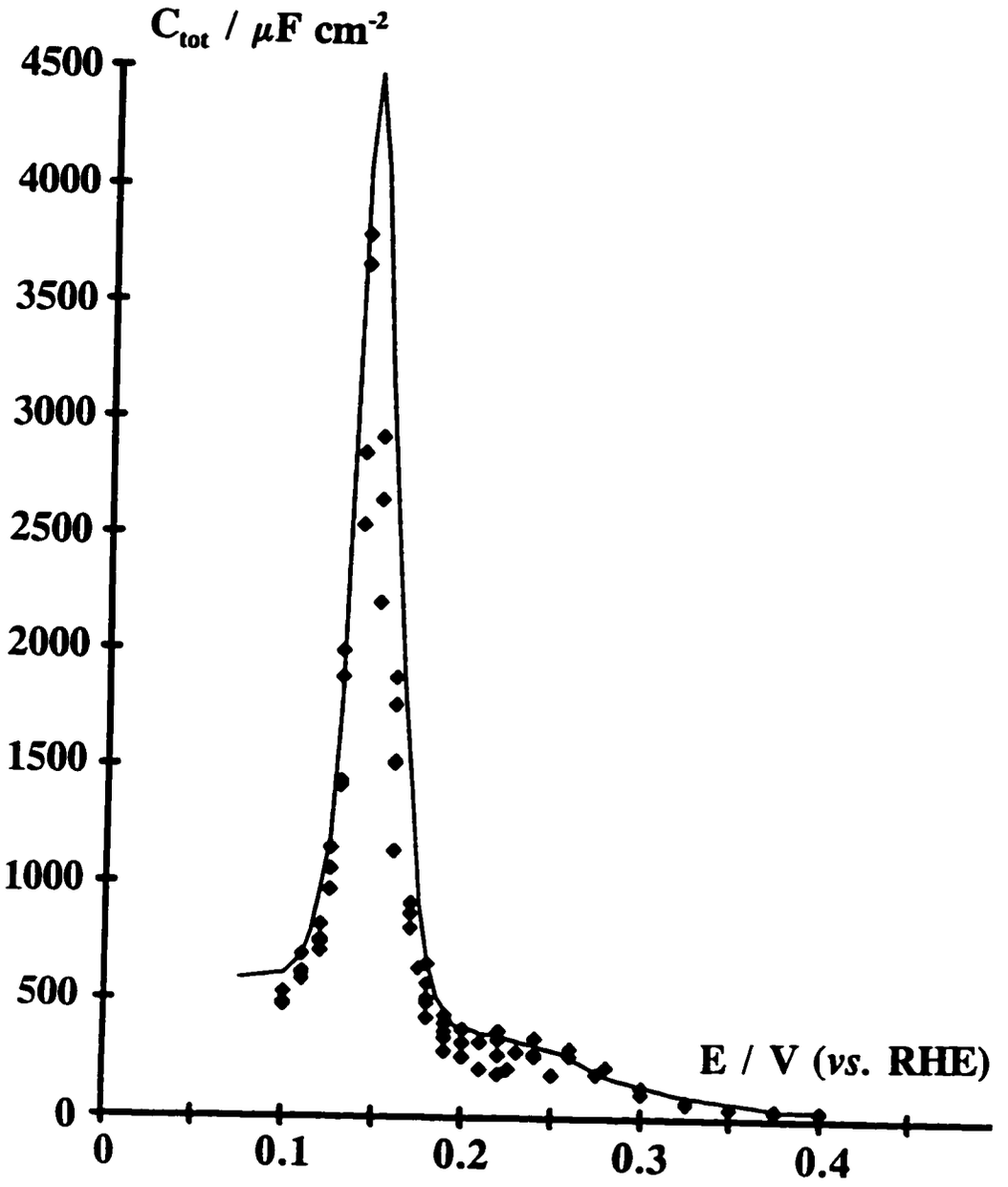

Fig. 5.3 Total capacitance C_{tot} as a function of the applied potential (*vs.* RHE) for the adsorption-desorption of H on Pt(110) in contact with a 0.5 mol dm^{-3} aqueous H_2SO_4 solution at 273 K. The solid line corresponds to the C_{tot} calculated from the CV (current density / sweep rate = total capacitance); it is not drawn as a fit to the experimental points.

5.2.1.2 Evaluation of the charge transfer rates for the Pt(111) surface

In this work attempts were made to evaluate the charge transfer rate at Pt(111); this was of great importance since this surface displays a very different profile for UPD of H from those for the other surfaces (as discussed in Chapter 3).

Unfortunately, the charge-transfer rates at Pt(111) were not accessible at frequencies smaller than 300 kHz even at 273 K in 0.5 mol dm^{-3} H_2SO_4.

However, it is possible to evaluate roughly the magnitude of the exchange rate on this face using the data of Oelgeklaus *et al.* [5] for polycrystalline Pt and Pt(111) determined in 1 mol dm^{-3} KOH. Under these experimental conditions the H adsorption-desorption process follows eq. 4.28b (in Chapter 4), and an exchange rate of 7 x 10^{-8} mol s^{-1} cm^{-2} was found for Pt(111) while an exchange rate of 7 x 10^{-9} mol s^{-1} cm^{-2} was observed at the polycrystalline Pt electrode. If it were to be assumed that the observed differences in these exchange rates remain unchanged when H_2SO_4 is used instead of KOH, an exchange rate of the order of 4 x 10^{-5} mol s^{-1} cm^{-2} could be expected for Pt(111) in 0.5 mol dm^{-3} H_2SO_4. This would correspond to a turn-over rate at 293 K, 16 times greater than that measured at 273 K for Pt(110) in the same solution.

5.2.2 Effect of temperature on the kinetics of UPD of H at Pt(100) and determination of the apparent activation energy

Figure 5.4 shows the cyclic voltammograms for Pt (100) in 0.5 mol dm^{-3} H_2SO_4 at 293 K, 283 K, and 273 K, where the potential scale has been corrected to a "constant-temperature" one, *i.e.* the SHE. This is done according to ref. 6 by correcting the standard potential, E^o, of the reversible hydrogen reference electrode using the fairly reliably known, but extra-thermodynamic, absolute temperature dependence of E^o, (dE^o/dT), which is equal to 8.4 x 10^{-4} V K^{-1} in acidic solutions, derived from the standard entropy change for the H_2/H^+ reversible electrode. Over the range of temperature studied only minor changes were observed in the CV's recorded at lower temperatures; the height of the current peak (~350 mV) increased slightly and the small peak around 250 mV became better resolved. When the potential scale was not corrected to constant temperature, all the CV's were almost superimposable; to avoid confusion, the results

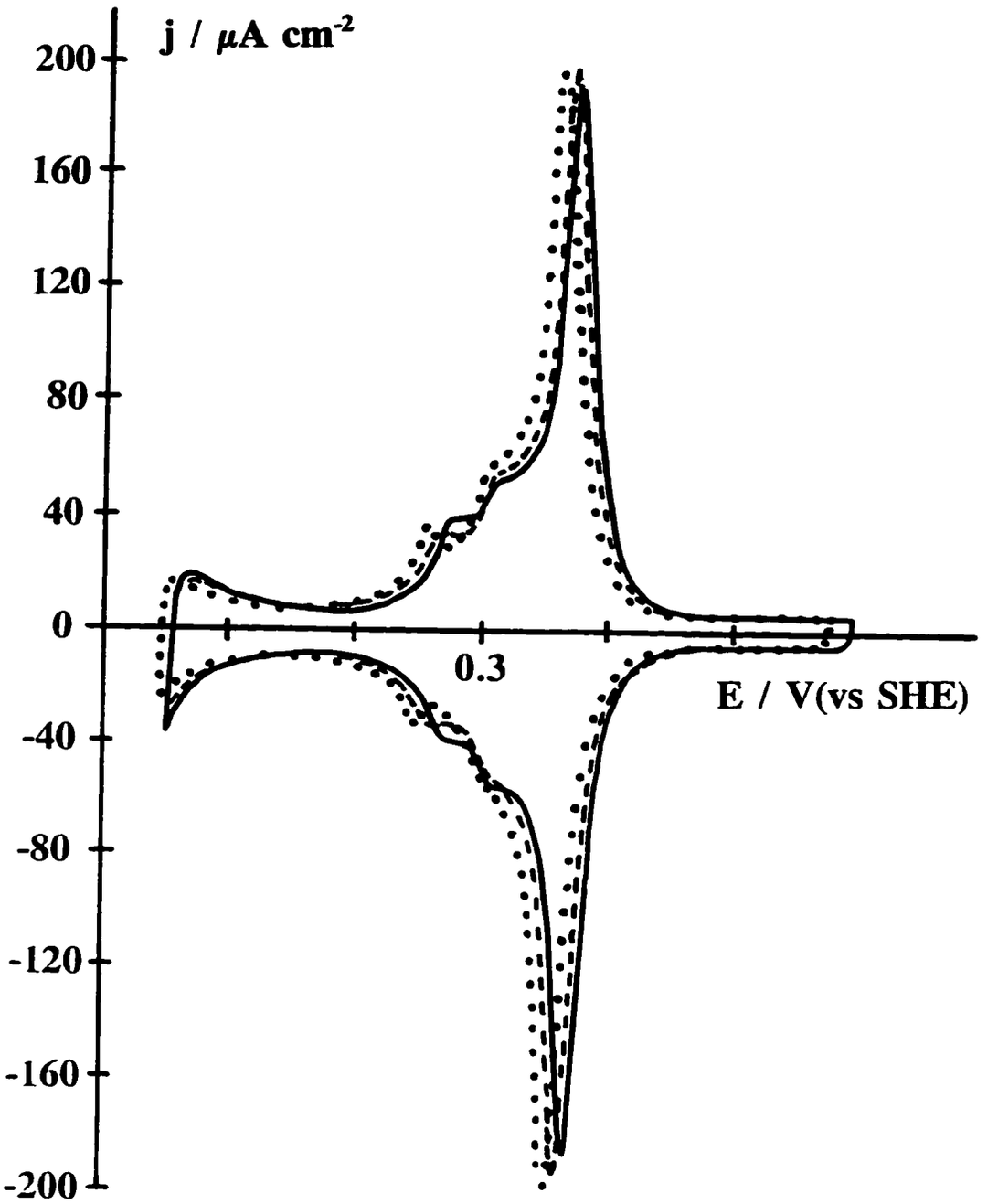

Fig. 5.4 Cyclic voltammograms for Pt(100) in 0.5 mol dm^{-3} aqueous H_2SO_4 solution at 293 K (solid line), 283 K (dashed line), and 273 K (dotted line); sweep rate: 50 mV s^{-1}. Potential scale is *vs.* T-independent SHE (see text).

shown in Fig. 5.5 are, however, plotted vs RHE at the corresponding temperatures.

For Pt (100) both C_p and C_{dl} remained almost unchanged when the temperature was lowered from 293 K to 283 K and 273 K, whereas the exchange rate decreased markedly with temperature (see Fig. 5.5). Using eqn. 4.35 (Chapter 4) to derive the exchange rate constant, the Arrhenius plots shown in Fig. 5.6 were constructed for the range of potential values (50 to 375 mV) within which no anion adsorption-desorption takes place. In calculating $k_{o,\theta}$, β was assumed to be equal to 0.5, since the range of temperature studied is not very large and hence the β value is not expected to vary much. The resulting E_a^* values are given in Table 5.1 for various coverages. At intermediate coverages (θ_H = 0.58 and 0.82) the E_a^* is 48 ± 2 kJ mol^{-1} and tends to become smaller as the coverage increases. Although the number of temperatures studied is small the author reported the E_a^* values only in order to show the general trend in the variation of E_a^* with the coverage. In particular, the measurements down to temperature below 298 K were performed mainly to achieve a better resolution of the R_{ct} for all the surfaces studied.

Table 5.1 Apparent activation energy E_a^* for Pt (100) in contact with 0.5 mol dm^{-3} aqueous H_2SO_4 solution as a function of H coverages (θ_H).

Coverage, θ_H ± 0.05	0.97	0.94	0.82	0.58	0.1*
E_a^* / kJ mol^{-1}	29 ± 4	42 ± 6	48 ± 3	48 ± 6	38 ± 2

For the θ value marked by *, the corresponding potential values are positive to the capacitance peak. Hence, this θ is in the region of potentials where the surface is changing during the ac polarisation (see Fig. 4.7, p.127) and also in the region where anion adsorption takes place.

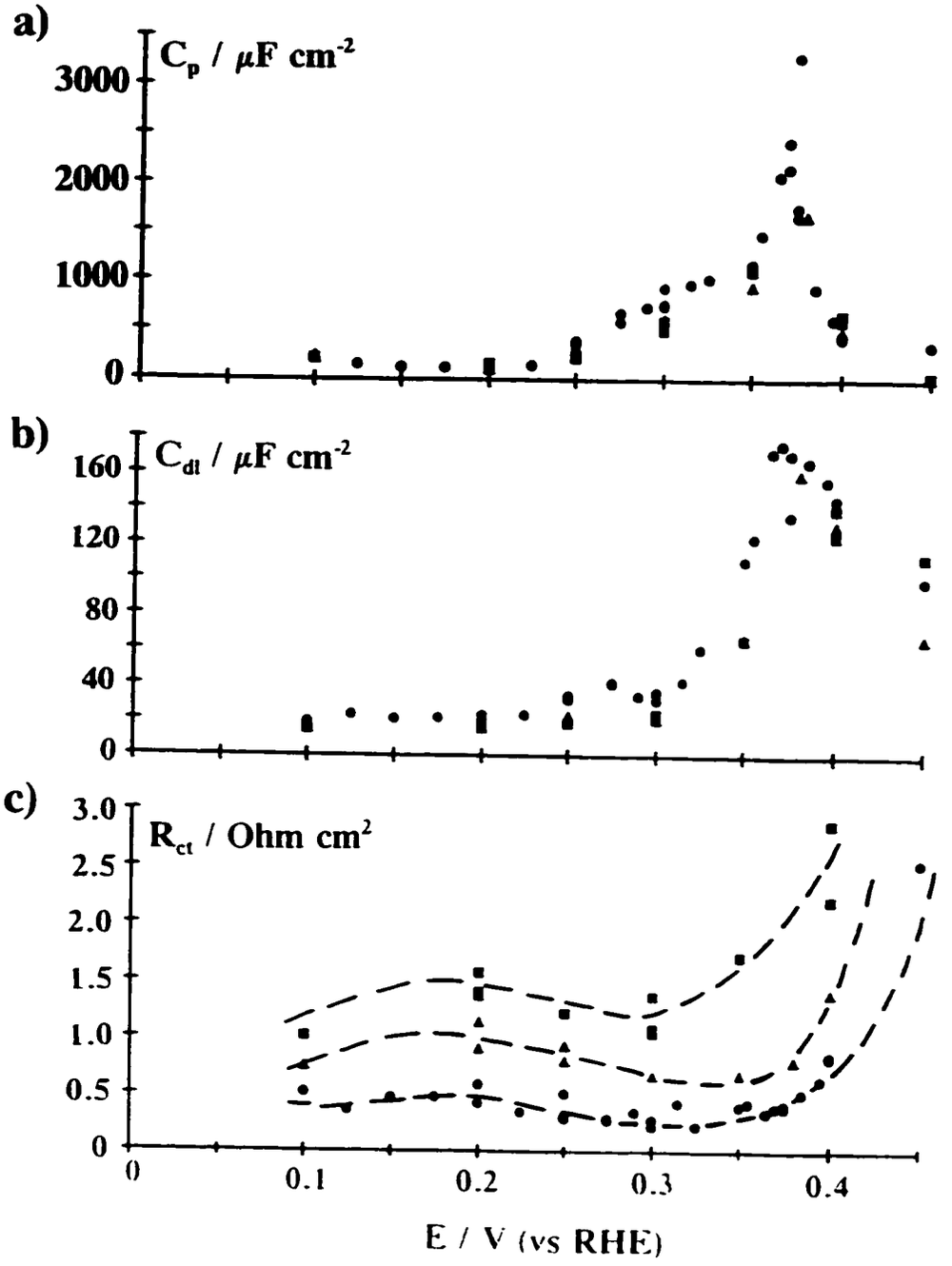

Fig. 5.5 Effect of lowering the temperature on a) the pseudocapacitance (C_p), b) the double-layer capacitance (C_{dl}), and c) the charge-transfer resistance (R_{ct}) as a function of potential (vs RHE) for the adsorption-desorption of hydrogen on Pt (100) in contact with a 0.5 mol dm^{-3} aqueous H_2SO_4 solution at 293 K (●), 283 K (▲), and 273 K (■).

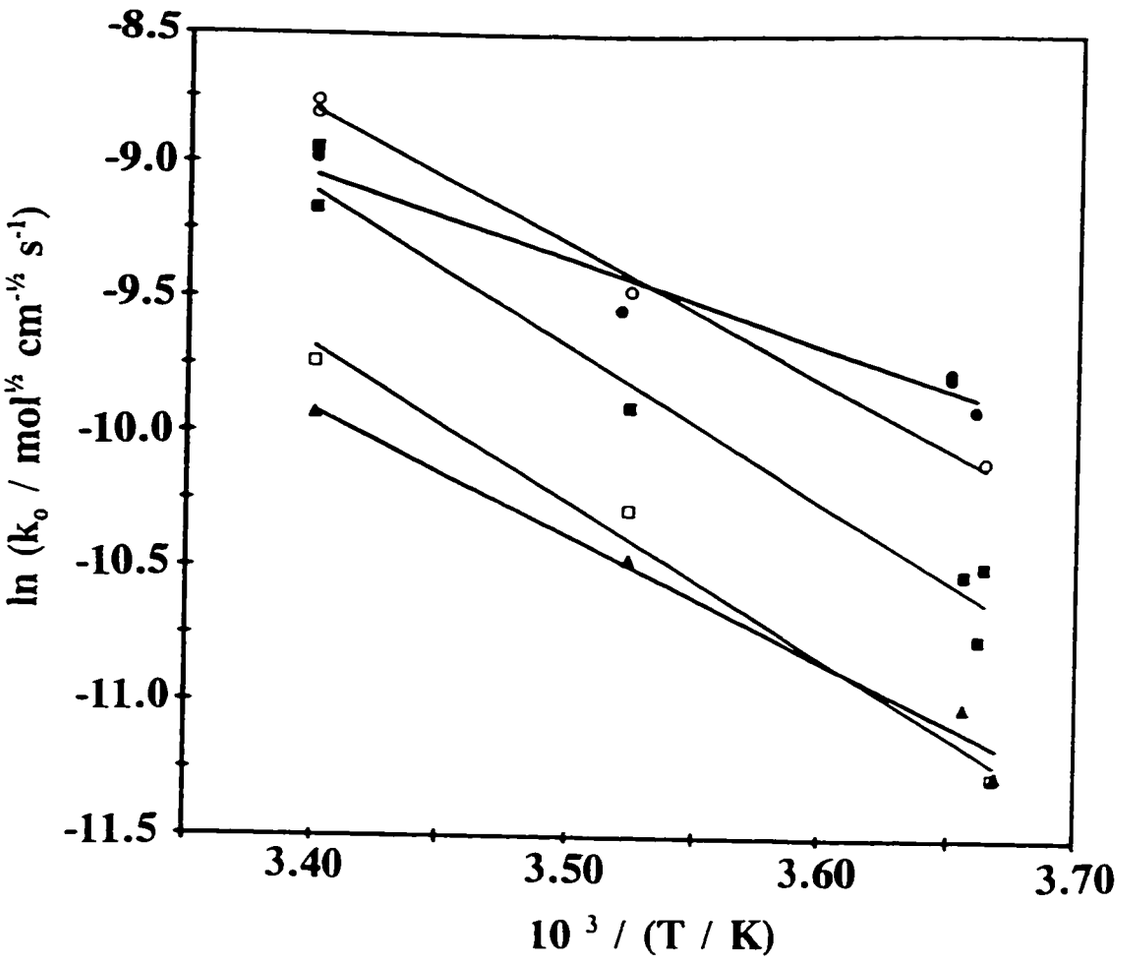

Fig. 5.6 Arrhenius plots: logarithms of the apparent rate constant for H deposition-desorption on Pt (100) in contact with a 0.5 mol dm^{-3} aqueous H_2SO_4 solution as a function of the reciprocal of the temperature (K^{-1}) for various coverages (θ_H): 0.97 (●), 0.94 (○), 0.82 (■), 0.58 (□) and 0.1 (▲).

5.2.3 Effect of temperature on the kinetics of the UPD of H at Pt(311) and determination of the apparent activation energy

Following the procedure described in the previous section, the dependence of the UPD of H (and anions) was investigated at Pt(311) for the same three temperatures: 293, 283 and 273 K. However, in the case of Pt(311), resolution of both H and HSO_4^- anion adsorption-desorption processes was possible, as shown in Chapter 4 for the same face at 293 K.

Figure 5.7 shows the pseudocapacitances (C_{p1} and C_{p2}) and the double-layer capacitance C_{dl} as a function of potential for the three temperatures studied. Again the C_p's follow the cyclic voltammograms (not shown, see Fig. 4.5b for the CV at 293 K) recorded at the corresponding temperatures.

The C_{dl} values for Pt(311) in contact with a 0.5 mol dm^{-3} H_2SO_4 solution at 293 K were also reported in Fig. 4.11b (Chapter 4), these values are plotted in Fig. 5.7b along with the ones obtained at 283 K and 273 K. Surprisingly, the C_{dl} values (Fig. 5.7b) obtained at the latter temperatures are much lower, between 0.075 and 0.2 V, than those first shown in Fig. 4.11b and correspond more to the expected behaviour of C_{dl} with potential for a solution containing large amounts of electrolyte. A similar scatter in the data to that observed here at 293 K was noted for Pt(110) at 273 K (see Fig. 5.1b).

Over the narrow range of temperature investigated (*ca.* 20 K) such a large variation of the C_{dl} value is not expected (see Fig. 5.7b). Two possible explanations can be proposed: i) the time constant of the charge-transfer process is too small to be evaluated correctly and/or b) there is interference on these two faces, Pt(311) at 293 K and Pt(110) at 273 K, from incipient OPD H currents which affect the C_{dl} determination.

The first proposed explanation could be more or less ruled out from the fact that similar time constant (RC) values were found for Pt(100) around 0.2 V and *no scatter* was observed in those C_{dl} data.

On the other hand, it is clear from the cyclic voltammograms for Pt single-crystal surfaces, as well as for polycrystalline Pt, that there is a small current component associated with the HER which arises already around the least positive limit of potential

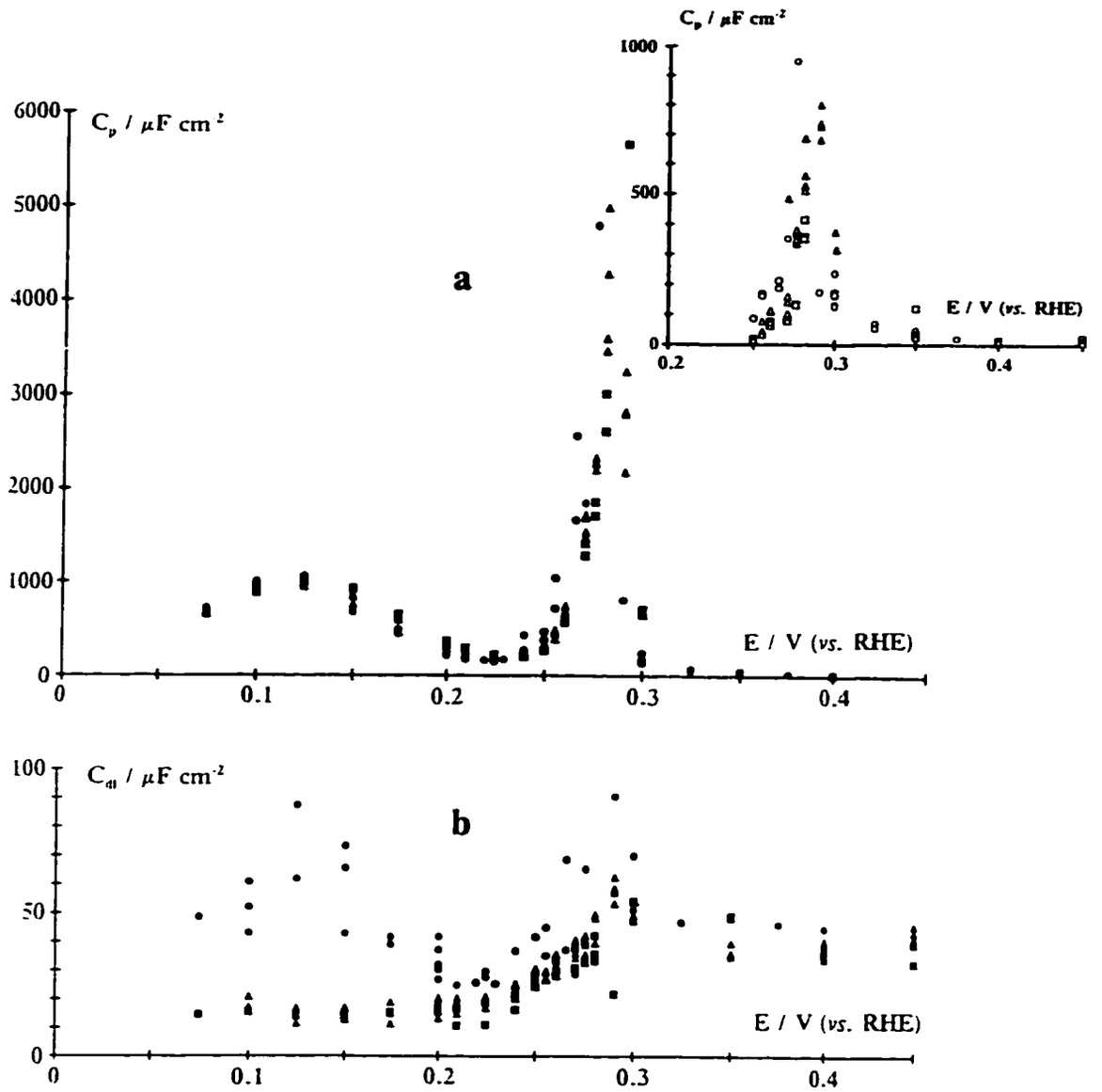

Fig. 5.7 a) pseudocapacitances C_{p1} (filled symbols) and C_{p2} (open symbols) and b) double-layer capacitance C_{dl} as a function of the applied potential (*vs.* RHE) for the adsorption-desorption of H and HSO_4^- anions at Pt(311) surface in contact with a 0.5 mol dm^{-3} aqueous H_2SO_4 solution at 293 K (●,○), 283 K (▲,△) and 273 K (■,□). C_{p2} values are shown in the inset of a) on an expanded potential scale.

on these curves. The difference observed in Fig. 5.7 between the C_{dl} values at 293 K and the ones reported at lower temperatures could be attributed to the formation of small amounts of overpotential-deposited H. This effect would then be significantly reduced as the temperature is lowered.

In a similar fashion, as in Fig. 4.11c and 4.12, the $R_{\alpha 1}$ and $R_{\alpha 2}$ are shown in Fig. 5.8 as a function of potential for the three temperatures studied. For reasons of clarity, the data associated with H adsorption-desorption are shown in the inset of Fig. 5.8 while those associated with HSO_4^- adsorption-desorption are displayed in the main graph (Fig. 5.8). This assignment of the R_α to each process (H and HSO_4^- adsorption-desorption) is based on the arguments given previously in Chapter 4 (section 4.3.4).

Similarly to the other surfaces studied the total capacitance ($C_{dl} + C_{p1} + C_{p2}$) was calculated and compared to that calculated from the voltammetry current responses. The results are reported in Fig. 5.9 for the three temperatures investigated (to avoid confusion each set is shown in a separate graph). The observed C_{tot} are in very good agreement for potential values $\leq$ 260 mV and $\geq$ 300 mV; however, some discrepancies are observed over the remaining 40 mV in the sharply peaked region. This region of potential was found to be more difficult to investigated; the scatter in the data (see for example Fig. 5.9b) gives an estimate of the error bars in that narrow potential region (between *ca.* 260 and 300 mV).

Following the procedure given in the previous section, the exchange rate constant could be calculated and the Arrhenius plots constructed (Fig. 5.10). From these data the apparent activation energy as a function of coverage (θ_H) was evaluated and the resulting $E_a^{\ddagger}$ values are given in Table 5.2 for various θ_H values.

Table 5.2 Apparent activation energy $E_a^{\ddagger}$ for Pt(311) in contact with 0.5 mol dm^{-3} aqueous H_2SO_4 solution as a function of H coverage (θ_H)

θ_H ± 0.05	0.89	0.81	0.71	0.65	0.54	0.47	0.41	~1 for anions
$E_a^{\ddagger}$ /kJ mol^{-1} ± 4	48 ± 4	59 ± 9	41 ± 3	34 ± 6	37 ± 2	48 ± 4	41 ± 4	46 ± 9

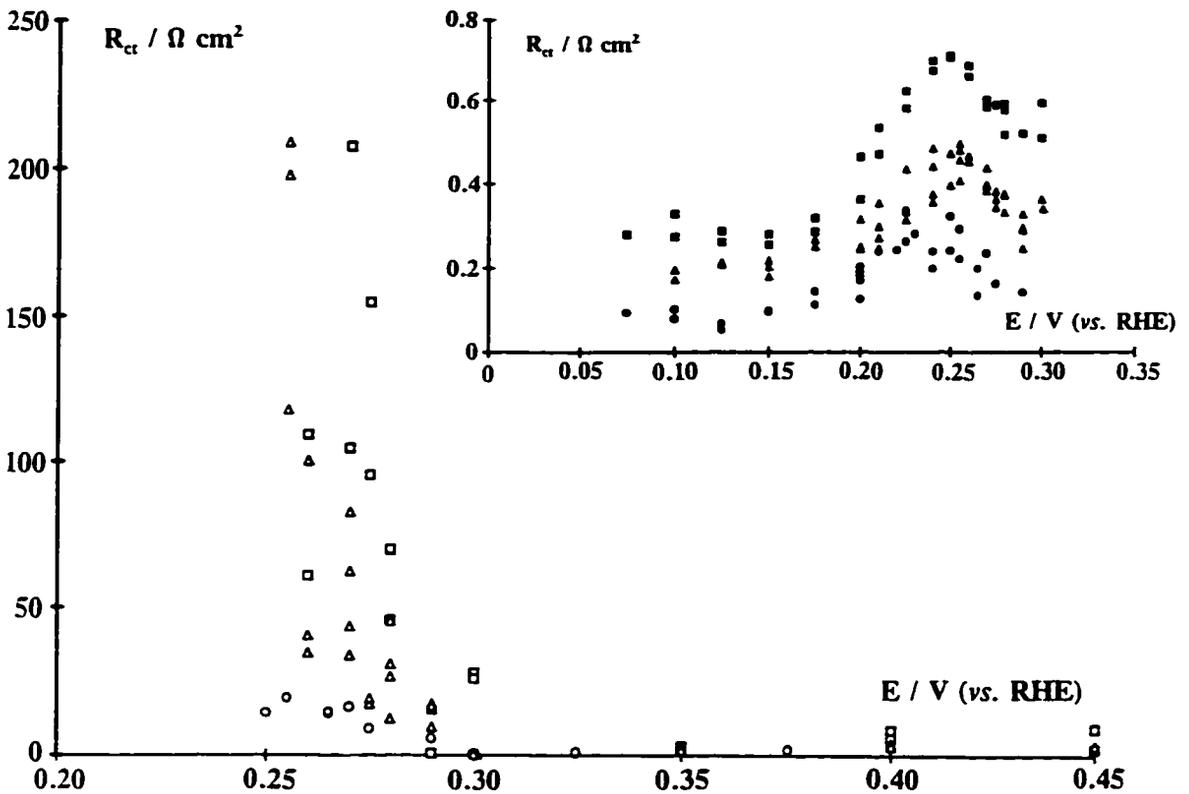

Fig. 5.8 Charge-transfer resistances R_{ct1} (filled symbols) and R_{ct2} (open symbols) as a function of the applied potential (*vs.* RHE) for the adsorption-desorption of H and HSO_4^- anions at Pt(311) surface in contact with a 0.5 mol dm^{-3} aqueous H_2SO_4 solution at 293 K (●,○), 283 K (▲,△) and 273 K (■,□). The R_{ct1} values are shown in the inset on a different potential scale.

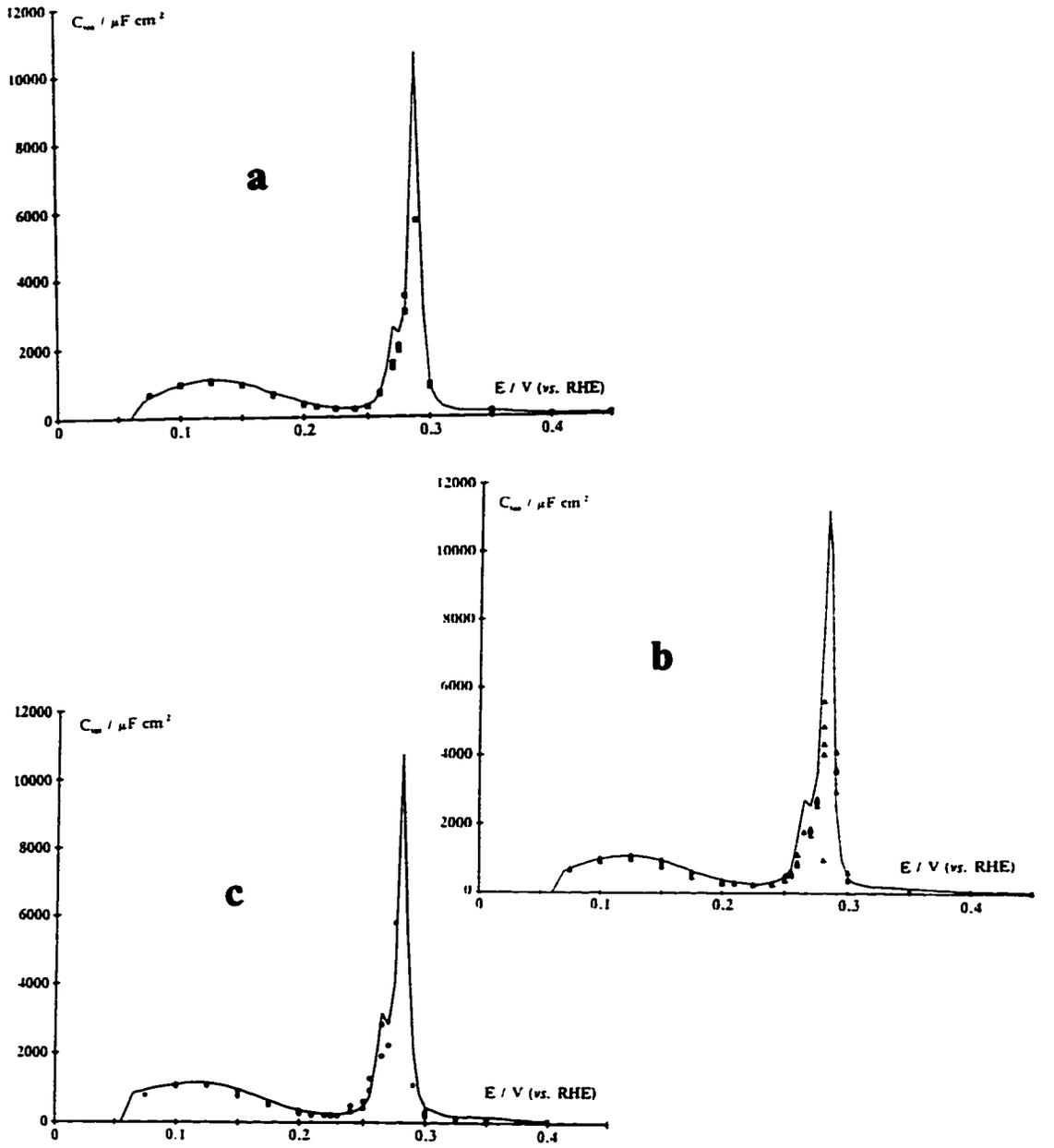

Fig. 5.9 Total capacitance, C_{tot}, as a function of the applied potential (*vs.* RHE) for the adsorption-desorption of H and HSO_4^- anions on Pt(311) in contact with 0.5 mol dm^{-3} aqueous H_2SO_4 solution at a) 293 K (●); b) 283 K (▲) and c) 273 K (■). The solid lines correspond to the C_{tot} calculated from the CV's (current density / sweep rate = total capacitance) at the respective temperature; it is not drawn as a fit to the experimental points.

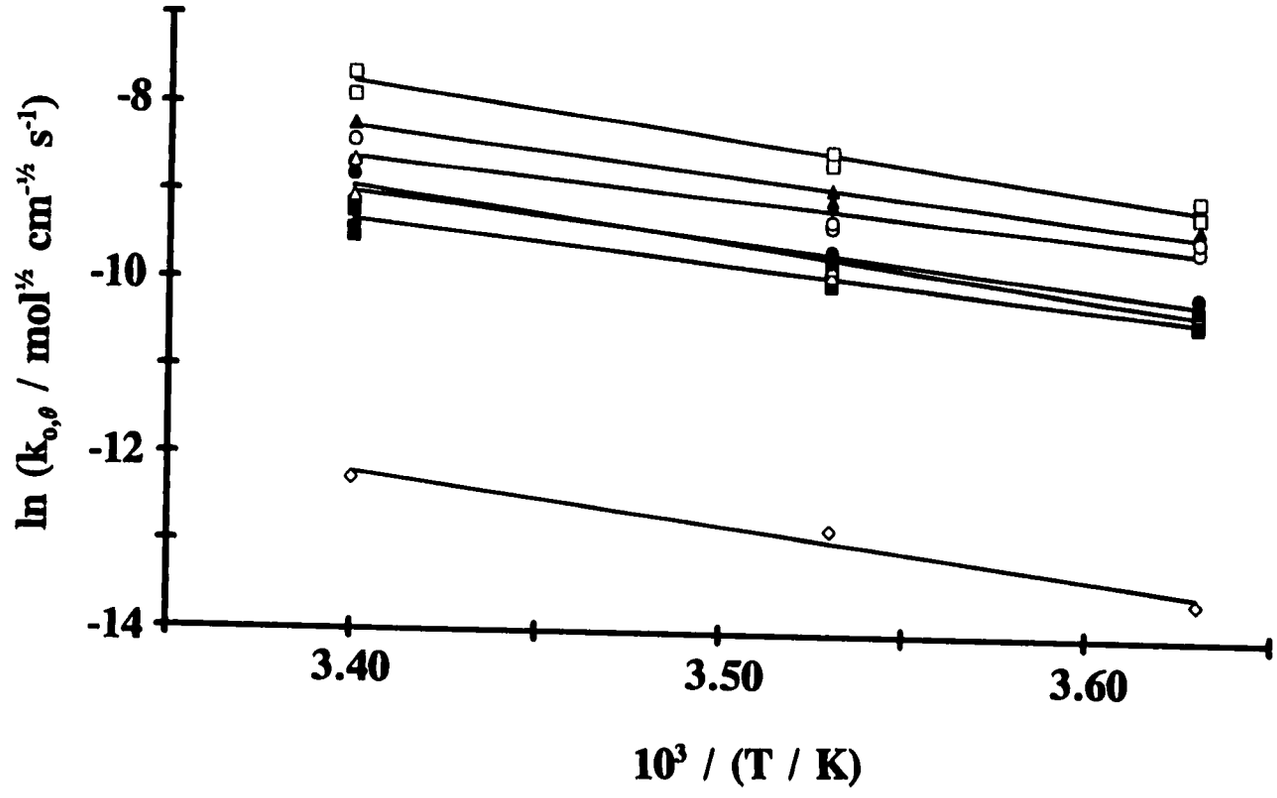

Fig. 5.10 Arrhenius plots: logarithms of the apparent rate constant for H deposition-desorption at Pt(311) in contact with a 0.5 mol dm^{-3} aqueous H_2SO_4 solution as a function of the reciprocal of the temperature (K^{-1}) for various coverages (θ_H): 0.89 (□), 0.71 (▲), 0.65 (○), 0.54 (■), 0.47 (△), 0.41 (●) and ~ 1 for HSO_4^- (◇).

The apparent activation energy was determined here only for the R_{ct1} values (inset in Fig. 5.8) since the standard deviation resulting from the fitting of the second semicircle (hence R_{ct2}) of the impedance plot is greater (*ca.* 20%) than that for R_{ct1} (*ca.* 2%). Moreover, as the temperature is lowered, the small R_{ct1} becomes larger, *i.e.* easier to fit, while the increase of R_{ct2} makes it even more difficult to fit (see Fig. 4.12 inset for an example of the impedance response at 293 K). In Table 5.2 the apparent activation energy is given for an almost full coverage of the surface by anions, although, in this case, the standard deviation on the R_{ct} values used to evaluate $k_{o,\theta}$ are much greater, a value of $E_a^{\ddagger}$, comparable in magnitude to that determined for the various coverages of H is obtained (see also Fig. 5.10).

Apparent activation energy values similar to the ones found for Pt(100) (see Table 5.1) were determined from Fig. 5.10, as shown above in Table 5.2. At this point, it is somewhat difficult to reach any definite conclusions on the variation of $E_a^{\ddagger}$ with θ_H since only the minimum number of temperatures were investigated over a relatively narrow range of temperature, *ca.* 20 K.

5.3 Conclusions

In Part I of this thesis (Chapters 4 and 5) the kinetics of the UPD of H (as well as HSO_4^- anions) were investigated for the three low-index planes and for the Pt(311) stepped surface. The main conclusion from this part of the work is that the charge-transfer rate for these processes depends substantially on the two-dimensional geometry of the Pt single-crystal surfaces; according to the following decreasing order of their respective average rates: (111) > > (110) > polycrystalline > (100) while for the (311) surface the rate was found to be greater on the (111) sites than on the (100) sites. Table 5.3 gives the average exchange rates for the process of UPD of H as well as the turn-over rate as calculated from the surface concentrations of H at the various Pt surfaces studied.

Using impedance spectroscopy, it was possible, for the first time, to quantify the charge-transfer rates for both H and HSO_4^- adsorption-desorption processes as well as to characterise the double-layer capacitance and adsorption pseudocapacitance as a function

of potential. This approach shows a promising new possibility that would allow, for example, resolution of other co-adsorption processes involving *e.g.* organic molecules and anion adsorption, or anions adsorbing through an organic film (*e.g.*, a self-assembled monolayer). Using more dilute solutions of electrolyte, it would also become possible to measure the *pzc*'s of Pt surfaces accurately using electrolytes containing less strongly adsorbed anions. Moreover, these impedance measurements have yielded valuable information that can now be used to compare data for UPD and OPD of H at Pt single-crystal electrodes, which would help the understanding of the role of the surface in the overall HER process and other related processes.

Table 5.3 Summary of the average exchange rates and turn-over rates for the three Pt low-index planes and the Pt(311) stepped surface at 293 K

Single-crystal planes	Average exchange rate/ mol s^{-1} cm^{-2}	Turnover rate/ monolayer of H s^{-1}
(111)	4×10^{-5} *	16 000 *
(110)	1×10^{-6} **	1022 **
(100)	7×10^{-7}	350
(311)		
(100) sites	7×10^{-7}	700
(111) sites	3×10^{-6}	2000

* These values have been evaluated from the data in ref. 5
** These values are for T = 273 K

References

1. R.A. Marcus and N. Sutin, Biochimica et Biophysica Acta, 811 (1985) 265.
2. B.E. Conway, "Theory and Principles of Electrode Processes", The Ronald Press Company, New York, 1965.
3. a) J.M. Feliu, J.M. Orts, R. Gomez, A. Aldaz and J. Clavilier, J. Electroanal. Chem., 372 (1994) 265; b) J. Clavilier, J.M. Orts, R. Gomez, J.M. Feliu and A. Aldaz, Proceedings of the symposium on "Electrochemistry and materials Science of Cathodic Hydrogen Absorption and Adsorption", (eds. B.E. Conway and G. Jerkiewicz), The Electrochem. Soc. Inc., New Jersey, Vol. 94-21, 1994, p.167.
4. R. Gomez and J. Clavilier, J. Electroanal. Chem., 354 (1993) 189.
5. R. Oelgeklaus, J. Rose and H. Baltruschat, J. Electroanal. Chem., 376 (1994) 127.
6. B.E. Conway, H.A. Angerstein-Kozlowska and W.B.A. Sharp, J. Chem. Soc., Faraday Transactions I, 78 (1978) 1373.

Part II

Chapter 6

Surface structure dependence of the reactive chemisorption of acetonitrile on single-crystal platinum surfaces

6.1 Introduction

The study of electrochemical adsorption and reactivity of small molecules at single-crystal surfaces, especially of noble metals, constitutes a major sector of the growing field of electrochemical surface science. Surface reactivity studies involving the oxidation of small organic molecules is of fundamental importance in fuel-cell research and electrosynthesis. These studies encompass a large number of molecules e.g. CH_3OH [1,2], HCOOH [3,4], lower molecular weight alkenols [5] and many more. Many of these molecules have been studied at single-crystal surfaces and their reactivity has been shown to be highly surface selective, as it is in gas-solid heterogeneously catalysed processes [6]. This chapter reports a section of the work concerned with the interesting but little studied case of electrosorption and surface reactivity of acetonitrile (CH_3CN) at Pt single-crystal surfaces [7].

In an early paper from Conway's group [8], it was reported that CH_3CN undergoes irreversibly, chemisorption to a bound state on Pt from dilute aqueous solutions within the potential range from 0.05 to *ca.* 0.75 V *vs.* RHE at a Pt polycrystalline electrode and, *in the bound state*, undergoes an almost reversible reduction/reoxidation process as demonstrated by linear-sweep voltammetric experiments (see Fig. 6.1). Slower processes, involving a partially blocked surface, also arise in the UPD H region at Pt. Because of the surface reactions which arise involving CH_3CN in an electrosorbed state, this system constituted one of the earliest examples [8] of a reactive, "chemically modified electrode", related to other types of such electrodes studied and constructed subsequently (1974-75), e.g. by Murray and co-workers [9] and Lane and Hubbard [10].

In comparison with the behaviour of other chemisorbed small organic molecules,

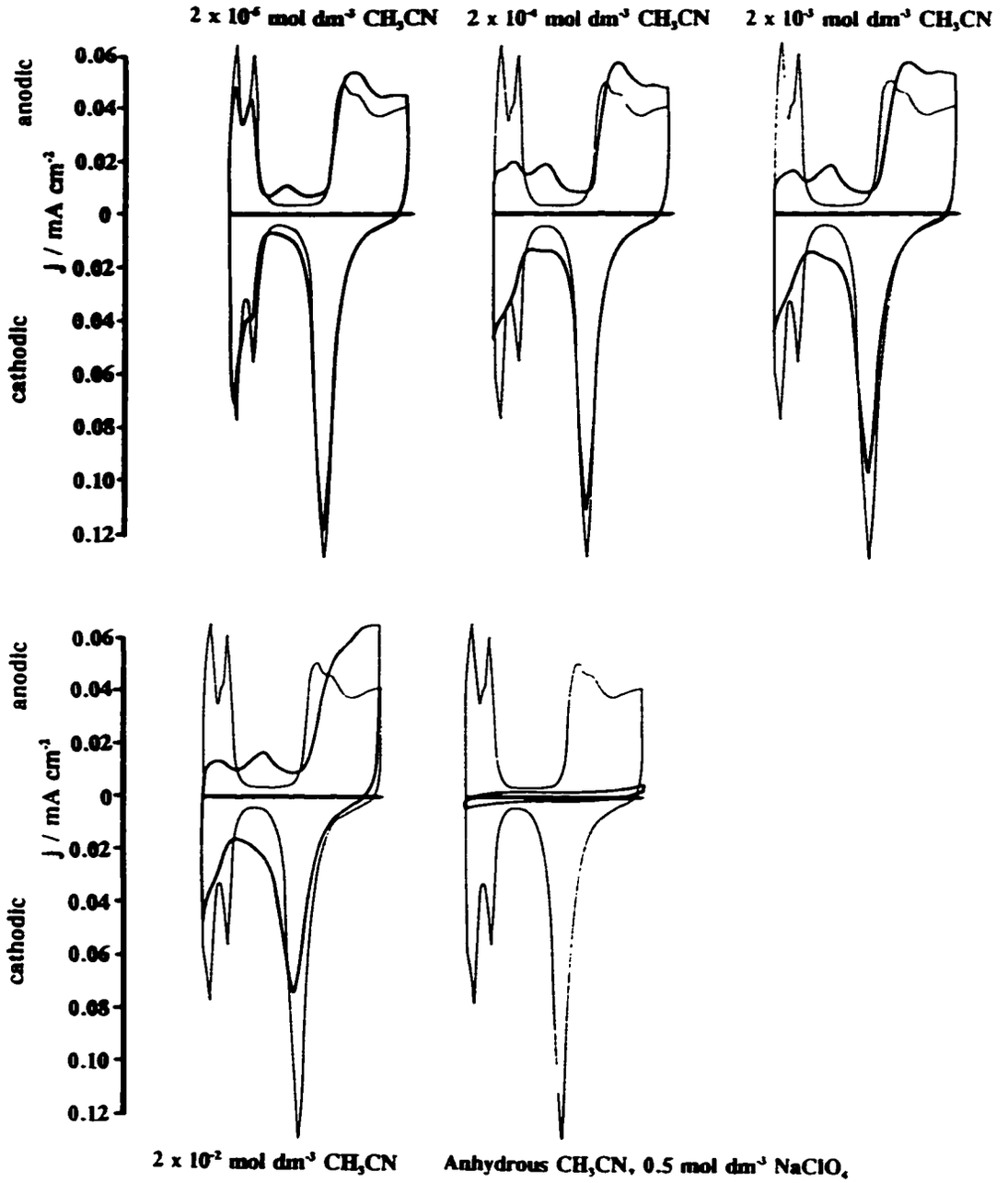

Fig. 6.1 Potentiodynamic j-E profiles for adsorbed acetonitrile at polycrystalline platinum as a function of concentration in relation to background curves for hydrogen (H) and oxygen (as OH and O) electrosorption from 0.5 mol dm^{-3} H_2SO_4. Also shown is the j-E relation for anhydrous CH_3CN and $NaClO_4$ as the electrolyte. Sweep rate: 50 mV s^{-1} [8].

e.g. CH_3OH, HCHO or HCOOH, the behaviour of CH_3CN is fundamentally different in that reversible reduction/reoxidation processes can be conducted in a cyclic manner with little or no desorption of the adsorbate species from the electrode surface, except in the case of potential excursions well into the surface oxide formation region (to *ca.* 1.4 V) at a polycrystalline Pt where irreversible oxidative desorption takes place.

The reactive electrosorption of CH_3CN, discovered in the earlier work of Conway and co-workers [8] on Pt, provides a very interesting system in electrochemical surface science where examination of the complementary aspects of electrosorption and subsequent surface reactivity of the resulting chemisorbed species can be made quantitatively by means of cyclic voltammetry and complementarily by recording the current transients for H desorption [11] in time. An example of an H-displacement current transient is shown in Fig. 6.2. They arise [11] from addition of small quantities of CH_3CN to an initially CH_3CN-free solution (solid line in Fig. 6.2) at various, potentiostatically held, constant potentials.

Additionally, over the UPD of H region at Pt, CH_3CN becomes chemisorbed at a given controlled potential with anodic desorption of H [11] (the so-called "anodic hydrogen desorption effect" [11]) (Fig. 6.2) and from the characterization of this effect, further information on the electrosorption of CH_3CN has been derived by integrating the current transients (see section 6.3.5 for a more detailled discussion on the "anodic hydrogen desorption effect"). It was found that CH_3CN becomes reductively chemisorbed at potentials near to or just less positive than about 0.40 V down to *ca.* 0.26 V *vs.* RHE, [8] at an initially clean Pt surface whereas in the H UPD region the net transient current can become anodic owing to the superposition of the "anodic H desorption" effect.

Upon cycling right after the addition of CH_3CN from 0.40 V to *ca.* 0.75 V an anodic current peak and, when the potential sweep is reversed, a matching cathodic peak is observed. A continuing negative-going potential sweep gives a cathodic response current profile in the UPD of H region but with substantial diminution of the extent of coverage by H then co-adsorbed with a reduced state of CH_3CN, as shown in Fig. 6.2 (-·-·- trace) [8,11].

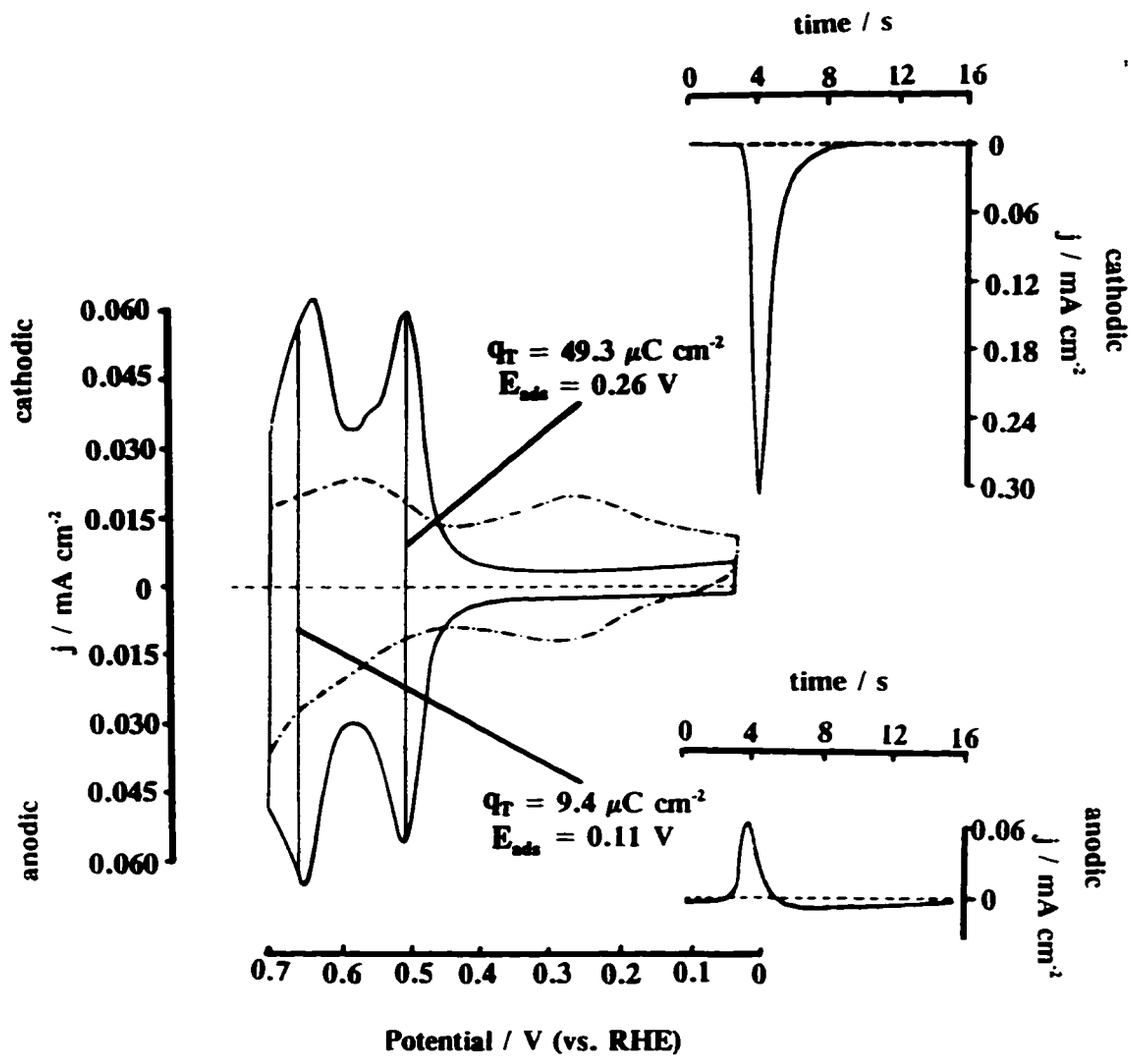

Fig. 6.2 Potentiodynamic profile for 3 x 10^{-3} mol dm^{-3} CH_3CN (-·-·-) and background (___) at 50 mV s^{-1}, together with typical anodic and cathodic transients which arise on potentiostatic adsorption at 0.11 or 0.26 V, with the anodic H displacement effect arising in the former case [12].

It should be mentioned that the above behaviour of CH_3CN is not specific to this particular lowest alkyl nitrile but has also been observed with a series of other nitriles [8], so that the electrosorptive reactivity is associated with the CN function rather than the CH_3 group. However, no reactive chemisorption of acetonitrile was observed in anhydrous acetonitrile conditions [8].

The principal features of the behaviour of adsorbed CH_3CN, observed in the previous work [8] on polycrystalline Pt, can be summarized as follows: (a) reductive electrosorption of CH_3CN at potentials within the "double-layer" potential region (Fig. 6.2); (b) chemisorption in the UPD of H region accompanied by an anodic H displacement charge (Fig. 6.2); (c) two principal and conjugate cathodic and anodic current response regions of CH_3CN in the adsorbed state in cyclic voltammetry over the "double-layer" and "UPD of H" regions (Fig. 6.1); (d) these response currents are associated [8] with CH_3CN in the chemisorbed state, i.e. the processes are surface-reaction controlled, rather than diffusion-controlled, for concentrations of $CH_3CN \geq 2 \times 10^{-3}$ mol dm^{-3}; (e) no continuous faradaic processes occur; and (f) slow processes take place as a result of holding the potential (after initial chemisorption) at 0.05 V *vs.* RHE for 90 s (Fig. 6.3) and lead to subsequent increases of anodic response currents in positive-going, linear-sweep voltammograms.

These results suggested (i) a $1e^-$ reversible e^-, H^+ reduction/reoxidation process over the "double-layer" region, (ii) a second but slower reduction and reoxidation stage over the "UPD of H" region and (iii) from charge integration measurements, attainment of a limiting coverage by adsorbed CH_3CN species less than saturation, i.e. leaving a significant fraction of the available Pt surface free for co-adsorption of H. Thus, the CH_3CN-covered Pt behaved as a "chemically modified electrode".

More recently, two research groups have re-examined this process, one of them using potentiodynamic and radiometric techniques [12] and the other emplying potentiodynamic techniques coupled with on-line mass spectroscopy (DEMS) [13]. In the first study ammonia was detected during the electroreduction of acetonitrile below 0.15 V and it was assumed that ethane must also be produced [12]. In the latter study [13], it was observed that during electro-oxidation of acetonitrile, only processes

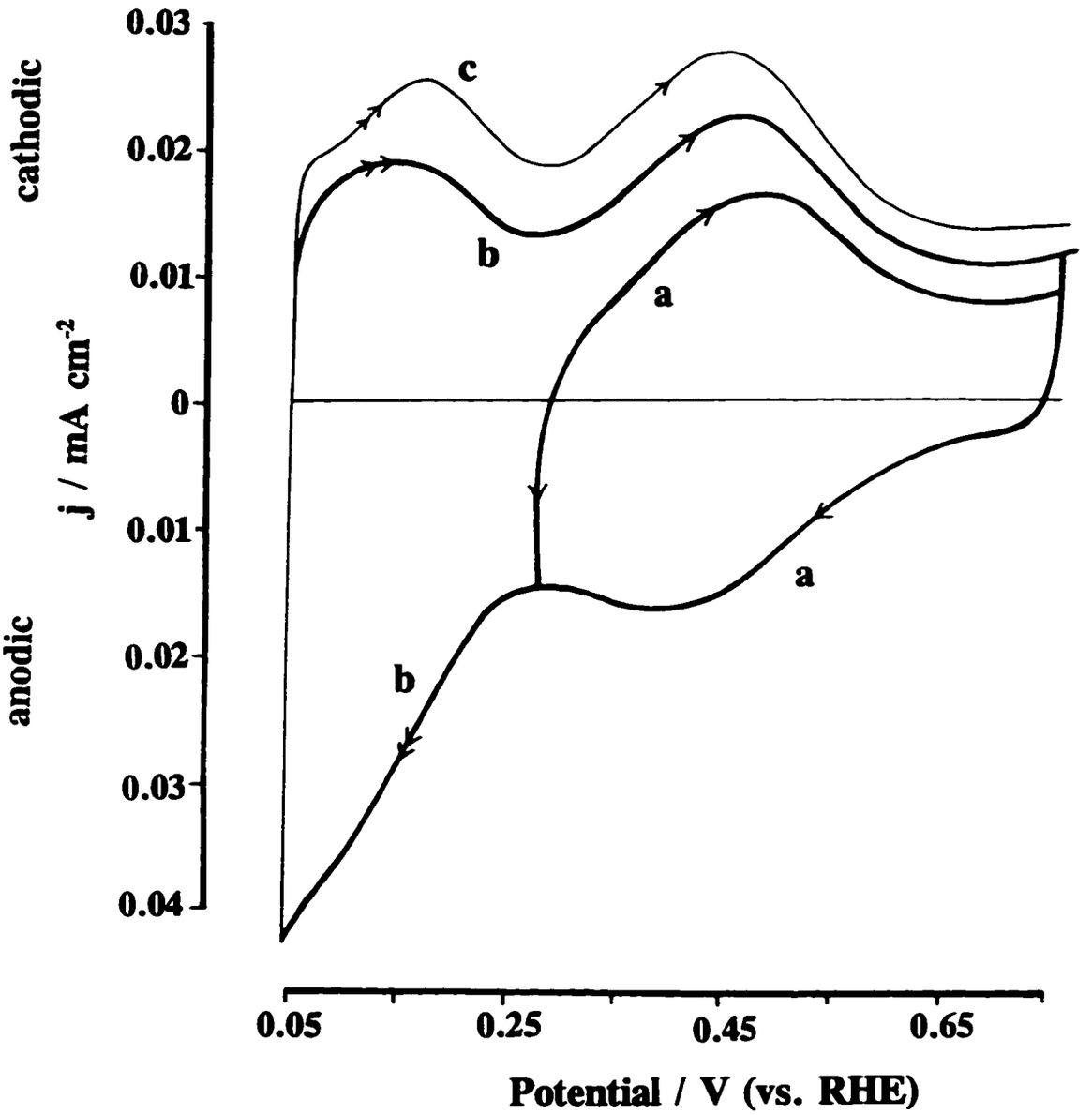

Fig. 6.3 Anodic and cathodic peaks in potentiodynamic j-E profiles for adsorbed acetonitrile at platinum showing the effect of the H-region and cathodic holding at 0.06 V on the reactions in the "double-layer region"; curve (a) for the "double-layer region"; curve (b) for the "double-layer and H UPD region"; curve (c) with holding of potential at 0.06 V for 90 sec. Concentration of CH_3CN: 5 x 10^{-3} mol dm^{-3}, sweep rate: 50 mV s^{-1} [8].

involving adsorbates were involved, where desorption of acetonitrile as the intact compound was observed at potentials above 0.5 V. Additionally, CO_2 was observed for potential excursions above 0.7 V, while NO_x is produced above 1.2 V.

On the other hand, electroreduction of bulk and adsorbed acetonitrile at potentials below 0.1 V was found to produce ethane. The use of deuterated H_2SO_4 and deuterium oxide produced under the same conditions 1,1,1-trideuteroethane. Moreover, from their experiments these authors have reached two important conclusions that confirms assumptions made in ref. 8 and 12: a) the adsorption of acetonitrile take place through the CN group, otherwise acetonitrile with deuterium atoms should have been observed during its desorption; and b) that the CH_3 group remains unaffected during the electroreduction of acetonitrile, as supported by the absence of ethane with more than three deuterium atoms.

Similarly to the experiments of Conway *et al.* [8], Wasmus and Vielstich recorded cathodic adsorption transients in the potential range of 0.2 V to 0.6 V, *vs.* RHE. However, the major difference between the results in refs. 12 and 13, and 8, concerns the behaviour of adsorbed acetonitrile at potentials below 0.1 V. In the work of refs. 12 and 13, large-area porous Pt electrodes were used whereas, in ref. 8, smooth Pt electrodes were employed; this could be the cause of the discrepancies observed for potentials below *ca.* 0.1 V.

In the present chapter, procedures will be described by which the dependence of the processes of reactive chemisorption of acetonitrile on surface structures of various single-crystal planes of Pt can be characterized and elucidated.

6.2 Electrochemical procedures

All experiments were conducted under the very high-purity conditions that have been used for some years in various other works in this laboratory and elsewhere. For more details concerning the preparation of the single-crystal electrodes, the electrolyte solutions and the electrochemical cell see Chapter 2.

The current as a function of the electrochemical potential behaviour of CH_3CN in the adsorbed state was examined by the potentiodynamic method at various Pt single-

crystal electrodes, namely the (100), (111), (110) planes and the stepped (311) plane, and also at a polyoriented Pt sphere and polycrystalline Pt wire electrodes. As noted in previous work [14], potentiostatic steady-state techniques are inapplicable since the results of interest for adsorbed CH_3CN are concerned only with surface processes for which no continuous faradaic currents arise. Determinations of variation of the potentials of current peaks with sweep-rate were performed using a palladium wire loaded with hydrogen as the reference electrode. This electrode was very stable over the whole duration of each of the experiments and was mounted close to the Pt experimental electrode, inside the working electrode compartment of the cell, in order to minimize intra-cell impedance, as required in potentiodynamic experiments conducted up to high sweep-rates.

Additionally, the modulated potential sweep procedure [15] was applied, as in ref. 8, to distinguish fast- and slow-responding processes to sweep-rate changes. All charges evaluated for cyclic voltammograms (CV's) were corrected for double-layer charging contributions, as will be given in Tables 6.1 and 6.2 later.

6.3 Results and discussion

6.3.1 Review of behaviour at polycrystalline Pt

For comparison with the present, new results on CH_3CN chemisorption and reactivity at Pt, we show first the cyclic voltammetric behaviour of adsorbed CH_3CN at a clean, regular polycrystalline wire for reference (Fig. 6.4, inset) as in ref. 8, in relation (Fig. 6.4) to the behaviour at the single-crystal bead, polyoriented-face electrode. At this electrode, small contributions arise from UPD H currents at (111) facets on the bead's surface but the main features for adsorbed acetonitrile in Fig. 6.4 are similar to those (solid line in Fig. 6.4, inset) for polycrytalline wires [8], except that the current peaks in the "double-layer" potential range (0.40 V to 0.75 V vs. RHE) are sharper; also, there is significant difference between the current-peak potentials on the positive and negative sweeps. This is not due to an IR-drop effect.

It is noteworthy, in relation to very different behaviour to be described below for the single-crystal surfaces, that at polycrystalline Pt wire, the oxidation/reduction

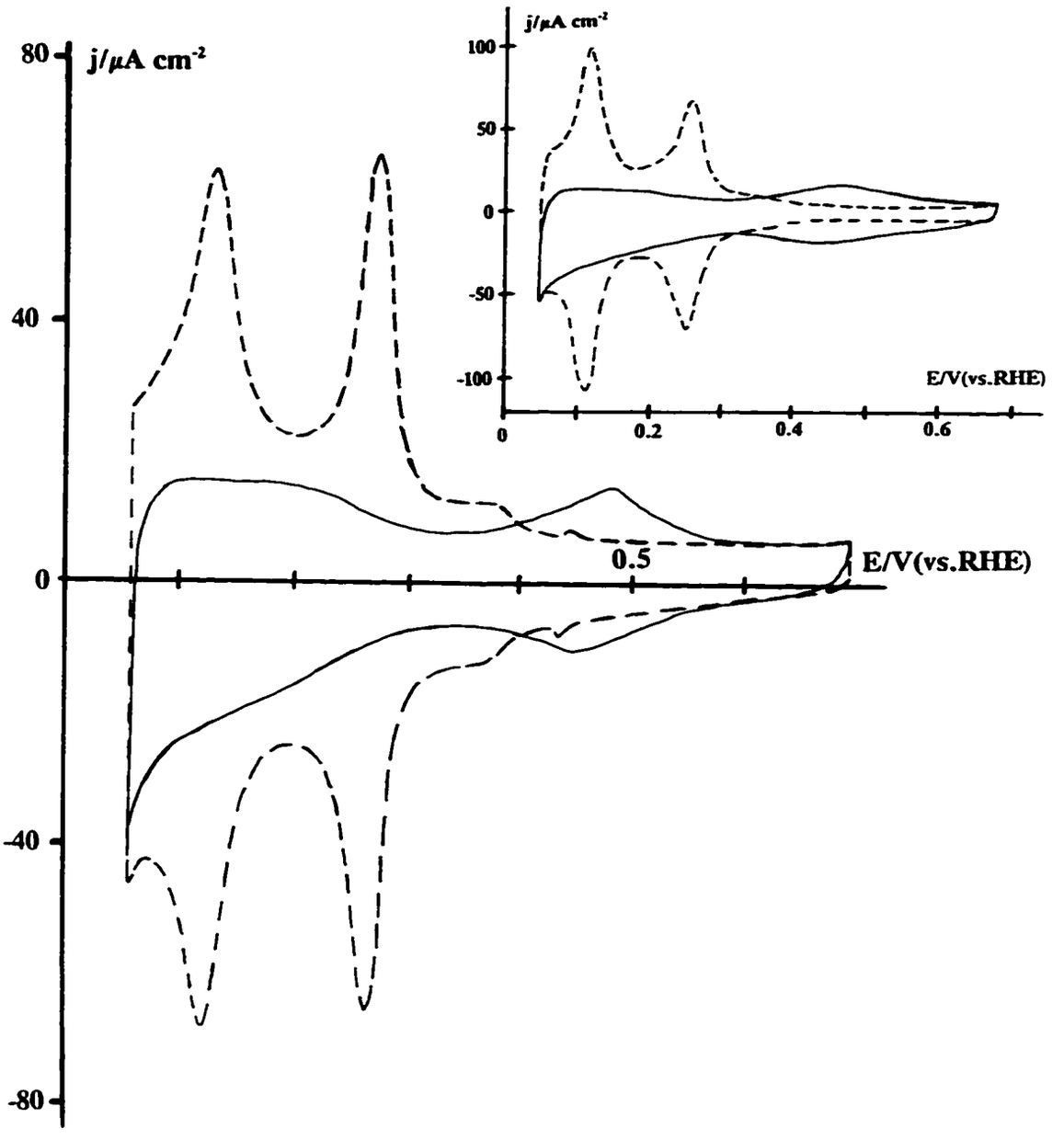

Fig. 6.4 Cyclic voltammograms obtained for flame-treated Pt polyoriented sphere after cooling in air: (- - -)in 0.5 mol dm^{-3} H_2SO_4; (___) in 0.5 mol dm^{-3} H_2SO_4 + 0.8 x 10^{-4} mol dm^{-3} CH_3CN. Inset: cyclic voltammograms obtained for Pt polycrystalline wire: (- - -) in H_2SO_4; (___) in 0.5 mol dm^{-3} H_2SO_4 + 0.8 x 10^{-4} mol dm^{-3} CH_3CN.

process(es) over the "double-layer" potential region is almost reversible [8] although, in the UPD H region, less so but with more or less quantitative anodic/cathodic charge balance.

6.3.2 Behaviour of adsorbed acetonitrile at Pt(111) in 0.1 mol dm^{-3} $HClO_4$ and 0.02, 0.5 and 2.0 mol dm^{-3} H_2SO_4

In this section we first compare the reactive chemisorption of acetonitrile at Pt(111) in 0.1 mol dm^{-3} $HClO_4$ with that in 0.02, 0.5 and 2.0 mol dm^{-3} H_2SO_4. This type of comparison is important since the UPD H behaviour at Pt(111) in CH_3CN-free $HClO_4$ is substantially different from that in H_2SO_4 (HSO_4^- ions [16]) owing to the stronger chemisorption of HSO_4^- than that of ClO_4^- [17], as is also found in OH electrosorption studies at Au [18].

Figure 6.5 shows the current response for acetonitrile adsorbed at Pt(111) in 0.1 mol dm^{-3} $HClO_4$ (solid line) compared with the background voltammogram (dashed line) in CH_3CN-free solution. The voltammogram for the CH_3CN-free $HClO_4$ solution exhibits the two, now well known [19], separated "butterfly" regions over the potential ranges 0.06-0.38 V and 0.55-0.87 V *vs.* RHE. It is seen that the behaviour with acetonitrile adsorbed is substantially different from that for polycrystalline or poly-oriented Pt in Fig. 6.4; in particular, the continuing anodic and cathodic current response in the $HClO_4$ solution at potentials greater than *ca.* 0.32 V, is much more spread out, in fact over two further well separated regions between 0.4 and 0.9 V in which the respective anodic/cathodic peaks are not at the same potentials (as they are the polycrystalline wire or in H_2SO_4 (see below)). The first and third current-response regions in Fig. 6.5 are evidently related in some way to the first and second principal UPD H regions (the well known [19] two "butterfly" patterns), although the respective charges due to H ionization or deposition are substantially (but not by any means completely) reduced by the presence of the chemisorbed acetonitrile. As was shown in ref. 8, for steric reasons, CH_3CN, initially adsorbed axially through the CN group, could leave a substantial and well defined fraction of the surface still available for adsorption of H. This seems to be the case here also.

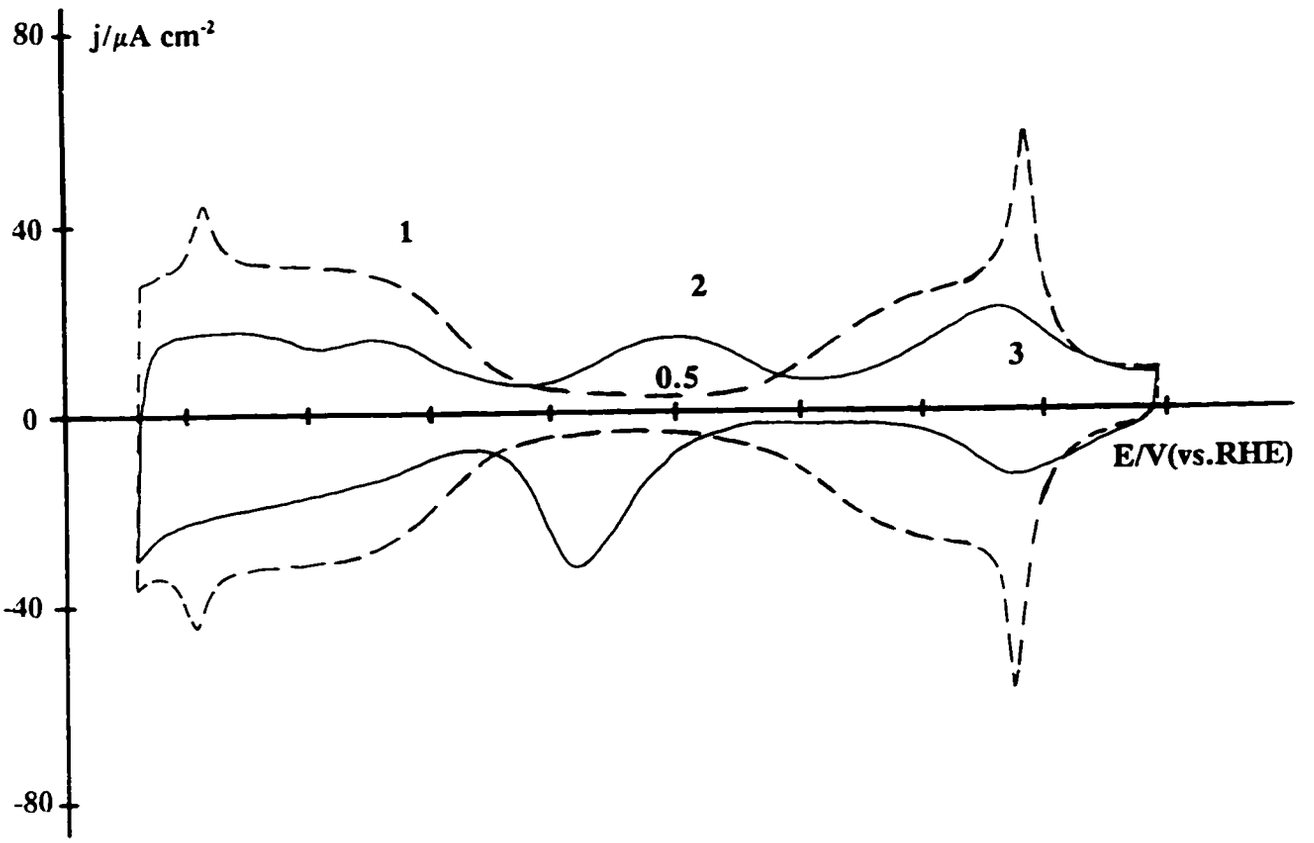

Fig. 6.5 Cyclic voltammograms obtained for flame-treated Pt(111) after cooling in air: (- - -) in 0.1 mol dm^{-3} $HClO_4$; (___) in 0.1 mol dm^{-3} $HClO_4$ + 0.8 x 10^{-4} mol dm^{-3} CH_3CN.

While the forms of the voltammograms for the surface reactions of adsorbed acetonitrile at the four surfaces examined (see Figs. 6.5, 6.6, 6.8, 6.9, 6.11 and 6.12) are clearly different and, in fact, represent one of the most striking cases of specificity of electrochemical surface processes to the orientation and respective two-dimensional structure of single-crystal planes, besides of course anion specific adsorption and UPD of metals. It is informative to examine, more quantitatively, the charges, q, associated with the distinguishable peaks. First we examine the data derivable for the (111) plane (Figs. 6.5 and 6.6).

In the absence of CH_3CN, as discussed in Chapter 3, the usually distinguished two UPD regions are observed, as outlined in Fig. 6.6 by the dashed and dotted lines, the latter corresponding to 160 $\mu C\ cm^{-2}$, i.e. two thirds of the total observable charge (240 $\mu C\ cm^{-2}$) between 0.06 and 0.55 V for the (111) surface [20].

In the first (UPD H) region (0.06 to *ca.* 0.38 V), the current profile for Pt (111) in the presence of CH_3CN (Fig. 6.5) is similar to that at polycrystalline wire and also almost the same as that for the same surface in the 0.5 mol dm^{-3} H_2SO_4 (Fig. 6.6). In fact, when CH_3CN is present (concentration 0.8 x 10^{-4} mol dm^{-3}) half of the UPD H charge is apparently lost over the first region, with 87 $\pm$ 3 $\mu C\ cm^{-2}$ remaining in the positive sweep profile and in the conjugate negative sweep profile over this region; this value is for the H_2SO_4 supporting electrolyte solution (Fig. 6.6) but very similar respective results are found for corresponding experiments in $HClO_4$ (Fig. 6.5). However, in the 0.5 mol dm^{-3} H_2SO_4 the two further regions beyond 0.38 V (up to 0.85 V) become "compressed" into what appears to be an highly reversible, sharply peaked region between 0.38 and 0.55 V but one in which some structure is still discernable. The apparent reversibility of processes corresponding to this sharp peak appears to be the result of "compression" of the two non-matching regions 2 and 3 in Fig. 6.5 (in $HClO_4$) possibly caused by the effect of HSO_4^- anions, anions which are known to be adsorbed over that range of potential [16]. In this region, both the anodic and cathodic current peaks are much better defined that at the polycrystal.

For all the faces studied in this part of the work, the CV's were taken after reproducibility in the current response had been attained (usually after about three

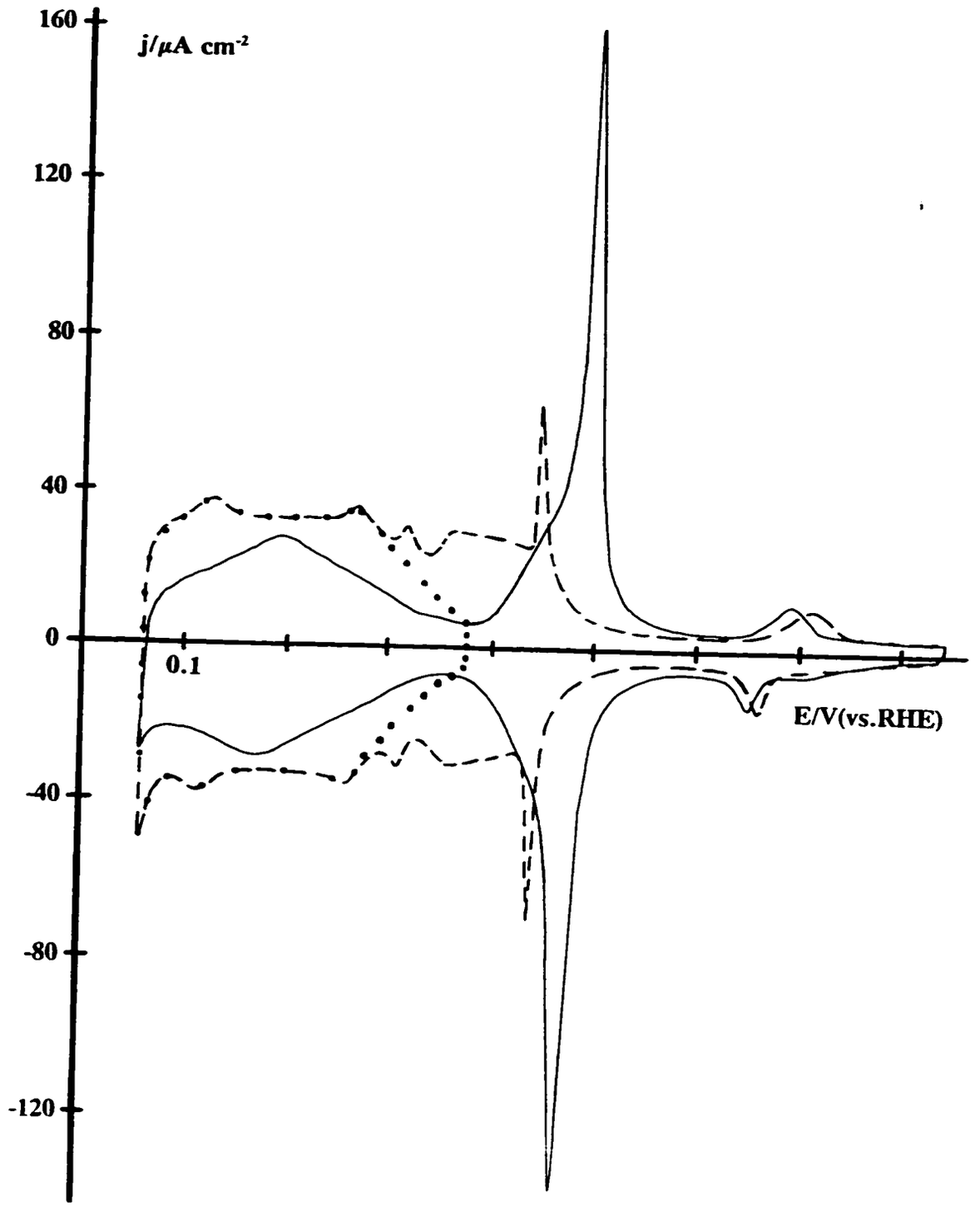

Fig. 6.6 Cyclic voltammograms obtained for flame-treated Pt(111) after cooling in air: (- - -) in 0.5 mol dm^{-3} H_2SO_4; (____) in 0.5 mol dm^{-3} H_2SO_4 + 0.8 x 10^{-4} mol dm^{-3} CH_3CN. Dotted line delineates the first UPD H region as known from experiments in dilute H_2SO_4 solutions.

cycles). In the case of Pt (111), the current response observed in the more positive potential region is the sharpest for the first cycle and its current intensity subsequently tends to decrease with continuation of cycling. (This was not observed when the UPD of H behaviour was recorded and so is not due to any impurity in the supporting electrolyte solution). However, when quantitative analysis of the results is performed for the first five cycles by determination of the charge over the first and second regions, values for both anodic and cathodic current responses are the same, viz. 87 $\pm$ 3 μC cm^{-2} for the first region and 107 $\pm$ 3 μC cm^{-2} for the second. With subsequent cycling the charges within the two regions become redistributed. Thus, the charge for the first anodic region becomes larger (92 μC cm^{-2}) than in the case mentioned above (87 μC cm^{-2}), but smaller than that for the conjugate cathodic peak (99 μC cm^{-2}); similar behaviour is observed in the second region but there it is the sharper cathodic current response which passes a smaller charge (91 μC cm^{-2}) than the anodic one (105 μC cm^{-2}). Overall, however, the total anodic and cathodic charges are equal and remain unchanged in both of these cases (193 $\pm$ 4 μC cm^{-2}).

If the electrode is cycled further, the sharpness of the peak is diminished and the total anodic and total cathodic charges each become 122 $\pm$ 3 μC cm^{-2}. Similar diminution of the peak's sharpness arises when the concentration of added CH_3CN is increased to above 5 x 10^{-3} mol dm^{-3}. It seems that these evaluated charges could be associated with long-term modification of the species on the surface, e.g. due to some oligomerization.

For the (111) Pt in 0.5 mol dm^{-3} H_2SO_4, with the above concentration of CH_3CN present, the large reversible current response (0.38-0.55 V) in Fig. 6.6 corresponds to a charge of 107 $\pm$ 3 μC cm^{-2} and these anodic and cathodic peak charges here are identical with one another, within 4 μC cm^{-2}. This charge is also 20 μC cm^{-2} larger than that for the H (36 % of the total initial H charge) apparently remaining (see above) over the first region in the anodic profile, i.e. corresponding to the differences of the integrated areas beneath the initial UPD profile (up to 0.38 V) and that with CH_3CN present.

The effects of increasing concentration of H_2SO_4 (i.e. correspondingly of HSO_4^-

and SO_4^{2-} ions) on the current profile for CH_3CN-free Pt (111) were characterized by Clavilier *et al.* [17]. Similar experiments were conducted here from 0.02, through 0.5 to 2.0 mol dm^{-3}, as shown in Fig. 6.7(b) in relation to the behaviour in the respective CH_3CN-free, acid solutions shown in Fig. 6.7(a).

Figure 6.7(a) shows (cf. ref. 17) the effect of increasing HSO_4^- and SO_4^{-2} ion concentrations on the form of the CV's for Pt (111), where displacement of the current peaks to less positive potentials (typical of specific adsorption of anions) arises. With CH_3CN present (Fig. 6.7(b)), this is paralleled by a similar, easily distinguishable effect on the two current-response regions of the adsorbed acetonitrile oxidation/reduction in relation to the three regions in Fig. 6.5 for $HClO_4$ electrolyte. We presume that these effects are due to interactions associated with competitive adsorption of HSO_4^- as, e.g., for halide-ion effects on the UPD H behaviour [21,22] or on the initial OH electrodeposition of OH at Pt or Au [18,21,23] which commences at 0.85 and 1.35 V (*vs.* RHE), respectively.

In 0.02 mol dm^{-3} H_2SO_4 (Fig. 6.7(b), dotted line), the sharp-peaked reversible regions observed in 0.5 or 2.0 mol dm^{-3} H_2SO_4 become broadened, i.e. there is less effect of co-adsorbed HSO_4^- ions and the peaks are at more positive potentials; the behaviour just begins to acquire features characteristic of the weaker anion adsorption arising in the $HClO_4$ solution and, in fact, region 3 in Fig. 6.7(b) then overlaps the original UPD H region 3 in Fig. 6.7(a).

It should be noted that the reversible (acetonitrile) current response regions, referred to above, lie outside the H UPD profile and more so when the behaviour in 2.0 mol dm^{-3} H_2SO_4 is examined (Fig. 6.7(b), full line); in fact, the anodic and cathodic peak potentials for these regions are changed substantially less, relative to those in Fig. 6.7(a) for the UPD H states, by the fourfold increase in H_2SO_4 concentration but it is the most positive region of the UPD H profile, where the spike arises, that becomes progressively more "compressed" to less positive potentials as illustrated by Fig. 2 in ref. 17. This region is observed to be "sharp-peaked" only on the (111) face in comparison with the other faces studied. It can be identified, however, to a small but significant extent on the polyoriented single-crystal sphere containing (111) facets (Fig. 6.4) at its surface.

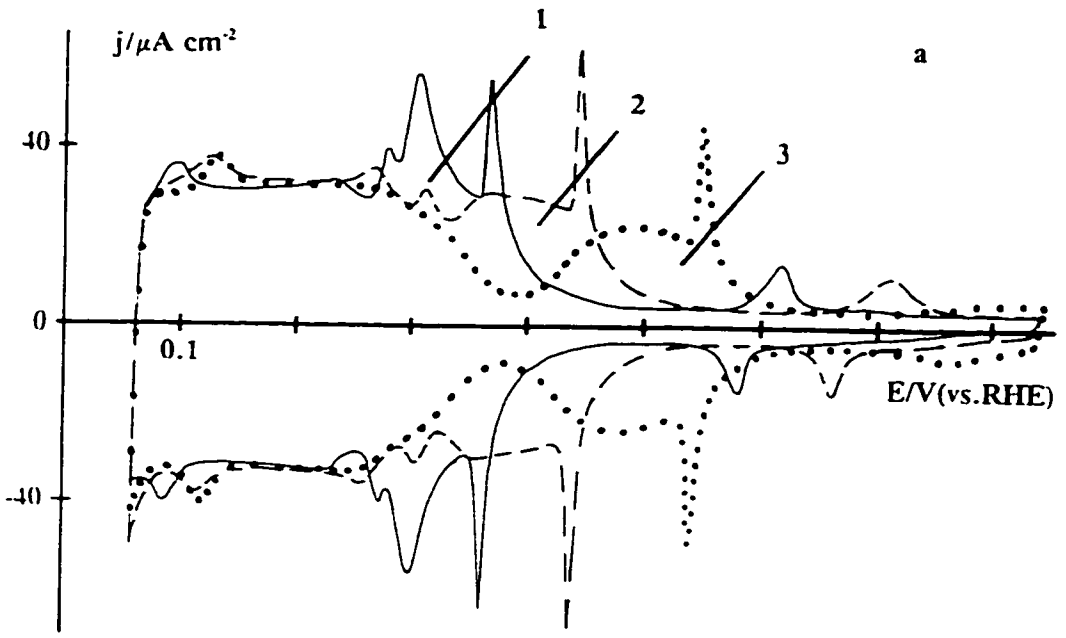

Fig. 6.7 a) Effect of H_2SO_4 concentration on the voltammetric behaviour of Pt(111) in CH_3CN-free H_2SO_4 solutions. Fig. 6.7b is on the next page.

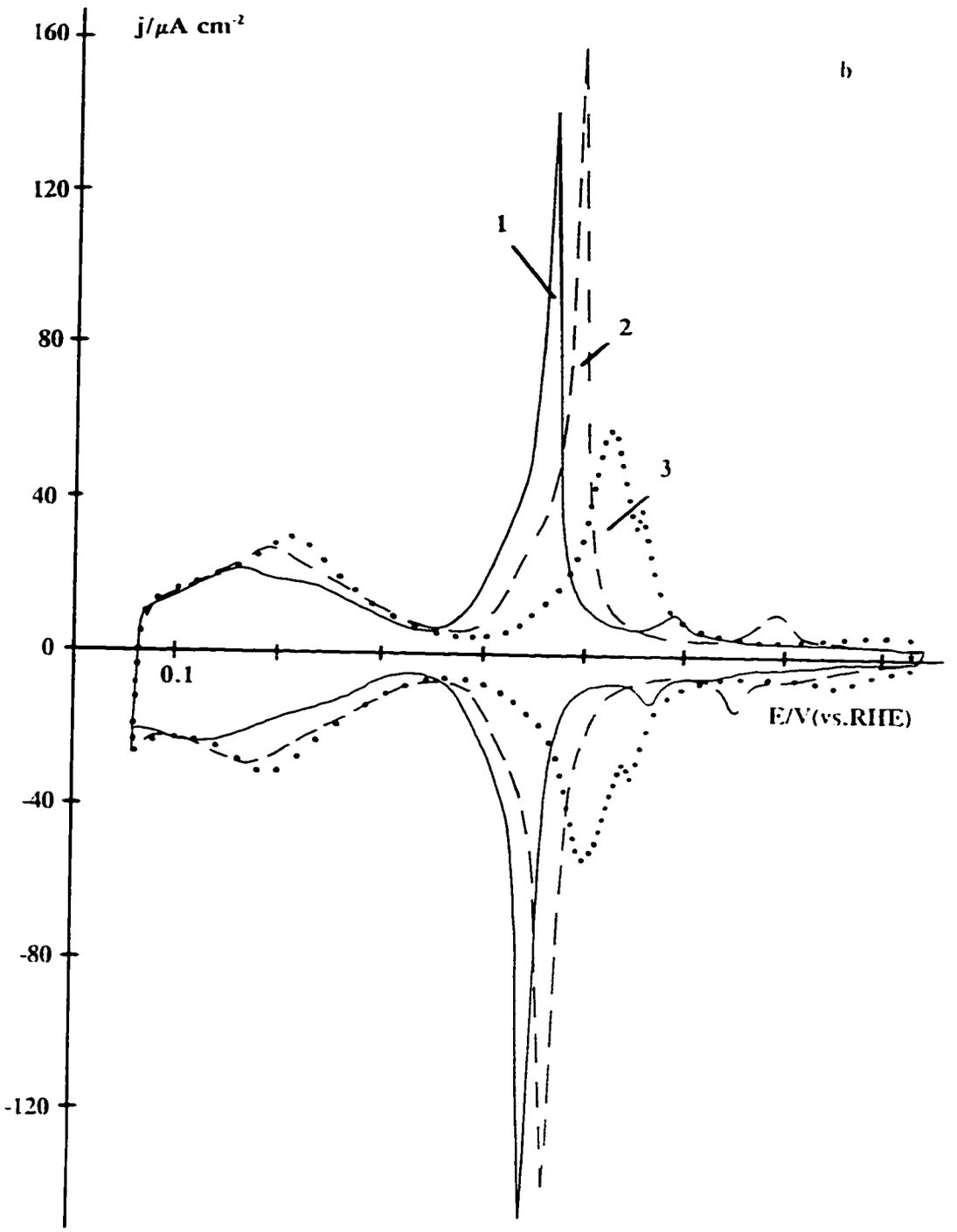

Fig. 6.7 b) Effect of H_2SO_4 concentration on the voltammetric behaviour of Pt (111) in the presence of 0.8 x 10^{-3} mol dm^{-3} CH_3CN. H_2SO_4 concentration: (___) 2.0 mol dm^{-3}; (- - -) 0.5 mol dm^{-3}; (••••) 0.02 mol dm^{-3}.

From this we can conclude that the process related to this peak is dependent on the fraction of (111) sites. Future studies on stepped faces containing (111) terraces of various widths could probably quantify these effects.

6.3.3 Behaviour of adsorbed acetonitrile at Pt(100)

Here experiments were conducted comparatively in 0.1 mol dm^{-3} $HClO_4$ and 0.5 mol dm^{-3} H_2SO_4 in an analogous way to those described in the previous section for Pt(111). In Figs. 6.8 and 6.9, for $HClO_4$ and H_2SO_4 respectively, the dashed-line voltammograms are for CH_3CN-free solution and the solid lines are for acetonitrile electrosorbed from 0.8×10^{-4} mol dm^{-3} CH_3CN present in the solutions. Here two regions of anodic current response are observed over well separated potential ranges. Corresponding cathodic current responses are also seen but without the reversibility observed at polycrystalline wire (Fig. 6.4). However, the solid line for acetonitrile is repeatable on multiple cycling with little change.

Neither of the current-response peaks in Fig. 6.8 corresponds to the UPD H peaks; the more positive peak (0.60-0.90 V) is outside the UPD H region (0.20-0.70 V) on this face (as it is at the polycrystal) while the first, least positive region arises within the potential range where the (100) surface would have been almost fully covered by H in the absence of CH_3CN.

In 0.5 mol dm^{-3} H_2SO_4 the H UPD region is again "compressed" by competitive HSO_4^- adsorption (Fig. 6.9, dashed line), but two distinguishable acetonitrile current response regions are still well separated, but with less sharp peaks. As for $HClO_4$, the first region in H_2SO_4 arises over that for almost full coverage by H (in the absence of CH_3CN) while the second arises where H would be absent in CH_3CN-free $HClO_4$. The behaviour of the two current response regions for adsorbed acetonitrile in $HClO_4$ vis à vis H_2SO_4 at Pt(100) (Figs. 6.8 and 6.9) is in contrast to the anion effect observed at Pt(111) (Fig. 6.6 compared with Fig. 6.5) where a substantial "compression" of the profiles is to be seen.

The "compression effect" referred to here originates because of an interaction effect due to the presence of HSO_4^- ions which are adsorbed competitively at the Pt

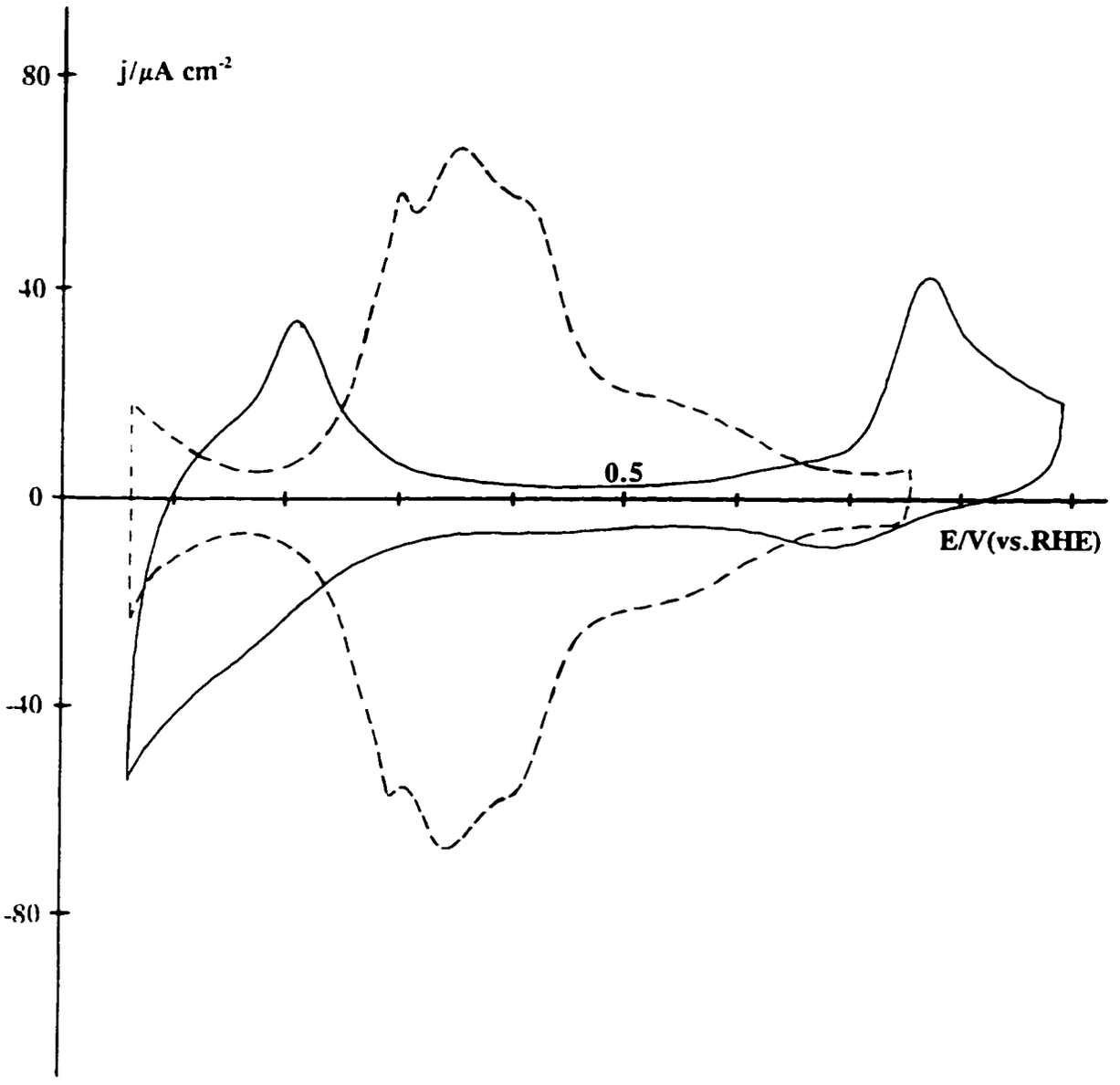

Fig. 6.8 Cyclic voltammograms obtained for flame-treated Pt(100) after cooling in H_2 + Ar: (- - -) in 0.5 mol dm^{-3} $HClO_4$; (___) in 0.5 mol dm^{-3} $HClO_4$ + 0.8 x 10^{-4} mol dm^{-3} CH_3CN.

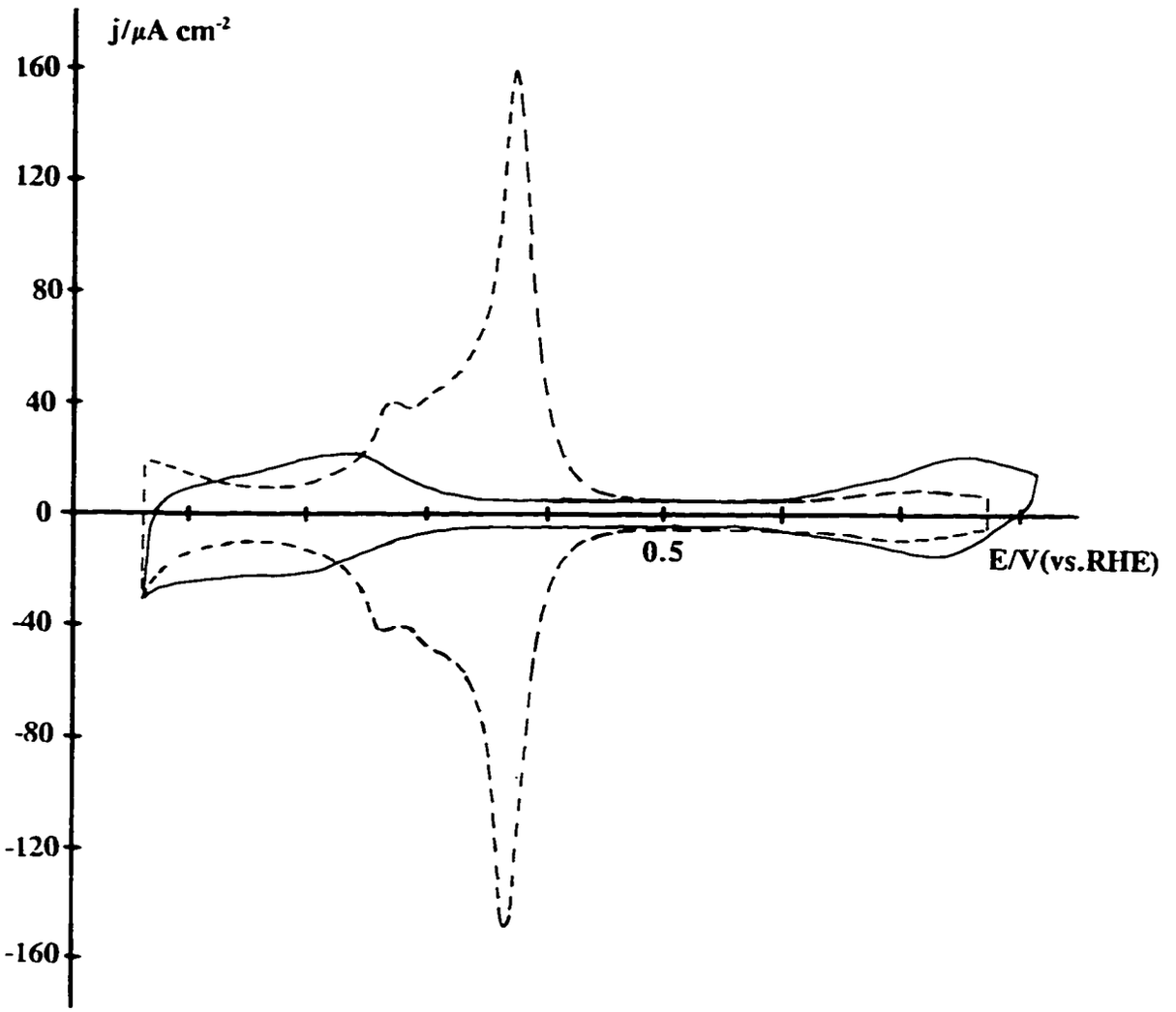

Fig. 6.9 Cyclic voltammograms obtained for flame-treated Pt(100) after cooling in H_2 + Ar: (- - -) in 0.5 mol dm^{-3} H_2SO_4; (____) in 0.5 mol dm^{-3} H_2SO_4 + 0.8 x 10^{-4} mol dm^{-3} CH_3CN.

surface sites, vis à vis H atoms. Thus H atoms which would normally commence being electrosorbed say at some potential $+E_\theta$ (*vs.* RHE) become adsorbable only at some *less positive* potential $+(E_\theta - \Delta E_\theta)$, following competitive desorption of the HSO_4^- ions. Consequently, the charge for H electrosorption has to be passed over a narrower potential range than in the absence of co-adsorbed anions; hence a sharper, *i.e.* narrower and higher, peak arises.

At this (100) surface in $HClO_4$ solution (with CH_3CN at 10^{-3} mol dm^{-3}), on holding the potential at the least positive end (0.06 V) of the sweep range for 15 min, an appreciable increase (by a factor of about two) of the current peak arises at the same potential as for the peak initially observed (0.21 V, Fig. 6.8) and a second at the potential of the second peak (0.78 V, Fig. 6.8). A similar experiment in 0.5 mol dm^{-3} H_2SO_4 gives a much smaller potential-holding effect, suggesting the remaining presence of strongly bound HSO_4^- ion.

These latter results seem to indicate that on holding the potential at 0.06 V, the adsorbed species is further reduced (as it also is at a polycrystalline wire [8]) in the adsorbed state. The extent of this reduction (in terms of charge) is measured by the new extra charges recovered (in the following positive-going sweep, Fig. 6.10) in the current peaks at 0.19 and 0.79 V. On reversing the sweep at 0.90 V, these reoxidation charges quantitatively return the behaviour of the adsorbed acetonitrile species to that of its initial state after one or two cycles, electrochemically, and therefore probably chemically.

Next, the charges and ratios for the current peaks at the (100) surface, based on Fig. 6.10, were recorded over the two principal potential ranges 0.06-0.32 and, 0.65-0.90 V where the holding effect arises. The charges associated with this behaviour are enumerated in Table 6.1 in relation to the designations of current peaks and curves shown in Fig. 6.10: peaks 1a and 2a are the anodic current responses under cycling conditions (50 mV s^{-1}) and peak 1b and 2b are the anodic current responses following the potential holding at 0.06 V. The respective extra charges due to reduction on holding are 73 and 71 μC cm^{-2}, respectively, and are thus in close agreement.

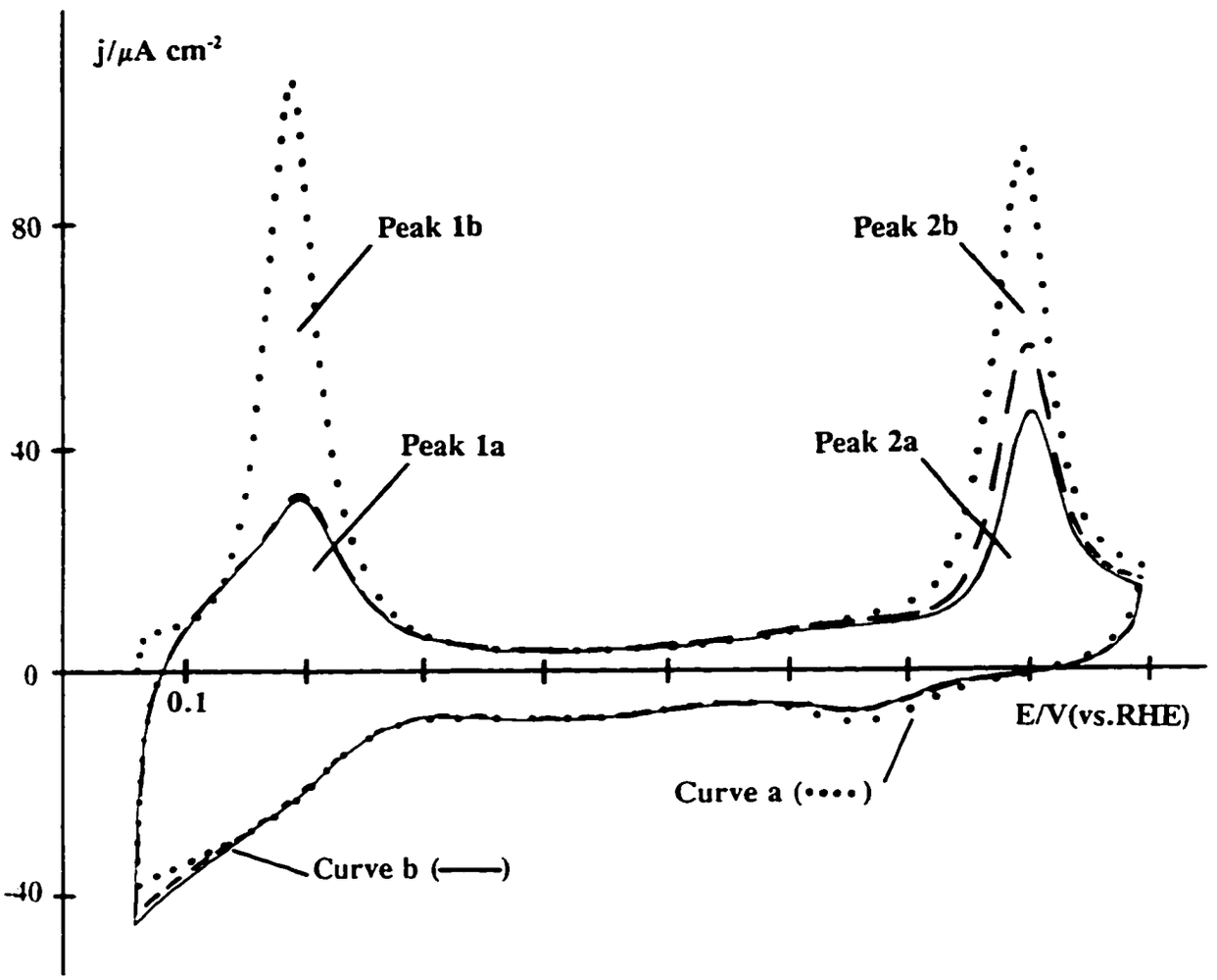

Fig. 6.10 Cyclic voltammograms for Pt(100) in the presence of 0.1 mol dm^{-3} $HClO_4$ + 1 x 10^{-3} mol dm^{-3} CH_3CN: (••••) first CV after holding the potential at 0.06 V for 15 min; (- - -) second CV; (___) third CV.

Table 6.1 Charges under indicated peaks in Fig. 6.10 for Pt(100) with acetonitrile adsorbed

Charge	Peak			
	before holding		after holding	
	1a	2a	1b	2b
$q/\mu C\ cm^{-2}$	64 ± 5	93 ± 5	137 ± 5	164 ± 5
$q/q_H/\%$	31	45	66	78
Total $q_{cathodic}/\mu C\ cm^{-2}$	Curve a (dotted)		Curve b (solid)	
	142 ± 6		136 ± 6	

In Fig. 6.10, it is seen that the effect of holding the potential at 0.06 V is much more specific and spectacular at this (100) surface than at the Pt(111), (110) and (311) surfaces. Thus, at the latter surfaces, holding the potential at the least positive value (0.06 V) of the scan gives only a small increase in the anodic reoxidation charge over the UPD H region in the following anodic sweep, and a small shift for (111) in 0.5 mol dm^{-3} H_2SO_4 to less positive potentials of the sharper peak.

The q value for peak 1a (Fig. 6.10) after holding the potential at 0.06 V is close to *twice* that observed in the cycling experiment, and for peak 2a, it is 1.76 times larger. The total cathodic q is reproducible (138 ± 6 $\mu C\ cm^{-2}$) and thus constant (± 6 $\mu C\ cm^{-2}$) during cycling. The total anodic q is *ca.* 157 $\mu C\ cm^{-2}$ during cycling; these total anodic/cathodic q values thus agree to within 10% and the cathodic value is 88% of the anodic charge. These charges represent 66% and 75% respectively, of the UPD H accommodation charge (209 $\mu C\ cm^{-2}$ in the absence of CH_3CN) on the (100) surface. The individual charges under peaks 1a, 2a and 1b, 2b, as a fraction of H accommodation charges, are listed in comparative summary fashion in Table 6.1 above as q/q_H (%).

6.3.4 Behaviour of adsorbed acetonitrile at the Pt(110) and Pt(311)

Figures 6.11 and 6.12 show the respective voltammograms for these faces in the

absence (dashed lines) and in the presence (solid lines) of adsorbed acetonitrile. At both these surfaces, the first acetonitrile current response region arises within the sharper-plus-broader UPD H regions 0.06-0.31 V for Pt(311) and 0.06-0.25 V for Pt(110). The second acetonitrile regions are again well outside the respective UPD H profiles over the range *ca.* 0.35-0.60 V for Pt(311) and 0.25-0.60 V for Pt(110). The current responses of acetonitrile at these two surfaces are evidently not specifically related to the sharpness of the peaks for UPD of H at these surfaces observed in the absence of CH_3CN.

It should be noted that the sharper peaks developed on the (111) plane and the polyoriented sphere (Fig. 6.4 and 6.6) are not distinguishable on the CV for Pt(311) in the presence of CH_3CN (Fig. 6.12, solid line). We believe that this is due to the restricted width of the (111) terraces which are too narrow on the (311) surface to give rise to the effect observed in Figs. 6.4 and 6.6.

It is of interest, qualitatively, that the CV behaviour of acetonitrile on the Pt(110) and (311) planes is most similar to that on the polycrystal, particularly with regard to current response in the "double-layer" region. Such surfaces are coordinatively the most open of the four structures examined, and this may hence be the situation predominating at the polycrystalline surface.

6.3.5 Charge transients on addition of acetonitrile and its adsorption at initially clean surfaces

Current transients arise [8,11] at the Pt electrode when CH_3CN is added to an initially CH_3CN-free acid solution, as explained in the Introduction (Fig. 6.2). In the UPD H region, anodic H displacement currents arise which are accounted for formally by the process

$$CH_3CN + xPtH \rightarrow Pt{\cdot}CH_3CN + xH^+ + xe^-$$

where one CH_3CN molecule occupies effectively x sites previously occupied by UPD H, so that x H's are displaced per acetonitrile chemisorbed. The transient experiments also show that CH_3CN can suffer Faradaic reduction on chemisorption (depending on the potential) so that the sign and magnitude of the observed transient charge is potential dependent, being the algebraic sum of the H displacement charge and the Faradaic

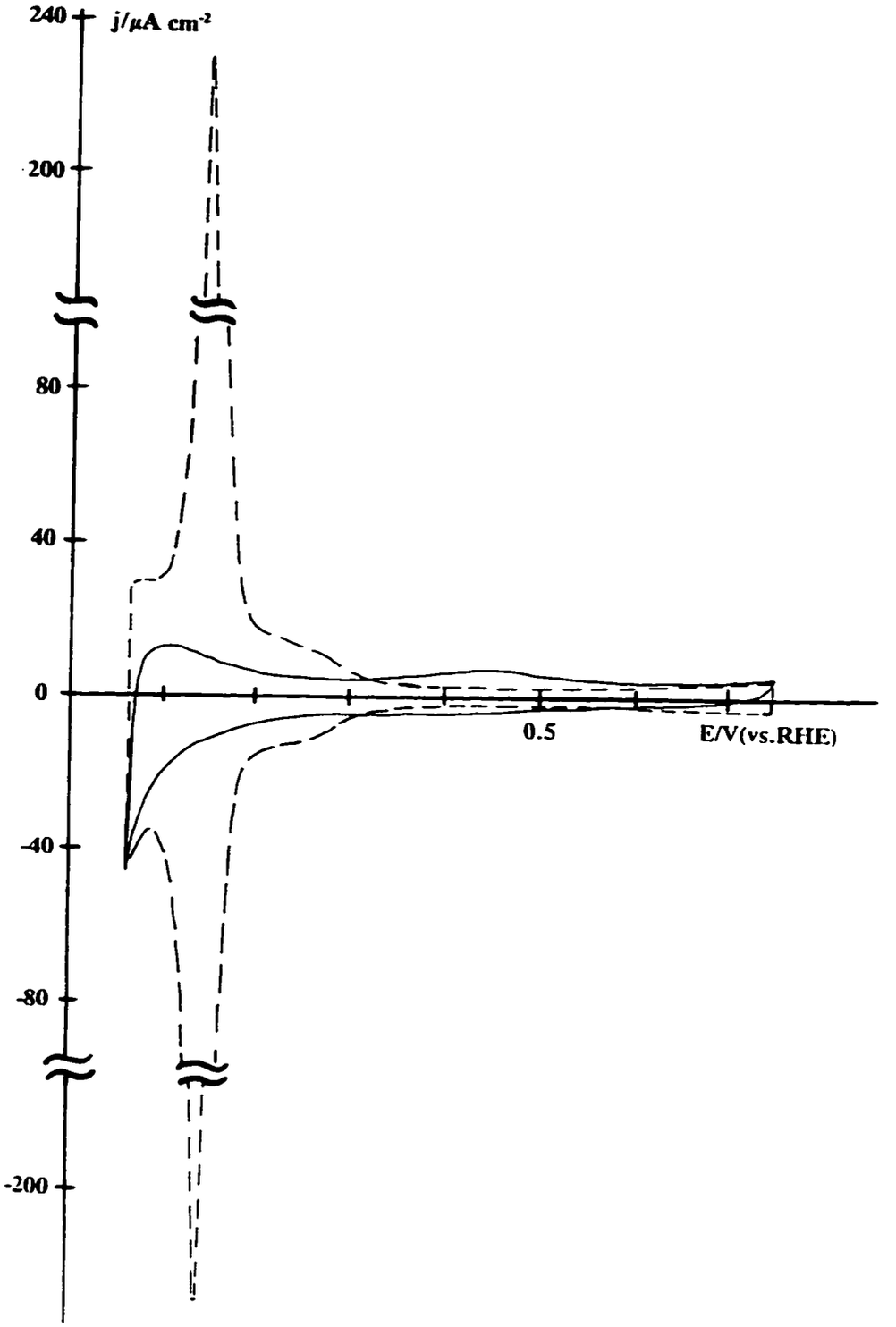

Fig. 6.11 Cyclic voltammograms obtained for flame-treated Pt(110) after cooling in H_2 + Ar: (- - -) in 0.5 mol dm^{-3} H_2SO_4; (___) in 0.5 mol dm^{-3} H_2SO_4 + 0.8 x 10^{-4} mol dm^{-3} CH_3CN.

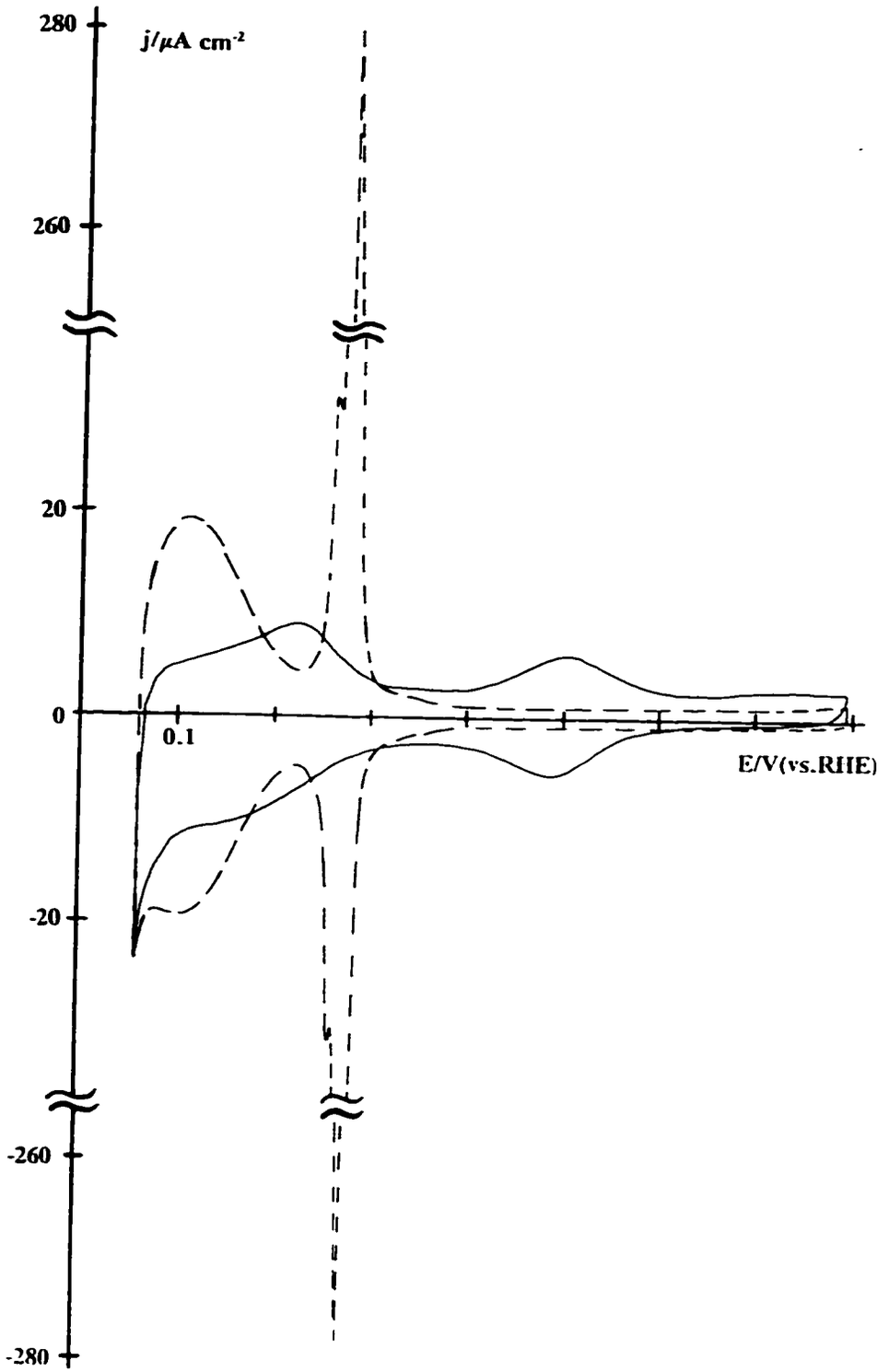

Fig. 6.12 Cyclic voltammograms obtained for flame-treated Pt(311) after cooling in H_2 + Ar: (- - -) in 0.5 mol dm^{-3} H_2SO_4; (___) in 0.5 mol dm^{-3} H_2SO_4 + 0.8 x 10^{-4} mol dm^{-3} CH_3CN.

surface-reaction charge for acetonitrile itself.

At Pt(111), it happens that this sum is zero (Fig. 6.13) at 0.25 V in the H region. Figure 6.13 also shows the transients arising in current-time plots for CH_3CN addition at two other potentials, one further in the UPD H region (anodic) and one in the double-layer region (cathodic). The respective derived charges are indicated by annotations on Fig. 6.13; apart from the value at 0.25 V, they are substantially larger than the changes of double-layer charge would be; hence they are associated with the reactive chemisorption of acetonitrile and/or H displacement by competitive adsorption of acetonitrile. More quantitatively, as an example, the charge passed in the negative-going sweep, in Fig. 6.13, from 0.70 V, where acetonitrile would be in its oxidized form (**I**) (see below p. 198), to 0.55 V, at which the transient is initiated, is 30 $\pm$ 3 μC cm^{-2}, while the observed transient charge at the latter potential is 29 μC cm^{-2}; these values are thus in quite good agreement. This confirms that the adsorption at the initially CH_3CN-free surface is accompanied by a reductive Faradaic reaction corresponding to a process such as **I**→**III** (see reaction scheme later; p. 199).

Pursuing this "charge accounting" further, we can deduce that at the potential of the zero charge transient (here 0.25 V), the quantity of H displaced (calculated as charge) should be equal to the acetonitrile reduction charge that would correspond to the integral, Δq_T, of the cathodic current response profile for acetonitrile from 0.70 to 0.25 V. This Δq_T is 110 μC cm^{-2}; it agrees well with the value (115 μC cm^{-2}) of charge that corresponds to the amount of UPD H that would have been present at this potential in the absence of CH_3CN (dashed curve in Fig. 6.13). The above charge values have an evaluation error of about 3%, so the agreement is fairly good (*ca.* 4%).

6.3.6 General question of current response assignments

In previous work [8] and in the discussion up to this point, it has been assumed that the current responses observed at Pt in the presence of CH_3CN are due mainly to surface reaction(s) of the acetonitrile itself in some chemisorbed state. However, during the course of analysis of the new results of the present work, it appeared necessary to examine the possibility that the response currents arising over all regions of the CVs

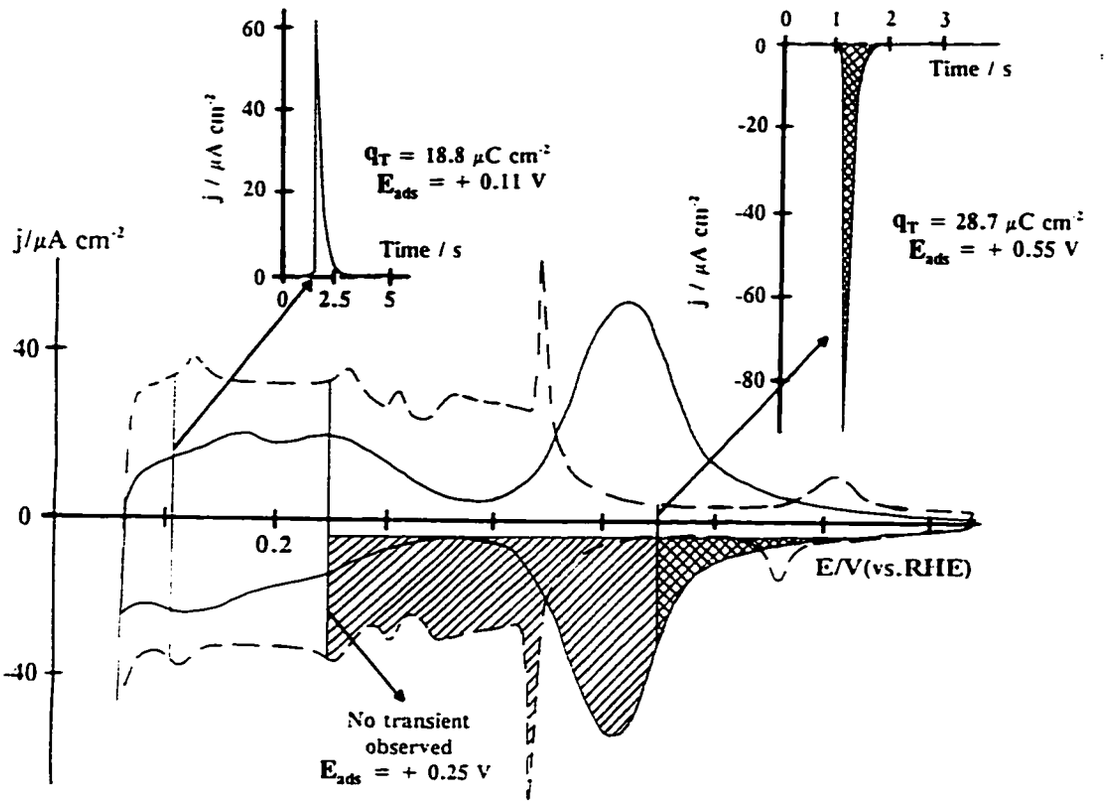

Fig. 6.13 Potentiodynamic profile for 1 x 10^{-2} mol dm^{-3} CH_3CN (___) and background (- - -) in 0.5 mol dm^{-3} H_2SO_4 together with typical anodic and cathodic transients which arise on potentiostatic adsorption of added CH_3CN at 0.11 and 0.55 V, with the anodic H displacement effect arising in the former case. No transient charge passes at 0.25 V. Cross-hatched region corresponds to integrated reduction charge from 0.70 to 0.55 V; single-hatched region corresponds to reduction charge passed down to 0.25 V in the negative-going sweep.

could be due to deposition and desorption of H in states modified, through interactions, by the presence of acetonitrile itself, in this scenario existing in an adsorbed but electrochemically inactive state.

The following facts and arguments, we believe, speak against such an overall alternative interpretation of the results that have been presented in earlier sections of this chapter. (a) The current transients associated with addition of CH_3CN (at Pt(111), see Fig. 6.13) correspond to charges that are negative (cathodic adsorption) at the more positive potentials, then pass though zero around 0.25 V and become positive (anodic) in sign over the region of less strongly bound H (anodic H desorption effect). It is thus clear that over a certain potential range where UPD H is initially absent, acetonitrile can itself be electroactively chemisorbed through a reduction process. Then, in that state, it can be reversibly reoxidized and re-reduced in the potential range 0.38-0.55 V. (b) At several of the surfaces studied here, the acetonitrile current response peaks in cyclic voltammetry lie well outside the region where UPD processes involving H arise (in the absence of CH_3CN), especially at the (100), (110) and (311) planes. (c) The substantial effect of holding the potential at the least positive potential in linear sweep voltammetry at polycrystalline Pt [8], and especially at Pt(100) (Fig. 6.10), would be very difficult to explain if the acetonitrile in the chemisorbed state was itself unreactive.

6.3.7 Kinetics of reduction and reoxidation of adsorbed acetonitrile

6.3.7.1 Dependence of current response on sweep rate

In the earlier work from this laboratory [8], the extent of kinetic reversibility of the processes involved in reduction and reoxidation of acetonitrile in the chemisorbed state was evaluated at polycrystalline wire by estimating the s_o value [24] analogous to the j_o quantity for regular, continuous faradaic processes. s_o is the value of sweep-rate, s, below for which the process remains kinetically reversible (*i.e.* without any overvoltage) as indicated by the peak-potential, E_{peak}, remaining independent of s (*e.g.* see Fig. 1.7 in Chapter 1). Figure 6.14 shows a comparison of the shifts of peak potential (ΔE_{peak}) for the current response peak in the "double-layer" region at the polyoriented single-crystal sphere in comparison with the previous results [8] obtained

at polycrystalline wire. The s_o value, as $\log(s_o / \text{mV s}^{-1})$, = 1.6, is closely similar to that previously observed for a wire. There is, however, some curvature in the anodic and cathodic ΔE_{peak} plots but this was not due to *IR*-drop effects. At the (111) surface, a very clear and sharp peak arises (Fig. 6.6) outside the UPD H region, as described above. The potential of this peak as a function of log s can also be monitored with the result shown in Fig. 6.14. These responses correspond to Tafel-like deviations from reversibility (especially for the polycrystal) in the reduction/reoxidation of the acetonitrile species in a chemisorbed state beyond $s \approx 40$ mV s^{-1}, the s_o value here.

6.3.7.2 Behaviour under modulated potential sweep conditions

In an earlier paper [15] it had been shown how repetitive modulation of the sweep rate from a low to a higher value, e.g. from 5 to 50 mV s^{-1}, over a continuously varying range of potential covered in a cyclic voltammogram enabled the resolution of relatively fast-responding processes from slower ones to be made (Fig.6.15). This technique had been applied to the behaviour of adsorbed acetonitrile at polycrystalline Pt wire [8] and, in the present work, to that at Pt(111), as shown in Fig. 6.16. The method was subsequently extensively applied in works of Arvía and co-workers [25] on oxidation of Pt.

The dashed lines in Fig. 6.16 show the locus of the termination of fast current responses as a function of potential as sweep-rate was increased periodically during the sweep from 5 mV s^{-1} (inner solid line profile) to 50 mV s^{-1}, leading to the manifold of curves in this figure, in both the positive- and negative-going directions of potential scan.

As at polycrystalline Pt [8], distinguishable regions of fast-responding processes are resolved in the UPD H region at Pt(111) both on the anodic and cathodic sweeps, while the sharper peak in the double-layer region exhibits mainly fast-response behaviour over all of the charge passed. This behaviour is nearest to that observed previously on polycrystalline Pt where the fast-responding processes were suggested to be due to electrosorption and desorption of co-adsorbed H remaining amongst the adsorbed (slowly responding) acetonitrile molecules.

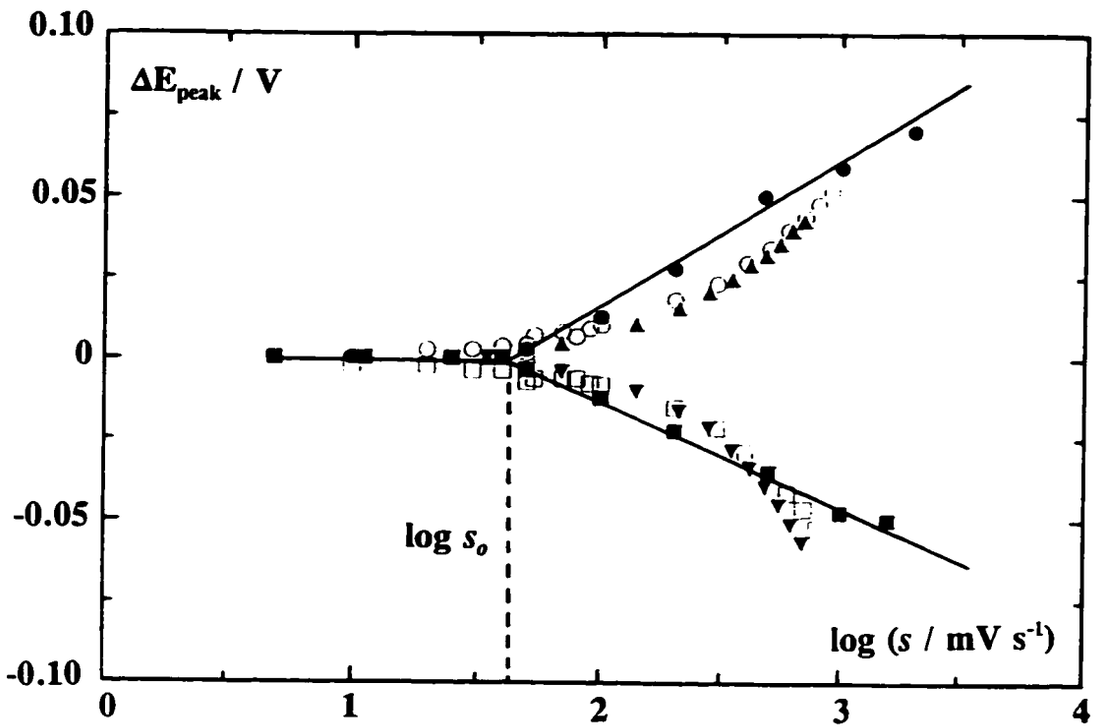

Fig. 6.14 Change of peak potential in negative and positive sweeps in double-layer region with log (sweep rate) showing limit of reversibility (as log s_o) of double-layer reduction/oxidation process for polycrystalline Pt (•,▪), Pt polyoriented sphere (○,□), and Pt(111) (▲,▼) in 0.5 mol dm^{-3} H_2SO_4 aqueous solution containing 2 x 10^{-3} mol dm^{-3} CH_3CN.

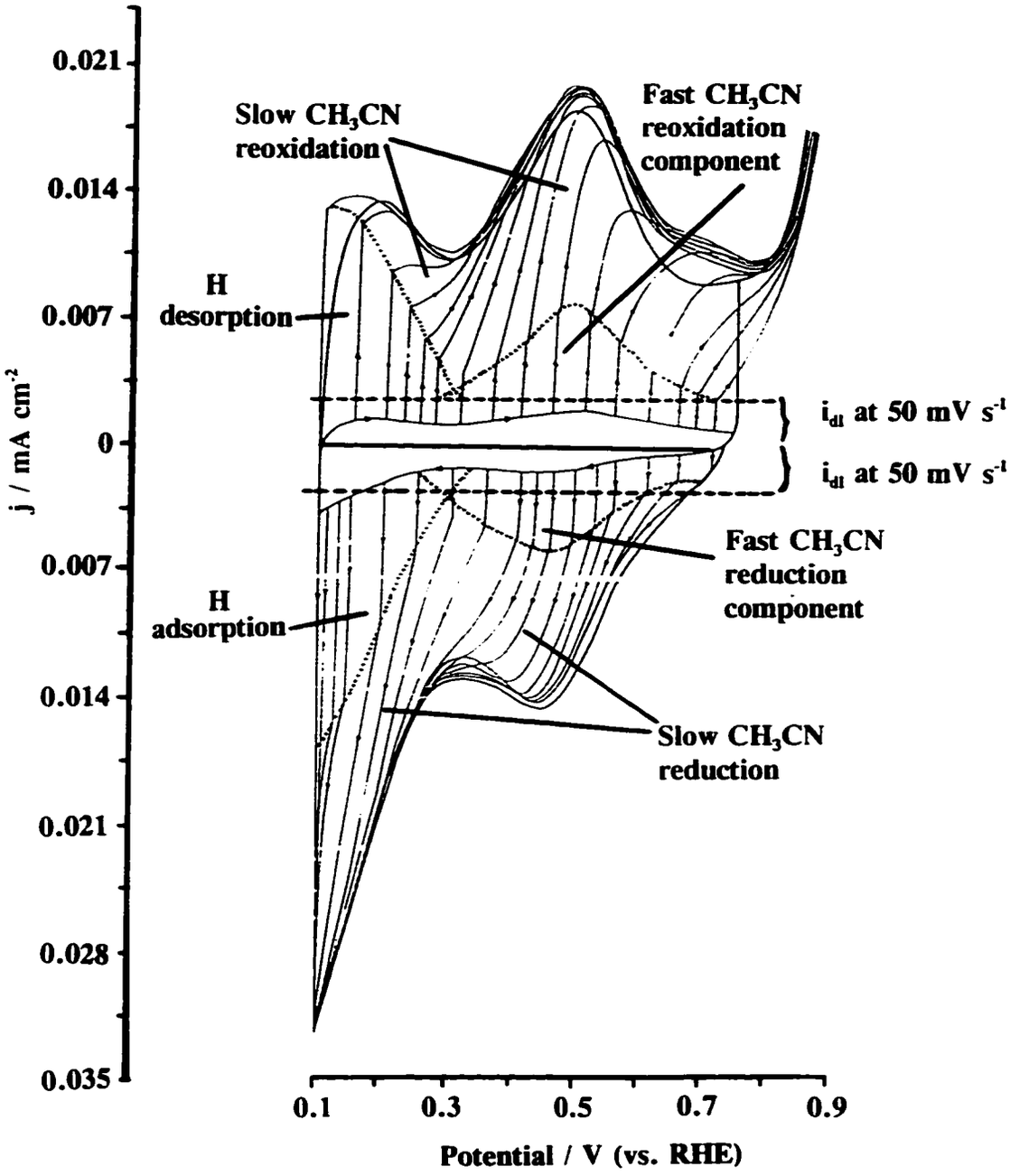

Fig. 6.15 Resolution of the fast atomic hydrogen and acetonitrile processes obtained by initiating faster transients (50 mV s^{-1}) on a slower anodic or cathodic-going one (5 mV s^{-1}) for the polycrystalline Pt electrode in contact with 0.5 mol dm^{-3} H_2SO_4 solution containing 2 x 10^{-3} mol dm^{-3} CH_3CN [8].

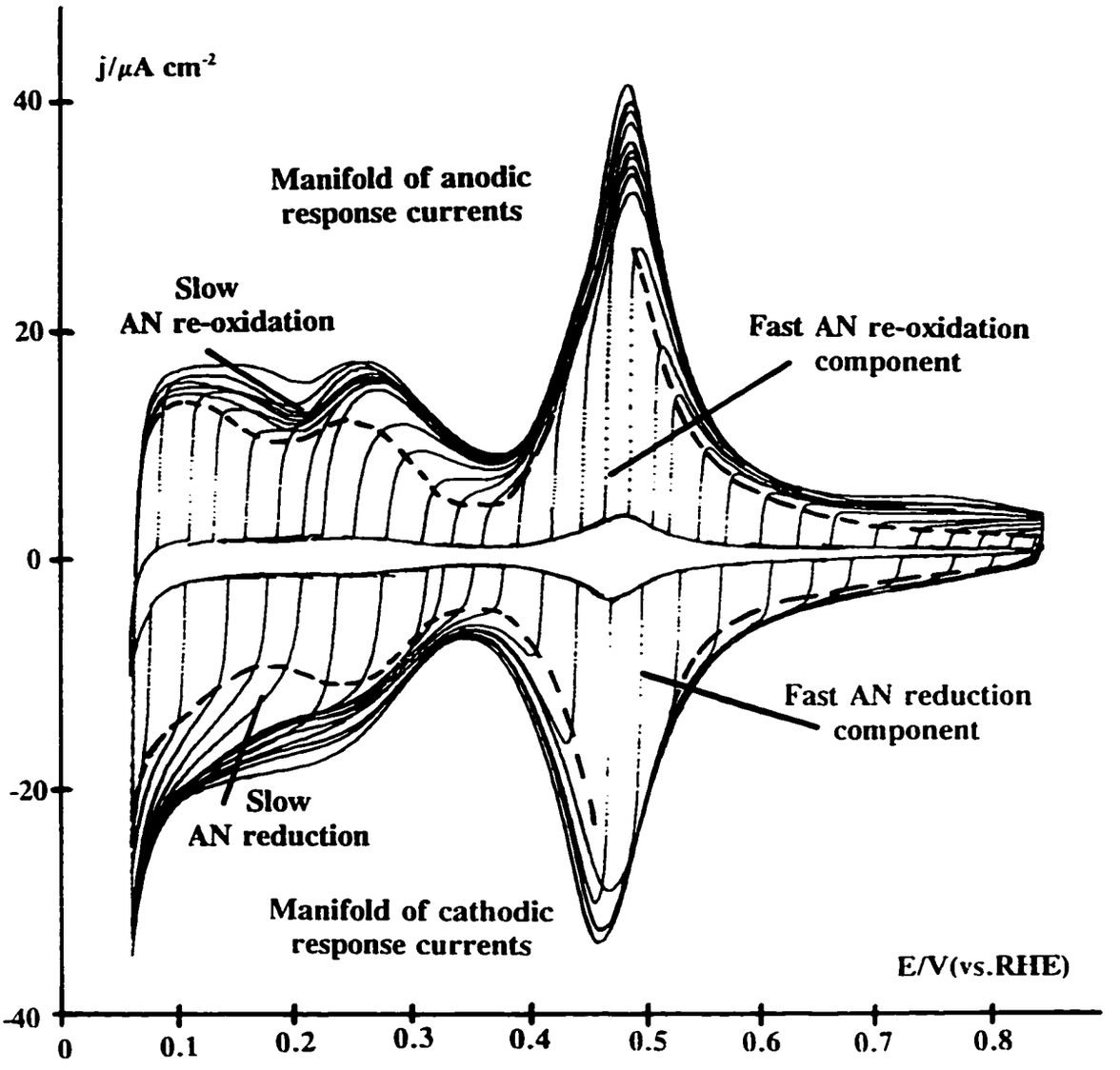

Fig. 6.16 Manifolds of fast and slow current responses for change of sweep rate from 5 to 50 mV s^{-1} in CV's for adsorbed acetonitrile and UPD H processes at Pt (111) in 0.5 mol dm^{-3} H_2SO_4 solution containing 2 x 10^{-3} mol dm^{-3} CH_3CN, indicating locus (- - -) of limits of fast current responses in the positive- and negative-going sweeps.

6.3.8 Possible mechanisms of the observed reactive chemisorption effects

In the previous papers [14,8] from this laboratory, several possibilities were identified for the chemical processes occurring; first a donative (I) or associative (II) chemisorption of acetonitrile were proposed, thus:

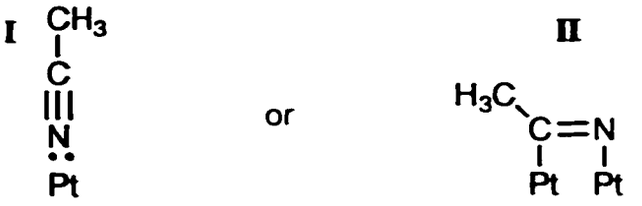

coupled with two consecutive electron and proton transfer processes such as:

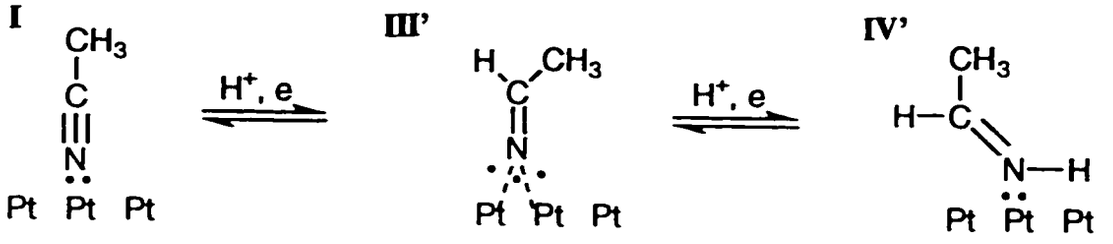

Unfortunately, deductions about the identity of the chemisorbed species are difficult to make on the basis of the cyclic voltammetric and chemisorption charge-transient data alone. In the present part of the work being described here we have concentrated on demonstrating the specificity of the overall current-response profiles to the four single-crystal surfaces examined and shown the directions and magnitudes of the charge-transfer transients that arise upon chemisorption of acetonitrile at the (111) plane (Fig. 6.13).

At this surface, there is a clear relation of the charges passed in the current-response profiles for acetonitrile, cathodically and anodically, over the first H UPD region to those for acetonitrile over the second region in Fig. 6.6. In the first region, the anodic and cathodic charges are equal and are half the original H charge (in the absence of acetonitrile) over the same potential range. In the second (reversible response) region, the anodic and cathodic charges are again equal, and also equal to the

anodic or cathodic charges in the first region.

These results suggest that two closely related processes are taking place: in the second region over the more positive potential range of Fig. 6.6, Faradaic reductive chemisorption occurs with protonation according to:

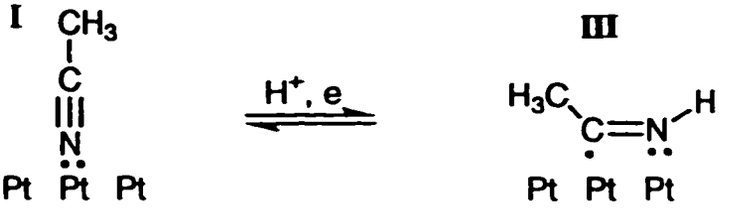

where the product **III** is formally an adsorbed free radical but the bonding to the surface probably involves interaction with an additional electron in a *d*-orbital of the Pt surface. This chemisorption would have a site requirement of two Pt atoms per acetonitrile molecule and involve a change of configuration of the CH_3CN to that of molecule **III**. In the chemisorbed state, this reduced form of acetonitrile ($1e^-$ per two occupied Pt sites) can be reoxidized to **I** reversibly, corresponding to the sharp peak in Fig. 6.6 or that observed at polycrytalline Pt (Fig. 6.4).

In the UPD H region (at (111)), this site occupancy reduces the accommodation for H but this is not directly determinable from the anodic or cathodic voltammetric curves in that region since some components of current are associated, respectively, with further reoxidation or re-reduction of the adsorbed acetonitrile [8]. However, from application of the modulation procedure (Fig. 6.16), the envelope of fast-responding currents assumed to be associated with H adsorption or desorption (plus double-layer charging) corresponds to about 67% of the charge passed in that region, i.e. ca. 33.5 % of the original UPD H charge passed over that potential range (0.06-0.38 V).

The effect of potential holding is to lead to the formation of a species on the surface that either requires an increased charge for its reoxidation and/or allows an increase of sites for accommodation of H. A possible process associated with the holding effect is:

III

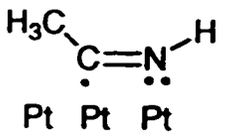

H^+, e, time

IV

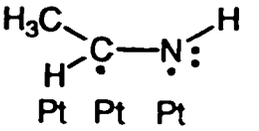

where III is a dissociatively chemisorbed form of ethylamine. However, the process III → IV is almost structurally, if not kinetically, reversible since, after a single cycle, following holding, the voltammogram is restored almost to its initial form prior to the holding condition.

Further analyses of the reactive chemisorption of adsorbed acetonitrile are given in the next chapter, where these processes are examined in the light of results of further experiments using in-situ infrared spectroscopy.

References

1. B.B. Damaskin and A.N. Frumkin, Electrochim. Acta, 12 (1967) 1323.
2. M.W. Breiter, J. Electrochem. Soc., 109 (1962) 1099.
3. a) M.W. Breiter, Electrochim. Acta, 8 (1963) 457; b) M.W. Breiter, *ibid*, 10 (1965) 503.
4. a) R.R. Adzic, W.E. O'Grady and S. Srinivasan, Surf. Sci. Lett., 94 (1980) L191; b) R.R. Adzic, W.E. O'Grady and S. Srinivasan, *ibid*, J. Electrochem. Soc., 128 (1981) 1913.
5. a) N. Batina, S.A. Chaffins, F. Lu, C.H. Lin, J.W. McCargar, B.E. Kahn, J.Y. Gui, D.G. Frank, G.N. Salaita, D.A. Stern and A.T. Hubbard, Electrochim. Acta, 34 (1989) 1031; b) S.A. Chaffins, J.Y. Gui, C.H. Lin, F. Lu, G.N. Salaita, D.A. Stern, B.E. Kahn and A.T. Hubbard, J. Electroanal. Chem., 284 (1990) 67.
6. a) G. Somorjai, Surf. Sci., 89 (1979) 469; b) G. Somorjai, *ibid*, Principles of Surface Chemistry, Prentice Hall, Englewood Cliffs, NJ, 1972.
7. S. Morin and B.E. Conway, J. Electroanal. Chem., 376 (1994) 135.
8. B.E. Conway, H.A. Kozlowska and B.R. MacDougall, J. Electroanal. Chem., 39 (1972) 287.
9. a) R.W. Murray, Acc. Chem. Res., 13 (1980) 135; b) P.R. Moses, L. Wier and R.W. Murray, Anal. Chem., 47 (1975) 1882.
10. R.F. Lane and A.T. Hubbard, J. Phys. Chem., 79 (1980) 808.
11. B.R. MacDougall, B.E. Conway and H.A. Kozlowska, J. Electroanal. Chem., 32 App. (1971) 15.
12. M. Szlarczyk and J. Sobkowski, Electrochim. Acta, 25 (1980) 1597.
13. S. Wasmus and W. Vielstich, J. Electroanal. Chem., 345 (1993) 323.
14. B.E. Conway, B.R. MacDougall and H.A. Kozlowska, J. Chem. Soc., Faraday Trans. 1, 68 (1972) 1566.
15. B.E. Conway, H.A. Kozlowska, F.C. Ho, J. Klinger, B.R. MacDougall and S. Gottesfeld, Faraday Discuss. Chem. Soc., London, 56 (1973) 199.
16. see section 3.1.2 in Chapter 3, and reference therein.

17. J. Clavilier, K. El Achi and A. Rodes, Chem. Phys., 141 (1990) 1.
18. H.A. Kozlowska, B.E. Conway, B. Barnett and J. Mozota, J. Electroanal. Chem., 100 (1979) 417.
19. D. Armand and J. Clavilier, J. Electroanal. Chem., 270 (1989) 331.
20. J. Clavilier, J. Electroanal. Chem., 107 (1980) 211.
21. D.M. Novak and B.E. Conway, J. Chem. Soc., Faraday Trans. 1, 77 (1981) 2341.
22. M.W. Breiter, Electrochim. Acta, 8 (1963) 925.
23. V.S. Bagotskii, Y.B. Vasil'yev, J. Weber, J.N. Pirtskhalava and B. Knots, J. Electroanal. Chem., 27 (1970) 31.
24. H.A. Kozlowska and B.E. Conway, J. Electroanal. Chem., 95 (1979) 1.
25. a) N.R. de Tacconi, J.O. Zerbino, M.E. Folquer and A.J. Arvia, J. Electroanal. Chem., 85 (1977) 213; b) J.O. Zerbino, N.R. de Tacconi, A.J. Calandra and A.J. Arvia, J. Electrochem. Soc., 126 (1979) 592; c) R. Cordova, M.E. Martins and A.J. Arvia, Electrochim. Acta, 25 (1980) 453.

Chapter 7

The reactive chemisorption of acetonitrile on Pt(111) and Pt(100) electrodes as examined by *in situ* infrared spectroscopy

7.1 Introduction

Over the years, spectroscopy techniques have provided molecular level information, with high sensitivity and selectivity, and have been shown to provide invaluable information in many areas of chemistry. This has also been beneficial to surface science which employs some of these spectroscopic methods to probe solid surfaces in vacuum and the gas phase. These methods include electron diffraction techniques, such as low energy electron diffraction (LEED), for characterizing long-range atomic and molecular order, and the techniques of Auger electron (AES), ultraviolet photoelectron (UPS), electron energy loss- (EELS), X-ray photoelectron (XPS) and infrared reflection absorption (IRRAS) spectroscopies, which can be used to obtain information concerning the chemical composition and structure of surface layers or adsorbates. However, the electron spectroscopies, which have been proven so valuable to the study of clean surfaces and adsorbate-covered surfaces in high vacuum, cannot be used to study the electrochemical interface owing to the extremely low path length of electrons in condensed media, *i.e.* through the solution.

In recent years there has been a major effort to develop spectroscopic methods for characterizing the electrode-electrolyte interface. These spectroscopic techniques can be either performed *in situ*, meaning that the electrode-electrolyte interface is studied directly, or *ex situ*, meaning that the electrode is transferred from the electrolyte to an ultrahigh vacuum (UHV) chamber allowing the use of the gallimaufry of surface spectroscopies mentioned above. However, the latter transfer technique involves a drastic change in the electrode environment and the loss of potential control; this limits the systems that can be studied to processes involving strongly (and thus irreversibly) chemisorbed molecules, as in UPD of metals [1], or the potential-induced restructuring of metal surfaces [2].

In situ techniques, in which the structural integrity of the electrode-solution

interface is maintained, do not involve the uncertainties of *ex situ* methods. A plethora of *in situ* spectroscopies has been developed including Raman spectroscopy [3], UV-visible reflectance spectroscopy [4], surface plasmon spectroscopy [5], ESR spectroscopy [6], Mössbauer spectroscopy [7], surface-EXAFS [8], and infrared (IR) reflection spectroscopy. This chapter will be concerned mainly with a discussion of results obtained by applying the latter technique to study further the reactive chemisorption of acetonitrile at Pt(111) and (100) surfaces.

The first *in situ* IR spectroelectrochemical experiments used the internal reflection method [9,10]. This technique employs multiple reflections from the electrode surface to increase the signals for absorbance that are too weak to be observed by direct measurement. This technique requires optically transparent materials (n-type germanium) or thin film electrodes deposited on infrared-transmitting substrates. These were not very successful at the time and it is only recently that these configurations have again been used, this time for Fourier Transform spectroscopy [11,12]. Nevertheless, the most successful technique has been the external reflection method [13].

This latter procedure yields direct molecular information concerning the structure and bonding of adsorbates on electrode surfaces. The first experiments employed a dispersive infrared spectrometer and modulation of the electrode potential, with synchronous detection of the modulated infrared absorbance. This method was later developed for use with Fourier transform infrared spectrometers [14,15] and sensitivity levels allowing the detection and characterisation of submonolayer quantities of adsorbates were achieved [16]. In the subsequent sections of this chapter, use of the latter IR spectroscopy method for investigation of the adsorbed species involved in the reactive chemisorption of acetonitrile discussed in the previous chapter (6) will be described, as first outlined below.

As is now well documented [17], the recent emergence of an increasing variety of *in situ*, microscopic-level techniques is exerting a major impact on our understanding of the nature and properties of species originating from electrosorption processes. Given that the foregoing interpretations have been based solely on results derived from conventional electrochemical methodology, further insight into the molecular-level

processes involved should be forthcoming by utilizing such microscopic-level techniques.

From the work presented in Chapter 6, a two-stage mechanism for the surface reactivity was suggested, as illustrated in Fig. 7.1 on the basis of electrochemical cyclic voltammetry and adsorption charge-transient measurements [18-20].

In the present context, a natural strategy to employ is infrared spectroscopy. The method is well established as an invaluable means of examining adsorbate structure and bonding, at least for systems displaying strong infrared absorption bands that are sensitive to the interfacial environment and exhibiting potential-dependent states of adsorption [21]. Since, as the potential is stepped to less positive values, possible reorientation of the adsorbed acetonitrile and change in the bond order can occur; thus the first 1e, $1H^+$ reduction could transform the triply bonded -C≡N to the doubly bonded form >C=N-. Hence, it is anticipated that the sensitivity of the "C=N" vibrational chromophore to the manner in which acetonitrile is oriented at, and bonded to the surface, should provide direct evidence supporting (or otherwise) the mechanism summarised in Fig. 7.1. For reactive systems, infrared spectroscopy has been utilised extensively to examine electrosorption of CO and a range of organic adsorbates yielding CO and other species arising from dissociative adsorption [21]. However, the range of electrochemical reactions involving surface-attached reactants and products that has been examined by means of *in situ* infrared spectroscopy is, hitherto, quite narrow.

There are no previous *in situ* spectroscopic studies of the present aqueous acetonitrile system on Pt electrodes. Several reports have considered the behaviour of pure acetonitrile, which is widely used as an aprotic solvent in electrochemistry; for example, infrared spectroscopic studies on its stability at high positive potentials (> 2 V *vs.* SCE) [22], and on the effects of the presence of trace amounts of water [22,23], have been made. However, it is only when a large excess of water is present [18] that the phenomenon of reactive chemisorption of CH_3CN under examination here, takes place.

In this present section of the work, *in-situ* infrared spectroscopy has been used to examine the validity of the mechanism proposed in Chapter 6 (see also [19]), specifically by probing the C-N vibrational modes of the species arising from reactive

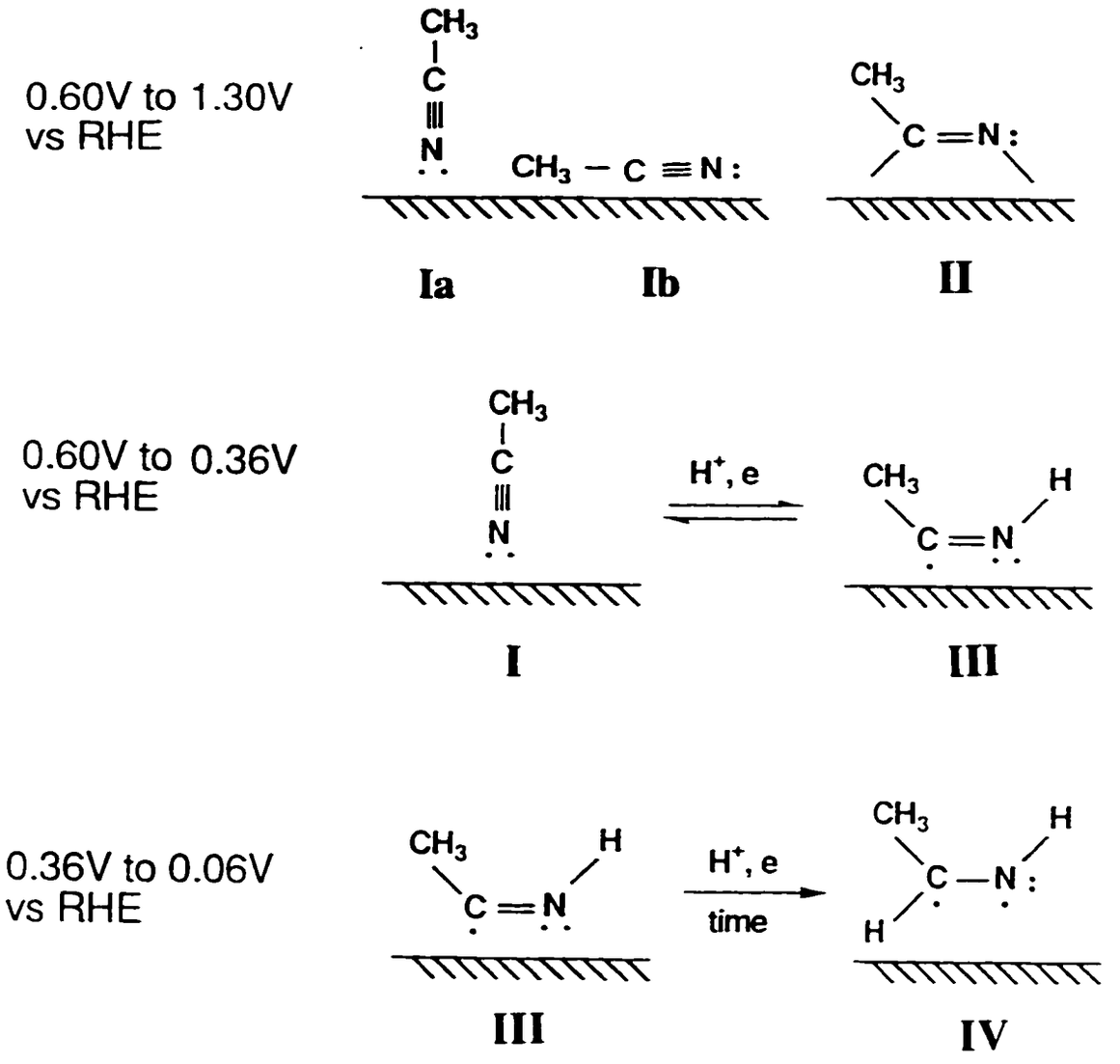

Fig. 7.1 Mechanism for the reductive chemisorption of CH_3CN on Pt(111) and (100) as proposed in ref. 19; see Chapter 6.

chemisorption of acetonitrile at Pt.

7.2 Experimental and theoretical considerations

The detection of infrared absorbances by submonolayer quantities of species at the electrode-electrolyte interface requires a high level of sensitivity, which has been achieved by using a thin layer cell and by modulating the potential or the state of polarization of the infrared radiation. These two latter strategies [21] will be detailed below.

Infrared reflection absorption spectroscopy (IRRAS) consists in modulating the polarization state (s and p) of the incident IR light and recording the difference in the absorbance intensity (I_p - I_s) as a function of potential. This technique relies on the fact that the two polarization states behave differently on reflection at surfaces: thus only the p-component of the incident IR beam can interact with the adsorbate, since the s-component has a near to zero electric field strength at the metal surface. Hence the (I_p - I_s) signal contains spectral information for species on (and near to) the electrode surface, while randomly oriented species in the rest of the path of the beam produces no (I_p - I_s) signal. The spectrum is obtained by taking the ratio of the (I_p - I_s) difference signal, and the sum of the two signals (I_p + I_s).

Similarly, the alteration of the electrode potential between two values (E_1 and E_2) produces a modulation in the electrochemistry in the interfacial region, and potential-difference IR spectroscopy monitors the accompanying changes in the absorbance of IR ratio. The change of reflectivity between E_1 and E_2, (ΔR), *i.e.* the difference spectrum, can be obtained by dividing by R, the total reflectivity.

Two variants of the potential-modulation method are commonly utilised: subtractively normalized interfacial Fourier transform infrared spectroscopy (SNIFTIRS) and electrochemically modulated infrared spectroscopy (EMIRS). EMIRS involves relatively rapid (*ca.* 10 Hz) potential modulation between the E_1 and E_2 values while the incident infrared wavelength is scanned slowly with a grating spectrometer. The alternative approach, SNIFTIRS, involves recording a series of interferometer scans sequentially at the two E_1 and E_2 potential values, the spectra resulting from the series

of scans then being subtracted from each other to yield the potential-difference infrared (PDIR) spectra [21]. Recently, Weaver and co-workers [24] have proposed another PDIR method called single potential alteration infrared spectroscopy (SPAIRS). This method is a modification of the SNIFTIRS technique and finds application in the study of irreversible (or less reversible) electrode reactions. It consists in recording the interferometer scans at E_1 and then at E_2 by stepping the potential only once. It will be shown below that this technique is suitable for the investigation of the reactive chemisorption of acetonitrile at Pt single-crystal electrodes.

Most of the experimental details concerning the infrared instrumentation and procedures used are given in refs. [25-29]. The specific potential-step strategies employed are outlined in sections 7.3.2 and 7.3.3 of the present chapter.

Details concerning the infrared spectrometer are given in Chapter 2. The spectral resolution was $\pm$ 4 cm^{-1} and the incident infrared light was p-polarized.

7.3 Results and discussion

7.3.1 Cyclic voltammetry

The choice of Pt(111) and (100) surfaces for this study was motivated by the fact that it is on these surfaces that the reactive chemisorption of CH_3CN gives the most informative current responses as described in Chapter 6 and ref. 18. On the (111) face, higher positive potentials (> 1.3 V) are required before interfering surface oxidation currents arise, thus allowing a wider range of potentials over which the reactive chemisorption can be examined by spectroscopic as well as voltammetric means (Fig. 7.2a).

Figure 7.2a shows typical anodic/cathodic cyclic voltammograms at 50 mV s^{-1} from 0.06 to 0.90 V, and return, for reactive chemisorption from a 1 x 10^{-3} mol dm^{-3} CH_3CN solution in 0.1 mol dm^{-3} $HClO_4$ on Pt(111). The dashed trace corresponds to the current response before addition of CH_3CN to the electrochemical cell. The voltammograms for the CH_3CN-free electrolyte exhibit the well known features diagnostic of ordered Pt(111) (Chapter 3). The behaviour observed in the presence of adsorbed acetonitrile (solid trace) is essentially the same as that reported earlier in

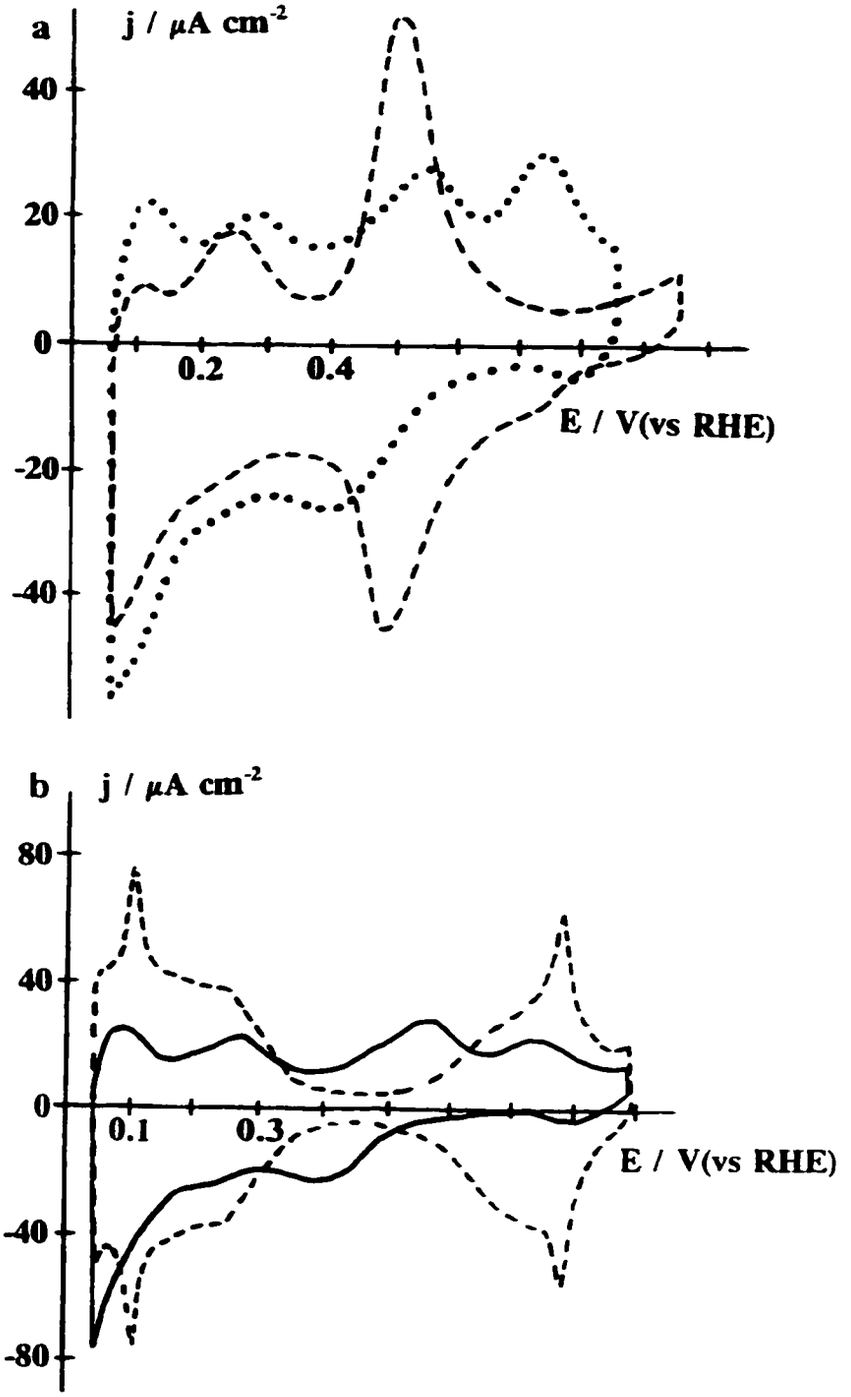

Fig. 7.2 Cyclic voltammograms obtained for a flame-treated Pt(111) after I_2-CO treatment: a) CV's recorded in the preparation cell (---) in 0.1 mol dm^{-3} $HClO_4$; (solid line) in 0.1 mol dm^{-3} $HClO_4$ + 7 x 10^{-3} mol dm^{-3} CH_3CN; b) CV's recorded in the in-situ IR cell (....) in 0.1 mol dm^{-3} $HClO_4$ + 7 x 10^{-3} mol dm^{-3} CH_3CN; (---) in 0.1 mol dm^{-3} H_2SO_4 + 7 x 10^{-3} mol dm^{-3} CH_3CN.

Chapter 6. For instance, from the anodic and cathodic current responses shown in Fig. 7.2a, it is clear that CH_3CN chemisorption (or a species derived from it) is occurring over a wide potential range and thus affects the electrochemical responses arising from the adsorption of the species (H and anions) that would otherwise be present. Above 0.6 V, the adsorbed species could be ClO_4^- or even hydroxyl ions [30], but their identity is still not well characterized. However, the potential region between 0.32 V and 0.6 V is clearly associated with the first stage of reduction/reoxidation of adsorbed acetonitrile [19]. At potentials below 0.32 V, the voltammetric features in the presence of CH_3CN are qualitatively similar to those observed on polycrystalline Pt except that the extent of blocking of adsorption of H is much less on Pt(111) than on the other surfaces studied, bearing in mind that acetonitrile species never completely eliminate H-adsorption at the Pt surface even at relatively high (1 mol dm^{-3}) concentrations of that solute (cf. ref. 18) in the solution.

Figure 7.2b shows typical cyclic voltammograms obtained in the thin-layer infrared cell for Pt(111) in contact with a 7 x 10^{-3} mol dm^{-3} CH_3CN solution in 0.1 mol dm^{-3} $HClO_4$ (dotted trace) and 0.5 mol dm^{-3} H_2SO_4 (dashed trace). These current responses are essentially the same as those previously reported [19] and shown in Chapter 6, confirming the electrochemical integrity of the infrared spectral arrangement. The main difference between the behaviour in the perchloric and sulphuric acid electrolytes in Fig. 7.2b, is the overlap observed in the case of the H_2SO_4 solution, between 0.35 V and 0.55 V, of the current responses for bisulphate anion adsorption [31] with the currents in the region where acetonitrile is reduced and reoxidized.

7.3.2 Infrared spectral behaviour of species derived from adsorbed acetonitrile

Figures 7.3 and 7.4 show a series of infrared spectra obtained in 0.1 mol dm^{-3} H_2SO_4 in D_2O containing 7 x 10^{-3} mol dm^{-3} of CH_3CN and CD_3CN, respectively, at Pt(111). D_2O (99.8 %) was utilized as the solvent primarily in order to minimize solvent spectral interferences in the frequency range, 1300-2000 cm^{-1}, covered in Figs. 7.3 and 7.4. The procedure used, that has been termed potential-difference infrared (PDIR) spectroscopy as explained above, involves obtaining a set of interferometer scans (say,

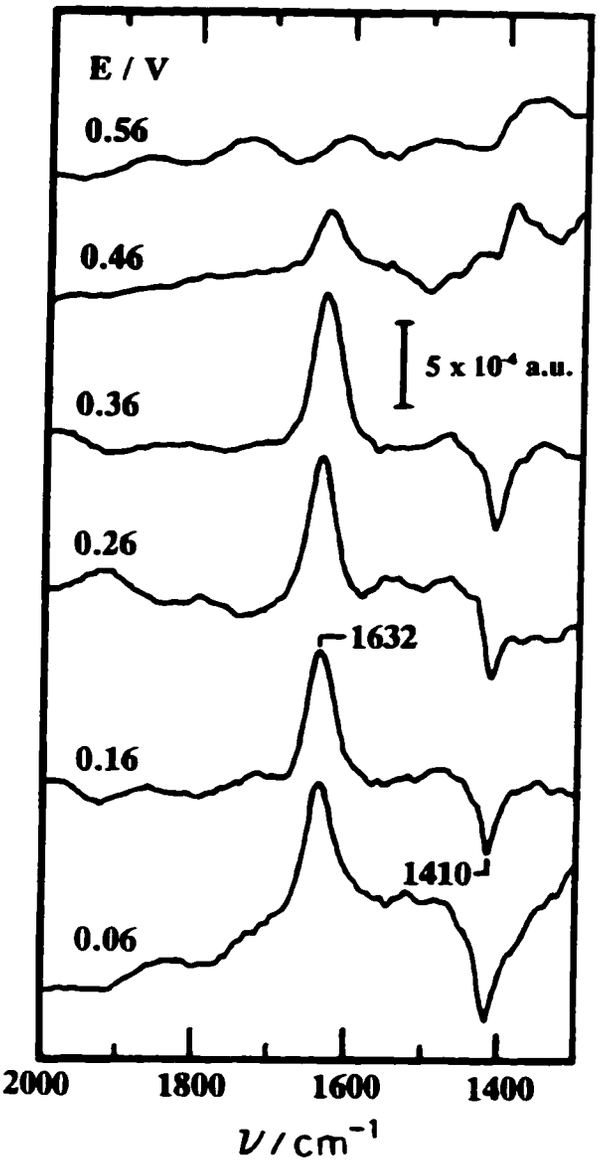

Fig. 7.3 Single potential-step PDIR spectra in the 1300-2000 cm^{-1} region for 7 x10^{-3} mol dm^{-3} CH_3CN in 0.1 mol dm^{-3} $HClO_4$ with D_2O as the solvent on Pt(111). Each spectrum was acquired by using 100 interferometer scans; the potentials indicated beside each spectrum are the sample potentials. A corresponding set of interferograms obtained at 0.76 V was used as the reference and the result was subtracted from each spectrum so as to remove solvent and other spectral interferences. The units of the intensity axis are in absorbance units (a.u.).

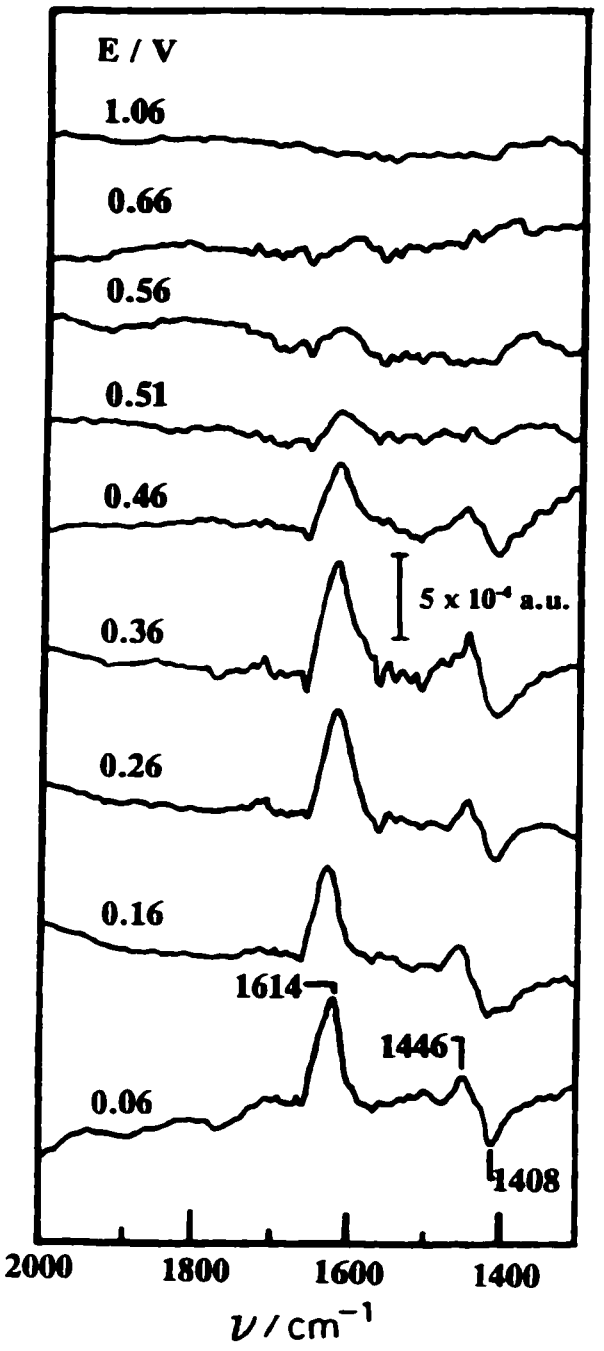

Fig. 7.4 As in Fig. 7.3 but for a 0.1 mol dm^{-3} $HClO_4$ solution containing 7 x 10^{-3} mol dm^{-3} CD_3CN.

100) taken sequentially at a pair of electrode potentials, and subtracting one from the other, *i.e.* the spectra acquired at the sample potential minus the one at the reference potential; this yields the difference absorbance spectra [24] shown. This conventional procedure therefore removes solvent and other unwanted spectral interferences, leaving only the components that yield differences between spectra of the species existing at the two (reference, sample) potentials. Specifically, for the spectra in Figs. 7.3 and 7.4, the "reference" spectra were all obtained at 0.76 V, with the sequence of decreasing positive "sample" potentials being indicated on those figures. Hence, the potential was stepped from 0.76 V to the first sample potential (*e.g.* 0.56 V) back to the reference potential (0.76 V), then stepped back to the next sample potential (*e.g.* 0.46 V). The former value was chosen as the potential at which the adsorbed acetonitrile is stable towards reduction, so that the positive- and negative-going spectral features refer to species generated and consumed, respectively, upon decreasing the potential to the "sample values" indicated in the figures.

Inspection of Figs. 7.3 and 7.4 shows clearly resolvable positive-going vibrational features at 1632 ($\pm$2) cm^{-1} and 1614 ($\pm$2) cm^{-1}, respectively, which appear at *ca.* 0.55 V (see Fig. 7.4) and reach a constant intensity by *ca.* 0.35 V. The band frequency and also intensity remain unchanged towards lower potentials, down to the less positive limit, *ca.* 0.06 V. The band frequency observed in Fig. 7.3 is downshifted from 1632 to 1614 cm^{-1} upon acetonitrile deuteration, as seen by comparing the spectra in Figs. 7.3 and 7.4. In addition, a negative-going band at 1410 cm^{-1} appears over the potential range where the 1632 cm^{-1} feature is observed. While the 1410 cm^{-1} band is seemingly unaffected by reactant deuteration (see Fig. 7.4), an additional weaker positive-going feature is evident at *ca.* 1450 cm^{-1} for deuterated acetonitrile (Fig. 7.4) but a corresponding absorption is detected for unlabelled acetonitrile (Fig. 7.3). Each of the spectral features were entirely absent for "blank" infrared experiments undertaken in the absence of acetonitrile. Also, no significant solute spectral bands were evident at higher frequencies.

While reproducible PDIR spectra were most reliably obtained in D_2O as solvent, some acceptable data were nonetheless acquired in a similar fashion to those in Figs. 7.3 and 7.4, but utilizing instead H_2O as solvent. Spectra b and c in Fig. 7.5 show a typical

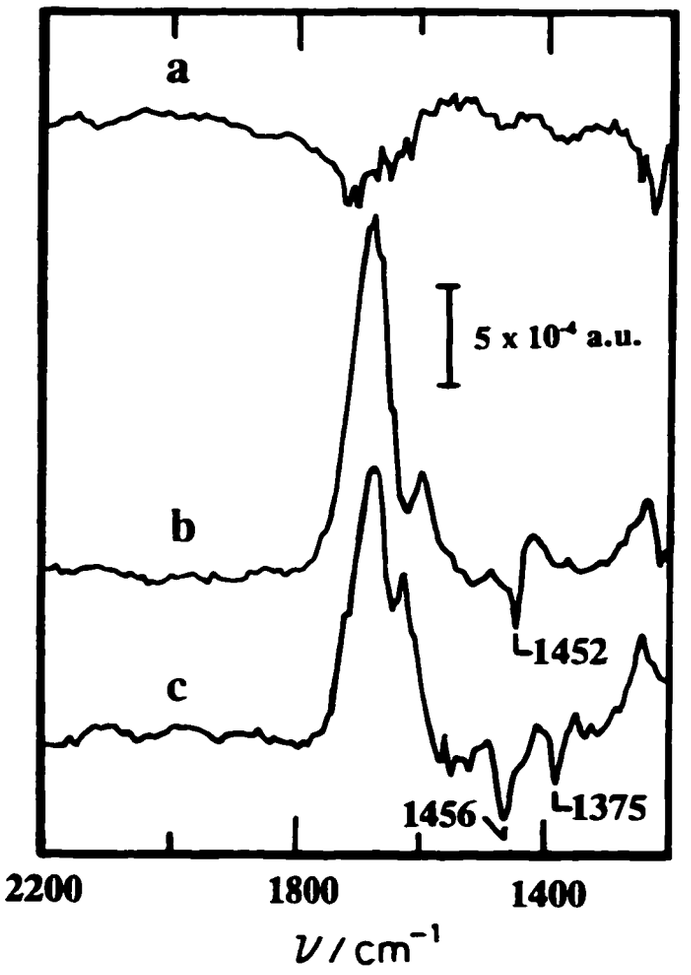

Fig. 7.5 Single potential-step PDIR spectra in the 1200-2800 cm^{-1} region for 0.1 mol dm^{-3} $HClO_4$ with H_2O as the solvent on Pt(111). The spectra acquisition followed the description given in the caption for Fig. 7.3. Spectra labelled **a** to **b** result from stepping the potential from 0.76 V (reference) to 0.26 V (sample). Spectrum **a** is recorded for a solution containing the electrolyte alone; Spectrum **b** is for 7 x 10^{-3} mol dm^{-3} CD_3CN; and spectrum **c** for 7 x 10^{-3} mol dm^{-3} CH_3CN. The units of the intensity axis in absorbance units (a.u.).

pair of examples of spectra in the latter solvent, with CD_3CN and CH_3CN, respectively as the solute. The 1630 cm^{-1} feature is still observable, albeit less clearly due to interference from H_2O bending modes arising from inexact cancellation of the solvent contributions in the reference and sample spectra. The weak bands seen in the *ca.* 1400-1450 cm^{-1} region are apparently altered by D_2O/H_2O solvent substitution. Thus a weak negative-going feature at *ca.* 1455 cm^{-1} is observed for both CH_3CN and CD_3CN in H_2O as solvent (Fig. 7.3) which is absent in D_2O solvent, and the negative-going band arising at *ca.* 1410 cm^{-1} in D_2O as solvent (Figs. 7.3 and 7.4) becomes absent in H_2O as solvent (Fig. 7.5). A possible interpretation of these subsidiary PDIR features is offered below.

Significantly, spectra obtained for the electrode that had been cycled with acetonitrile present in a separate solution and then transferred to the optical cell were essentially identical to spectra obtained with the same electrode but with the acetonitrile actually present in the thin-layer cell. This indicates that the vibrational features are due to irreversibly adsorbed acetonitrile. However, under the latter conditions of the transfer experiments, the reductively chemisorbed acetonitrile was not as stable with time as when that solute was already present in the thin-layer solution, as indicated by observation of a small but progressive diminution of the 1632/1614 cm^{-1} signals.

Additionally, repetitive potential modulation experiments were performed at Pt(111) in the presence of acetonitrile as solute, by periodically stepping the potential back and forth a number of times between the reference and sample values. This type of modulation experiment still yielded the same spectral bands seen in Figs. 7.3 to 7.5 but, as observed in the experiment described above, they became significantly attenuated as the number of modulations was increased. Again, this indicates that the formation of the reduced or reoxidized species during the reactive chemisorption of CH_3CN is not a rapid and/or fully reversible process. This behaviour could be related to the slow process observed in Chapter 6 occurring at less positive potentials (< 0.36 V, i.e. in the presence of the remaining UPD H).

A possibly surprising feature of the >C=N- band is that its frequency is not discernably dependent on the electrode potential (Stark effect, as with CO) as might be anticipated for an adsorbate mode. Nevertheless, clear evidence that this spectral feature

corresponds to an adsorbed, rather than a solution-phase, species can be deduced from the observation of similar behaviour for irreversibly pre-adsorbed acetonitrile, i.e. in the absence of acetonitrile in the thin-layer solution.

These spectral findings can be compared insightfully with the mechanism for acetonitrile adsorption and reduction proposed previously in Chapter 6 (see Fig. 7.1) [18,19]. The absence of any unipolar or dipolar bands at higher frequencies, specifically at 2250-2300 cm^{-1}, provides evidence against the presence of σ-bonded acetonitrile, since such a "perpendicular" (or tilted) form should be infrared-active and yield bands in this region [32,33]. Precedents for the above statements are to be found in the spectroscopy of nitrile complexes as summarized in Table 7.1 where, for example, upon coordination of $Cl_2Pt(CH_3CN)_2$ to Pt [32], the 2260 cm^{-1} $\upsilon(C\equiv N)$ band [34] becomes shifted to higher frequency, around 2309 cm^{-1}; on the other hand, for a π-coordinated nitrile, the $\upsilon(C\equiv N)$ would be expected to be shifted to a lower frequency, such as 1734 cm^{-1} in the case of $Pt(P(Ph)_3)_2CF_3CN$, Ph=phenyl [33]. The presence of π-bonded acetonitrile at higher potentials, as suggested in structure Ib (Fig. 7.1), is also in harmony with UHV-based experiments which indicate that the nitrile group becomes adsorbed in a flat orientation when acetonitrile is dosed directly onto Pt (111) at low temperature [35-37]. Reference 35 includes results of UHV-based infrared experiments which show the absence of a nitrile stretching vibration for chemisorbed acetonitrile, in harmony with the usual surface selection rule.

Most significantly here, the appearance of an *infrared-active* feature at 1632/1614 cm^{-1} at lower potentials, $\leq$ 0.35 V (Fig. 4.4), provides strong support to the previously suggested formation of a reduced acetonitrile state in which the "CN" function now consists of a *double bond* and is tilted with respect to the surface plane as shown in structure V:

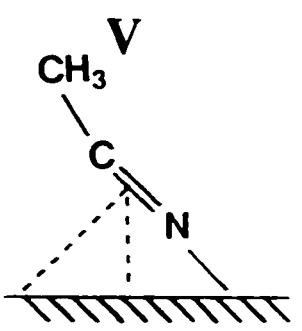

Table 7.1 Comparison of CN stretching frequencies in nitrile complexes

Compound	$\upsilon(C\equiv N)$/ cm^{-1}	Structure	References
CH_3CN	2268	Linear	[34]
$PtCl_2 \cdot 2CH_3CN$	2309	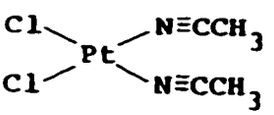	[32]
$Pt(PPH_3)_2 \cdot CF_3CN$	1734	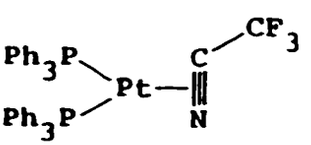	[33]
$Fe_3(CH_3CN)(CO)_9$	1610	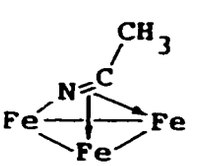	[38]
CH_3CN/Pt(111) monolayer	1615	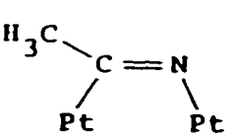	[36]
$CH_3CN_{(aq)}$/Pt(111) reductive chemisorption	1632	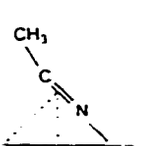	present work [41]

The present results apparently constitute the first time such a υ(C=N) stretching motion has been observed *in-situ* at a metal/solution interface. However, a similar υ(C=N) stretch is also observed at 1610 cm^{-1} for the bulk phase $Fe_3(CH_3CN)(CO)_9$ complex where the CN group, as C=N, is bonded via both the C and N atoms to an Fe_3 triad [38]. A similar frequency (1615 cm^{-1}) was also observed by EELS for acetonitrile adsorbed onto Pt(111) in UHV [36]. In the latter work, based on both EELS and XPS data (at 100 K), the authors suggested that, as a result of acetonitrile chemisorption at Pt(111), there must be considerable back-donation from Pt into antibonding π^*-orbitals of the CH_3CN molecule in order for the bond order to be reduced by one. The observation of the >C=N- double-bond frequency was explained by formation of an adsorbed, di-σ-bonded >C=N-, with the C=N bond being essentially parallel to the Pt surface plane in an η^2(C,N) configuration [36]. Table 7.2 gives a summary of the vibrational frequencies (cm^{-1}) of vapour phase and adsorbed acetonitrile as reported in ref. 36.

Beside the fact of the very observation of a >C=N- vibration in the infrared , another difference between the present >C=N- infrared vibration and that seen for adsorbed anhydrous acetonitrile on Pt(111) in UHV experiments concerns the significant (*ca.* 18 cm^{-1}) downshift arising upon deuteration of acetonitrile. This effect can be understood, at least qualitatively, in terms of an increase in the effective mass of the methyl group adjacent to the C=N moiety.

As a check on the validity of this notion, we examined the effect of deuterating the methyl groups on the carbonyl vibration in liquid-phase acetone [$(CH_3)_2CO$] as a model analogue. This molecule was chosen in view of its roughly similar C=O and C-C frequencies to our adsorbed acetonitrile in its reduced "C=N" form. Indeed, an effect of methyl deuteration on the carbonyl frequency, downshifting it by 10 cm^{-1} (from 1716 to 1706 cm^{-1}) *is* observed, comparable with that for the present acetonitrile case, thus supporting the assignment of the 1632/1614 cm^{-1} feature to a C=N vibration.

Interestingly, however, deuteration of liquid-phase acetonitrile leads to an *upshift* of 11 cm^{-1} in the -C≡N frequency from 2267 to 2278 cm^{-1} [39]. This unexpected effect is attributed [39] to a mechanical interaction between the symmetric C-D and -C≡N

Table 7.2 Vibrational frequencies (cm^{-1}) of vapour phase [34] and adsorbed CH_3CN on Pt (111) [36]

Vibrational mode	Description	CH_3CN gas	CH_3CN multi-layer	CH_3CN mono-layer	CD_3CN mono-layer	Ratio H/D
$\rho_t(CH_3CN)$	torsion	-	120			
$\upsilon_s(Pt\text{-}CH_3CN)$	Pt-CH_3CN stretch	-	-	280	265	1.06
$\upsilon_a(Pt\text{-}CH_3CN)$		-	-	410	385	1.06
$\delta(C\text{-}C\text{-}N)$	CCN bend	361	-	605	580	1.04
$\upsilon(C\text{-}C)$	CC stretch	920	920	950	930	1.02
$\rho_r(CH_3)$	Methyl rock	1041	1040	1060	850	1.25
$\delta_s(CH_3)$	Methyl sym. bend	1389	1430	1375	1100	1.27
$\delta_d(CH_3)$	Methyl deg. bend	1454		1435		
$\upsilon(C\equiv N)$	CN strech	2268	2270	1615	1625	0.99
$\upsilon_s(CH)$	CH_3 sym. stretch	2954	3010	2960	2120	1.40
$\upsilon_d(CH)$	CH_3 deg. stretch	3009		3005	2280	1.32

stretching motions. However, such coupling is unlikely in the present case of acetonitrile in the adsorbed reduced state, due to the markedly lower frequency of the >C=N- compared with the -C≡N band.

It remains to offer a tentative explanation of the subsidiary spectral features observed in the 1400~1450 cm^{-1} region which are apparently sensitive both to deuteration of the adsorbed solute and the solvent. First, the negative-going band at 1407 cm^{-1} in Fig. 7.3 (CH_3CN in D_2O solvent) and the 1375 and 1456 cm^{-1} bands observed in Fig. 7.5, spectrum c (CH_3CN in H_2O solvent), could be tentatively assigned to -CH_3 symmetric or/and asymmetric bending modes that become less absorbing as the CH_3CN molecules reorient upon reduction, i.e., from a -C≡N bond parallel to the surface to a >C=N- bond somewhat inclined with respect to the Pt surface plane (structure V). However, the 1375 cm^{-1} band is marginally significant, due to its small intensity but similar bands at 1375 cm^{-1} and 1435 cm^{-1} have been observed in the UHV experiments of Sexton and Avery [36] for the methyl bending modes (see Table 7.2). This reorientation would cause the methyl group to change its contribution to that absorption band.

Some evidence supporting the assignment of the 1410 cm^{-1} band seen for CH_3CN/D_2O (Fig. 7.3) to a methyl bending vibration could be deduced from the loss of most of its band intensity upon solute deuteration (Fig. 7.3), as indicated by the resulting large downshift of frequency. However, since weak bands are still observable in the *ca.* 1410 cm^{-1} frequency region, it seems reasonable to suggest that one of these bands could arise from υ(C=N) with protonated nitrogen (or carbon) atoms (in the case of the weak, positive-going band at 1446 cm^{-1}) whereas the negative-going one at 1408 cm^{-1} could arise from some vibrational mode(s) associated with anion/CD_3CN or D_2O/CD_3CN solvation structures in the interphase.

Lastly, attempts were made to provide further confirmation of the present 1632/1614 cm^{-1} band assignment to >C=N- from the effect of ^{13}C substitution (on the C=N carbon atom). Unfortunately, however, the ^{13}C isotopically labelled samples obtained commercially were insufficiently pure to enable reliable surface infrared spectra to be obtained.

After stepping the potential and recording the spectra for potentials less positive than 0.76 V, the potential was stepped to higher values in order to examine if the adsorbed CH_3CN might become oxidized. One of these spectra is shown at the top of Fig. 7.3 for a sample potential of 1.06 V; it is clear that for potentials more positive than 0.76 V, no indications of oxidation of CH_3CN are detectable spectroscopically.

7.3.3 Effects of potential holding on the PDIR spectra for Pt(100)

As was shown in ref. 1 in the work on polycrystalline Pt and confirmed in ref. 19, when the potential is held at the less positive limit (0.06 V) in the presence of acetonitrile there is an increase of the reoxidation charge as the potential, in a following sweep, is scanned up to 0.9 V. This effect is also observed on both Pt(110) and (111) single-crystal planes but it is on Pt(100) that the change of current response is much larger, as was shown in Fig. 6.10 of Chapter 6 [19]; in that case, the anodic charge for the two peaks observed became doubled.

In order to investigate this potential-holding effect at Pt(100), spectra were recorded immediately after stepping the potential from 0.86 V to 0.16V, with the potential being then held at the latter value for *ca.* 2 minutes followed by another series of spectra being recorded at that lower potential (holding time = 2 min). Figure 7.6 shows a pair of PDIR spectra which illustrate qualitatively the temporal growth of the >C=N- feature on Pt(100). Spectrum **a** was obtained by subtracting a spectrum obtained at a reference value taken as 0.86 V from that acquired at 0.16 V. Similarly to the results shown in Figs. 7.3-7.5, 100 interferometer scans were collected at both potentials, thereby requiring a duration of *ca.* 60 s in each case. As observed at Pt(111), the characteristic positive-going 1630 cm^{-1} feature is evident, indicating formation of the >C=N- moiety at the lower potential. Spectrum **b** in Fig. 7.6 was obtained subsequently to spectrum **a**, but after holding the potential at 0.16 V for an additional 2 min, and employing the sample spectrum in **a** (also acquired at 0.16 V) as the reference. Consequently, the positive-going feature at *ca.* 1630 cm^{-1} seen in spectrum **b** reflects the *additional* >C=N- species that has formed during the 2 min holding time at the lower potential. Hence the time effect arises from further slow formation of the double-bonded

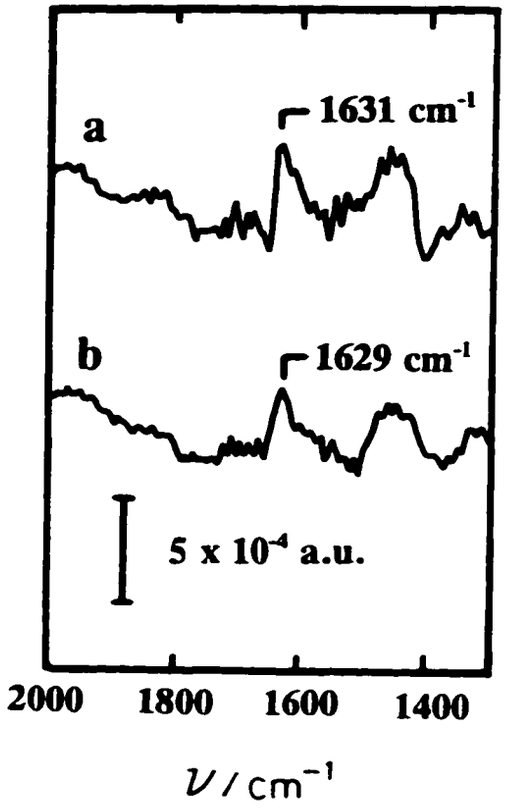

Fig. 7.6 Single potential-step PDIR spectra in the 1350-2000 cm^{-1} region for 7 x 10^{-3} mol dm^{-3} CH_3CN in 0.1 mol dm^{-3} $HClO_4$ with D_2O as the solvent on Pt (100). Each spectrum was acquired by using 100 interferometer scans at each of the (reference/sample) potentials; in Spectrum **a**, the reference potential is 0.86 V and the sample potential is 0.16 V; in Spectrum **b**, the reference potential is 0.16 V (no holding) and the sample potential is 0.16 V (holding time 2 min). See section 7.3.3 for more details. The units of the intensity axis are in absorbance units (a.u.).

C=N species, rather than from further reduction to a single-bonded C-N adsorbate as had been suggested in ref. 19.

The two spectra reported in Fig. 7.6 do not display bands that are so well resolved as those observed in the spectra for acetonitrile adsorption on Pt(111) (Fig. 7.3-7.5); we believe this is inherent to this face which displayed the least reversible features in its cyclic voltammogram in the presence of CH_3CN (see Fig. 6.10 of Chapter 6) [19].

In separate experiments, it was verified electrochemically that the species being formed during the potential-holding at 0.16 V was not diffusing away from the electrode, i.e. it remained adsorbed.

7.3.4 Further comparison with vacuum-based adsorption behaviour

In addition to the examinations of acetonitrile adsorption by low-temperature dosage onto Pt (111) in UHV already noted, Hubbard *et al.* [40] have reported a study entailing emersion of Pt(111) electrodes with adsorbed acetonitrile in aqueous solution into UHV for spectral examination, indicated both side-on and end-on chemisorptive bonding of CH_3CN to Pt(111) (cf. **I** in our Fig. 7.1) while adsorption from neat CH_3CN led to a species that supposedly reacted with traces of water, giving adsorbed acetamide, $CH_3.CO.NH_2$. This adsorbate could exist as an iminol tautomer $OH(CH_3)C=NH$, related to the structure of "reduced acetonitrile". Adsorption of CH_3CN from aqueous solution, followed by transfer to a UHV system, produced predominantly $CH_3.CO.NH_2$ (*cf.* 40). In our own work, comparative voltammetry experiments with $CH_3.CO.NH_2$ at Pt(111) was performed and after addition of acetamide the CV had none of the characteristics of the CV's of adsorbed CH_3CN, although the amide was strongly adsorbed as indicated by blocking of UPD of H and of co-adsorption of HSO_4^-; however, no evidence for a *reactive* chemisorption process was found. Note that Pt surfaces behave as hydrogenation or dehydrogenation catalysts rather than catalysts for hydration, the process required in conversion of CH_3CN to $CH_3.CO.NH_2$.

7.4 Conclusions

Using infrared spectroscopy, this present section of the work shows how it was possible to gain better molecular insights on the mechanism of reactive chemisorption of acetonitrile at Pt electrodes. A comparison of the information acquired spectroscopically with the proposed mechanism (Fig. 7.1) deduced mainly from electrochemical techniques (Chapter 6) is made in Table 7.3.

From this table the following conclusions are reached: a) the CH_3CN molecules initially adsorbed at the most positive potential limits are most likely adsorbed with their $C \equiv N$ bond parallel to the Pt(111) surface plane; b) there is a good consistency between the determination of the onset of the reduction of the adsorbed CH_3CN from the CV's shown in Fig. 7.2 and the appearance of an absorption band for a $>C=N-$ structure; c) from the spectra recorded for the reactive chemisorption of CH_3CN at Pt(100) it was possible to associate the observed increase of currents that arise in the linear sweep following holding the potential of the electrode at 0.16 V, with a continuing reduction process leading to $>C=N-$ species, the same as that referred to in point b); d) although the current responses in Fig. 7.2b depend on the acid solution used, the series of spectra (Figs. 7.3 to 7.5) remain unchanged upon substitution of ClO_4^- by HSO_4^-. This is consistent with the interpretation given in section 7.3.1 of the feature observed in Fig. 7.2b, above 0.6 V in $HClO_4$ and between 0.35 V and 0.55 V in H_2SO_4.

Although the use of infrared spectroscopy could not provide a full clarification of the electrochemical processes being addressed in this chapter, and described in Chapter 6, it allowed, however, for the first time, identification of the $C=N$ structure **V** as the principal species arising from reactive chemisorption of acetonitrile.

At this point, it could be added that although the recorded absorbance is of about the right magnitude for adsorbed species, there is always the possibility that another surface species not adsorbing in surface IR, (due to surface selection rules) could also be involved in the reactive chemisorption of acetonitrile. However, from the evidence found in section 7.3.3, related to the potential holding effect, the adsorbed species involved in the reactive chemisorption of acetonitrile are having the structure proposed as **V** (see page 216).

Table 7.3 Vibrational frequencies (cm^{-1}) for the reduction of chemisorbed acetonitrile

Potential / (V)	Suggested structures	Vibrational modes / (cm^{-1})
0.76	Structure II or	υ (C≡N) not observed
	Ib (see Fig. 7.1)	υ (C=N) not observed
		δ_s $(CH_3)^{**}$ not observed
		δ_d $(CH_3)^{***}$ 1410 cm^{-1}
0.36 - 0.06*	Structure V	υ (C=N) 1614, 1632 cm^{-1}
	(see section 7.3.2)	δ_s $(CH_3)^{**}$ not observed
		δ_d $(CH_3)^{***}$ not observed

* The mechanism of Fig. 7.1 suggested protonation of the C and/or N atoms between 0.36 and 0.06 V, but no bands supporting this process was observed. Except maybe in Fig. 7.6, where a broad positive-going band is visible on both spectra **a** and **b**, around 1450 cm^{-1}.
** Methyl symmetric bending.
*** Methyl asymmetric bending.

References

1. A.T. Hubbard, J.L. Stickner, S.D. Rosasco, M.P. Soriaga and D. Song, J. Electroanal. Chem., 150 (1983) 165.
2. D.M. Kolb and J. Schneider, Electrochim. Acta, 31 (1986) 929.
3. M. Fleischmann and I.R. Hill in "Comprehensive Treatise of Electrochemistry", Vol. 8, J.O'M. Bockris, R.E. White, B.E. Conway and E. Yeager (Eds.), Plenum, New York, 1985, p. 373.
4. J. Robinson in "Electrochemistry", Vol. 9, D. Pletcher (Ed.), Royal Society of Chemistry, London, 1984, p. 101.
5. A. Otto, Surf. Sci., 101 (1980) 99.
6. G.H. Brilmeyer and A.J. Bard, Anal. Chem., 52 (1980) 685.
7. D.A. Scherson, S.B. Yao, E.B. Yeager, J. Eldridge, M.E. Kordesch and R.E. Hoffman, J. Electroanal. Chem.,150 (1983) 535.
8. M.J. Albarelli, J.H. White, G.M. Bommarito, M. McMillan and H.D. Abruna, J. Electroanal. Chem.,248 (1988) 77.
9. H.B. Mark and S.B. Ponds, Anal. Chem., 38 (1966) 119.
10. A.H. Reed and E. Yeager, Electrochim. Acta, 15 (1970) 1345.
11. H. Neugebauer, G. Bauer, N. Brinda-Konopik and G. Gidaly, J. Electroanal. Chem., 122 (1981) 381.
12. D.L. Dubois and J.A. Turner, J. Am. Chem. Soc., 104 (1982) 4989.
13. A. Bewick, K. Kunimatsu and S.B. Ponds, Electrochim. Acta, 25 (1980) 465.
14. S. Pons, T. Davidson and A. Bewick, J. Electroanal. Chem., 160 (1984) 63.
15. S. Pons, J. Electroanal. Chem., 150 (1983) 495.
16. a) J.W. Russell, J. Overend, K. Scanlon, M. Severson and A. Bewick, J. Phys. Chem., 86 (1982) 3066; b) J.W. Russell, M. Severson, K. Scanlon, J. Overend and A, Bewick, *ibid*, 87 (1983) 293.
17. a) M.J. Weaver and X. Gao, Chem. Rev. Phys. Chem., 44 (1993) 459; b) H.D. Abruña, "Electrochemical Interfaces: Modern techniques for in-situ interface characterization", VCH Publishers, Inc., New York, 1991.
18. H.A. Kozlowska, B.R. MacDougall and B.E. Conway, J. Electroanal. Chem.,

39 (1972) 287.

19. S. Morin and B.E. Conway, J. Electroanal. Chem., 376 (1994) 135.
20. B.R. MacDougall, B.E. Conway and H.A. Kozlowska, J. Electroanal. Chem., 32 App. (1971) 15.
21. R.J. Nichols in "Adsorption of Molecules at Metal Electrodes", J. Lipkowski and P.N. Ross (Eds.), VCH Publishers, New York, 1992, Chapter 7.
22. K. Ashley and S. Ponds, Chem. Rev., 88 (1988) 673; and references therein.
23. P. Krtil, L. Kavan and P. Novak, J. Electrochem. Soc., 140 (1993) 3390.
24. D.S. Corrigan, L.-W. H. Leung, M.J. Weaver, Anal. Chem., 59 (1987) 2252.
25. S.-C. Chang, L.-W.H. Leug and M.J. Weaver, J. Phys. Chem., 94 (1990) 6013.
26. S.-C. Chang, A. Hamelin and M.J. Weaver, J. Phys. Chem., 88 (1991) 1615.
27. S.-C. Chang and M.J. Weaver, J. Phys. Chem., 92 (1990) 4582.
28. S.-C. Chang and M.J. Weaver, J. Phys. Chem., 94 (1990) 5095.
29. S.-C. Chang, J.D. Roth and M.J. Weaver, Surf. Sci., 244 (1991) 113.
30. a) J. Clavilier, R. Albalat, R. Gómez, J.M. Feliu and A. Aldaz, J. Electroanal. Chem., 330 (1992) 489; b) R. Gómez, Ph.D. Thesis, Universitat d'Alacant, Alacant, Spain 1994.
31. see section 3.1.2 of Chapter 3.
32. R.A. Walton, Spectrochim. Acta, 21 (1965) 1795.
33. W.J. Bland, P.D.W. Kemmit and R.D. Moore, J. Chem. Soc. Dalton Trans., (1973) 1292.
34. J.E.D. Davies, J. Mol. Struct., 9 (1971) 483.
35. I. Villegas and M.J. Weaver, J. Am. Chem. Soc., 118 (1996) 458.
36. B.A. Sexton and A.R. Avery, Surf. Sci., 129 (1983) 21.
37. A. Cassuto and G. Tourillon, Vacuum, 46 (1995) 583.
38. M.A. Andrews and H.D. Kaesz, J. Am. Chem. Soc., 101 (1979) 7255.
39. W.H. Fletcher and C.S. Shoup, J. Mol. Spec., 10 (1963) 300.
40. A.T. Hubbard, E.Y. Cao, M.A. Smith and D.A. Stern, Electrochim. Acta, 39 (1994) 1007.
41. S. Morin, B.E. Conway, G.J. Edens and M.J. Weaver, J. Electroanal. Chem., in proof (1996).

Chapter 8

Final conclusions and contributions to original research

During the course of this thesis work, two electrochemical surface processes were investigated in detail: the fast kinetics of the UPD of H and the reactive chemisorption of acetonitrile at platinum single-crystal surfaces. Although these processes are very different in their kinetics and mechanism, they both display great sensitivity towards the surface geometry of the various platinum surfaces studied. While impedance spectroscopy was found to be suitable for the investigation of the UPD of H, the reactive chemisorption of acetonitrile could be investigated adequately using various potential cycling programs and transient measurements, as well as *in situ* reflection FTIR spectroscopy.

The contributions to original research are the following:

a) Investigation of the reactive chemisorption of acetonitrile at various Pt single-crystal planes showed that this process was highly sensitive to the different surface geometries studied and provided a new example of reactivity of a small organic molecule, in this case having a nitrile functionality, at Pt single-crystal surfaces.

i) A large effect of the nature of the anions (ClO_4^- or HSO_4^-) on the cyclic voltammetry for this process at Pt(111) was also demonstrated.

ii) Similar to the previous work from this laboratory on polycrystalline Pt, the H displacement and the effect of potential holding at the less positive potential limit was also observed at the single-crystal surfaces. However, a much larger potential holding effect was seen at Pt(100).

iii) In order to elucidate some of the behaviours observed (points i and ii) as well as to validate the proposed mechanism, *in situ* IR spectroscopy was utilized.

iv) In accordance with the mechanism proposed, based on the results of the electrochemical studies, the IR spectra show, at potentials below 0.35 V *vs.* RHE at Pt(111), the presence of a vibrational frequency of a lower C

to N bond order than that in acetonitrile; confirming the presence of a reduced form of chemisorbed acetonitrile. This >C=N- stretching frequency was observed at 1630 cm^{-1} and it was downshifted to 1614 cm^{-1} upon deuteration.

v) A similar spectral feature was observed upon reduction of chemisorbed acetonitrile at Pt(100) which was also shown to develop with time, indicating slow reduction as was suggested on electrochemical grounds (point ii).

vi) It is also the first time that such a reduced chemisorbed-nitrile vibrational band has been observed by *in situ* IR spectroscopy at an electrode surface.

b) Using impedance spectroscopy, the kinetics of the UPD of H were evaluated for the first time at various single-crystal planes, and at three temperatures.

i) The methodology employed in the kinetic studies of the UPD of H allowed determinations of the double-layer capacitance, the adsorption pseudocapacitance and the charge-transfer resistance.

ii) From the analysis of the impedance results an order of reactivity could be determined for the various surfaces investigated, where the exchange rate was found to be decreased in the following order: (111)>>(110)>polycrystalline>(100), while determination of the kinetics of UPD of H at Pt(311) showed faster adsorption-desorption rates on the (111) sites than on the (100) sites present on that surface.

iii) These kinetic studies on adsorbed H importantly allowed determination of the *coverage-dependence* of the rates of electrosorption at several of the single-crystal surfaces of Pt examined in the research.

iv) It was also observed that the double-layer capacitance recorded as a function of potential did have the characteristic features that are expected when a large concentration of electrolyte is present in solution.

v) Moreover, the impedance technique allowed separation in some cases of both the pseudocapacitance and the charge-transfer resistance for the co-

adsorption of H and HSO_4^-.

vi) The conditions for onset of anion adsorption obtained from these methods are in agreement with the results obtained by the method based on displacement of previously chemisorbed H or anions (HSO_4^-) by CO and yield a good approximation for the location of the *pzc* on the experimental potential scale.

vii) For each of the surfaces studied, the sum of all the capacitance components yielded a value very similar to that calculated from the cyclic voltammetry results, providing validation of the impedance data.

viii) The dependence of the kinetic parameters on temperature was also investigated and from it the energy of activation was determined for the UPD of H; a value of 48 $\pm$ 5 kJ mol^{-1} was obtained at intermediate coverages for Pt(100) and (311).

c) In the course of the research and examination of the pertinent literature, a critical review on the states of H and co-adsorbed anions on single-crystal surfaces of Pt was prepared (Chapter 3) and will be published as a review article in due course.